

UNIVERSITY OF SHEFFIELD
Department of Civil and Structural Engineering

LATERAL-TORSIONAL BUCKLING STRENGTH
OF
CASTELLATED BEAMS

by

DJAMEL EL-DDINE Kerdal
Ing. ENPA (Algiers), MEng (Sheffield)

A thesis submitted to the University of Sheffield
for the degree of Doctor of Philosophy.

November, 1982

TO
MY PARENTS
AND
PAMELA ANN

SUMMARY

A review of the research carried out on the subject of castellated beams revealed that one subject had remained largely untouched -lateral stability. This was despite the fact that the fabrication process had increased their strength and rigidity about the plane of loading at the expense of lateral stiffness.

This emphasis on in-plane behaviour stemmed from the need to catalogue the failure modes particular to castellated beams. However because of the high number of parameters necessary to describe a castellated beam and their high degree of internal redundancy, little that can be regarded as firm design recommendations and no provisions against lateral buckling have been included in national codes of practice, particularly in the present British codes.

This is why the draft of the new British code for structural steelwork B/20 to be published as BS 5950 suggests the use of the simple Vierendeel analogy for in-plane behaviour and has adopted the conservative approach of cl.11.3.2 to the prevention of lateral buckling in which the contribution of the web and tension flange are ignored.

The work undertaken herein had the aim of mainly providing the missing quantitative data on the lateral-torsional buckling strength of castellated sections currently available in the U.K. Eight full size castellated beams were tested. The results of these plus the few cases reported in the literature were used as a basis for a critical evaluation of several design approaches.

Comparisons between the test results and the strength predicted by B/20 were found to be generally acceptable provided cross-sectional properties at a castellation were used in the calculations.

Similar results were obtained for the two-stage procedure of BS 449 and BS 153 whereas the use of Table 3 in the former was shown to lead to rather low load factors.

A preliminary test programme on small scale beams showed the negligible effect that the holes had on lateral buckling behaviour. Finally a computer program which was used to calculate a value of elastic critical load confirmed that the web post did not distort when the beams failed.

ACKNOWLEDGEMENTS

This research was carried out in the Department of Civil Engineering at the University of Sheffield.

The author would like to express his sincere appreciation and gratitude to Dr. D. A. Nethercot for his excellent guidance and supervision throughout.

Many thanks are due to the Ministry of Higher Education, Algeria, for the scholarship awarded to the author.

The author also wishes to thank Constrado for the financial support provided for the tests reported in this thesis. The assistance of Mr. F. H. Needham, of that organisation, is greatly appreciated.

He acknowledges the assistance of the technical staff of the department and in particular that of Messrs. R. Foster, H. Cass and D. Thompson. He also extends his thanks to the secretarial staff of the department for helping in many ways and to Miss S. Krajewski for typing the tables so diligently.

CONTENTS

	<u>Page</u>
Summary.....	i
Acknowledgements.....	iii
Contents.....	iv
List of Figures.....	xi
List of Tables.....	xiv
List of Plates.....	xvi
Notation.....	xvii
CHAPTER 1 <u>INTRODUCTION</u>	
1.1 Castellated beams	1
1.1.1 General introduction	1
1.1.2 Fabrication process.....	1
1.1.3 Applications and advantages of castellated beams.....	3
1.2 Brief literature survey.....	4
1.2.1 Present state of the research.....	4
1.2.2 Lateral buckling considerations.....	5
1.3 The present situation regarding the British codes of practice.....	6
1.3.1 Reasons for the present gaps in research.....	6
1.3.2 Consequences.....	7
1.4 Aim of the project.....	8
1.5 Presentation of the thesis.....	9
CHAPTER 2 <u>LITERATURE REVIEW</u>	
2.1 Introduction.....	10
2.2 British tests.....	10
2.2.1 The Rotherham tests.....	10
2.2.1.2 1958 tests (16).....	12
2.2.1.3 1960 and 1961 tests (17,18).....	13
2.2.2 Other British tests.....	13
2.3 American tests.....	13
2.4 Belgian tests.....	14

2.5	French tests.....	15
2.6	Canadian tests.....	15
2.7	Miscellaneous.....	16
2.8	Theoretical investigations.....	17
2.8.1	Deflection predictions.....	17
2.8.1.1	Empirical methods.....	17
2.8.1.2	Matrix methods.....	18
2.8.2	Stress distribution.....	18
2.8.3	Web buckling.....	19
2.9	Design procedures.....	19
2.10	Lateral buckling of castellated beams.....	20
2.10.1	General considerations.....	20
2.10.2	Description of the method.....	20
2.10.3	Comparison with methods for plain-webbed beams.....	21
2.11	Conclusions.....	22

CHAPTER 3 SMALL SCALE TESTS

3.1	Introduction.....	23
3.2	Previous work on model testing.....	24
3.2.1	Stresses and deflections.....	24
3.2.2	Effect of openings on the lateral buckling of beams.....	24
3.3	Test rig.....	25
3.3.1	Description.....	25
3.3.2	Loading system.....	26
3.4	Specimens.....	26
3.4.1	Choice of dimensions.....	26
3.4.2	Fabrication process.....	27
3.4.3	Material properties.....	28
3.5	Testing programme.....	28
3.6	Theoretical predictions.....	29
3.6.1	Calculations of failure loads.....	29
3.6.2	Failure modes.....	30
3.7	Results and conclusions.....	30
3.7.1	Short girders CM8 and CM10.....	30
3.7.2	Long girders (CM12 to CM18).....	31
3.7.3	Conclusions.....	32

CHAPTER 4 DESIGN OF THE TEST BEAMS

4.1	Introduction.....	33
4.2	Lateral-torsional buckling considerations.....	34
4.2.1	Influence of the holes.....	34
4.2.2	Elastic lateral buckling.....	35
4.2.2.1	General.....	35
4.2.2.2	Comparison of the values of elastic critical moment calculated at a hole and web post cross-section.....	36
4.2.2.2.a	Elastic critical moment from ref.62.....	37
4.2.2.2.b	Elastic critical moment from ref.55.....	38
4.2.2.3	Conclusions.....	39
4.2.3	Inelastic lateral buckling.....	39
4.3	B/20 proposals.....	40
4.3.1	Existing practices.....	40
4.3.2	B/20 approach.....	41
4.3.2.1	Design of plain-webbed beams.....	41
4.3.2.2	Design of castellated beams in B/20.....	42
4.4	Review of experimental data.....	43
4.4.1	Introduction.....	43
4.4.2	Redwood and McCutcheon tests (73).....	44
4.4.3	B.S.C. tests (15,16).....	45
4.4.4	Kolosowski's test (20).....	46
4.4.5	French tests (24).....	47
4.4.6	Toprac and Cooke tests (22).....	48
4.4.7	Other tests.....	49
4.5	Conclusions of the survey.....	50
4.6	Selection of the test beams.....	52
4.6.1	Procedure.....	52
4.6.2	Dimensions of the test beams.....	53
4.6.3	Initial deformations.....	54
4.6.4	Slenderness of the test beams.....	54
4.6.5	Material properties.....	55
4.7	Design of the sidespans.....	56
4.7.1	Introduction.....	56
4.7.2	Longitudinal stresses.....	56
4.7.2.1	Elementary theory of bending.....	56
4.7.2.2	Vierendeel analysis of castellated beams.....	57

4.7.2.2.a	Vierendeel analogy.....	57
4.7.2.2.b	1st method.....	57
4.7.2.2.c	2nd method.....	59
4.7.2.2.d	Conclusions.....	60
4.7.3	Rupture of welded joints.....	61
4.7.3.1	Description.....	61
4.7.3.2	Horizontal stresses in the welded joints.....	62
4.7.4	Stability of the web posts.....	62
4.7.4.1	Web post buckling due to horizontal shear force.....	62
4.7.4.1.a	Description.....	62
4.7.4.1.b	Calculation of the failure load.....	63
4.7.4.2	Web buckling due to compression.....	64
4.7.5	Failure due to the formation of a collapse mechanism.....	66
4.7.5.1	Introduction.....	66
4.7.5.2	The Vierendeel mechanism.....	66

CHAPTER 5 TEST RIG

5.1	Test set-up.....	69
5.2	Loading system.....	69
5.2.1	Description of the transfer of load.....	69
5.2.2	Jack system.....	70
5.3	Support system.....	70
5.3.1	Lateral support.....	70
5.3.2	Transfer of loads within the boxes.....	71
5.3.3	Vertical supports.....	72
5.3.4	Longitudinal girder movement.....	73
5.3.5	Summary.....	73
5.3.6	Structural bracing.....	73
5.3.7	Load bearing stiffeners.....	73
5.4	Loading of the beams in the test rig.....	74
5.5	Instrumentation.....	75
5.5.1	Introduction.....	75
5.5.2	Measurement of the displacement of the beams at mid-span..	75
5.5.3	Measurement of the distortion of the web posts.....	77
5.5.3.1	Method of measurement.....	77
5.5.3.2	Description.....	78
5.6	Test procedure.....	79

CHAPTER 6 RESULTS OF THE TEST PROGRAMME

6.1	Introduction.....	80
6.2	Failure loads.....	80
6.2.1	Presentation.....	80
6.2.2	Friction Losses.....	81
6.3	Load-deflection behaviour of the test beams.....	82
6.3.1	Presentation of the load-deflection curves.....	82
6.3.2	Short span beams.....	82
6.3.3	Long span beams.....	83
6.3.4	Medium-span beams.....	83
6.3.5	Unloading behaviour.....	84
6.4	Local buckling failure.....	85
6.5	Buckled shape.....	87
6.5.1	Overall buckled shape.....	87
6.5.2	Distortion of the web posts.....	87
6.6	Comparison of predicted failure loads for collapse modes other than lateral-torsional buckling with the experimental failure loads.....	89
6.6.1	Collapse modes.....	89
6.6.2	Vierendeel mechanism.....	90
6.6.3	Web post buckling.....	91
6.6.3.1	Web post buckling due to compressive force.....	91
6.6.3.2	Lateral buckling.....	91
6.6.4	Web weld fracture.....	93

CHAPTER 7 DISCUSSION OF THE RESULTS

7.1	Introduction.....	95
7.2	Comparison of B/20 with ECCS approach.....	96
7.3	B/20 other procedures.....	97
7.3.1	Description.....	97
7.3.2	Comparison between the various λ_{LT}	98
7.4	Beams S6-2 and S5-1.....	101
7.4.1	Hole cross-sectional properties.....	101
7.4.1.1	B/20 approach.....	101
7.4.1.2	Permissible stress approaches.....	102

7.4.2	Web post properties.....	102
7.4.2.1	Effect of using web post properties on the slenderness....	102
7.4.2.2	Comparison of the various approaches.....	103
7.5	Beams M4-2 and M5-1.....	103
7.5.1	Allowance for moment gradient.....	103
7.5.2	Hole cross-sectional properties.....	105
7.5.2.1	B/20 predictions.....	105
7.5.2.2	ECCS predictions.....	106
7.5.2.3	Other predictions.....	107
7.5.3	Web post cross-sectional properties.....	107
7.6	Beams L6-4, L4-2, L5-3 and L4-1.....	108
7.6.1	Hole cross-section.....	108
7.6.1.1	Limit state approaches.....	108
7.6.1.2	Permissible stress approaches.....	109
7.6.2	Web post properties.....	110
7.7	Results from other tests.....	110
7.7.1	Introduction.....	110
7.7.2	Hole Cross-section.....	111
7.7.2.1	Permissible stress approaches.....	111
7.7.2.2	B/20 and ECCS approaches.....	112
7.7.3	Web post cross-section.....	112
7.8	Comparisons based on the full set of results.....	113
7.8.1	B/20 Recommendations.....	113
7.8.2	ECCS Recommendations.....	115
7.8.3	Permissible stress approaches.....	115

CHAPTER 8 ANALYSIS OF THE CASTELLATED BEAM BY THE STIFFNESS METHOD

8.1	Introduction.....	116
8.2	Out-of-plane analysis.....	116
8.2.1	Stability analysis of a frame.....	116
8.2.2	Load-deflection approach.....	117
8.2.3	Eigenvalue approach.....	118
8.2.4	Application to castellated beams.....	118
8.3	Analysis of the castellated beam treated as a plane frame.	119
8.3.1	Matrix stiffness method.....	119
8.3.2	Geometry of the frame.....	119
8.4	Flow chart of the computer program.....	120

8.4.1	General description.....	120
8.4.2	Preliminary.....	121
8.4.3	In-plane analysis.....	121
8.4.4	Out-of-plane analysis.....	123
8.4.5	Determination of the buckled shape.....	125
8.5	Results.....	125
8.5.1	Initial verification of the computer program.....	125
8.5.2	Calculation of the elastic critical load.....	126
8.5.2.1	Frame used in the analysis.....	126
8.5.2.2	Verification of the out-of-plane part of the program.....	127
8.5.2.3	Elastic critical load.....	127
8.5.2.4	Influence of the size of the holes on the elastic critical load.....	128
8.5.3	Shape of the buckled frames.....	129
8.6	Conclusions.....	130
CHAPTER 9	<u>CONCLUSIONS AND SUGGESTIONS FOR FUTURE WORK</u>	
9.1	General behaviour of castellated beams.....	131
9.2	Design of the sidespans.....	132
9.3	Lateral-torsional buckling.....	133
9.4	Suggestions for future work.....	134
REFERENCES	136

LIST OF FIGURES.

<u>Figure No.</u>	<u>Title</u>
1.1	Castellated beam.
1.2	Litzka module.
1.3	British module.
1.4	Terms used.
2.1	Elastic critical loads for the section 609X140X46.
3.1.a	Model beam.
3.1.b	Dimensions of hole and cross-section.
3.2	Load deflection curves of some of the small scale girders.
3.3	Experimental failure loads of small scale girders.
4.1	Comparison of elastic critical loads of section 609x140x46 calculated at a hole and at web post cross-sections by the method of ref.56.
4.2	B/20 design curve for lateral-torsional buckling.
4.3	Comparison of test data with B/20 proposals for solid web beams having the properties of the hole cross-section.
4.4	Coupons for tensile tests.
4.5	Vierendeel analysis of the castellated beam.
4.6	Secondary bending moment due to shear force.
4.7	Distribution of shear force.
4.8	Longitudinal stresses.
4.9.a	Behaviour of beam with single opening subjected to bending and shear (from ref. 54).
4.9.b	Behaviour of beam with multiple openings subjected to pure bending (from ref. 54).
4.10	Behaviour of beam with multiple openings subjected to bending and shear (from ref. 54).
4.11	Free body diagram of the web post.
4.12	Web buckling due to compression.

- 4.13 Vierendeel mechanism.
- 4.14 Flexural mechanism.
- 4.15 Halleux's shear force mechanism.
- 5.1 Castellated beam under two point loading.
- 5.2 Schematic arrangement of test rig.
- 5.3 Section 1-1 of Fig.5.2, details of test girder support box frame and lateral support frame.
- 5.4 Mid-span deflections.
- 6.1 Variation of end support loads with time.
- 6.2 Variation of end support loads with time.
- 6.3 Variation of $\beta = M_D/M_B$ with time.
- 6.4 Rate of lift of jack.
- 6.5 Load deflection curves of beam S6-2 (L=1650mm).
- 6.6 Load deflection curves of beam S5-1 (L=1650mm).
- 6.7 Load deflection curves of beam M4-2 (L=3000mm).
- 6.8 Load deflection curves of beam M5-1 (L=3000mm).
- 6.9 Load deflection curves of beam L6-4 (L=4026mm).
- 6.10 Load deflection curves of beam L4-2 (L=4268mm).
- 6.11 Load deflection curves of beam L5-3 (L=4268mm).
- 6.12 Load deflection curves of beam L4-1 (L=4268mm).
- 6.13 Displacement of end A for beams S6-2 and S5-1.
- 6.14 Location of the target points on beam L4-2.
- 6.15 Displacements of points 1-7 on beam L4-2.
- 6.16 Displacement of web post W1.
- 6.17 Displacement of web post W2.
- 6.18 Displacement of web post W3.
- 6.19 Displacement of web post W4.

- 7.1 Comparison of B/20 design curve with ECCS proposals for solid web beams.
- 7.2 Comparison of test data with B/20 proposals for solid web beams having the properties of the hole cross-section.
- 7.3 Comparison of test data with B/20 proposals for solid web beams having the properties of the web post cross-section.
- 7.4 Comparison of test data with approximate B/20 proposals for solid web beams having the properties of the web post cross-section.
- 7.5 Comparison of test data with approximate B/20 proposals for solid web beams having the properties of the web post cross-section.
- 7.6 Comparisons of test data with ECCS proposals for solid web beams having the properties of the hole cross-section.
- 7.7 Comparison of test data with ECCS proposals for solid web beams having the properties of the web post cross-section.
- 8.1 Comparison of eigenvalue and load-deflection methods.
- 8.2 Castellated beam treated as a plane frame.
- 8.3 Properties of the members.
- 8.4 Second idealisation of the castellated beam.
- 8.5 Flow-chart of computer program.
- 8.6 Symmetrical half-frame.
- 8.7.a Buckled shape of the web posts for section 609x140x46.
- 8.7.b Buckled shape of the web posts for section 609x140x46.

LIST OF TABLES

<u>Table No.</u>	<u>Title</u>
2.1	Summary of test data from ref.15.
2.2	Summary of test data from ref.16.
2.3	Summary of tests reported in the literature.
2.4	Details of tests where beams failed by lateral-torsional buckling.
3.1	Elastic critical loads for various levels of loading.
3.2	Lengths, effective length factor, slendernesses, predicted strengths and test results of small scale beams.
4.1	Elastic critical moment M_E for lateral buckling of the original UB beams (1) and the castellated beams having the properties of the hole (2) and the web post (3) cross-sections.
4.2	Slenderness ratios for section 609x140x46.
4.3	Summary of test behaviour of 8WF17 beams from Redwood and McCutcheon (ref.73).
4.4	In-plane moment capacities of beams which failed in a flexural mode with or without lateral buckling.
4.5	Moment capacities of beams which failed by lateral-torsional buckling.
4.6	Dimensions of the cross-section of the test beams.
4.7	Properties of test beams.
4.8	Details of the present experimental programme.
4.9.a	Values of static yield stresses.
4.9.b	Material stresses.
4.10	Nominal stresses at various locations of the beam.
4.11	Predicted shear loads when web post buckling is considered.
4.12	Compressive loads causing web buckling.
4.13	Predicted failure loads when shear mechanism is considered.
6.1	Ratios end moments β of span BD at failure.
6.2	Loads at failure and at end of test and time corresponding to these loads.
6.3	Failure loads for Vierendeel mechanism.

- 6.4 Moment capacities of the beams of ref.16 which failed by web post buckling.
- 6.5 Comparison of predicted failure loads R_p with experimental failure loads for beams which failed by web post buckling.
- 7.1 Slenderness of test beams.
- 7.2 Predicted values of M_b calculated using the various λ_{LT} values of Table 7.1.
- 7.3 Comparison of accurate and approximate values of λ_{LT} for the beams of the present series.
- 7.4 Comparison of accurate and approximate values of λ_{LT} for beams with U.K. shaped holes from other test series.
- 7.5 Moment capacities for beams with short central spans.
- 7.6 Moment capacities for beams with medium length central spans.
- 7.7 Moment capacities for beams with long central spans.
- 7.8 Comparisons of test moments with various design predictions for beams with short central spans.
- 7.9 Comparisons of test moment with various design predictions for beams with medium central spans.
- 7.10 Comparisons of test moments with various design predictions for beams with long central spans.
- 7.11 Values of allowable bending stresses p_{bc} calculated using BS 449 and BS 153 methods.
- 7.12 Moment capacities calculated at a hole cross-section.
- 7.13 Comparison of test moments with various design properties. Properties at a hole cross-section.
- 7.14 Moment capacities calculated at a web post cross-section.
- 7.15 Comparisons of test moments with various design predictions. Properties at a web post cross-section.
- 7.16 Means and standard deviation values obtained for the various predictions for the beams of the present series.
- 8.1 Comparison of Euler buckling load P_E with program buckling load W
- 8.2 Elastic critical loads for section 458x102x33.
- 8.3 Elastic critical loads for section 458x127x37.
- 8.4 Elastic critical loads for section 534x127x39.
- 8.5 Elastic critical loads for section 609x140x46.
- 8.6 Elastic critical loads for different widths of web post for section 609x140x46.

LIST OF PLATES.

<u>Plate No.</u>	<u>Title</u>
3.1	Test set-up for small scale tests.
3.2	Local buckling of short small scale girders.
3.3	Lateral-torsional failure of long small scale girders.
5.1	Test rig.
5.2	Jack driving mechanism.
5.3	Jack at end support A.
5.4	Support box frame and side wall with corner studs.
5.5	Lateral support plate.
5.6	Support box frame enclosing the test beam.
5.7	Bearings.
5.8.a	Spherical bearings between portal frame and spreader beam.
5.8.a	Spherical bearings.
5.9	Cylindrical bearing.
5.10	Load bearing stiffener.
5.11	Transducers and pulleys arrangement.
5.12	Lightweight frame.
5.13	Data logging arrangement.
6.1	Local buckling failure of beam S6-2.
6.2	Local buckling failure of beam S5-1.
6.3	Beams S5-1 and S6-2 after test.
6.4	Beams M4-2 and M5-1 after test.
6.5	Beams L4-1, L4-2, L5-3 and L6-4 after test.
6.6	Displacements of beam L4-2 at various stages of loading.
6.7	Side-view of beam S6-2 after test showing no distortion of the web posts
6.8	Side-view of beam L4-2 after test showing no distortion of the web posts.
6.9	Beam M4-2 in a late stage of the test and showing no distortion of the web posts.

NOTATIONS

A	- Area of section.
A_{tee}	- Area of tee section.
B	- Breadth of flange.
C_{ii}	- coefficients of the slope deflection equation.
C_W	- Warping constant.
d	- Distance between neutral axes of tee section.
D	- Depth of section.
D_c	- Depth of castellated section.
D_s	- Depth of original UB section.
E	- Modulus of elasticity.
f_i	- Stiffness coefficient in the element matrices.
G	- Shear modulus of elasticity.
h	- Distance between flange centroids.
I_y, I_z	- Moments of inertia of the members of the frame.
J	- Effective torsion constant.
k	- Effective length factor.
L	- Effective length.
L_{AB}, L_{BD}, L_{DE}	- Length of spans of test beams.
m	- Pitch of castellation.
M_b	- Buckling moment of resistance.
M_{exp}	- Experimental moment.
M_E	- Elastic critical moment.
M_p	- Maximum in-plane carrying capacity.
M_B, M_C, M_D	- Moments at points B, C and D of the test beams.
M_{1a}, M_{1b}	- Moments at points 1a and 1b of the test beams.
n	- Length of web weld joint.

N	- Axial force (ch.4), number of panels in a frame (ch.8).
N_p	- Squash load.
p_{bc}	- Allowable bending stress.
p_c	- Allowable compressive stress.
p_y	- Nominal yield stress.
P	- Compressive load.
P_E	- Euler load.
r_y	- Radius of gyration.
R_{AF}	- Load at failure.
R_{AP}	- Predicted failure load.
R_{AS}	- Load at end of test.
S_{tee}	- Plastic section modulus of tee section.
S_x	- Plastic section modulus.
T	- Thickness of flange.
u	- Buckling parameter.
U	- Total strain energy.
U_w	- Potential energy of the external forces.
v	- Slenderness factor.
V	- Shear force.
w	- Thickness of web.
W	- Force equivalent to bending moment.
W_{cr}	- Elastic critical load.
x	- Torsional index.
Z	- Elastic section modulus.
Z_{tf}, Z_{ts}	- Elastic section modulus at top and stem of tee section.
y_{tee}	- Depth of neutral axis of tee section.
$[k_I^e]$	- In-plane element stiffness matrix.
$[k_L^e]$	- Out-of-plane stiffness matrix.

$[P_L]$	- Out-of-plane load vector.
$[K_L]$	- Overall out-of-plane matrix.
$[\delta_L]$	- Displacement vector.
α	- Shape factor.
β	- Ratio of end moments.
γ	- Ratio allowing for influence of in-plane deflection.
γ_m	- Material factor.
δ_r	- Reduction factor.
η_{LT}	- Perry coefficient for beams.
λ	- Slenderness ratio.
λ_{LT}	- Equivalent slenderness ratio.
σ	- Longitudinal stresses.
σ_{1a}	- Longitudinal bending stresses at point 1a.
σ_{1b}	- Longitudinal bending stresses at point 1b.
$\sigma_{cr,D}$	- Design bending stresses.
$\sigma_{M,N}$	- Bending stresses due to axial force and shear force.
σ_r	- Material yield stress.
σ_{tee}	- Secondary bending stresses.
τ_w	- Shear stress in the web weld joint.
τ_y	- Ultimate shear stress
ϕ	- Angle of cut of the castellated beam.
ϕ_i	- Stability coefficient.

CHAPTER 1

INTRODUCTION

1.1 Castellated beams

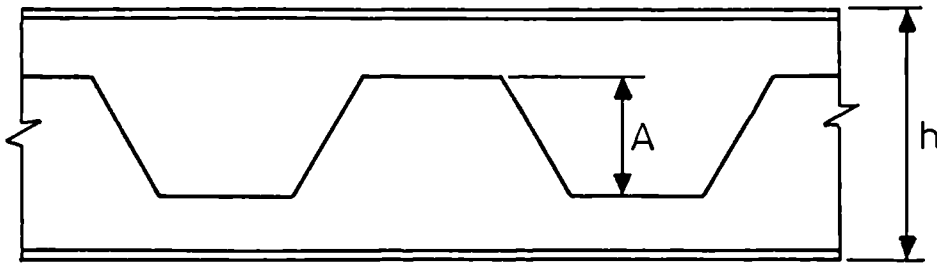
1.1.1 General Introduction

A rather simple aid in assessing the load carrying capacity of steel I-beams is to assume that the applied moment is resisted solely by the flanges with the shear being carried by the web. Examination of typical situations reveals that it is usual to find that the bending stresses are much closer to their allowable limit than are the shearing stresses.

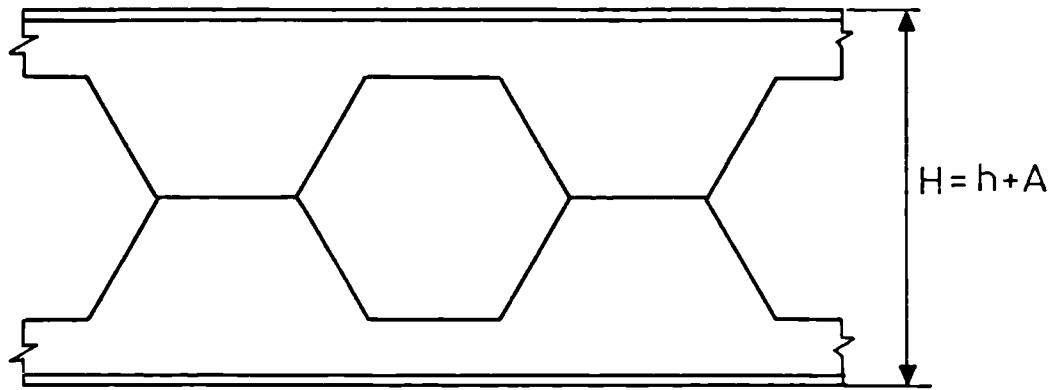
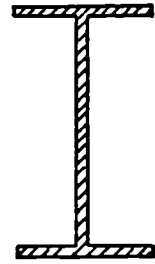
Castellated beams, which are sometimes called castella beams or open-web expanded beams, are one way of correcting this discrepancy. They also bring about added improvements on the performance of the original section from which they were made and help achieve savings in weight over equivalent plain webbed sections. They were first used in the U.S.A. by the Chicago Bridge and Iron Works as early as 1910 and in Great Britain their use appears to have been originated by G.M. Boyd in the 1930's. Nowadays castellated beams are used throughout the developed world.

1.1.2 Fabrication process

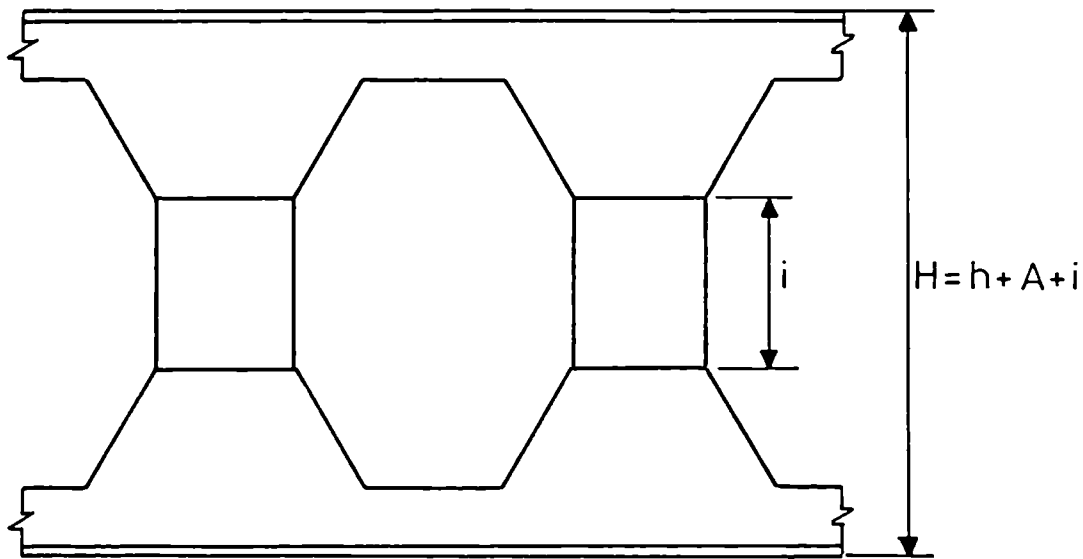
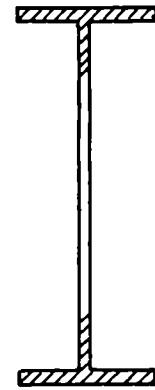
Castellated beams are made by expanding a standard rolled shape in a manner which creates a regular pattern of holes in the web. Fig.1.1 illustrates the production of a castellated beam. It is made by separating a standard section into two halves by cutting the web in a regular alternating pattern. The halves are then rejoined by welding after offsetting one portion so that the high points of the cut beams come into contact to form a castellated beam with hexagonal openings. Its depth can be further increased by welding rectangular plates, the



a) Burning Pattern.



b) Castellated beam formed.



c) Castellated beam with increment plates.

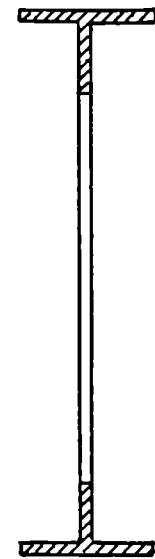


FIG.1-1. CASTELLATED BEAM.

increment plates, between the crests of both halves of the original beam.

This process of fabrication was originally performed entirely by hand until its automation was initiated by H. Litzka (1). Until then castellated beams met with only limited success owing to their high production costs although substantial savings could be made in multi-storey steel framed buildings as reported in ref.2 which also describes their shop fabrication. The manufacturing process, which is now entirely automatic both in cutting and welding, has helped to popularize the use of castellated beams. It is possible to use any geometrically available steel shape and to vary the amplitude and the geometry of the cut. This enables designers to choose the resulting height of the beams, the hole geometry and the spacing between the holes to best suit the design requirements.

The proportions of castellated beams have been standardised in Great Britain to facilitate their mass production and the various sections are available in the Handbook of Structural Steelwork(3). Fig.1.2 gives the geometry of the cut of commercially available British sections: the angle of cut is kept constant at 60 degrees and the height of the hole is equal to the serial height D_s of the unexpanded section thus making the resulting depth of the beam equal to 1.5 times that of the original beam and the pitch of castellation equal to $1.08 \times D_s$. In contrast to the British castellated module of cut, the module of cut used for continental beams which is sometimes called the Litzka module can be divided into six equal parts as seen in Fig.1.3. Finally Fig.1.4 gives the terminology used in referring to the parts of a castellated beam.

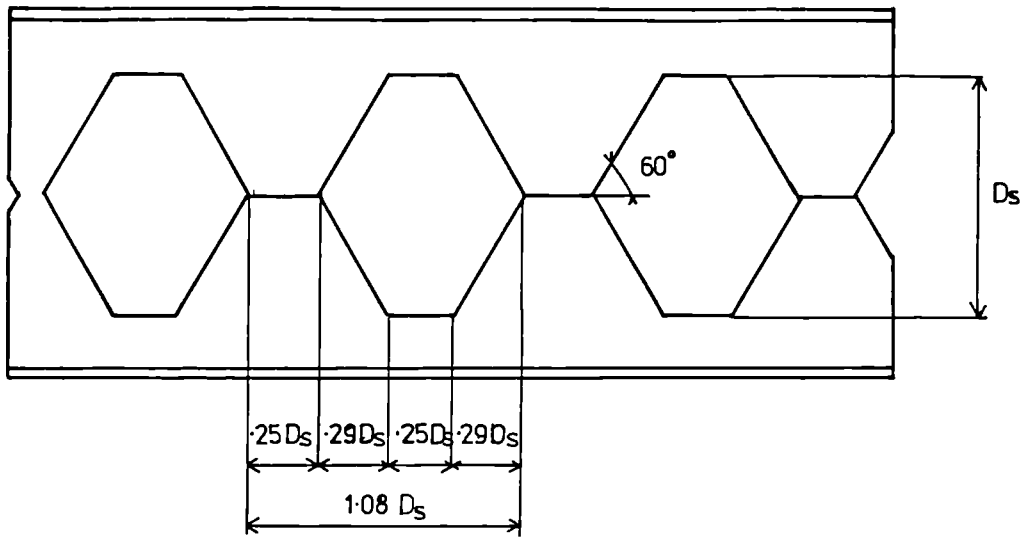


FIG. 1.2 BRITISH MODULE

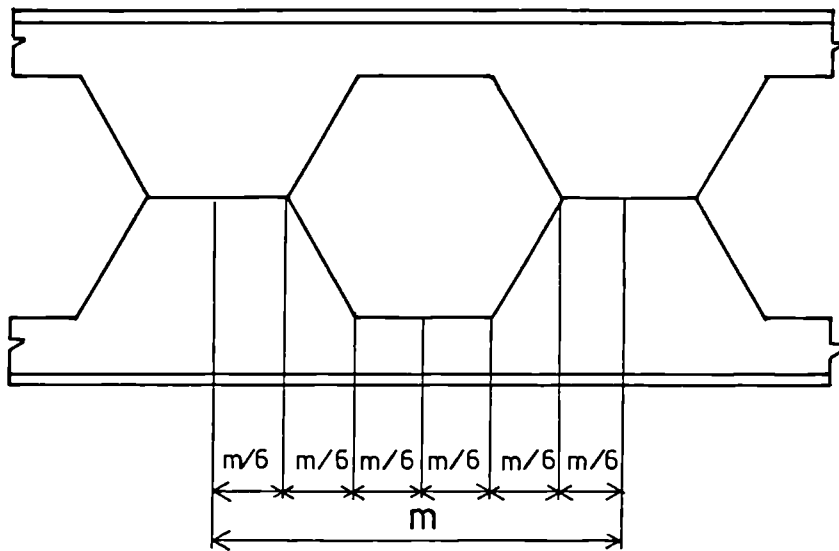


FIG. 1.3 LITZKA MODULE

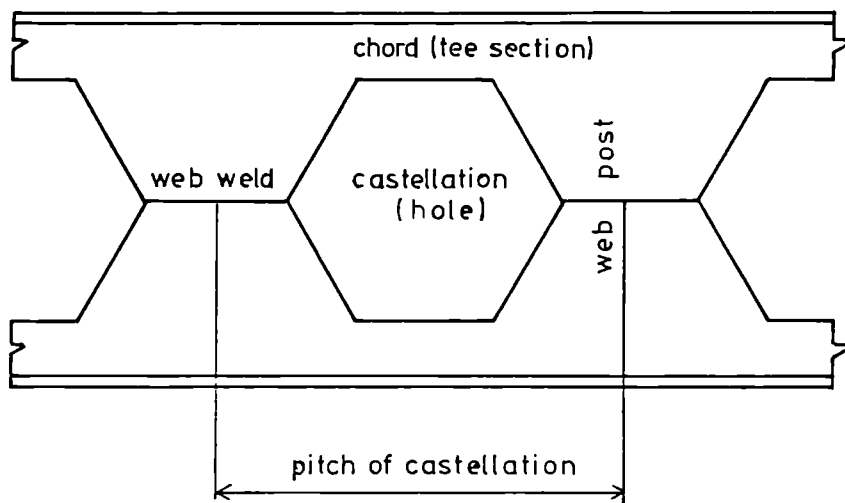


FIG. 1.4 TERMS USED

1.1.3 Applications and advantages of castellated beams

Numerous examples can be seen of the application of castellated beams used as secondary or main units in light to medium construction and medium to long spans. Soon after the automation of the fabrication process, which made castellated beams widely available, several reports describing their application were published in various countries.

The most frequent instance is the use of castellated beams in multi-storey blocks as trusses or purlins which can afford savings in weight of up to 50% as compared with solid web sections (4-6). This can be very important when structures have to be founded on poor soil conditions. They are also used in commercial and industrial buildings, warehouses and portal frames (1,7,8), in bridges as deck stiffeners and in the shipbuilding industry. Built up plate girders can sometimes be advantageously replaced by castellated beams (ref.1 shows castellated beams spanning length of up to 37m). Their use as stanchions is more restricted but they have been incorporated in many structures (1,7). Generally speaking they are not suitable for use in applications involving either heavy concentrated loads or dynamic or repeated loadings.

Web holes can help improve the aesthetic appearance of many buildings when castellated beams are exposed to view as in showrooms and entrance porches(7). They can also perform a very useful functional role when accommodating pipes, conduits and duct works, thus helping to decrease the thickness of floors. However, probably the most important advantages of castellated beams is the economy they can help achieve which can be very substantial(1,2,4), resulting from their high strength to weight ratios and their lower maintenance and painting costs.

1.2 Brief literature survey

1.2.1 Present state of the research

This widespread use of castellated beams as structural members prompted a number of theoretical and experimental investigations into their structural behaviour. Early studies concentrated on in-plane response both in the elastic and plastic ranges. Extensive measurements were made of the stress distribution over the cross-section and these were compared with the predictions of various theoretical studies ranging from the simple Vierendeel analogy to the sophisticated analyses based on finite differences techniques, various finite element schemes and a complex variable method. Deflections were calculated using a variety of approximate methods, based on elementary bending theory suitably modified so as to take into account the beam's reduced shear stiffness, or by using more rigorous methods based on flexibility, stiffness or finite element approaches. A number of different failure modes particular to castellated beams, i.e. Vierendeel collapse mechanism where plastic hinges form at the sections touching the four re-entrant corners of a castellation, buckling of a web post, web weld fracture etc., have been observed as a result of the various series of tests which have been carried out in several countries. Several collapse mechanisms have been proposed and the lateral buckling of the web posts has been analysed. The outcome of this research has been the development of procedures for both elastic and plastic designs as well as the preparation of optimum expansion ratios.

1.2.2 Lateral buckling considerations

This thorough survey of the literature showed that despite the considerable volume of research available, one important topic remained largely untouched - lateral stability, although one theoretical solution to the elastic buckling of castellated beams was proposed. Because researchers were concerned with in-plane behaviour, bracing was always provided in tests so as to prevent any adverse lateral deflection from affecting the results. Nevertheless a few instances exist in which lateral-torsional buckling was observed in tests where either inadequate bracing had been provided or the beams had already attained their maximum in-plane carrying capacity.

The usual explanation for the lack of interest in the lateral-torsional buckling of castellated beams was that bracing would be provided by floor slabs or that they would be carrying small loads. This is despite the fact that any flexural members are liable to fail by lateral buckling and that the collapse of castellated beams which are mostly used as flexural members is enhanced by their particular geometry. The increase in depth over the original section brought about by the fabrication process has significantly increased the moment of inertia of the beam about its major axis without affecting the moment of inertia about its minor axis. This increase in the major second moment of area results in greater strength and rigidity about the plane of loading but is obtained at the expense of the lateral stiffness which has in effect been decreased relative to its transverse stiffness leading to a greater likelihood of failure by lateral instability. Moreover the presence of holes in the web tends to reduce the section's overall torsional stiffness as well as introducing the possibility of lateral torsional buckling being accompanied by web distortion.

1.3 The present situation regarding the British codes of practice

1.3.1 Reasons for the present gaps in research

It might seem surprising that in spite of the extensive literature that exists, little that can be regarded as firm design recommendations - and not surprisingly, no provisions against lateral buckling - are presently available in national codes of practice, particularly in the British codes (9,10), the nearest being rules for the design of beams with large holes in the web in Canada (11) and the U.S.A.(12).

It is a direct consequence of the particular nature of castellated beams. Firstly their high degree of internal redundancy makes an accurate stress analysis prohibitive and secondly the number of parameters necessary to describe a particular beam is large. Among the more important of these are:

1. geometry of the cut (amplitude, angle and weld length).
2. resulting height of the section.
3. loading arrangement.
4. support and bracing system.

Halleux(13) counted that one hundred thousand different castellations could be obtained from the 120 sections available on the European market in 1966 if the first two parameters were considered separately from the others and this when the geometry of the cut was restricted to the Litzka module. This number can therefore be increased manifold if various geometries of cuts are considered or if intermediate plates are used. A further reason for this lack of interest in castellated beams was that researchers tended to consider a castellated beam as a structure in its own right, the members of which were the chords and the web posts. They concentrated more on the design of the separate members than that of the beam as a whole, as is the norm in the

study of plain-webbed beams.

1.3.2 Consequences

A closer look at the available literature showed that the experimental study of the behaviour of castellated beams seemed of a very patchy nature despite the many experimental programmes which had been carried out in all main industrial countries such as Belgium, Canada, France, Great Britain and the U.S.A.. It was difficult to thread them together except on the behavioural level, several geometries of cut and different loading conditions having been used in the 122 tests recorded. It was found that although all the possible failure modes had been catalogued and described, the prediction of failure loads could not be done as accurately and confidently as for plain-webbed beams. This is why the draft of the new British code for structural steelwork B/20 (14), which will be published in its final form as BS 5950 largely unaltered, suggests the use of the simple and widely adopted Vierendeel analogy for in-plane behaviour (this takes into account the secondary moments produced by shear) and does not give any procedures for the design against any of the possible modes of failure except for lateral-torsional buckling. However in this case, largely due to the lack of information, it has adopted the conservative approach of clause 11.3.2.c to the prevention of lateral buckling in which the contributions of the web and tension flange are ignored.

1.4 Aim of the project

The work undertaken herein will therefore have the aim of mainly providing the missing quantitative data on the lateral-torsional buckling strength of castellated sections of the type currently available in the U.K.. Eight full scale beams were tested in order to observe their overall behaviour and more particularly their propensity to failing by lateral buckling under a four-point loading system. The results of these tests plus the few cases which were reported in the literature were then used as a basis for a critical evaluation of several design approaches and hence led to the proposal of an improved procedure for the prevention of failure by lateral-torsional buckling. It is ironic that whereas in past experimental programmes great care was taken in order to avoid the early termination of tests because of lateral-torsional buckling, the present programme had to ensure that failure due to any of the failure modes reported in the literature could not happen before lateral-torsional buckling caused the collapse of the beams. This therefore provided the opportunity for an appraisal of the current methods for designing the members of the castellated beams expanded by using the British module of cut.

A preliminary test programme on ten model beams with sectional properties similar to one of the full scale beams was carried out in order to provide a qualitative estimate on the influence of the holes on the lateral-buckling behaviour of castellated beams. Finally, a computer program based on the stiffness approach and modelling the beams as a Vierendeel frame whose members had the properties of the chords (tee sections) and the web posts of castellated beams was used to calculate a value of elastic critical load and find the shape of the frame in its laterally buckled state.

1.5 Presentation of the thesis

The organisation of the thesis flowed from the present state-of-the-art in the design of castellated beams which is reviewed in chapter 2. Chapter 3 presents the results of the testing of the small scale models whilst chapter 4 reports the design of the various members of the castellated beams and the process leading to the choice of a design method for lateral buckling. The rig used in the testing of the eight full scale beams is then described in chapter 5. The results of the test programme are given in chapter 6 whilst chapter 7 compares the various design procedures available and chapter 8 describes the computer program used in the calculation of an elastic critical load. Finally, the conclusions drawn from the present work and suggestions for future research are given in chapter 9.

CHAPTER 2

LITERATURE REVIEW

2.1 Introduction

A considerable amount of work, both experimental and theoretical, has been published on the general subject of castellated beams and its associated problem, beams with holes in the web. It was therefore important before embarking on any further research in the subject to review this past work and find its relevance to the present investigation on lateral-torsional buckling. However, appraisals of past research will not be the aim of this survey. A thorough understanding of the behaviour of castellated beams under loading is sought and in particular the influence of the holes on their lateral-torsional buckling behaviour.

Because this study was concerned with castellated sections of the type used in the U.K., the British test programmes will be described first, then, in chronological order, programmes reported in the U.S.A., Belgium, France and Canada. The subsequent analytical work will finally be briefly commented upon.

2.2 British tests

2.2.1 The Rotherham tests

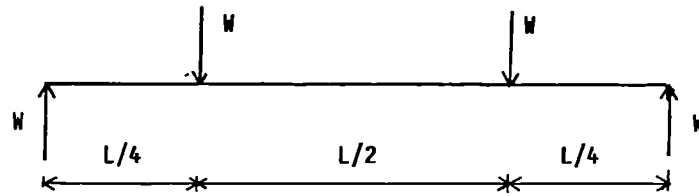
A series of tests were carried out between 1951 and 1961 at the Swinden laboratories of B.S.C. at Rotherham (15-18). These were basically for internal use by the steel company which fabricated castellated beams. The main purpose of the tests was to check the safety factors provided by the safe table loads published. The absence of a single load-deflection curve made the interpretation of the test results very difficult and in addition the failure loads recorded were quoted as the highest that the beams would sustain. Considerable deformation was

usually associated with these loads.

Twenty eight beams were tested in the same test rig which produced a four-point loading system and provided mid-span and end bracing. Although all the beams were made-up of R.S.J. sections which have since been removed from the catalogues, some useful information can be obtained on the type of failure likely to occur in castellated beams of similar hole geometry as the present ones. The dimensions given for the beams of refs. 15-30 are the depth of the section, the breadth of the flange and the thicknesses of the flange and web.

2.2.1.1 1951 tests (15)

Six 266.7x101.6x9.8x6.3 castella beams geometrically similar and of identical length were tested under the same conditions of loading and support. The principal objective of the test series was to check the need for reinforcing the beams by filling in the end castellations to prevent web buckling at the end support, and thus three of the beams had filled in end castellations whilst the other three were unreinforced. Two of the beams with open-end castellations failed by web buckling over one of the supports while the third failed because of rupture of the weld at the web post next to one end. This is the only reported case of web weld failure apart from those obtained by Hosain and Speirs (26) who specifically designed their beams to fail by shearing of the weld. The consequence of reinforcing the end castellations was to change the mode of failure of the beams with only a slight increase in load carrying capacity. Buckling of the web at one of the loading points was reported in two beams while the third failed by lateral buckling of the top flange between one end support and the nearest loading point. Table 2.1 gives a detailed account of the experimental results.



Section 266.7x101.6x9.8x6.3 (L=2896 mm)

Beam No.	End Castellation	W (kN)	Mode of failure
1	Open	108	Web buckling at one end
3	Open	123	
5	Open	104	
2	Filled	117	Lateral instability of top flange at one end
4	Filled	120	Web buckling under one load
6	Filled	123	

Table 2.1 Summary of Test Data from Ref. 15

2.2.1.2 1958 Tests (16)

These were a follow-up to the previous tests and in addition to checking the safe end reactions of unreinforced castellated beams (no filling-in end plates) they were used to try to establish a relationship between the mid-span deflections of castellated beams and those of a hypothetical rolled steel joist which had the properties of the sections taken through the holes of the castellated beams.

Five beams, each made from a different section, were tested first under quarter-span loading in order to obtain elastic load-deflection curves and then under an asymmetrical loading system so that failure would occur at the most heavily loaded end by web buckling.

The deflection data showed that the use of simple engineering bending formulae under-estimated the actual deflections by ratios varying between 1.14 for the most slender section to 1.35 for the stiffest section. The most interesting fact to emerge from this part of the investigation was that the first beam to be tested failed prematurely by lateral buckling, the mid-span bracing proving to be unable to restrain the beam in position. The test rig was subsequently reinforced for the following tests.

Three of the beams under the asymmetrical loading system reached their ultimate load when a web post buckled, whereas the fourth beam failed because of lateral buckling of the top flange between one loading point and the end support. Table 2.2 summarizes the results of the second part of this programme.

Beam Section	Length (mm)	Load at failure W (kN)	Mode of failure
342.9x101.6x11.6x7.6	4140	223	Lateral buckling of top flange
342.9x177.8x21.0x10.2	4216	473	Steady yielding in bending with end web posts beginning to buckle
381x127x14.0x9.1	4140	422	Buckling of end four web posts
381x203.2x19.9x10.2	4216	523	Buckling of end three web posts
381x114.3x12.8x7.6	4140	about 99.7	Lateral buckling of top flange during deflection test

Diagram 1: A beam of length L is shown with a point load W applied at the center. The distance from the left end to the load is $L/2$, and the distance from the load to the right end is $L/2$. The diagram is labeled with $2W/5$ and $3W/5$ at the ends, and $.3125L$ and $.479L$ below the beam.

Diagram 2: A beam of length L is shown with a point load W applied at the center. The distance from the left end to the load is $L/4$, and the distance from the load to the right end is $L/4$. The diagram is labeled with W at the ends, and $L/4$ and $L/2$ below the beam.

Table 2.2 Summary of Test Data from Ref. 16

2.2.1.3 1960 and 1961 tests (17,18)

The deflection characteristics of four castellated beams of different sizes were studied in the 1960 investigation (17). Each beam was tested at three different spans and no beam was taken up to failure. In 1961 (18) a castellated beam, 6477mm long, made from a large section, a 685.8x153.72x18.06x10.13 expanded from a 406.4x153.72x18.06x10.13 joist with an intermediate plate inserted, was tested to failure by web buckling.

2.2.2 Other British tests

Gibson and Jenkins (19) investigated the deflection behaviour and the stress distribution along the flanges and around the holes of castellated beams, simply supported and centrally loaded. They found that the local bending of the flanges altered very significantly the stress distribution as obtained from simple bending theory.

Kolosowski's investigation (20) was similar to the previous one but only one girder, with openings having a different shape from the standard U.K. shape, was tested. He was the first to point out that in castellated beams plane sections do not remain plane after bending because of the non-linearity of the stress distribution across a section.

2.3 American tests

In these tests, the structural behaviour of castellated beams was monitored in the elastic and plastic range and the yielding processes leading to various types of failure were described. The first ever elastic design method for the calculation of stresses was proposed by Altfillisch et al. (21) who performed seven tests on three beams of

different height. All the specimens were extensively braced to prevent premature failure by lateral-torsional buckling. However, the bracing system had to be reinforced twice during the series.

Toprac and Cooke (22) tested nine beams to failure under a six-point loading system which created three distinct zones of loading depending on the values of the shear force in the span. As a consequence a comprehensive set of failure modes were recorded with four beams failing because of lateral buckling of the span under pure moment loading. The detailed description of the tests and especially of the progress of yield within the beams gives an invaluable insight into the behaviour of castellated beams and more especially the connection between loading, geometry of the holes and failure modes can be better understood.

2.4 Belgian tests

Halleux (13,23) realised that the elastic methods available for designing castellated beams gave high but also very variable safety factors (the safety factors for elastic design for the twelve beams he tested varied between 1.53 and 5.53 with nine results higher than 2.70). He therefore proposed to apply plastic methods to the design of castellated beams. He started first by studying the elastic behaviour (13) and then identified two collapse mechanisms, one due to pure bending, the flexure mechanism, and the other, the Vierendeel mechanism, due to the combination of bending and shear. Although the effects of shear and axial forces on the plastic moment of the sections were neglected, a new area was opened in the calculation of the resistance of castellated beams (the safety factors varied now between 1.47 and 2.25). Two series of beams were tested. The pitch of castellation was kept

constant in each series while the amplitude of the cut was varied similarly. It is worth noting that Halleux, before embarking on his programme, checked the efficiency of his bracing system by testing an unbraced beam which failed by lateral-torsional buckling. It is unfortunate that although a photograph of the beams after failure was shown no value of failure load was given.

2.5 French tests

These tests were mainly conducted because castellated beams had never been investigated experimentally in France (24). This series had the limited aim of checking an elastic method of design proposed by the authors. This method was basically similar to those already in use elsewhere. The first set of four beams which were expanded from a wide flanged section had a constant pitch of castellation but variable depths of section whereas the second set of three beams had a constant depth of section but variable pitches. Eight load points were used to approximate a uniformly distributed load. The beams of the first series and the beam with the shortest pitch of castellation in the second series failed by buckling of the web. The last two beams with the longest unsupported lengths (which corresponded to two holes) failed because of lateral buckling of the compression flange.

2.6 Canadian tests

Three series of tests were conducted in this investigation (25-27) which was a follow-up to Halleux's plastic design proposals. They confirmed the existence of the two collapse mechanisms (25) and considered the possible occurrence of a third caused by the rupture of the welded joints in the webs (26). The authors finally presented

optimum expansion ratios (27) based on the strength of fully braced castellated beams as derived from elastic and plastic methods of analysis. The five beams tested for optimum expansion all developed signs of lateral deflection of the compression flange after extensive local deformation of the webs and flanges had taken place.

2.7 Miscellaneous

Four other test programmes have been reported in the literature. Clarke (28) was studying shear stress distribution and web stability in castellated beams. Three out of the five beams he tested reached their ultimate load because of lateral buckling but they showed considerable local distortion of the webs and flanges.

Douty and Baldwin (29) tested three beams which were representative of the beams used in a floor system for a building. The beams were more than 11m long and had depths varying between 600mm and 700mm. Several castellations were enlarged by removing the web post between two consecutive holes. The behaviour of these three beams was similar to those tested by previous investigations.

Sherbourne (30) was investigating the post-buckling behaviour of castellated beams with a view to defining the maximum length of the laterally unbraced spans which would still enable the beams to reach their maximum in-plane moment of resistance and develop their maximum rotation capacity.

Mandel et al. (31) compared experimental stresses obtained from the testing of nine beams to stresses calculated from the theory of elasticity.

Finally, a new type of castellated beams (32) has been developed in Rumania. The process of fabrication is entirely automatic and consists

of cutting a combination of semi-circles and straight lines on the web of the beam to be expanded. The two half-beams are then welded together. Circular holes eliminate corners where stress concentration develops. These beams can therefore be used in situations where fatigue is an important factor in the design, such as bridge decks and crane gantry girders. The tests carried out showed that longitudinal stresses in the tee sections of beams with circular holes were about 15% lower than those in castellated beams when bending and shear were present.

2.8 Theoretical investigations

2.8.1 Deflection predictions

2.8.1.1 Empirical methods

The vertical deflection of a castellated beam is the sum of the deformation due to the beam bending as a unit and of the deformation due to the holes in the web. The effects of axial and shear forces cannot be ignored. Several methods have been proposed. The simplest which were used in refs. 15-18 and by Toprac and Cooke (22) consisted of applying the simple engineering formula to an equivalent plain-webbed beam and then scaling up the numbers obtained to match experimental and predicted deflections. Halleux (34) demonstrated that these methods were not reliable and depended too much on the particular properties of each beam.

Several authors have tried to improve the predicted deflections by including the additional deformations brought about by the distortion of the panels around each hole (21,24). Others like Gibson and Jenkins (19) produced a method, later improved by Gardner (33), in which the discontinuous web was replaced by a continuous medium, while the moment distribution method was used by Kolosowski (20). Halleux (34) developed

a method, based on Mohr's theorem, which made extensive use of graphs. The accuracy of these methods is questionable despite the amount of computation required.

2.8.1.2 Matrix methods

The advent of computers and the widespread availability of elastic frame analysis have eased the problem of calculating the deflections of castellated beams. If a castellated beam is modelled as a Vierendeel frame the deflections are obtained automatically (25,42). Van Oostrom and Sherbourne (44) developed a program, based on the flexibility approach, which could predict the load-deflection behaviour in the elastic and plastic ranges. Finally several authors used the finite element method (37,39-41,43) to compare predicted deflections to experimentally measured ones.

2.8.2 Stress distribution

Approximate elastic analyses using the Vierendeel analogy were used in all the experimental investigations to calculate the longitudinal stresses in the test beams. However these methods cannot predict the real stress distributions across a web post. Numerical methods based on finite difference (31,35) and finite element (37,41,43) techniques were therefore used to calculate the stress in the web post. These numerical methods could also predict quite accurately the shear stresses at various sections which simpler methods could not do. Finally Gotoh (38) obtained similar results by using a complex variable method.

2.8.3 Web buckling

The possibility of preventing lateral buckling of the web between two holes, which caused the failure of several test beams, was investigated theoretically by several authors. Delesques (45) used a strain energy approach to show that elastic lateral buckling of the web was unlikely to occur. Aglan and Redwood (46) produced design aids in the form of graphs as a means of checking the possibility of web post buckling. Dougherty (47) studied the buckling of the web post in the beams with two closely spaced holes.

2.9 Design procedures

Nearly all researchers who reported the results of experimental programmes suggested approximate procedures for the design of castellated beams. However these procedures did not always cover every aspect of the behaviour of castellated beams and could not be available to designers of other countries. This led several authors to produce sets of design recommendations based on the results of the research carried out locally and elsewhere, which could be applied in their own country. The early papers by Bazile (48), Faltus (49) and Boyer (50) responded to the need for simple criteria and treated castellated beams as plain-webbed beams. Later papers (51-54) analysed castellated beams as structures composed of vertical and horizontal members and gave procedures for the calculation of stresses and for checking the stability of each member.

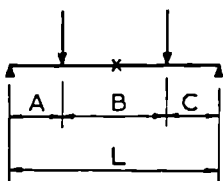
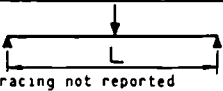


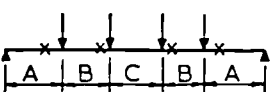
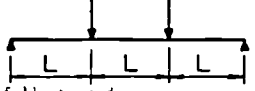
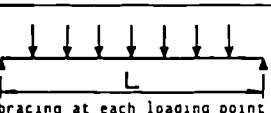


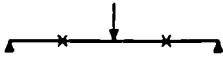
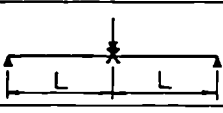
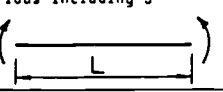
Some of these proposals (48,50,53,54) were orientated towards the use of national codes of practice. It is interesting to note that design against lateral buckling was mentioned only by Boyer (50) and McCormick (54). They suggested using the existing codes of practice

recommendations for plain-webbed beams.

2.10 Lateral buckling of castellated beams

2.10.1 General considerations

The review of the literature has revealed that nearly all aspects of the behaviour of castellated beams had been studied either experimentally or theoretically. Table 2.3 gives a summary of the experimental test programmes surveyed. However one topic has remained largely untouched, lateral-torsional buckling. Because researchers were concerned with in-plane behaviour bracing was always provided in tests so as to prevent any adverse lateral deflection. Nevertheless a few instances exist in which lateral-torsional buckling was observed in tests where either inadequate bracing was provided (16) or the beams had already attained their maximum in-plane moment capacity (15,16,20,24,27,28). A detailed account of these tests can be found in Table 2.4. This apparent lack of interest in the lateral-torsional buckling of castellated beams was usually explained by the fact that they were likely to carry light or uniformly distributed loads or that they would be part of a floor system which would provide lateral restraint. Nevertheless a solution to the problem of elastic lateral-torsional buckling has been proposed by Pattanayak and Chesson (55). It was felt necessary to assess their solution and in particular to compare the values of critical loads found by using their method with those of the equivalent plain-webbed beam.

Ref.	Loading System	Nb. of Sections used	Nb. of tests (tests to failure)	Main Purpose	Variables	Comments	Occurrence of lateral-torsional buckling (LTB)
15	 <p>x: point of lateral support</p>	1	6(6)	web strength stresses	stiffening of end panels	U.K. standard section	1 LTB
16		5	9(5)	deflection web strength stresses	A, B, C	U.K. standard sections	2 LTB
17		4	12(0)	deflection	L	U.K. standard sections	-
18		1	1(1)	web strength	large section intermediate plate	U.K. standard section	-
19	 <p>bracing not reported</p>	1	7(?)	in-plane-elastic stresses deflection	L	U.K. standard section	-
20	 <p>bracing not reported</p>	1	1(1)	in-plane-elastic stresses deflection	-	U.K. hole not cut to standard U.K. size	1 LTB
21		1	7(3)	in-plane-elastic -plastic deflection	B d, n, μ	U.S.A.	-
22		1	9(9)	in-plane-elastic -plastic deflection	A, B, C d, n, μ	U.S.A.	4 LTB
13, 23	 <p>fully braced</p>	1	12(12)	in-plane-elastic -plastic stresses deflection	d, n, μ intermediate plates	Belgium	-
24	 <p>bracing at each loading point</p>	2	7(7)	in-plane-elastic -plastic stresses deflection	L d, n, μ intermediate plates	France	2 LTB
25		1	12(12)	in-plane-plastic web strength	A, B n, μ , ϕ	Canada	-
26		1	6 6	web weld strength	A, B n, μ , ϕ	Canada	-
27		2	5(5)	optimum expansion ratio	d, ϕ	Canada	5 LTB with local buckling
28		2	7(5)	web strength stresses	L d, n, μ , ϕ	Canada	3 LTB with local buckling
29	Loading system not described	1	5(3)	deflection stresses enlarged web holes	L d	U.S.A.	-
30	various including 3 	1	7(7)	in-plane-plastic	L	Canada	-
31	Loading system not described	-	9(?)	stresses	-	U.S.A.	-

d: depth of expanded section μ : pitch of castellation n: length of weld ϕ : angle of cut

Table 2.3 Summary of Tests Reported in the Literature

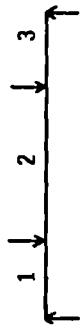
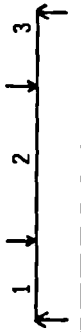
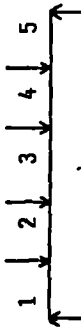
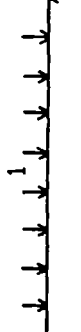

Refs.	Loading system	Buckled span	Length of buckled span (mm)	Section	Comments
15		1	724	266.7x101.6x9.8x6.3	-
16		2	2070	381x114x12.8x7.6	Premature failure due to inadequate bracing
16		1	1294	342.9x101.6x11.6x7.6	-
20		1	1133	457.2x127x12.9x8.38	Failure of span 1 due to lack of top bracing
		3	1010	266.7x101.6x5.1x4.57	All the beams were expanded to various height from the same section
22		3	832	297.9x100.3x5.13x4.8	
		3	695	297.2x99x5.08x4.7	
		3	820	295.9x100.3x5.15x4.4	
24		1	1008	500x135x10.2x6.6	Pitch of castellation was varied and intermediate plates inserted
		1	1260	500x135x10.2x6.6	
30		-	329		Tested for length of unbraced span but no failure by LTB
		-	494	228.6x76.2x9.6x5.8	
		-	658		

Table 2.4 Details of Tests where Beams Failed by Lateral-torsional Buckling

2.10.2 Description of the method

Pattanayak and Chesson used the principle of minimum potential energy for calculating the elastic critical load. The beam was considered to be made up of two independent parts, the tee sections and the web posts. Geometrical and material imperfections were neglected.

The total potential energy of the beam, which is the sum of the strain energy U stored in the beam and the potential energy of the external forces U_w , is zero when the beam is in its naturally deflected configuration. The strain energy stored in the beam is that due to the bending and twisting of the top and bottom tee sections and the bending and twisting of all the web posts. The possible distortion of the web posts is therefore taken into account. The procedure allows for the various types of loading and different levels of application of the load.

2.10.3 Comparison with methods for plain-webbed beams

A design procedure for the calculation of elastic critical load of laterally unsupported plain-webbed beams loaded with transverse loads exists (56). It was used to calculate values of critical loads of one of the test beams to be used in the present programme. Because of the presence of the holes the properties of the beam were calculated at two different sections. A section taken through a castellation gave the minimum values for the geometrical properties of the beam whereas a section through a web post gave the maximum values. A uniformly distributed load was acting on the beam at three levels; the top flange, the shear centre and the bottom flange. Fig.2.1 shows the values of critical loads obtained for both cross-sectional properties compared to the values obtained by using the minimum potential energy approach (55).

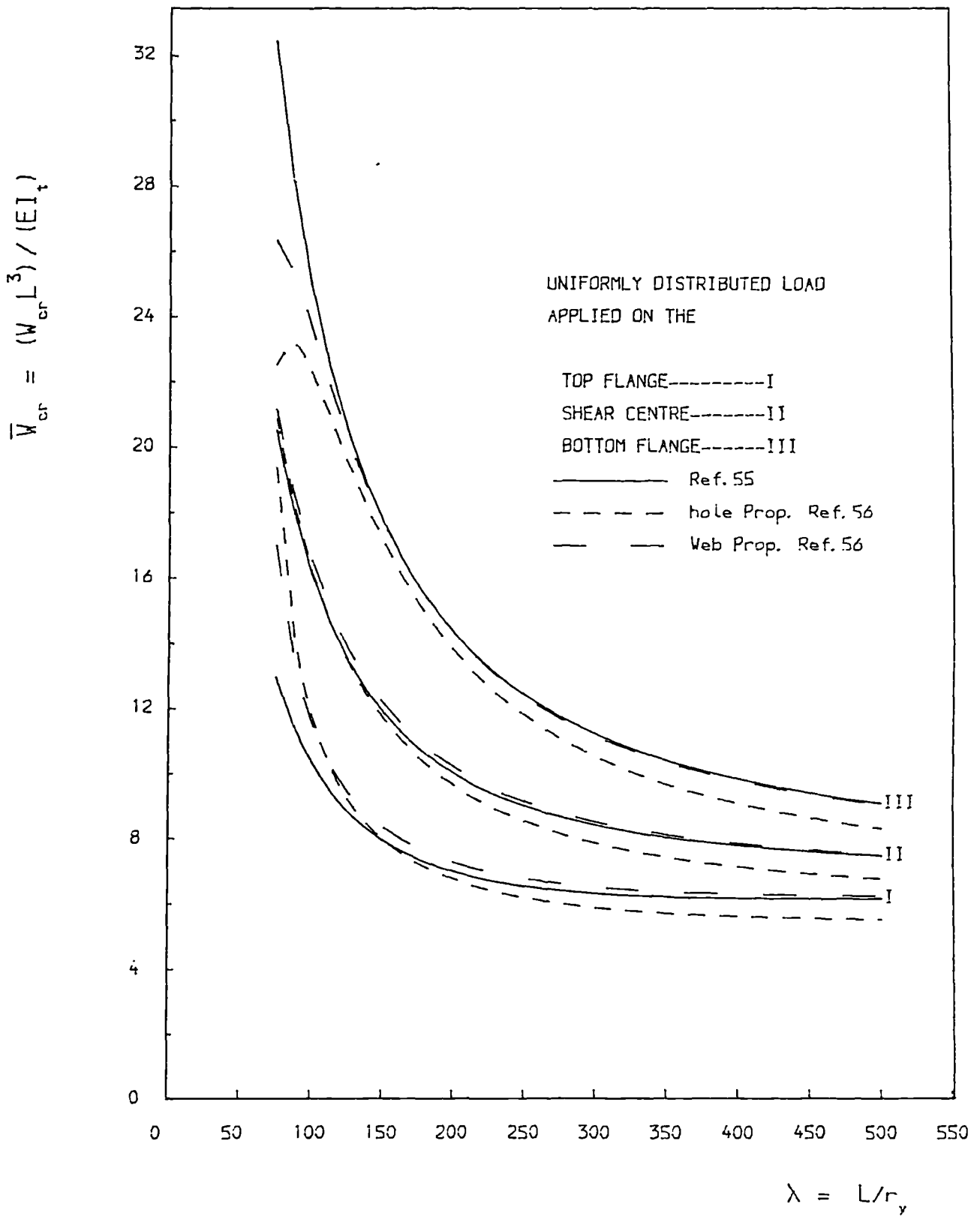


FIG. 2.1 ELASTIC CRITICAL LOADS FOR THE SECTION 609x140x46

It becomes apparent from the graphs that the additional computational effort involved in the use of the method proposed by Pattanayak and Chesson is not warranted. Therefore the elastic critical loads of castellated beams will be calculated in a way similar to that used for plain-webbed beams.

2.11 Conclusions

The survey of the literature has revealed that a considerable amount of research has been carried out on the subject of castellated beams. However because of the many parameters necessary to describe a given castellated beam, in particular the shape of web holes which makes several modes of failure unknown to plain-webbed beams possible, it is difficult to thread together all the experimental results except on the behavioural level. In addition the computational effort required to design a castellated beam and the various parts forming it such as tee-sections and web posts is greater than that for the equivalent plain-webbed beam. Furthermore one area of the behaviour of castellated beams has not been investigated, lateral-torsional buckling, despite being the cause of the failure of several test beams.

The lack of design recommendations in the national codes of practice (9,10,11,57,58) and in particular BS 449 (9) is therefore not surprising although rules for the design of beams with large holes are available (11,12).

CHAPTER 3

SMALL SCALE TESTS

3.1 Introduction

The scarcity of the information available on the subject of lateral-torsional buckling of castellated beams made it important that a better understanding of their behaviour be obtained before embarking on the main experimental programme. Although the review of the literature revealed several cases of failure because of lateral buckling, these usually occurred when the beams had reached their maximum in-plane moment carrying capacity and no obvious difference in the buckling behaviour between them and plain beams was reported. It was felt that the more slender beams which were to be tested might show a somewhat different behaviour in the elastic or inelastic ranges. In particular the presence of the holes in the web of castellated beams might affect in some unforeseen way the behaviour of the more slender beams.

It was therefore decided to construct a series of small scale castellated girders and test them as cantilevers. The test rig needed to carry out the testing programme could then be very simple and thus easily and cheaply made. However, because the models were to be fabricated by the author in a workshop the quality of workmanship could not be maintained consistently and complete straightness of the beams obtained. This limited the scope of the testing programme which could only really be expected to provide qualitative information on the influence of the holes on the buckled shape. In consequence only ten girders were made.

3.2 Previous work on model testing

3.2.1 Stresses and deflections

Model beams have been used previously for various purposes. The type of experiments chosen for model beams usually reflected the gaps in knowledge at the time of carrying out the experiments. For example Gibson and Jenkins (19) and later Halleux (13) investigated photoelastically the stress distribution in model beams before they embarked on their main experimental programmes which were concerned partly with the distribution of stresses over the cross-section of full-size beams. A very accurate picture of the flow of stresses was obtained. Worley (59) carried out ultimate strength tests on aluminium beams containing several openings. However the holes were in most cases closely spaced and extended over the full web depth between the fillets at the web-flange intersections. The hole dimensions were therefore not typical of castellated beams and the results were not used in the present investigation. Finally Srimani and Das (42) tested ten model beams made of perspex. The authors were checking theoretical results obtained from a computer programme based on the displacement method.

3.2.2 Effect of openings on the lateral bucklings of beams

A series of tests on slender model cantilever beams containing a set of rectangular or circular openings along the centre line of the beams, in which the size and spacing of the opening were varied were carried out by Coull and Alvarez (60). The beams were cut from plexiglass sheet and had a rectangular section. The range of slenderness ratios chosen indicated that the beams would fail in an elastic lateral buckling mode. The tests seemed to indicate that for a given number of holes in a beam, the elastic critical load was more influenced by an

increase in the depth of the holes rather than by an increase in their length. However the castellated beams in our present series were of I section for which the presence of holes in the web does not affect the values of the second moment of area about the minor axis of the section in as dramatic a fashion as for rectangular sections and therefore their study had a largely academic interest.

3.3 Test rig

3.3.1 Description

The girders were tested as cantilevers and a clamping system to hold the girder in position at one end was built. It consisted of two blocks, two thick plates made of steel and five set-screws. The clamping device was fixed on the edge of a heavy steel table which would provide the necessary reaction to the applied load and the overall stability of the system.

One plate was used as the base for the bottom flange at the support point. The second plate was then placed on the top flange of the girder and the two blocks were positioned against the web of the girder, one on each side. The height of the block was the same as the depth of the web so the inside of the top and bottom flanges and each side of the web were in contact with the blocks. Four set-screws held the two blocks and the two plates together as well as securing the assembly to the table. One set-screw was then threaded across the two blocks to fix them together. The end of the girder once fixed could not slide out of the clamping device nor could it move longitudinally nor rotate.

3.3.2 Loading system

The level of application of the load at the free end of a cantilever has been shown to have a considerable influence on the critical load (61) and in particular loads applied at the level of the top flange. It was therefore necessary to use the same loading conditions throughout the tests. The load was applied to the shear centre of the section at the free end of the girder by means of weights hung on a load pillar. This pillar was suspended on a loop of wire which passed over a large disc clamped to the end of the girder. By means of this system, the line of action of the loading which passed through the centre of the disc remained vertical throughout the test and in particular during the lateral buckling of the beam. Plate 3.1 gives a good indication of the overall set-up. Throughout each test the lateral deflections were recorded by a dial gauge placed at the loaded end of the cantilevers.

3.4 Specimens

3.4.1 Choice of dimensions

The girders were geometrically modelled on one of the castellated sections used in the main programme, the castellated section 609x140x46. This section was chosen because it was deeper and had wider flanges than the other sections, thus making the fabrication of the models slightly easier.

A scaling factor of 1/10 was chosen and the resulting dimensions were adjusted to meet the availability of the commercially available material. Therefore the thickness of the flanges became 1.2mm instead of the nominal value of 1.12mm and the thickness of the web 0.8mm instead of 0.69mm. However it was possible to keep the dimensions of the

hexagonal holes and their spacing very close to the scaled nominal dimensions of the holes of the full scale beam. Fig.3.1 shows the nominal dimensions of a small scale girder.

3.4.2 Fabrication process

Because it was not possible to make the girders in the same conditions as a castellated beam in a factory, i.e. expand it from a plain webbed beam by cutting the web and welding back together the two halves, the process similar to that used in fabricating welded plate girders was used. Two sheets of mild steel, one of 1.2mm thickness and the other of 0.8mm were purchased (however, measurements showed the average thickness of each sheet to be higher, 1.25mm and 0.83mm respectively).

Strips from each sheet were cut on a guillotine to the required width in order to make the components of the girders, i.e. flanges and web. Then the position of the holes on the strip which made the web were marked and a punch of hexagonal shape which was machined to the required dimensions (see fig.3.1) was used to cut the holes. This strip was firmly clamped on a jig made of wood and the two flange strips were held tightly on each side of the web while the soldering of one side of the girder was carried out. After completion the girder was turned over to finish soldering the other side. Soldering was chosen in preference to welding because firstly the lower heat generated could not distort the steel between the holes and the flanges and secondly the process was simpler and therefore the help of a qualified technician was not required. This method of fabrication was very slow and it was not possible to eliminate the initial distortions resulting from the cutting process. The cutting of the strips on the guillotine released stresses

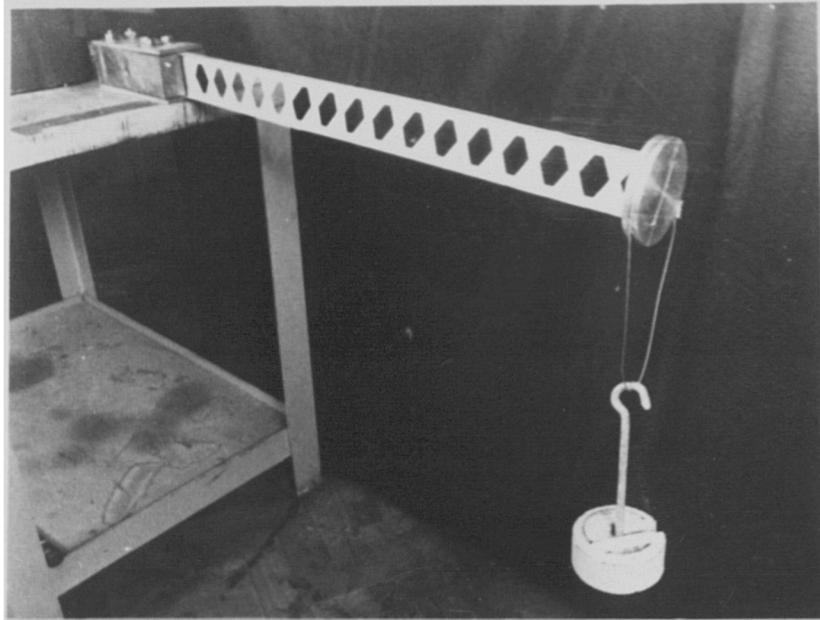


PLATE 3.1 TEST SET-UP FOR SMALL SCALE TESTS

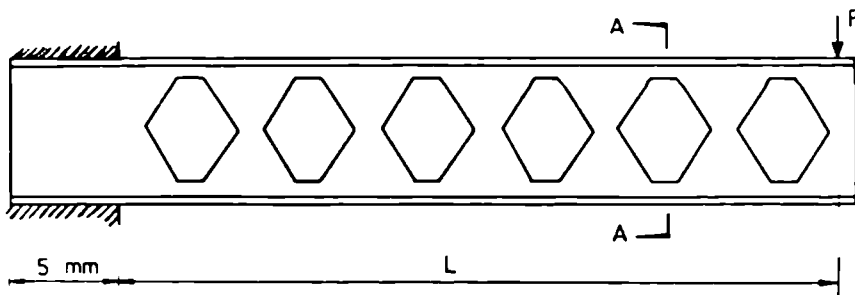


FIG. 3.1.a. MODEL BEAM.

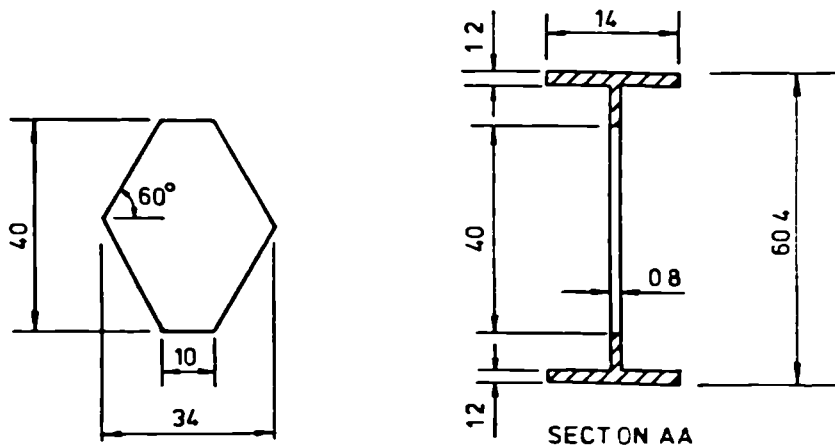


FIG. 3.1.b. DIMENSIONS OF HOLE AND CROSS-SECTION (mm)

in the material and the narrow flange strip tended to exhibit a marked bow which could not be completely eliminated by the soldering together of the three strips. The other consequence of the use of the guillotine was that the widths of the strips tended to be larger than the chosen sizes (59mm for the height of the web instead of 58mm and 14.5mm for the breadth of the flange instead of 14mm).

3.4.3 Material properties

Three coupons were cut from each sheet and tensile tests were performed in order to find the properties of the material. They revealed that the steel from which the web was made from had an average yield stress of only 212 N/mm² while the steel used for the flanges had an average yield stress of 264 N/mm².

3.5 Testing programme

Ten girders were made and their lengths were dictated by the number of holes in the web. The number of holes was varied between eight and eighteen with an increment of two between two consecutive girders (longer girders would have been impractical to construct). A first batch of six girders was made, each having between eight and eighteen holes, CM8, CM10, CM12, CM14, CM16 and CM18. Two further girders with fourteen and sixteen holes were made to check the repeatability of the test results and the quality of the fabrication process. Finally, two girders CMP14 and CMP16 of the same length as the CM14 and CM16 girders were made without the holes in the web in order to compare their behaviour to that of the castellated girders and check the influence of the holes on the lateral-torsional buckling behaviour.

All the girders were tested in the test rig described above. The

testing procedure was very simple and consisted of hanging weights at the free end of the cantilever, waiting for the girder to stabilize, taking the reading from the dial gauge and adding the next increment of load until complete failure occurred.

3.6 Theoretical predictions

3.6.1 Calculations of failure loads

Estimates of values of critical loads were calculated using a method proposed by Nethercot(61). The method enabled values of effective lengths and consequently elastic critical loads to be computed for three levels of loading, shear centre, bottom and top flanges for each girder. The various values of effective lengths and critical loads are given in Table 3.1 which clearly shows the influence of the level of application of the load. In the case of specimen CM8, the elastic critical load for bottom flange loading is nearly eight times that for top flange loading. However, this ratio decreases as the length of the specimens increases (the ratio is only three for specimen CM18). These values could only be used as an indication for the loads at failure because of the imperfections resulting from the fabrication of the girder, such as distortion of the flanges and the varying thickness of the solder along the web-flange joints which was caused by the use of a large soldering iron. Because each half flange was only 7mm wide, the solder had a tendency to spread over the whole width of the flange therefore increasing its thickness and contributing to the overall resistance of the girder. The influence of the solder on the strength of the girders and the strength of the solder itself were not quantified.

Level of application of the load	Top flange		Shear centre		Bottom flange	
	k	$P_E(N)$	k	$P_E(N)$	k	$P_E(N)$
Specimen						
CM8	2.04	298	0.885	1263	0.641	2329
CM10	1.57	252	0.782	839	0.594	1406
CM12	1.37	196	0.744	549	0.584	858
CM14	1.25	153	0.726	374	0.583	554
CM16	1.17	121	0.715	266	0.585	378
CM18	1.11	97.4	0.708	197	0.588	271

Table 3.1 Elastic Critical Loads for Various Levels of Loading

3.6.2 Failure modes

By comparing values of elastic critical loads calculated for shear centre loading with the maximum in-plane moment of resistance of the section, two types of failure could be predicted depending on the lengths of the girders. The shorter girders, CM8 and CM10, were expected to fail by crippling of the section at the root of the cantilever because of excessive in-plane deflection whereas the longer girders were expected to fail because of large lateral deflection. Table 3.2 gives the length L of the ten girders, the slenderness ratio $\lambda = kL/r_y$, the $B/20$ equivalent slenderness ratio $\lambda_{LT} = u.v.\lambda$, the elastic critical moment given by ref.61, the maximum in-plane capacity at a hole and a web post which is equal to that calculated for a plain-webbed beam, the corresponding critical tip loads, the experimental failure loads and the type of failure experienced.

3.7 Results and conclusions

3.7.1 Short girders CM8 and CM10

The short girders CM8 and CM10 failed at the support as predicted. Under the increasing loading they deflected vertically until the root of the cantilever completely yielded causing the weights to drop from the load pillar. The experimental failure loads were more than 25% lower than the calculated ones. This was probably due to the combination of two factors, the lower yield stress of the web and the limited strength of the solder. The web between the support and the first hole which started at 10mm distance from the support was distorted, the web and the flanges had been separated from each other but the hole next to the support was not involved in the sequence of failure. The web post between the first and second holes was undistorted in both specimens.

Specimens	L (mm)	k	$\lambda = kL/r_y$	$\lambda_{LT} = u.v.\lambda$	M_E ($10^6 N.mm$)	$P_E = M_E/L$ (N)	M ($10^6 N.mm$)	$P = M/L$ (N)	$P_{pw} = M/L$ (N)	P_{ex} (N)	mode of failure
CM8	350	0.885	99.6	81.8	0.439	1254	0.358	0.436	1246	942	Y*
CM10	444	0.782	125	88.5	0.365	822	0.358	0.436	982	598	Y
CM12	534	0.744	149	98.7	0.286	536	0.358	0.436	816	479	L†
CM14-A	613	0.726	174	110	0.228	372	0.358	0.436	711	392	L
CM14-B	613	0.726	174	110	0.228	372	0.358	0.436	711	376	L
CMP14 #	613	0.714	222	116	0.243	396	-	0.436	711	383	L
CM16-A	700	0.715	199	120	0.185	264	0.358	0.436	623	343	L
CM16-B	700	0.715	199	120	0.185	264	0.358	0.436	623	336	L
CMP16 #	700	0.707	254	127	0.198	283	-	0.436	623	326	L
CM18	790	0.708	224	130	0.154	195	0.358	0.436	552	213.6	L

†L = lateral-torsional failure

*Y = failure at the support by yielding

Specimens CMP14 and CMP16 are solid web beams

Table 3.2 Lengths, Effective Length Factor, Slendernesses, Predicted Strengths and Test Results of Small Scale Beams

local buckling of the web and flanges at the support can be seen very clearly in Plate 3.2.

3.7.2 Long girders (CM12 to CM18)

The longer specimens CM14 to CM18 deflected sideways under loading and their shape before failure was that of a single half wave. The recorded failure loads were larger than expected but the differences were not substantial given the techniques used for constructing the girders. The differences could also be explained by the slight changes in the depth of the girders which resulted in the disc used for hanging the weights having to be adjusted for each test, thus making the level of application of the load slightly above or below the shear centre. Girder CM12 had a behaviour which was intermediate between the shorter and longer girders. It did not deflect laterally under load but when its critical load was reached, it deflected suddenly sideways and collapsed immediately.

The two plain-webbed specimens were then tested and they behaved in the same fashion as the two castellated girders of the same length CM14 and CM16. They exhibited the same laterally buckled shape and when removed from the test rig, the girders of the same length could be perfectly matched as Plate 3.3 shows. Furthermore the recorded failure loads failed to suggest any differences between plain and castellated specimens.

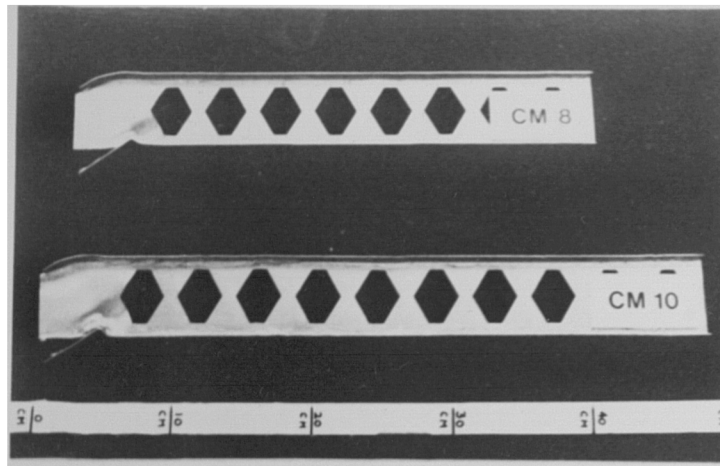
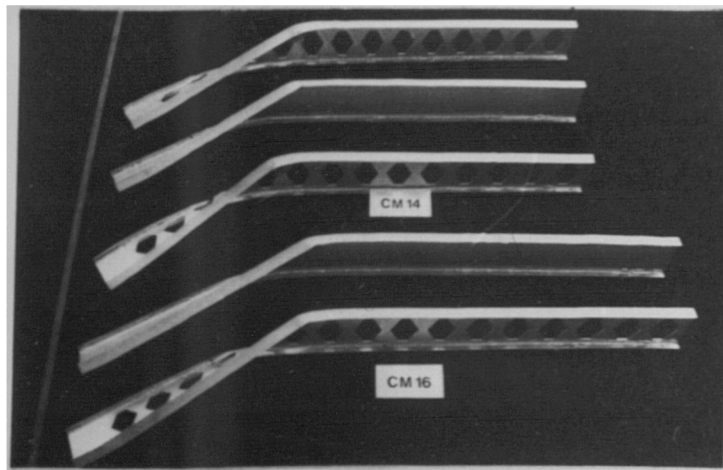
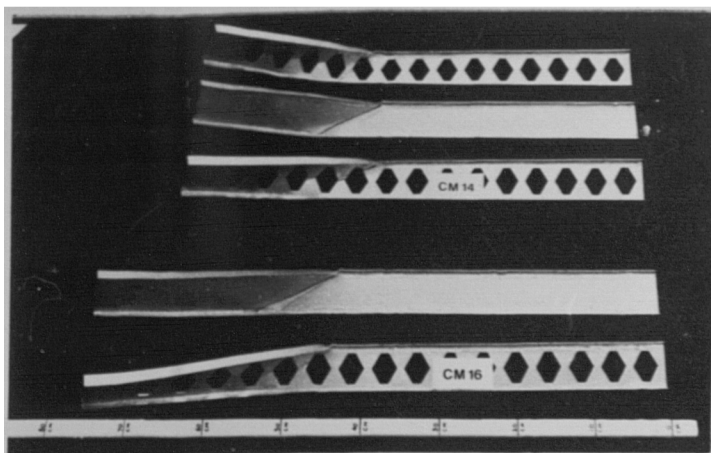


PLATE 3.2 LOCAL BUCKLING FAILURE OF SHORT SMALL SCALE GIRDE S



a.



b.

PLATE 3.3 LATERAL-TORSIONAL FAILURE OF LONG SMALL SCALE GIRDERS

3.7.3 Conclusions

The tentative conclusions which can be drawn from this short series of tests are :

1. the holes do not appear to have any influence on the shape of the girders in their laterally buckled configuration.
2. the holes do not seem to have any paramount effect on the failure load of the small scale girders.

Loads-deflection curves for some of the girders are given in Fig.3.2 and these seem to confirm the negligible influence of the holes. Finally plots of the experimental failure loads versus length L are given in Fig.3.3.

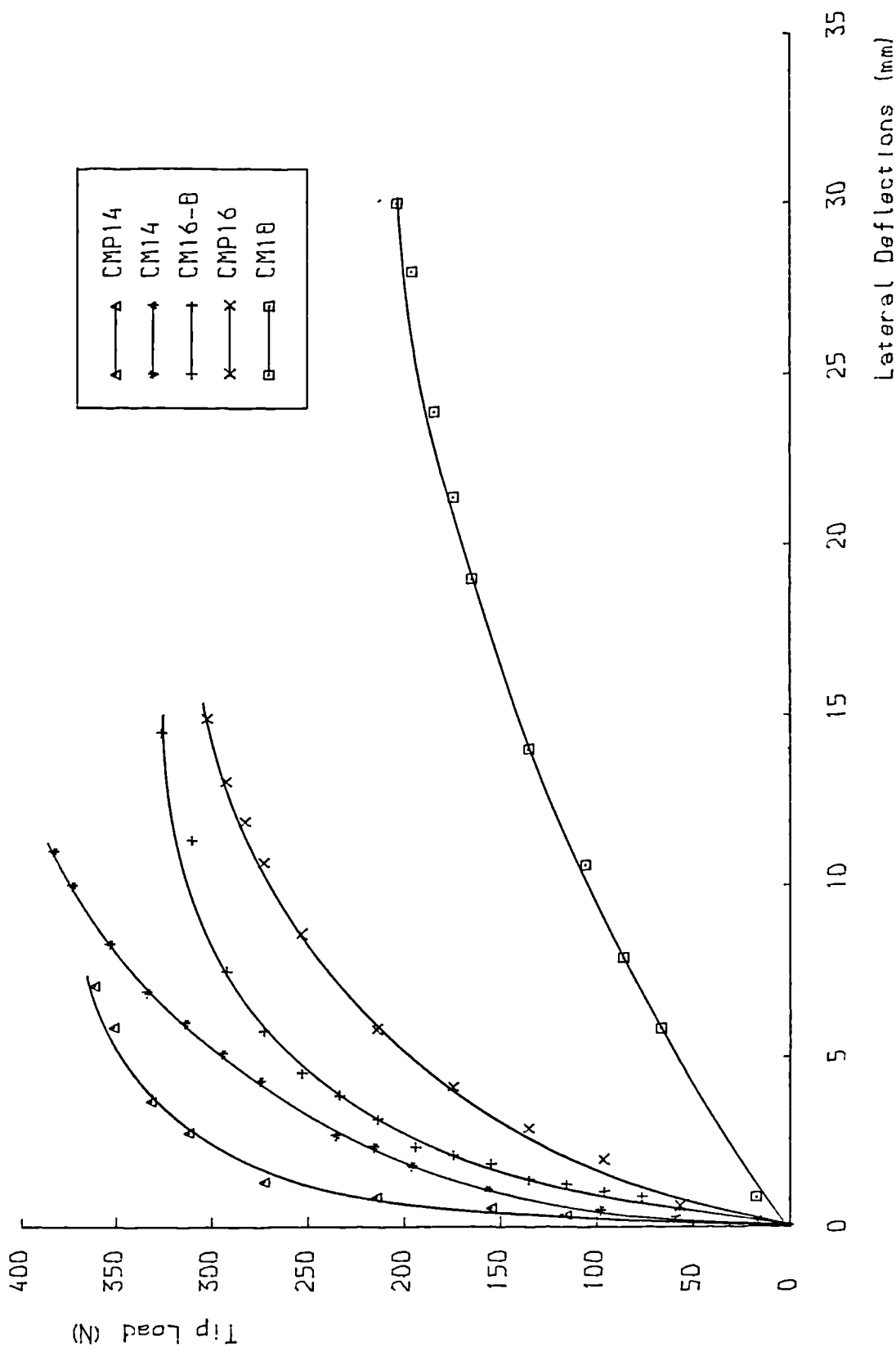


FIG. 3.2 LOAD DEFLECTION CURVES OF SOME OF THE SMALL SCALE GIRDERS

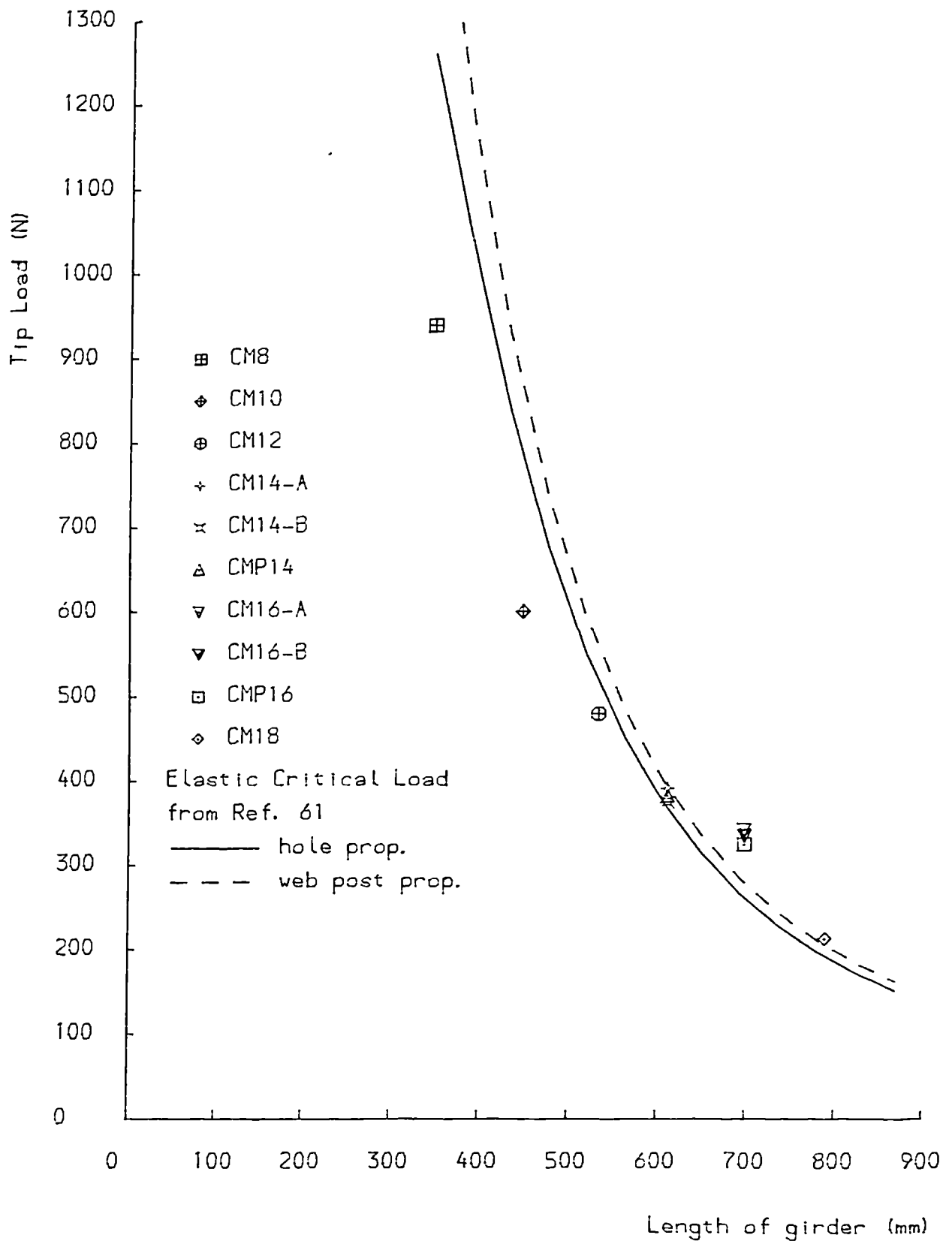


FIG. 3.3 EXPERIMENTAL FAILURE LOADS OF SMALL SCALE GIRDERS

CHAPTER 4

DESIGN OF THE TEST BEAMS

4.1 Introduction

The comprehensive survey of the literature has shown that the in-plane behaviour of castellated beams has received considerable attention and that design procedures have been proposed. The survey also revealed that the lateral buckling of castellated beams has never been the subject of an experimental investigation although they are mostly used as flexural members whose particular geometrical properties would tend to make them prone to develop this type of instability.

Castellated beams have been expanded from UB sections thus increasing the depth of the original section and its major moment of inertia. That increaseⁱⁿ in-plane strength is obtained at the expense of lateral stiffness since the minor moment of inertia remains largely unchanged. As a consequence the lateral stiffness of the beams is decreased relative to their transverse stiffness. The presence of holes in the web will also reduce the section's overall torsional stiffness and introduce the possibility of lateral buckling being accompanied by web distortion.

The test rig which was used in the present investigation created two separate zones of loading, one of pure bending and one of combined shear and bending moment. Because several modes of failure typical of castellated beams were due to the combination of shear and moment loading, the problem of checking the strength of the test beams was divided into two parts depending on whether shear was present in a span. The main concern of the present investigation was to study the tendency of castellated beams towards lateral buckling. The worst loading condition for lateral buckling is created in a span under pure bending.

It is also the easiest to treat analytically and it is the basis of the design procedures for plain-webbed beams in the various codes of practice. However the presence of shear introduced the possibility of unwanted failure modes taking place before the span under pure bending could reach its maximum predicted load and fail in the desired mode i.e. by lateral buckling. This entailed a study of all possible failure modes linked with shear which could develop. It is fortunate that the experimental and theoretical work that was available provided in most cases sufficient information to carry out these checks.

The slenderness of a plain-webbed beam will usually determine its failure mode if local types of failure are prevented. At low slenderness a beam will reach its maximum carrying capacity and fail by plastic buckling; at intermediate slenderness failure will occur in an inelastic buckling mode at a fraction of its maximum carrying capacity and at high slenderness, failure will be by elastic buckling. The study of the lateral buckling of castellated beams will therefore follow the same division.

4.2 Lateral-torsional buckling considerations

4.2.1 Influence of the holes

The effect that the holes have on the behaviour of castellated beams is the main problem that faces any investigation on their stability. The holes in the web of beams have a definite influence on local stability, i.e. weakening at a given section under a particular loading but their influence on the overall stability of the beams is less clear. The preliminary investigations carried out on model beams showed that very little difference could be found between the behaviour of castellated model beams and plain-webbed model beams. The survey of

the literature revealed that the effect of the holes on the lateral stability of cantilever beams of rectangular section had been the subject of a recent investigation (60). However because castellated beams derive their strength mainly from the flanges, this study was really only of academic interest. The influence of the holes on the stability of the beams will therefore have to be discussed in relation to the three zones of slenderness.

4.2.2 Elastic lateral buckling

4.2.2.1 General

The elastic lateral buckling of I-beams has been extensively studied and general solutions which can be found in the works of Timoshenko (62) and Galambos (63) are available. Solutions have been developed for a wide range of section types, loading patterns and support arrangements and these have generally been substantiated by laboratory tests. The advent of numerically-based approaches for the problem has meant that today virtually any elastic buckling problem is capable of solution. Nethercot and Rockey (56) have summarized the available theoretical solutions and presented a unified approach to the problem. As far as elastic lateral buckling of castellated beams is concerned, the limitations of the only solution to the problem were commented upon in chapter 2.

Castellated beams are part of the more general problem of beams with single or multiple holes of various shape in the web. A number of investigations have been carried out, particularly on the stress distribution around the holes and the need for reinforcing them. Several reports have been published which summarized the state-of-the-art (12,54,64). Because none of the investigations looked at the problem of

lateral stability of I-beams with isolated holes in the web, the Task Committee Report of the A.S.C.E. (12) proposed to limit the compressive stress in the top flange of I-beams allowed by the American code of practice (57) by using a reduction factor. However, Dougherty (65) showed that the problem had been oversimplified with the consequence of greatly overestimating the effect of a web hole on the lateral buckling strength.

4.2.2.2 Comparison of the values of elastic critical moment calculated at a hole and web post cross-sections

The main difference between castellated beams and beams with holes cut in the web is that the depth of the original section is increased by 50% in the case of the former whereas for the latter the depth remains the same. A castellated beam is therefore an entirely new beam with its own geometrical properties while beams with web holes keep all their original properties except around the holes. Although it is pointless to compare the strength of the resulting castellated beam with that of the original beam, it is necessary to understand the effect that the change in properties brought about by the fabrication process has on the elastic critical moment when the properties of the beam are calculated at the section of minimum and maximum area, i.e. through a hole and through a web post.

4.2.2.2.a Elastic critical moment from ref.62

The general equation for the elastic lateral buckling moment M_E of a beam with a symmetrical section and under equal end moment loading is well known. It is equal to:

$$M_E = \frac{\pi}{l} \left[EI_y GJ \right]^{1/2} \left[1 + \frac{\pi^2 EC_w}{l^2 GJ} \right]^{1/2} \quad (4.1)$$

The effect of the castellation is to reduce the values of I_y , J and C_w for the beam section. Since the web of an I-section makes a negligible contribution to I_y , the second moment of area about the vertical axis, the effect of I_y can be ignored. The values of I_y , J and M_E calculated at the two sections are given in Table 4.1 for the four sections chosen in the present series and for two sections chosen at the two ends of the range of castellated sections. It can be seen that the values of I_y are nearly identical and so will the warping section constant C_w which depends on I_y . On the other hand the values of J , the torsion constant, calculated at a section through a castellation are about 25% lower than those for the plain section. However this does not lead to a proportional decrease in the strength of the beam since J appears in the two parts of the formula and its effect on the value of M_E seems to partially cancel out. As a consequence the value of M_E calculated at either section are nearly equal for the short spans, the difference increasing to about 11% for spans of 10m. The values of M_E for the original UB section which are also given in the Table are generally between 7 to 10% lower than those of the expanded beam. In the case of the first two sections in the Table, the values of M_E tend to become equal as the length increases.

Section	I_{yy} (cm ⁴)	J (cm ³)	$M_E \times 10^6$ N.mm					
			2000 (mm)	4000 (mm)	6000 (mm)	8000 (mm)	10000 (mm)	
305x102x33 (1)	194	11.5	17.9	6.16	3.66	2.61	2.04	
hole (2)	194	10.0	24.2	7.19	3.91	2.66	2.02	
web (3)	194	13.0	24.7	7.61	4.24	2.93	2.24	
305x127x37	337	13.7	29.2	9.55	5.52	3.89	3.02	
hole	336	11.84	40.4	11.6	6.07	4.03	3.01	
web	337	15.63	41.2	12.2	6.55	4.43	3.36	
356x127x39	357	13.4	34.6	10.7	5.93	4.10	3.14	
hole	357	11.8	49.2	13.6	6.88	4.45	3.27	
web	358	15.1	49.7	14.0	7.27	4.79	3.56	
406x140x46	540	17.6	58.0	16.9	9.05	6.09	4.59	
hole	539	15.4	83.8	22.5	11.0	6.92	4.97	
web	541	19.8	84.5	23.0	11.5	7.37	5.36	
305x102x25	119	4.07	10.2	3.2	1.82	1.27	0.98	
hole	119	3.08	14.2	3.94	2.00	1.30	0.956	
web	120	5.06	14.6	4.25	2.27	1.52	1.15	
406x178x74	1550	61.1	173.	51.4	27.9	18.9	14.4	
hole	1549	54.9	245.	66.7	33.2	21.2	15.3	
web	1552	67.3	247.	68.2	34.5	22.3	16.4	

Table 4.1 Elastic Critical Moment M_E for Lateral Buckling of the Original U.B. Beams (1) and the Castellated Beams having the Properties of the Hole (2) and the Web Post (3) Cross-sections

4.2.2.2.b Elastic critical moment from ref.55

Although the specific solution to the problem of elastic lateral buckling of lateral beams of ref.55 was found to yield results similar to those of Eq.4.1 its derivation, which involved considering separately the flanges and the web posts and took into account the presence of the holes, made it suitable for studying the effect of changing the size of the holes on M_E .

In the first approach the presence of the holes was simply neglected in the equations provided by ref.55. The resulting curves plotted for section 609x140x46 were compared to those obtained when the original equations were used. Fig.4.1 shows that at low slendernesses each set of two curves calculated for each level of application of the load are nearly identical. For a value of slenderness equal to 250 which is equivalent to a beam length of 8.7m, the difference between the two values of M_E is about 1.2%.

In the second approach the size of the hole was decreased gradually. This would be equivalent to considering a plain-webbed beam, when the hole size would become very small. However the castellated beam appeared to be stiffer than its equivalent plain-webbed beam, the value of M_E increasing instead of decreasing. This could only be explained by the fact that the paramount term in the equation of ref.55 included a term representing the distance between the neutral axis of the bottom and top tee sections. Any change in its value had an important influence on the value of M_E , especially for lengths of beam up to 10m. A reduction in the depth of the hole meant the lowering of the neutral axis of each tee section leading in turn to a reduction in the distance between the two neutral axes. The elastic critical moment was therefore reduced.

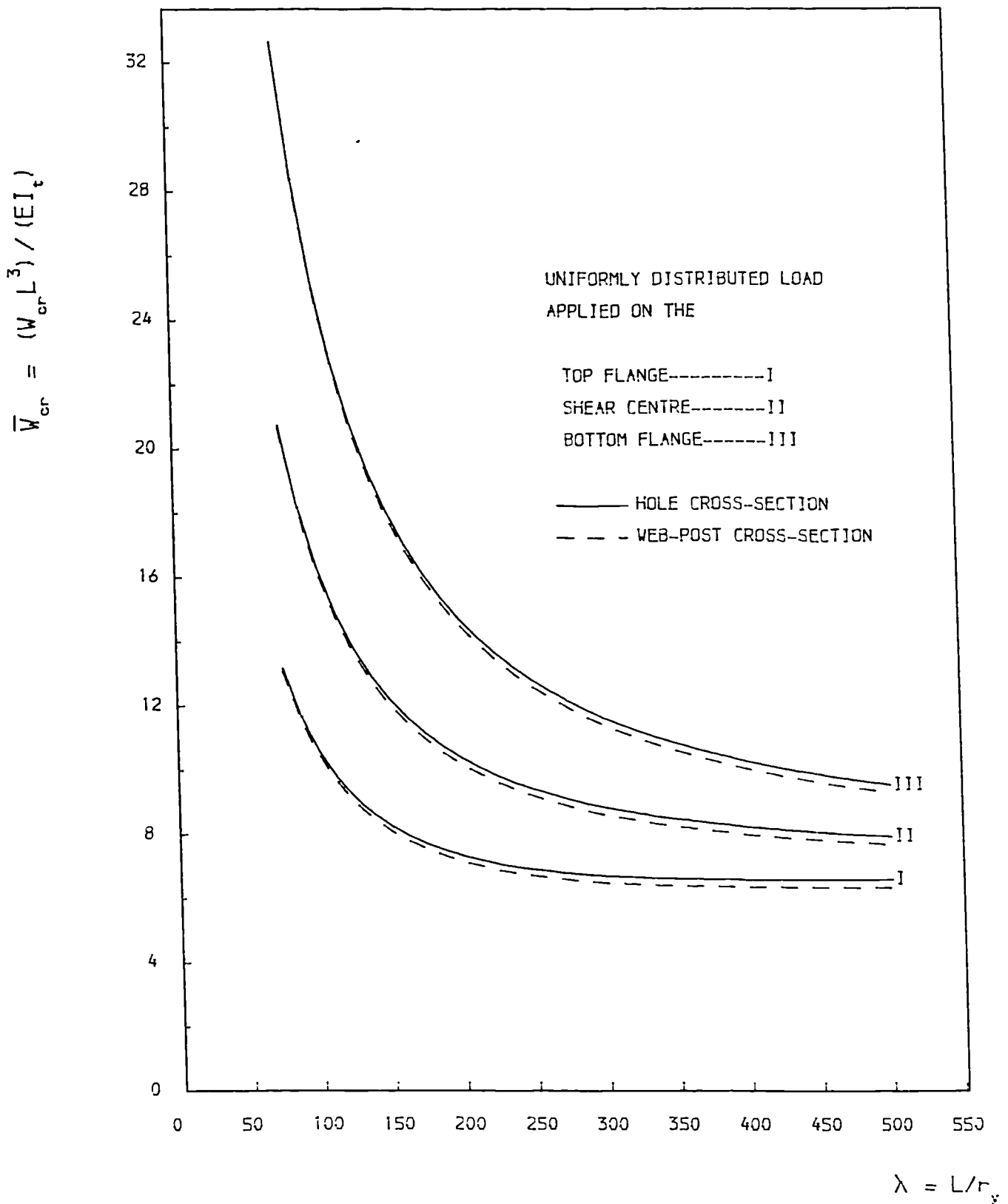


FIG. 4.1 COMPARISON OF ELASTIC CRITICAL LOADS OF SECTION 609x140x46 CALCULATED AT HOLE AND WEB POST CROSS-SECTIONS BY THE METHOD OF REF.56

4.2.2.3 Conclusions

The conclusion that emerged from comparing plain-webbed beams and castellated beams was that as far as elastic lateral buckling was concerned the presence of the holes does not weaken castellated beams dramatically.

4.2.3 Inelastic lateral buckling

In contrast to the problem of elastic buckling, inelastic lateral buckling of plain-webbed beams has not been so extensively investigated. Early investigations aimed at developing theoretical models which took into account the effect of partial yielding on the various factors controlling lateral stability. They had concentrated on simply supported beams subjected to uniform moment and considerable simplifications and approximations were needed to extend this work to other loading cases. A summary of this work has been carried out by Nethercot (66). Recent studies by Nethercot (67) have involved the analysis of the effect of unequal end moments while Kitipornchai and Trahair (68,69) investigated both theoretically and experimentally the effect of moment gradients due to concentrated loads. This led Nethercot and Trahair (70) to propose a design method for the design of single spans under a variety of load conditions. Finally Hollinger and Mangelsdorf (71) presented an approximate procedure which can be used to design beams in the elastic and inelastic ranges. This solution was based on the use of finite difference methods while previous proposals (67-70) were based on the use of the finite element method.

The idea of using the sophisticated method described above (67-70) can be discussed and its possible use argued. The main difficulty lies in adapting the procedure to the complications introduced by the

presence of the holes. The holes are hexagonal and therefore in addition to reducing the stiffness of the beam, this reduction is not constant along the length of the hole. This would lead to the subdivision of the beam into extra elements in order to cater for the change in stiffness. Another problem which can prove cumbersome is that the presence of other loading creates secondary bending moments in the region of the holes and that these vary very rapidly across a hole. Furthermore the magnitude of these secondary moments at each hole is different. This would lead to premature yielding of the tee section across the hole and away from the centre of the beam, thus initiating unsymmetrical yielding. It is therefore doubtful that these suggestions could lead to any straight forward design procedures.

Because the aim of the work undertaken herein is to provide mainly experimental data in order to check the applicability of the specification of the draft of the new British code of practice B/20 (14), the basis of these specifications for the design of beams against lateral buckling will be explained next.

4.3 B/20 proposals

4.3.1 Existing practices

The treatment of lateral buckling in many codes of practice is to give the design formula for the allowable compressive stress due to bending in the top flanges of beams. These formulae are based on simplifications of eq.4.1 usually obtained by replacing the three rigidities EI_y , GJ and EC_w by more easily calculated quantities. This normally requires the use of some approximations which reduce the range of application of the design rules. The calculation of elastic critical buckling stress is very similar in the codes of many countries, but the

treatment of inelastic behaviour varies a good deal.

4.3.2 B/20 approach

4.3.2.1 Design of plain-webbed beams

Unlike the present code of practice BS 449, the draft of the new code for the structural use of steelwork in building, the B/20 adopts the philosophy of limit states. Therefore since the theoretical maximum moment capacity of a beam that is not susceptible to prior failure by buckling is its fully plastic moment M_p the draft code expresses the strength of the beam, the buckling resistance moment M_b , directly as the proportion of M_p that can be developed. The new code employs the idea of a lateral-torsional slenderness λ_{LT} to write the ratio M_b/M_p as a function of $(1/\lambda_{LT}^2)$. λ_{LT} is defined as

$$\lambda_{LT} = \left[\frac{\pi^2 E}{p_y} \right]^{1/2} \left[\frac{M_p}{M_E} \right]^{1/2} \quad (4.2)$$

if the analytical values of M_p and M_E are substituted, then λ_{LT} can be written as

$$\lambda_{LT} = u.v.\lambda \quad (4.3)$$

where

$$u = \left[(S_x/Ah)^2 4\gamma \right]^{1/4} \text{ is the buckling parameter}$$

$$v = \left[1 + \frac{1}{20} \left[\frac{\lambda}{x} \right]^2 \right]^{-1/4}$$

$$x = 0.566 (A/J)^{1/2} \text{ is the torsional index}$$

$$\lambda = kL/r_y \text{ is the slenderness ratio}$$

and the other terms have their usual meaning.

λ_{LT} is used directly to find the corresponding value for M_b from a design curve which has been based on an experimental adaptation of the Perry type of interaction formula. M_b is taken as the smaller root of

$$(M_E - M_b)(M_p - M_b) = \eta_{LT} M_E M_b \quad (4.4)$$

in which

$$\eta_{LT} = 0.007 \left[\lambda_{LT} - 0.4(\pi^2 E / p_y)^{1/2} \right]$$

The resulting design curve is shown in Fig. 4.2. This approach forms the basis for cl.6.3 of B/20 for the design of plain-webbed beams against lateral buckling.

4.3.2.2 Design of castellated beams in B/20

The B/20 draft requires castellated beams to be designed according to cl.11.3.2.c. This clause uses basically the specifications of cl.6.3 which were described in paragraph 4.3.2.1. Thus the lateral-torsional stability of castellated beams must be assessed by treating them as plain-webbed beams. However instead of using the equivalent slenderness ratio λ_{LT} , which is a function of M_p and M_E , cl.11.3.2.c uses the simpler approximation $\lambda_{LT} \approx \lambda$, the minor axis slenderness l/r_y (it should be noted that the values of r_y given in the Handbook of Structural Steelwork (3) represent the average of the values at a hole and a web post). This approach amounts to neglecting the contributions of the web and tension flange towards providing lateral stability i.e. the problem is regarded as one in which the compression flange buckles as a strut. This is a direct consequence of the presence of the holes in the web. Because the effect of the holes on the stability of the beam was not well understood, it seemed safe to neglect the contribution of

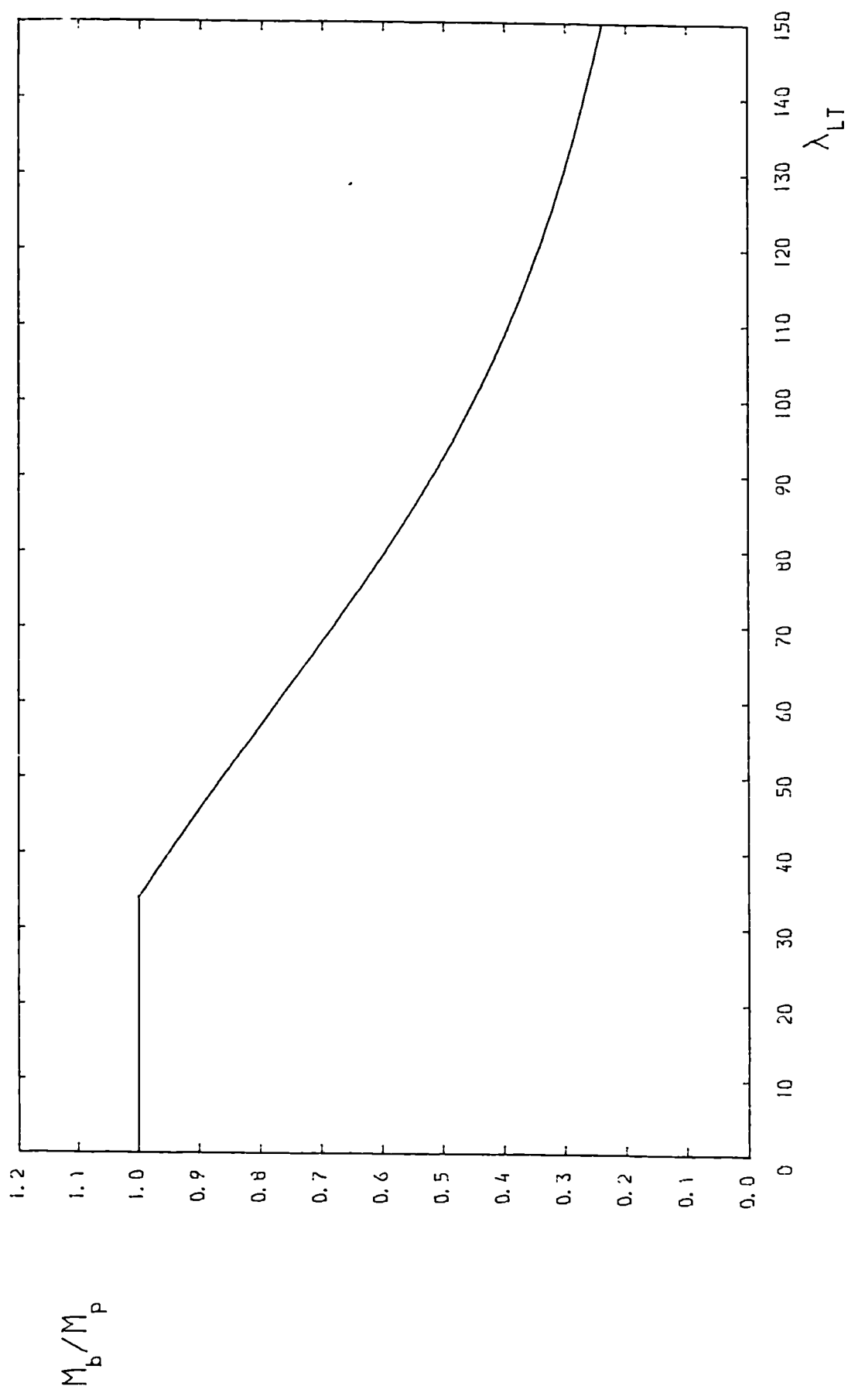


FIG. 4.2 B/20 DESIGN CURVE FOR LATERAL TORSIONAL BUCKLING

the web and the tension flange to the overall stability. The choice of $\lambda_{LT} = \lambda$ stems from the fact that if the properties of the section are calculated at a section taken through a hole, the values of u , the buckling parameter are close to unity for most sections and the torsional index takes large values, thus making the product $u.v$ in the formula $\lambda_{LT} = u.v.\lambda$ very close to 1. Table 4.2 gives comparative values for u , v , x , λ and λ_{LT} for section 609x140x46 when its properties are calculated at a hole cross-section.

An important question has just been raised. What is the effective section of a castellated beam? Should we calculate the properties of the section at a hole or at a web post or should we take average values for the properties? It is therefore necessary before embarking on the design of the castellated beams to be tested in our investigation to find out which section to use in the calculations. This will be done by taking a closer look at the various experimental programmes and especially at the tests where the beams failed in a lateral-torsional buckling mode.

4.4 Review of experimental data

4.4.1 Introduction

Chapter 2 revealed that no series of experiments were conducted with the specific aim of studying the lateral instability of castellated beams. Despite this, some useful information can be obtained from the tests conducted primarily to investigate in-plane response. A summary of all the test data was given in Table 2.3 while Table 2.4 gave a detailed account of the tests in which lateral buckling failure occurred. The cases of failure by lateral instability happened in tests where either the bracing proved inadequate (16) or after the beams had attained their maximum in-plane capacity (15,16,20,22,24,27,28). In some of the tests

Castellated Section 609x140x46		u = 0.9 x = 54.9 (=D/T)	u = 1.0 x = 54.9 (=D/T)	u = 0.973 x = 56.911 (exact)
L (mm)	$\lambda = kl/r_y$	λ_{LT}	λ_{LT}	λ_{LT}
1754	50.15	44.0	49.0	48.0
2630	75.2	66.0	73.0	71.0
3508	100.3	86.0	96.0	94.0
4385	125.4	106.0	115.0	115.0
5262	150.4	124.0	138.0	135.0
6139	175.5	142.0	157.0	154.0
7016	200.6	158.0	175.0	172.0
7893	225.7	173.0	192.0	189.0

Table 4.2 Slenderness Ratios for Section 609x140x46

(27,28) extensive local buckling was reported before the beams failed by lateral-torsional buckling. These tests and others carried out in refs. 23, 25 and 30, which although they did not report any lateral buckling failure used pure bending loading conditions, will as well as providing quantitative information regarding the choice of the relevant properties for the calculation of the various parameters necessary to enter the design curve of $B/20$, provide qualitative information on the failure modes of the beams.

Several series of tests were carried out on beams where holes were cut in the web (72-76). As for the tests on castellated beams, in-plane behaviour was the main subject of these investigations on beams with single or several web openings of various shapes. Most of the tests were concerned with the reinforcement requirements of the holes (72,75,76). However the series of tests conducted by Redwood and McCutcheon (73) dealt with the subject of unreinforced web openings in beams under a wide range of loading configurations and in particular several beams had holes in the region of pure bending moment which was therefore the nearest to the condition in which the beams of the present investigation were to be tested. From these tests valuable information can be obtained on the strength of the cross-section of a beam with a hole in the web.

4.4.2 Redwood and McCutcheon tests (73)

In these tests, one or two holes of rectangular or circular shape were cut in the web of the beams. These openings which had a depth equal to 57% of that of the beam were always situated in the least favourable zone of loading. Five ratios of shear to moment loading ranging from 0 to 0.425 were used and four beams were tested under the four-point loading arrangement which created a zone of pure bending for the central

span which contained the holes. The experimental moment capacities of these four beams were close to the values of the plastic moment capacity of the section at a hole. The average value of the experimental moments was 99.7% of the plastic moment calculated at a hole. This average value dropped to about 90% of the gross plastic moment. The average value of the plastic moment calculated at a hole was about 91% of the gross plastic moment.

For the other beams tested under central point loading, the measured plastic moment decreased as the shear to moment ratio increased. Significant reductions in strength were recorded and in some cases the experimental moment was as low as 40% of the plastic moment of the gross section. Table 4.3 gives a summary of a selection from the tests.

In the four tests where pure bending conditions existed, failure occurred at the openings without excessive deformation taking place. Yielding of the flanges was noticed before web yielding developed. This was consistent with the usual behaviour of an unperforated beam under pure bending in which yield spreads inward from the outer fibres of the flanges towards the neutral axis.

4.4.3 B.S.C. tests (15,16)

Three cases of lateral buckling of the compression flange were reported in these series of tests. Two beams failed when the span between the end support and the first load point buckled while one beam failed when its central span under pure bending buckled. The values of failure loads given were the maximum loads sustained by the test beams and might not have been the true failure loads. Table 4.4 which gives the in-plane moment capacities of the beams reviewed, indicates that

Test No.	($\frac{\text{shear}}{\text{moment}}$) ratio	Hole Description	M/M_p Section at a hole	M/M_p Section at a web	Failure Mode
1A	0.	1 Circular	0.982	0.890	Typical pure bending behaviour
1B	0.	1 Extended	1.02	0.920	Typical pure bending behaviour
1D	0.	2 Circular, close	0.945	0.855	Typical pure bending behaviour
1H	0.	2 Rectangular, wide	1.04	0.920	Typical pure bending behaviour
4F	0.160	1 Rectangular	0.775	0.700	4 hinges
4G	0.160	2 Rectangular, close	0.727	0.655	4 hinges
4H	0.160	2 Rectangular, wide	0.750	0.675	Opening nearest load failed
21G	0.319	2 Rectangular, close	0.445	0.400	Web buckling
21H	0.319	2 Rectangular, wide	0.560	0.500	Flange buckling
2F	0.425	1 Rectangular	0.452	0.410	Vertical cracks at opposite corners of opening

Table 4.3 Summary of Test Behaviour of 8WF17 Beams from Redwood and McCutcheon (Ref. 73)

strain hardening might have been the reason for the high failure load recorded in the test of ref.15. Because measurements of the yield stresses of the material were not carried out by the authors, a nominal value of 240 N/mm^2 was used to compute the moment capacities of the beams. If this value of yield stress was increased to 270 N/mm^2 , the ratio M_{exp}/M_p for the test of ref.15 would fall to 1.03 whereas the ratio for the corresponding beam of ref.16 would fall to 0.88. The third beam failed by inelastic lateral-torsional buckling and will therefore provide a further check for the design method of B/20.

4.4.4 Kolosowski's test (20)

Kolosowski tested one beam under a four-point loading system. The span under combined moment and shear loading failed by lateral buckling. The author remarked "the girder under test failed by buckling sideways at the ends, no lateral restraint having been provided for the top flange". This led him to comment on the desirability of providing adequate lateral bracing for castellated beams. He proposed to reduce the spacing of the lateral bracing points to $2/3$ of the spacing for the equivalent plain-webbed beam. The maximum capacity of the test beam was equal to the plastic moment calculated at a hole if the yield stress of the material was taken as 240 N/mm^2 . If the value of the yield stress was increased to 270 N/mm^2 , the ratio M_{exp}/M_p dropped to 0.90. This would suggest that the in-plane capacity of the test beams was reduced by the presence of the shear and axial force in the span.

4.4.5 French tests (24)

In this series of tests, three beams E, F and G had a constant depth but increasing pitches of castellation. The loads were applied at every two web posts and the length of each unbraced span corresponded to two pitches of castellations. Because the module of the cut was based on the Litzka module, an increase in the pitch of the castellation led to a proportional increase of the width of the web post and the hole. These three tests gave a good indication of the relationship between the width of the web post and the strength of the beam.

Beam E which had the shortest unbraced length of spans had also the shortest pitch of castellation and therefore the narrowest web post between two holes. Beam E failed when a web post twisted and buckled laterally. The failure load reached about 96% of the maximum in-plane capacity.

Beams F and G had longer pitches of castellations and therefore wider web posts. The increased width of the web posts prevented them from twisting before the beams reached the maximum in-plane capacity of the middle span under pure bending. The middle span then failed by lateral buckling of the top flange.

Although the three beams had intermediate plates 140mm wide inserted at the web weld, their behaviour was not in any way different from that of castellated beams without intermediate plates. The in-plane capacity of each beam was calculated by taking into account the presence of the intermediate plates.

4.4.6 Toprac and Cooke tests (22)

These tests which were conducted with the primary aim of studying in-plane behaviour provided the best insight into the failure pattern of castellated beams which collapsed in a lateral-torsional buckling mode. The progression of yielding throughout each beam up to collapse was reported in great detail. The nine beams were expanded from the same section and the expansion ratios varied between 1.33 and 1.78. The depth of the tee sections was varied respectively between 66.8mm and 22.4mm while the width of the web posts was varied between 38.1mm and 76.2mm. No comparative study was possible because all parameters were varied from test to test. However the six-point loading system created three combinations of moment and shear loading, thus making several failure modes possible.

In five beams A, B, C, D and E the width of the web post was kept constant while the expansion ratio increased from 1.33 to 1.67. Two parameters were varied, the length of the spans and the depth of the tee section. Beams A and C failed by lateral buckling of the compression flange in the zone of pure bending. The maximum recorded moment of these two beams which had the deepest tee section reached the maximum in-plane capacity of the section at the hole. Failure of beam E which had the longest central span but also the shallowest tee section occurred in the second span which was under a high moment and shear force of intermediate magnitude. Local buckling of the flange caused the collapse of the test beam. Beam D did not reach its maximum in-plane capacity although the tee section in the span under pure bending had completely yielded. The test of beam B had to be stopped prematurely before any sign of failure was noticed because of the moving out of line of the load beams.

The next beams F and G had similar width of web post but different depth of tee section. Beam F with the deepest tee section failed by lateral buckling of the top flange when it reached its maximum in-plane capacity while beam B failed in the zone of high shear when yielding of the web caused local buckling of the flange. The last two beams H and I behaved in a manner similar to that of beams F and G with beam H which had the deepest tee section failing by lateral buckling of the top flange when the maximum in-plane capacity of a section at a hole was reached in the zone of pure bending.

It was felt necessary to report in a detailed manner the series of tests carried out by Toprac and Cooke because of the need to understand the complexity of the interdependence between the shape of the holes, the depth of the beams, their slenderness and the loading system used. These tests have also highlighted the greater influence that shear and axial force have on castellated beams over plain-webbed beams.

4.4.7 Other tests

Although no other beams were found to have failed because of lateral buckling, several authors have reported cases of failure due to progressive yielding of the sections through the holes. Halleux (23), Hosain and Speirs (25) confirmed that when the influence of shear became secondary and local buckling was avoided a flexural mechanism formed in which the upper and lower tee sections at the critical sections through a castellation became completely plastic. The yielding pattern appeared to be similar to that of a solid web beam which had some material removed leading to a reduction of its in-plane carrying capacity.

Sherbourne (30) who investigated the plastic collapse behaviour of castellated beams, carried out three tests in order to check the

sensitivity of the section he used to lateral buckling. The three beams reached their moment capacity as can be seen in Table 4.4 without showing any signs of lateral buckling.

Finally Clark (28) and Galambos et al. (27) reported several cases of lateral buckling preceded by extensive local deformation. Galambos was investigating the optimum expansion ratio of expanded beams designed elastically and plastically. The two beams which were expanded to the optimum depth using elastic and plastic analysis reached their ultimate moment capacity while the other two which were expanded above and below the optimum expansion ratio just failed to reach their maximum load.

4.5 Conclusions of the survey

122 tests were carried out on castellated or expanded beams. 110 test beams were used and 82 tests were taken to failure. Lateral-torsional buckling was the primary cause of failure in 10 cases while several beams failed in flexure when the sections at a hole had fully yielded. Table 4.4 which gives the values of experimental moment M_{exp} and the in-plane capacity M_p of the sections calculated at the two positions considered shows that the maximum in-plane carrying capacity of castellated beams should be computed for a section through a hole. The average value of the ratio of M_{exp}/M_p which is 1.03 for all the tests excluding that of ref.16 for a hole cross-section drops to 0.86 for a web post cross-section.

It is possible to use the results of these tests to enter the design curve of cl.6.3 of B/20. Table 4.5 gives the dimensions of the sections considered, the values of elastic critical moment M_E , the maximum in-plane capacity M_p , the predicted buckling moment of resistance M_b , the experimental moment M_{exp} and the two slenderness

Ref.	Section	R*	M_{phole} $\times 10^8$ Nmm	M_{pweb} $\times 10^8$ Nmm	M_{exp} $\times 10^8$ Nmm	$\frac{M_{exp}}{M_{phole}}$	$\frac{M_{exp}}{M_{pweb}}$	$\frac{M_{pweb}}{M_{phole}}$
15	266.7x101.6x9.8x6.3	1.5	0.728	0.848	0.847	1.16	0.999	1.16
16	342.9x101.6x11.6x7.6	1.5	1.17	1.40	1.154	0.986	0.824	1.20
20	457.2x127x12.9x8.38	1.5	2.21	2.68	2.26	1.02	0.843	1.21
22	266.7x101.6x5.13x4.57	1.33	0.525	0.601	0.499	0.95	0.830	1.14
	297.9x100.3x5.13x4.83	1.50	0.560	0.715	0.577	1.03	0.807	1.28
	297.2x99.1x5.08x4.7	1.50	0.577	0.711	0.574	0.995	0.807	1.23
	295.9x100.3x5.15x4.4	1.50	0.591	0.719	0.605	1.02	0.841	1.22
24	500x135x10.2x6.6	1.85	2.43	2.98	2.62	1.08	0.879	1.23
	500x135x10.2x6.6	1.85	2.46	3.02	2.52	1.03	0.834	1.23
30	228.6x76.2x9.6x5.8	1.5	0.537	0.633	0.591	1.10	0.933	1.18
	228.6x76.2x9.6x5.8	1.5	0.537	0.633	0.581	1.08	0.918	1.18
	228.6x76.2x9.6x5.8	1.5	0.537	0.633	0.612	1.14	0.967	1.18
25	381x101.6x7.62x5.08	1.5	1.12	1.42	1.12	1.0	0.789	1.27
	381x101.6x7.62x5.08	1.5	1.50	1.87	1.58	1.05	0.845	1.25
27	302.5x100.5x6.78x6.25	1.2	1.054	1.11	1.051	0.997	0.947	1.05
	354.6x100.6x6.76x6.12	1.4	1.17	1.37	1.22	1.04	0.891	1.17
	340.6x100.6x6.58x6.12	1.35	1.16	1.33	1.19	1.026	0.895	1.15
	403.3x100.4x6.77x6.2	1.6	1.20	1.68	1.17	0.971	0.696	1.14

*R expansion ratio

Table 4.4 In-Plane Moment Capacities of Beams which Failed in a Flexural Mode with or without Lateral Buckling

Ref.	Sections	Yield stress (N/mm ²)		λ	λ_{LT}	M_E $\times 10^6$ Nmm	M_p $\times 10^6$ Nmm	M_b $\times 10^6$ Nmm	M_{exp} $\times 10^6$ Nmm	$\frac{M_{exp}}{M_p}$
		Web	Flange							
15	266.7x101.6x9.8x6.3	240.	240.	28.9	27.7	7.98	0.728	0.782	0.847	1.16
16	381x114.3x12.8x7.6	240.	240.	75.8	69.0	2.88	1.58	1.15	1.03	0.652
	342.9x101.6x11.6x7.6	240.	240.	47.8	45.2	4.82	1.17	1.08	1.15	0.986
20	457.2x127x12.9x8.38	240.	240.	35.5	34.2	16.0	2.21	2.26	2.26	1.02
22	266.7x101.6x5.13x4.57	274.5	302.1	42.7	40.0	2.42	0.525	0.500	0.499	0.95
	297.9x100.3x5.13x4.83	274.5	302.1	34.3	33.0	3.79	0.560	0.566	0.577	1.03
	297.2x99.1x5.08x4.70	274.	297.	29.0	27.9	5.14	0.577	0.603	0.574	0.995
	295.9x100.3x5.15x4.4	304.9	294.	33.4	32.1	3.90	0.591	0.595	0.605	1.02
24	500x135x10.2x6.6	335.	256.	30.4	29.2	20.6	2.43	2.52	2.62	1.08
	500x135x10.2x6.6	350.	255.	38.0	36.4	13.4	2.46	2.39	2.52	1.025
30*	228.6x76.2x9.6x5.8	282.3	282.3	16.6	16.0	14.9	0.537	0.617	0.591	1.10
				24.8	23.9	6.73	0.537	0.581	0.581	1.08
				33.1	31.5	3.86	0.537	0.547	0.612	1.14

* These did not fail by L.T.B.

Table 4.5 Moment Capacities of Beams which Failed by Lateral-Torsional Buckling

ratios. In these calculations the effective length of the spans under consideration was taken as the clear length of the spans. No attempt was made to assess the restraining effect of the adjacent spans or the loading system and consequently no effective length factors was used. The inclusion in the calculations of an effective length factor would have had the effect of reducing the values of λ_{LT} and of moving the test points nearer to the vertical axis. The shift to the left of the values of λ_{LT} would not have affected the points in the plastic zone but would have led to under-prediction in the elastic zone.

Thirteen points can be plotted against the design curve in Fig.4.3. Most of the points plot above the design curve in the plastic part of the curve. However the test point corresponding to the beam tested in ref.16 falls below the design curve; the actual strength being overestimated by about 10%. This can only be explained by the premature and unexpected failure of the beam, the failure load reported being approximate.

Another important conclusion from the survey was that castellated beams exhibit the same laterally buckled configuration as their equivalent plain-webbed beams consisting of a smooth continuous profile. Furthermore no distortion of the web posts in the parts of the beam which failed by lateral-torsional buckling was reported in any of the tests.

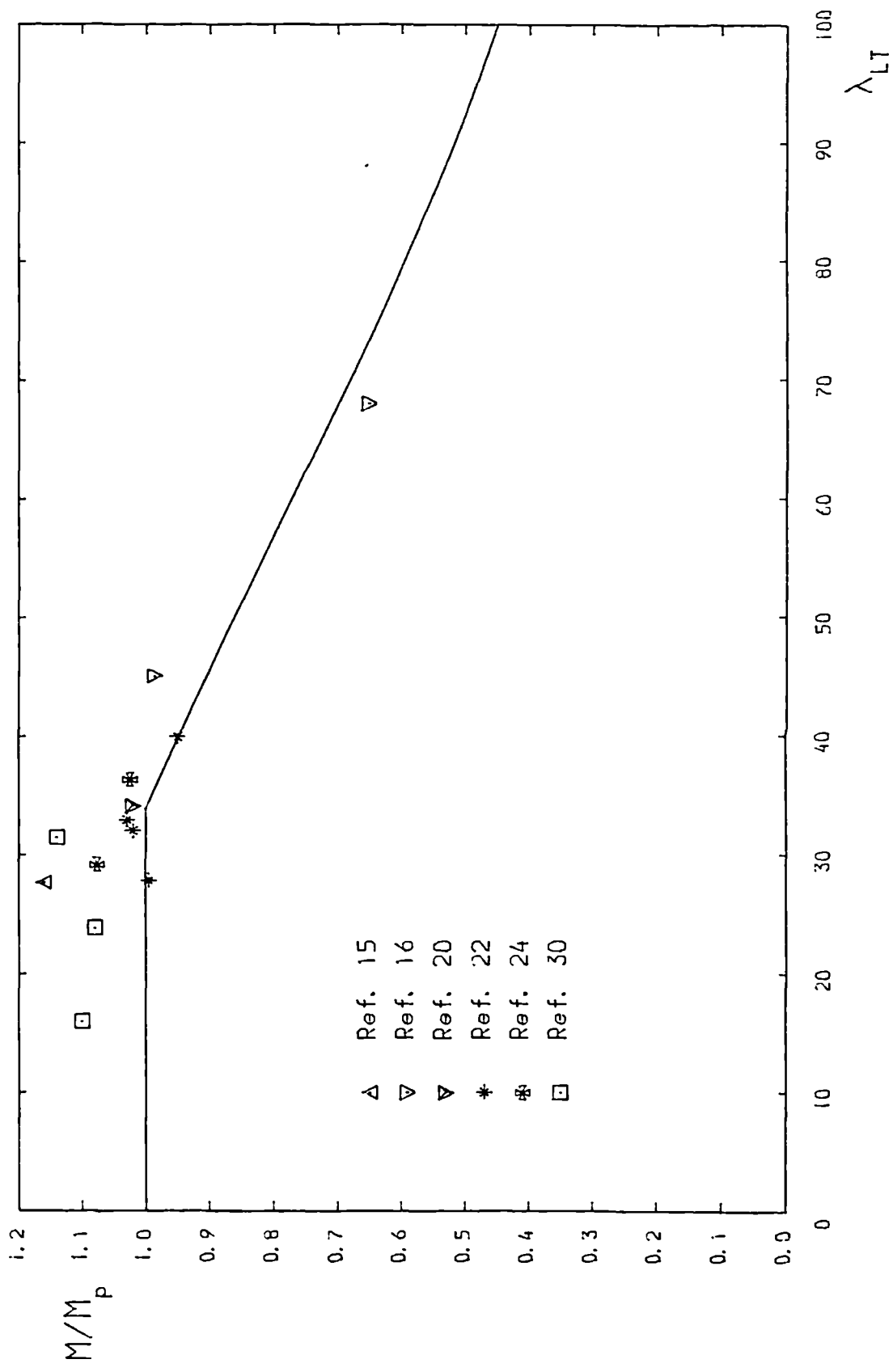


FIG. 4.3 COMPARISON OF TEST DATA WITH B/20 PROPOSALS FOR SOLID WEB BEAMS HAVING THE PROPERTIES OF THE HOLE CROSS-SECTION

4.6 Selection of the test beams

4.6.1 Procedure

The number of beams to be tested was determined by financial considerations. This number was fixed as eight. Because the aim of the investigation was to verify the proposals made in cl.11.3.2.c of B/20, the slenderness of the test beams, more specifically that of the central span, was the parameter chosen to be varied. The test rig divided the test beams into three spans, two sidespans which were subjected to a combination of shear force and bending moment loading and a central span under pure bending moment loading. The clause enabled an estimate of the strength of the central span, the buckling moment of resistance M_b , to be obtained as a fraction of the maximum in-plane capacity M_p .

The procedure therefore consisted of choosing both the cross-sectional dimensions and the length of the three spans such that the derived value of the ratio M_b/M_p was achieved in each case. The sections from which the test beams were made were selected from the Handbook of Structural Steelwork (3). Upper and lower limits to the depths and the lengths of the test beams were imposed by the test rig. Working within these limitations, a computer program was written which could calculate values of M_b and λ_{LT} for a given length. The values of λ_{LT} were determined from the expression $\lambda_{LT} = \sqrt{\pi^2 E / p_y} \sqrt{M_p / M_E}$ using the properties at a hole cross-section.

The lengths of the sidespans were determined once the length of the central span was chosen for each test beam. The next step was to assess the restraining effect of the sidespans on the central span. This was done by using the approach of ref.78 which gives a simple hand method for the calculation of the effective length factor k of laterally continuous beams. These values of k were fed back into the computer

program to calculate new values of M_p and λ_{LT} for the sections chosen. A check on the values of k was made by comparing them with values of k obtained from the more exact method of Trahair (79) which is valid only for the case of sidespans of equal length.

4.6.2 Dimensions of the test beams

Out of the eight beams selected for the testing programme, two were made from the castellated section 609x140x46, three from the castellated section 534x127x39, two from the section 458x127x37 and one from the section 458x102x33. Section 609x140x46 was expanded from the UB section 406x140x46, section 534x127x39 was expanded from UB section 356x127x39, section 458x127x37 was expanded from UB section 305x127x37 and finally section 458x102x33 was expanded from UB section 305x102x33. Beams with narrow flanges were chosen in preference to ones with wide flanges because lateral buckling would be more prevalent for deep sections with narrow flanges than for shallow sections with wide flanges.

The beams were fabricated at the Redpath Dorman Long factory in Manchester. The steel was mild steel of grade 43A and satisfied the specifications of BS 4360 (77). One specific demand was made during the making of the beams, the web posts had to be welded back straight.

The measured dimensions of the cross-section of each beam which were within the tolerance of fabrication as set out by the fabricator are given in Table 4.6. These dimensions were the average of several measurements taken along each beam. Because these measurements were different from the dimensions given by the Handbook (3), the properties of each test beam were calculated using the measured dimensions. Table 4.7 gives the values of the properties used in the calculations of M_p and λ_{LT} . Although it was suggested that the hole cross-section should be

Test Beams	Sections	D _{CL}	D _{CR}	D _C	B _{top}	B _{bot}	B	w _{top}	w _{bot}	w	T _{top}	T _{bot}	T
S6-2	609x140x46	602.8	608.1	605.4	142.4	145.	143.7	7.25	7.23	7.24	10.96	11.24	11.10
S5-1	534x127x39	525.0	524.0	524.5	125.0	124.0	124.5	6.99	7.01	7.0	10.58	10.61	10.60
M4-2	458x127x37	451.0	453.0	452.0	124.1	123.8	124.0	7.53	7.32	7.43	10.57	10.56	10.56
M5-1	534x127x39	524.9	525.7	525.3	124.01	124.89	124.45	7.05	7.03	7.04	10.58	10.6	10.59
L6-4	609x140x46	605.3	605.4	605.3	143.9	147.1	145.5	7.26	7.22	7.24	11.29	11.34	11.32
L4-2	458x127x37	450.4	453.0	451.7	123.8	124.17	124.0	7.64	7.42	7.53	10.7	10.64	10.67
L5-3	534x127x39	524.3	526.7	525.5	124.2	125.11	124.7	7.02	7.03	7.03	10.63	10.61	10.62
L4-1	458x102x33	458.9	460.2	459.6	102.64	103.76	103.2	7.23	7.23	7.23	10.75	10.63	10.69

Table 4.6 Dimensions of the Cross-section of the Test Beams (mm)

	S6-2		S5-1		M4-2		M5-1		L6-4		L4-2		L5-3		L4-1	
	hole	web post	hole	web post	hole	web post	hole	web post	hole	web post	hole	web post	hole	web post	hole	web post
D_c (cm)	60.54	-	52.45	-	45.20	-	52.53	-	60.53	-	45.17	-	52.55	-	45.96	-
D_c/T	54.54	-	49.48	-	42.80	-	49.60	-	53.47	-	42.33	-	49.48	-	42.99	-
A (cm ²)	44.73	74.13	36.69	61.61	35.54	58.20	36.79	61.85	45.72	75.12	35.90	58.86	36.89	61.91	31.75	53.80
I_{xx} (cm ⁴)	35668	40217	21948	24895	15748	17749	22047	25020	36506	41052	15876	17906	22129	250.96	14282	16254
I_{yy} (cm ⁴)	549.7	550.9	341.2	342.2	335.75	336.79	340.64	341.68	581.83	583.11	339.34	340.43	343.12	344.16	196.80	197.76
r_y (cm)	3.51	2.73	3.05	2.36	3.07	2.41	3.04	2.35	3.57	2.79	3.07	2.40	3.05	2.36	2.49	1.92
J (cm ⁴)	15.49	20.63	11.68	15.75	11.61	15.78	11.70	15.84	16.43	21.57	11.98	16.32	11.78	15.90	10.29	14.13
S_x (cm ³)	1265.1	1563.6	899.4	1121.2	750.12	922.92	902.57	1125.6	1294.0	1592.4	756.96	932.08	905.47	1128.2	675.46	843.60

Table 4.7 Properties of Test Beams

used for the calculation of the properties, the table also gives values of properties for a web post cross-section. These will be used to determine the theoretical strength of the test beams at a web post cross-section for comparison purposes.

4.6.3 Initial deformations

The initial out-of-straightness of the flanges which would be under compression during the tests was measured in each beam. A wire was stretched along the middle of the flange of the central span. The distance from the edges of the flanges to the wires was measured at several positions. As was first noticed from visual inspection, all the beams but two had negligible bow at the centre of the span. Beam M5-1 was found to have a bow of 4mm at the middle of the central span whilst a bow of 5mm was measured at the middle of the central span of beam M4-2.

The cross-section of beam S6-2 was found to be distorted. The measurements of the depth of the cross-section showed a difference of about 6mm between the two sides. Inspection of the web posts revealed that they were straight and that the welding back of the two halves of the beam had been executed satisfactorily.

4.6.4 Slenderness of the test beams

Table 4.8 gives for each test beam the length of the three spans L_{AB} , L_{BD} and L_{DE} , the effective length factor k of the span BD, the slenderness ratio λ , the equivalent slenderness λ_{LT} and the predicted ratio M_b/M_p . From the tables it can be seen that the eight beams fall conveniently into three groups depending on the slenderness of span BD:

Test Beams	L_{AB} (mm)	L_{BD} (mm)	I_{DE} (mm)	k	λ	λ_{LT}	M_b ($\times 10^6$ Nmm)	$R_A = M_b / L_{AB}$ (kN)
S6-2	1900	1650	1900	0.96	45.2	43.6	3.25	171.
S5-1	1900	1650	1900	0.895	48.4	46.5	2.25	118.2
M4-2	1900	3000	1200	0.665	64.9	61.4	1.70	86.2
M5-1	1900	3000	1900	0.695	68.5	65.2	1.84	97.
L6-4	2090	4024	2090	0.66	74.5	70.8	2.41	115.1
L4-2	1968	4268	1968	0.65	90.2	83.4	1.22	62.
L5-3	1968	4268	1968	0.65	90.9	85.2	1.42	72.
L4-1	1968	4268	1968	0.65	111.4	100.8	0.858	43.6

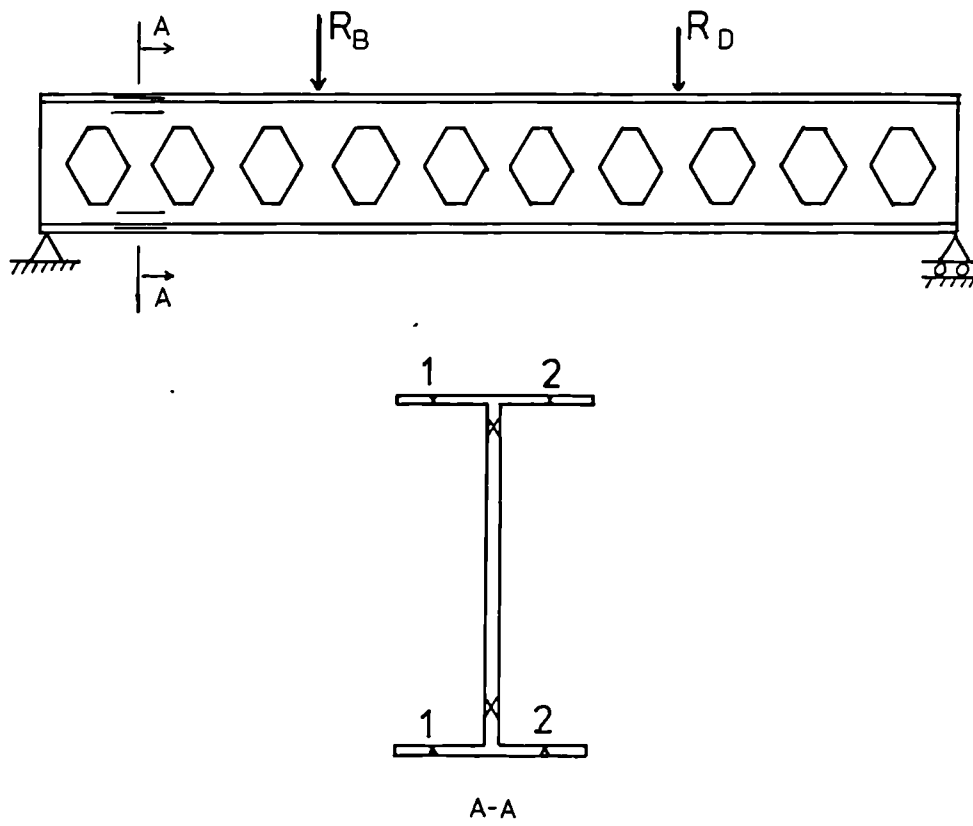
Table 4.8 Details of the Present Experimental Programme

1. Beams S6-2 and S-5-1 with λ_{LT} values of 43.6 and 46.6 respectively had a central span length of 1650mm and were expected to approach their full in-plane capacity.
2. Beams M4-2 and M5-1 with λ_{LT} values of 61.4 and 65.2 respectively had a central span length of 3000mm and were expected to fail by inelastic lateral-torsional instability.
3. Beams L6-4, L4-2, L5-3 and L4-1 with λ_{LT} values greater than 70 had a central span length of more than 4000mm and were expected to buckle elastically.

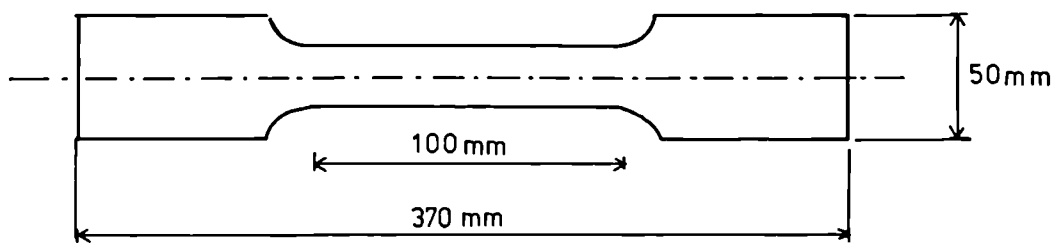
In all cases except M4-2, the two sidespans were kept equal to avoid any moment gradient. In the case of beam M4-2, the two sidespans were deliberately made unequal so as to produce a moment gradient along the critical span; the values of L_{AB} and L_{DE} were used such as to give $M_B/M_D = 0.8$ initially.

4.6.5 Material properties

Six tension coupons were cut from unyielded parts of each beam after test. Their dimensions satisfied the specifications given by BS 18 part 2 (80). Fig.4.4 shows the coupons location on the cross-section and their usual size. Two coupons were cut from the top flange, two from the bottom flange and two from the web. The coupons were tested in an Amsler testing machine at the slowest possible rate of strain which was the nearest to that at which the beam specimens were to be tested. Different values of yield stresses were obtained; upper, lower, static yield stresses and finally ultimate stresses. The static yield stresses which were obtained by following the recommendations of ref.81 were used in all the calculations of M_p and λ_{LT} and are given in Table 4.9.a. The other values of stresses are given in Table 4.9.b. The value of the



a. Location of coupons



b. Coupons cut out from beams

FIG. 4.4 COUPONS FOR TENSILE TESTS

Test Beams	Top flange 1	Top flange 2	Bottom flange 1	Bottom flange 2	Top web	Bottom web
S6-2	267.2	269.9	267.4	268.9	293.2	293.9
S5-1	274.2	269.8	270.	271.6	290.	291.2
M4-2	291.6	292.3	286.2	286.6	290.8	295.2
M5-1	272.	270.8	270.	271.7	294.7	300.8
L6-4	267.7	263.5	270.2	271.2	286.	277.
L4-2	280.8	284.2	283.7	281.8	299.7	297.3
L5-3	273.	270.3	272.3	271.8	310.4	295.5
L4-1	284.6	283.6	281.7	286.4	304.2	304

Table 4.9 a. Values of Static Yield Stresses (N/mm²)

Test Beams	Top flange 1			Top flange 2			Bottom flange 1			Bottom flange 2			Top web			Bottom web		
	u.y.s	l.y.s	r.															
S6-2	271.5	270.4	458.8	274.3	272.	478.3	278.2	276.4	486.	280.4	277.5	474.4	307.6	304.	-	305.	302.	472.
S5-1	284.7	278.	479.	279.	273.8	479.	283.	278.2	490.	282.7	281.6	494.	312.	305.	505.	311.	302.7	508.3
M4-2	301.3	-	518.	301.7	-	511.	294.5	291.5	511.	297.	286.6	509.4	300.2	-	509.	317.	311.	519.
M5-1	283.9	-	494.	284.	280.2	492.	283.8	281.2	493.	280.8	279.3	497.	312.3	305.5	-	312.3	-	512.5
L6-4	277.1	275.3	484.4	272.3	270.4	477.8	283.2	277.2	474.2	279.7	278.2	475.	299.7	298.	470.	291.3	288.5	473.
L4-2	289.3	-	512.	295.8	295.4	507.9	292.9	291.3	529.1	290.	288.1	513.6	306.9	-	-	306.1	-	531.
L5-3	287.6	286.8	491.	285.3	283.	482.	280.9	-	485.	285.5	282.5	487.	329.1	324.5	499.3	311.	308.	499.
L4-1	297.5	293.3	499.	295.2	293.	494.	293.	289.5	503.	299.7	-	500.	326.	317.	522.	323.	315.6	522.

u.y.s = upper yield stress
l.y.s = lower yield stress
r. = stress at rupture

Table 4.9 b. Material Stresses (N/mm²)

modulus of elasticity E was taken as 205000 N/mm^2 and the value of the shear modulus G was taken as 82000 N/mm^2 in the calculations.

4.7 Design of the sidespans

4.7.1 Introduction

The middle span was designed against possible failure by lateral-torsional buckling. However if the loads were to be transmitted to the middle span, the sidespans had to perform satisfactorily. The two sidespans which were under shear and moment loading were not likely to behave in a manner similar to that of the middle span.

For a plain-webbed beam, the point of maximum stress is very easy to determine once the bending moment diagram has been drawn. However this determination is not as straightforward in the case of castellated beams. The presence of the holes alters the stress distribution across the section of the beams which in turn introduces the possibility of several new failure modes. The various methods for evaluating the stresses in the test beams will be reviewed, the possible failure mechanism described and the likelihood of their happening assessed.

4.7.2 Longitudinal stresses

4.7.2.1 Elementary theory of bending

Although castellated beams are made by expanding a standard rolled shape, their design behaviour is different from that of a plain-webbed beam with a reduced web section. Stresses calculated by using the elementary theory of bending are not consistent with the experimental results and it cannot therefore be used.

4.7.2.2 Vierendeel analysis of castellated beams

4.7.2.2.a Vierendeel analogy

On the basis of the various experimental investigations (13,19-31) it is now accepted that a castellated beam behaves in a manner similar to that of a Vierendeel truss. The Vierendeel analogy is a consequence of the laws of equilibrium since a castellated beam has no effective means of transferring shear other than through bending of the tee sections above and below the holes. This approach is therefore recommended by cl.11.3.2 of B/20.

A Vierendeel frame is a highly indeterminate structure and in order to find the distribution of forces in the members it is necessary to assume that points of inflexion are located at the mid-lengths of the chords (tee section) and the vertical members (web posts) as shown in Fig.4.5. The longitudinal stresses are then calculated as the sum of the stresses from the bending moment created by the external loads and the local stresses caused by the shear force. Two methods for computing the longitudinal stresses have been proposed. These differ in the way the stresses due to the external bending moment are calculated.

4.7.2.2.b 1st method

This method (31,54) calculates the longitudinal stresses resulting from the conventional bending moment on the basis of the net section through an opening.

$$\sigma_M = \frac{M}{Z} \quad (4.5)$$

At each web opening the two tee sections act as members of a frame in resisting vertical shear force. It is assumed that the shear force is divided equally between the upper and lower chords and that points of

contraflexure for the bending caused by the shear occur at the vertical centreline through each opening (Figs. 4.5 to 4.7). The shear force applied at mid-opening produces a bending moment on the cantilevered tee section and the resulting secondary stresses are

$$\sigma_{tee} = \frac{Vn}{4Z} \quad (4.6)$$

where V is the shear force, n is the length of the weld and Z is the section modulus of the tee section.

For the loading case considered (four-point loading) the governing stresses will be the flexural stresses at the re-entrant corner of the web (section 1-1 in Fig.4.5) and at the extreme flange fibres of the tee section (section 2-2 in Fig.4.5) at the opening immediately before the applied load. The total resulting stresses are represented diagrammatically in Fig.4.8 and the expressions for computing them at sections 1-1 and 2-2 are:

section 1-1 :

$$\sigma_{1a} = \frac{M_{1a} D_s}{2I_g} + \frac{0.251 D_s V}{4Z_{ts}} \quad (4.7)$$

section 2-2 :

$$\sigma_{1b} = \frac{M_{1b} D_c}{2I_g} + \frac{0.251 D_s V}{4Z_{tf}} \quad (4.8)$$

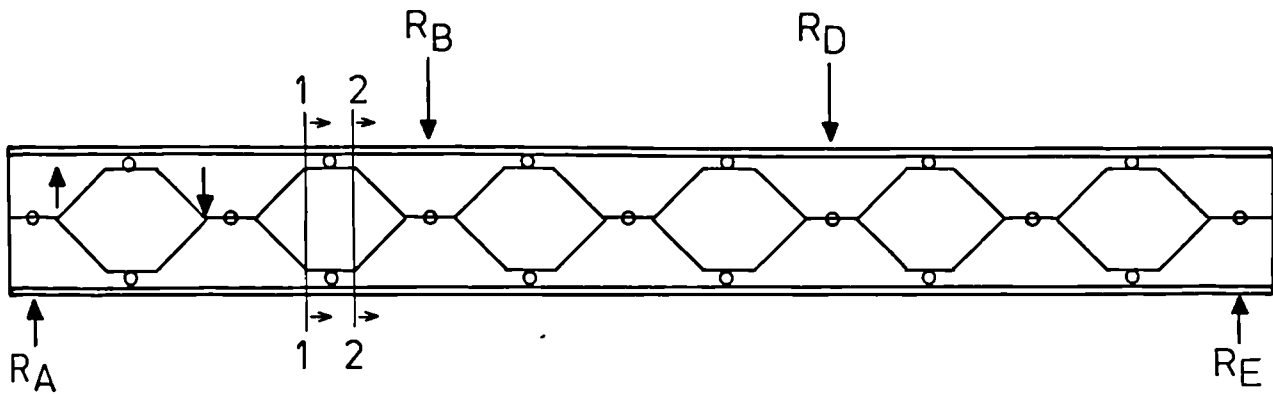


FIG. 4.5. VIERENDEEL ANALYSIS OF THE CASTELLATED BEAM.

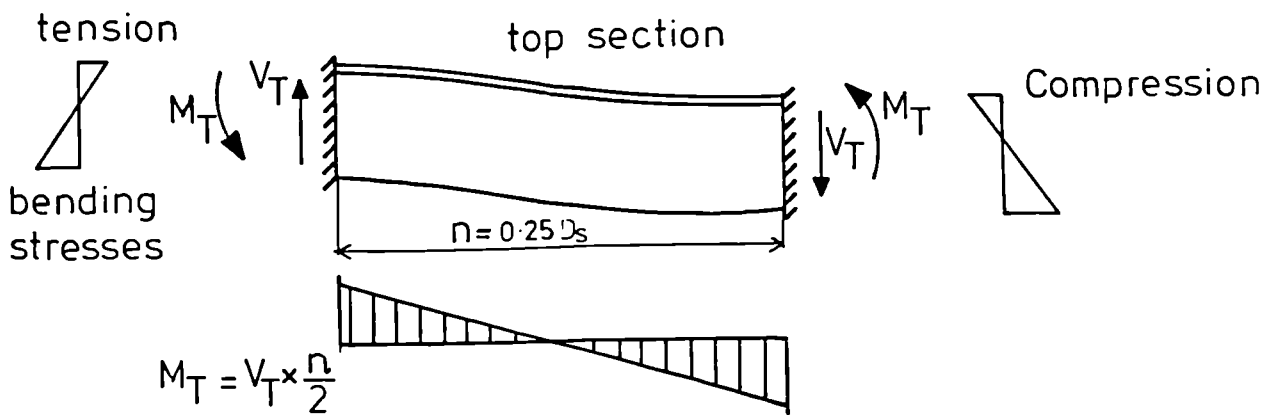


FIG. 4.6. SECONDARY BENDING MOMENT DUE TO SHEAR FORCE.

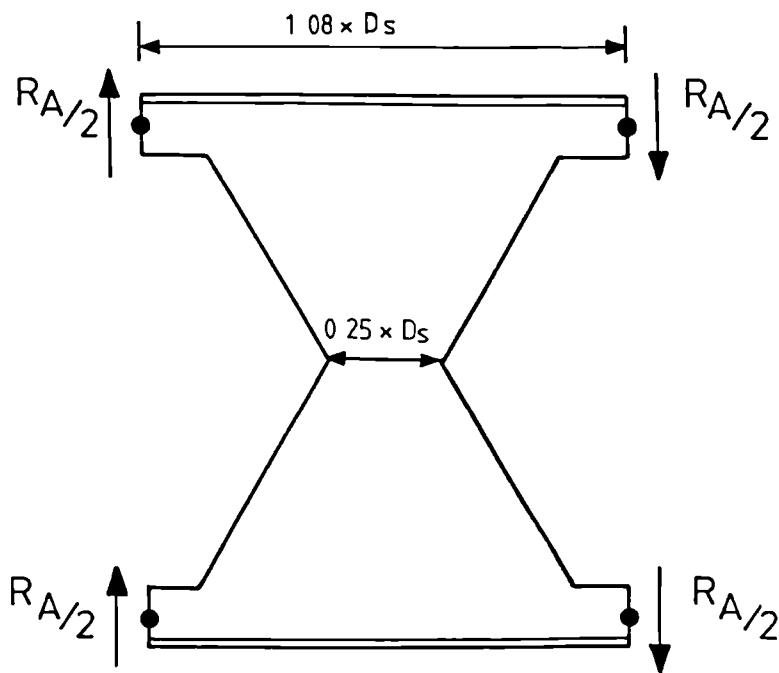


FIG. 4.7. DISTRIBUTION OF SHEAR FORCE.

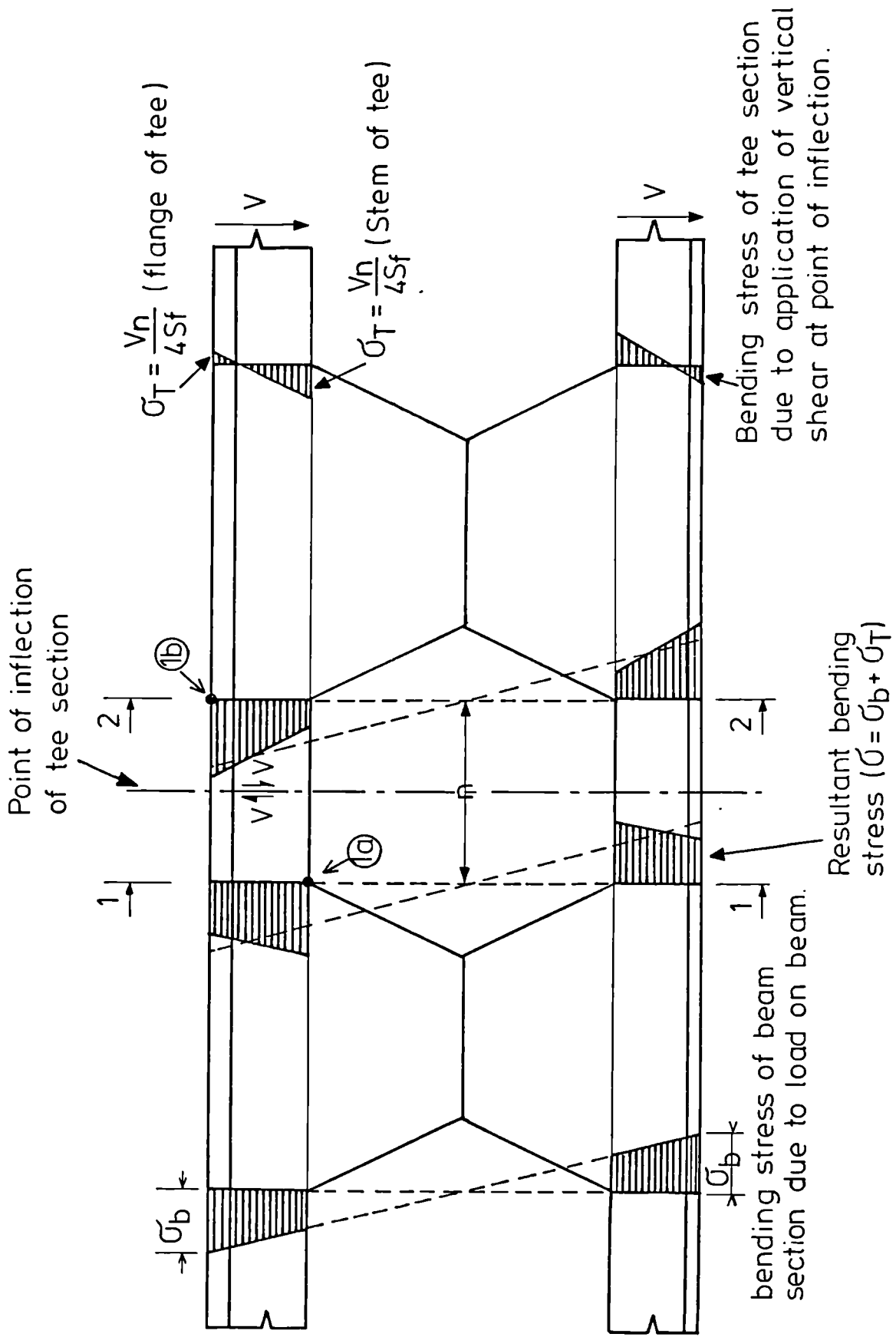


FIG. 4·8. LONGITUDINAL STRESSES.

where:

M_{1a} and M_{1b} are the moments at sections 1-1 and 2-2

Z_{tf} and Z_{ts} are the section modulus of the tee section at the extreme top fibres of the flange and at the stem respectively.

V is the shear force in the span

I_g is the moment of inertia of the open section

D_s is the serial height of the UB section from which the castellated beam has been expanded.

D_c is the depth of the castellated section.

4.7.2.2.c 2nd method

The second way of calculating the longitudinal stresses was first proposed by Altfillisch et al.(21) who noticed that the bending stresses in the tee section did not increase linearly and that in some cases the stresses at the stem of the tee section were higher than those at the outer fibres of the flanges. They therefore suggested that the stresses due to the external bending moment should be taken as uniform throughout the tee section. These stresses would result from a normal force N created by the external bending moment M at section 1 in Fig. 4.8

$$N = \frac{M}{D_c - 2y_{tee}} \quad (4.9)$$

where y_{tee} represents the depth to the neutral axis of the tee section. Because this section is the one where the shear force is applied for the secondary bending stresses, unlike the previous proposals it is only necessary to calculate the total bending stresses once.

They will be equal to

$$\sigma_{M,N} = \frac{M}{A_{tee} (D_c - 2y_{tee})} + \frac{0.251D_s V}{4Z_{ts}} \quad (4.10)$$

4.7.2.2.d Conclusions

The assumption that the stress distribution is linear across the sections of the beams and thus that plane sections remain plane across the full depth of the section is not verified either experimentally or theoretically. The removal of web material has removed any possibility of strain compatibility across the opening. Fig.4.9 shows stress and strain distributions across various sections of a beam with web holes when bending moment alone is present while Fig.4.10 shows the stress and strain distribution of a beam subjected to shear and bending.

However in most cases the magnitude of the error introduced by incorrectly assuming that plane sections remain plane is negligible. The number of tests performed so far have shown that the Vierendeel analogy gives the values of stresses at the extreme parts of the section with an accuracy satisfactory for design purposes and that the loads at which castellated beams cease to exhibit linear elastic behaviour can be predicted with confidence (13,20,25,27,31) if all the elements remain stable. It has been reported that at failure, the points of inflexion in the chords are no longer located at the mid-points.

It is also necessary to bear in mind that although the behaviour of a castellated beam can be modelled on the Vierendeel frame, its performance is not the same because of the difference in the proportions and the greater effect that shear deformations have.

Table 4.10 gives the stresses calculated at the various sections

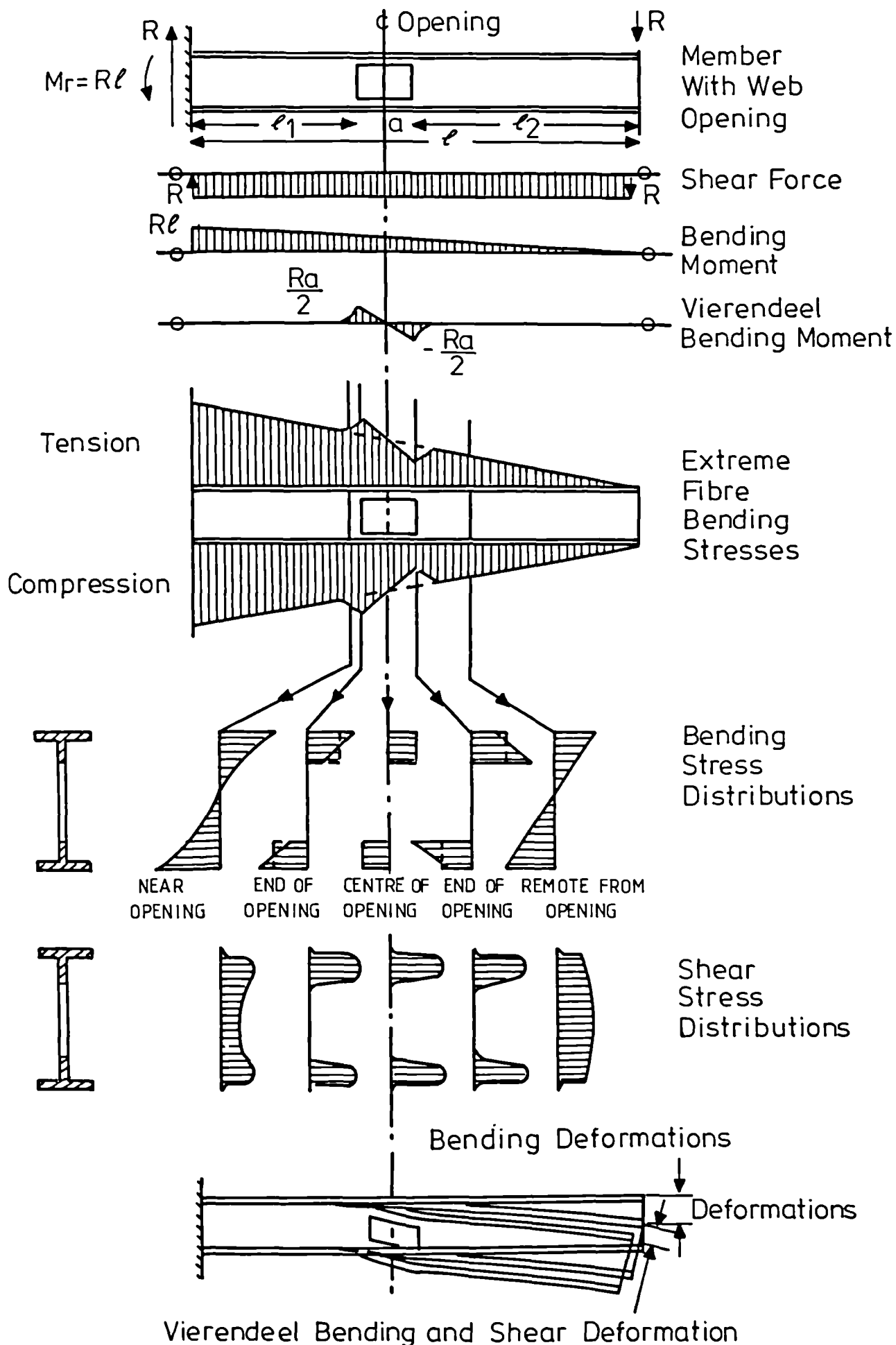


FIG. 4.9A. BEHAVIOUR OF BEAM WITH SINGLE OPENING SUBJECTED TO BENDING AND SHEAR. (From ref. 54)

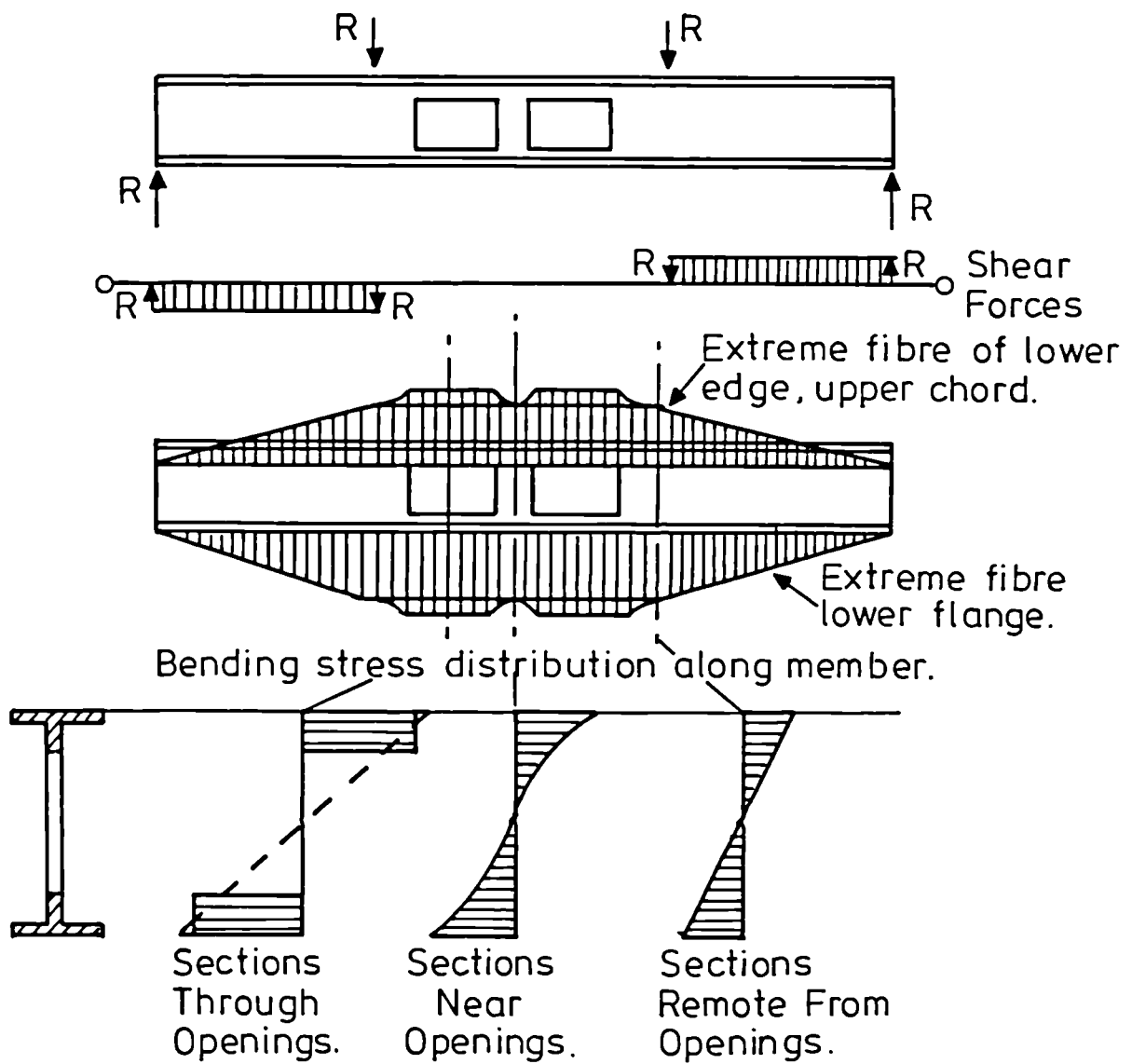
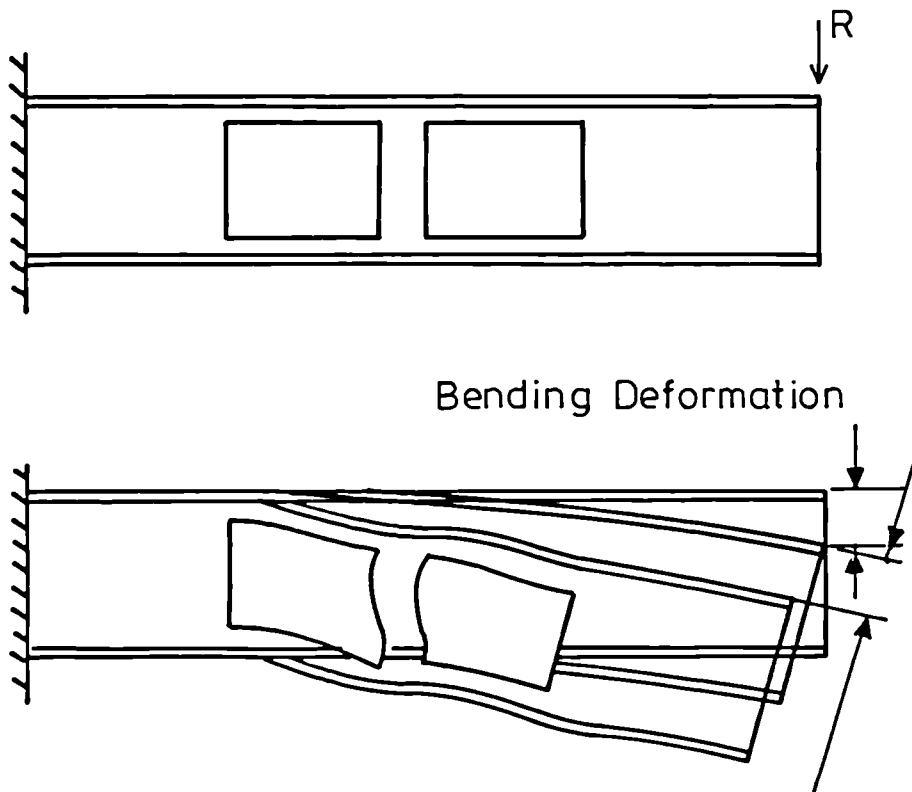
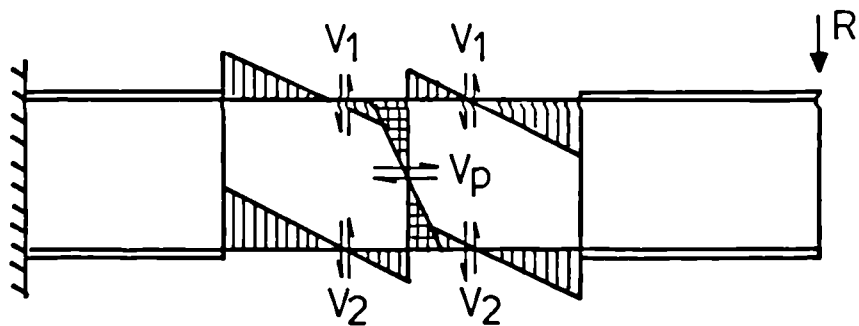


FIG. 4.9B. BEHAVIOUR OF BEAM WITH MULTIPLE OPENINGS SUBJECTED TO PURE BENDING. (From ref. 54)



Vierendeel bending and shear deformation.



Vierendeel bending and shear forces.

FIG. 4·10. BEHAVIOUR OF BEAM WITH MULTIPLE OPENINGS
SUBJECTED TO BENDING AND SHEAR.(From ref. 54)

Test Beams	$\sigma_{tee,1a}$	$\sigma_{M,1a}$	σ_{1a}	$\sigma_{tee,1b}$	$\sigma_{M,1b}$	σ_{1b}	σ_N	$\sigma_{M,N}$	τ_w
S6-2	130.	158.	288.	32.5	251.	283.	230.	360.	179.
S5-1	118.	159.	277.	30.0	247.	277.	223.	341.	148.
M4-2	95.1	130.	225.	24.5	202.	227.	184.	279.	121.
M5-1	94.5	141.	236.	24.1	219.	243.	199.	287.	118
L6-4	87.8	116.	204.	21.7	183.	205.	168.	256.	121.
L4-2	67.7	105.	173.	17.4	162.	180.	147.	215.	84.2
L5-3	70.6	100.	171.	18.1	155.	173.	141.	212.	89.9
L4-1	44.6	82.	127.	12.7	129.	142.	116.	161.	61.1

$$\sigma_{1a} = \sigma_{tee,1a} + \sigma_{M,1a}$$

$$\sigma_{1b} = \sigma_{tee,1b} + \sigma_{M,1b}$$

$$\sigma_{M,N} = \sigma_{tee,1a} + \sigma_N$$

Table 4.10 Nominal Stresses at Various Locations of the Beam (N/mm²)

using the two methods. Stresses calculated by method 2 are higher than those obtained from method 1. The calculations seem to indicate that for the shorter beams S6-2 and S5-1, yielding of the tee sections at the re-entrant corner and at the top of the flanges would cause premature failure of the sidespans.

4.7.3 Rupture of welded joints

4.7.3.1 Description

Hosain and Speirs (26) analysed this mode of failure which stemmed from a previous investigation on the optimization of the hole geometry in castellated beams (27). Rupture of the welded joint can become a possibility when its length is shortened in order to reduce the value of the secondary bending moment due to shear. They tested six expanded beams specifically designed to fail in the required mode and compared the experimental values of vertical shear corresponding to first yield along the web-weld and to fracture of the welded joints with the values of shear obtained from the statical analysis below.

However the review of the literature revealed that only one beam failed by rupture of the weld. It was reported in one of the B.S.C tests (15) and it therefore raised the possibility of this type of failure happening in the present series because of the similarity of the hole geometries. Although rupture of the welded joint was reported as being the cause of failure of the test beam, a photograph of the beam after test showed that the top flange of the beam had buckled laterally. The calculation of the stresses along the weld showed that at rupture the stresses were equal to 285 N/mm^2 .

4.7.3.2 Horizontal stresses in the welded joints

The rupture of the weld is caused by the horizontal force acting along the joint. This horizontal force V_h can be determined by considering a top segment of the beam as a free body diagram (see Fig.4.11) acted upon by the shear forces applied at the points of contraflexure and normal forces acting at the neutral axis of the tee section. These normal forces result from the external applied moment. V_h can then be calculated by taking the moments about point I in Fig. 4.11.

$$V_h = \frac{1.08D_s V}{(D_c - 2y_{tee})} \quad (4.11)$$

The average shear stress τ_w along the weld is obtained by dividing the shear force V_h by the area of the cross-section of the web:

$$\tau_w = \frac{4.31V}{w(D_c - 2y_{tee})} \quad (4.12)$$

where w is the thickness of the web.

4.7.4 Stability of the web posts

4.7.4.1 Web post buckling due to horizontal shear force

4.7.4.1.a Description

It is common practice to weld vertical stiffeners on the web of plate girders to prevent its buckling because of the diagonal compressive stresses resulting from the applied shear stresses. The stiffeners will carry the compressive stresses while the web transfers the diagonal tensile stresses. However the presence of the holes in the web of castellated beams will prevent this usual transfer of stresses.

The presence of the holes isolates the web posts. Furthermore the horizontal force V_h which has been shown to act along the welded joint

will stress the web post in bending. Therefore edge AB in Fig.4.11 will be stressed in tension whilst edge CD which is stressed in compression can now buckle laterally. Several authors have reported cases of lateral buckling of the web posts (16,21-25,30) and several methods have been proposed for predicting the value of vertical shear force which would cause failure by web post buckling. Although it has been recognized that the lateral buckling of the web posts usually occurs after yielding has started in the web, it is important to be able to predict the failure load if plastic methods are used to design the castellated beams. Hosain and Speirs (25) reported that it prematurely ended the rotation capacity of the beams.

4.7.4.1.b Calculation of the failure load

All the methods which calculate the value of shear force causing web post buckling in castellated beams treated the web post as a flexural element (45,46,53). Delesques (45) investigated the stability of the web post by assuming indefinite elastic behaviour of the material and used energy methods to calculate two values of shear force: an elastic shear force T_e which is the force at which yielding starts in the web and a critical shear force T_{cr} which is the limit of usefulness of the beam. However the application of the method to five beams tested by Bazile and Texier (24) showed wide discrepancies between experimental and calculated values of shear force. It can be safely said that elastic buckling is not likely to occur.

This view was confirmed by Aglan and Redwood (46) who analysed the problem by using a finite difference approximation and an ideally elastic-plastic hardening stress-strain curve. They presented design curves which related the critical loads to the geometry of the web

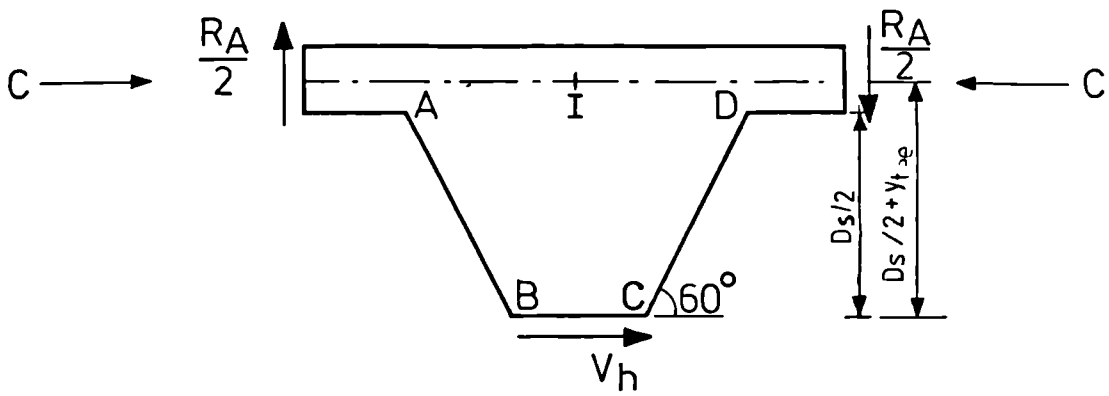


FIG. 4-11. FREE BODY DIAGRAM OF THE WEB POST.

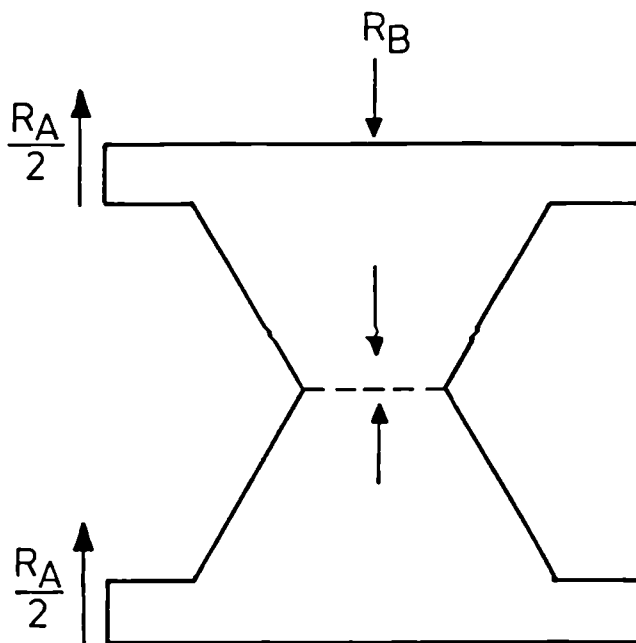


FIG. 4-12. WEB BUCKLING DUE TO COMPRESSION.

posts. From the curves provided, it can be seen that full yield of the web post is necessary before an elasto-plastic buckling mode would develop.

Finally Blodgett (53) presented an approximate elastic method of analysis which treated the web post as a tapered beam. Hosain and Speirs (25) have shown that for the two cases of web post buckling they experienced, the method was not reliable.

Three estimates of failure loads were calculated and are given in Table 4.11. The table would seem to indicate that web post buckling is a possible mode of failure but because of the wide range of predictions, no definite conclusions can be made.

4.7.4.2 Web buckling due to compression

Premature failure may occur because of web buckling caused by a load applied on the upper flange of the test beam. This load is carried as vertical shear on the beam and since the shear force is divided equally between the top and bottom tee sections, half this load applied to a unit panel segment must be transferred as compression down through the solid portion of the web into the bottom chords (see Fig.4.12). An approximate elastic analysis which treats the non-prismatic web as a column having the width of the welded joint is used to calculate the allowable load P acting on the web. P is equal to

$$P = 0.251D_s w p_c \quad (4.13)$$

The determination of p_c , the allowable compressive strength depends on the value of the column effective length chosen; several values were proposed.

The first investigations on the strength of the web posts of

Test Beams	$R_A = M_b / L_{AB}$	ref. 45			ref. 46	ref. 53
		T_e	T_{cr}	R_A	R_A	R_A
S6-2	171.	242.	149.	99.6	160.4	71.6
S5-1	118.	201.	153.	102.	134.	75.6
M4-2	86.2	184.	215.	143.	129.8	91.8
M5-1	97.	206.	157.	104.	137.	77.0
L6-4	115.	237.	149.	99.7	156.3	72.4
L4-2	62.	192.	223.	149.	128.3	95.6
L5-3	72.	216.	155.	104.	144.	76.7
L4-1	43.6	189.	198.	132.	126.3	89.6

Table 4.11 Predicted Shear Loads when Web Post Buckling is Considered
(kN)

castellated beams were carried out in refs. 15 and 16. Several of the test beams failed by web buckling over a support or under a load-point. An effective length factor of 0.75 which was later reduced to 0.5 in ref.16 was used. The permissible stresses which were obtained from BS 449 gave safety factors between 2.0 and 2.4. Hosain and Speirs (25) who assumed the web post column to be hinged at both ends calculated safety factors varying between 1.66 and 2.78 for the three beams which exhibited compression buckling of the web post. If both ends of the web post are assumed to be fixed as suggested in ref. 16 the safety factors of two of the beams become equal to 0.66 and 0.78.

Similar calculations were carried out for the specimens of the present series in order to evaluate the possibility of their failing by buckling of the web post. Values of effective length factors of 0.5 and 1.0 were used to calculate permissible compressive stresses from BS 449 and B/20. Table 4.12 which gives a summary of the predicted loads shows the wide variation in the range of values obtained. However, because the beams of refs. 15 and 16 were made from British castellated sections, the predictions obtained by using an effective length factor of 0.5 and the permissible stresses of BS 449 would seem reasonable reference values. Therefore beam S6-2 which will carry the highest load would probably fail because of web buckling at a load point. It was therefore decided to provide stiffeners not only for beam S6-2 but for all the beams of the present series.

Beam	$k_l = D_s$						$k_l = 0.5 \times D_s$					
	k _l	1/r _y	BS 449		B/20		k _l	1/r _y	BS 449		B/20	
			P _c *	P [†]	P _c	P			P _c	P	P _c	P
S6-2	406.	194.	28.	41.3	47.	69.3	203.	97.1	104.	153.	148.	218.
S5-1	356.	176.	34.	42.5	57.	71.3	178.	88.	123.	154.	167.	209.
M4-2	305.	142.	51.	58.	82.	93.3	152.5	71.1	169.	192.	203.	231.
M5-1	356.	175.	34.	42.8	57.	71.7	178.	87.6	123.	155.	168.	211.
L6-4	406.	194.	28.	41.3	47.	69.3	203.	97.1	104.	153.4	148.	218.
L4-2	305.	140.	53.	61.1	84.	96.8	152.5	70.2	172.	198.2	205.	236.
L5-3	356.	175.	34.	42.7	57.	71.6	178.	87.7	123.	154.5	167.	210.
L4-1	305.	146.	49.	54.2	80.	88.5	152.5	73.1	163.	180.4	199.	220.

* P_c = allowable compressive stress in N/mm² ; †P = load causing web buckling in kN

Table 4.12 Compressive Loads Causing Web Buckling

4.7.5 Failure due to the formation of a collapse mechanism

4.7.5.1 Introduction

Two different collapse mechanisms can develop in the specimens of the present series under the four-point loading system of the test rig: a flexural mechanism in the central span under pure moment loading has been described when the design against lateral buckling was discussed and a Vierendeel mechanism which can form in the sidespans under bending moment and shear force. The two modes of failure are shown in Figs. 4.13 and 4.14.

4.7.5.2 The Vierendeel mechanism

This mechanism is characterized by the formation of plastic hinges at the corner of the holes which then deform in the manner of the parallelogram. Each plastic hinge is the result of the complete plastification of the tee sections above and below the holes. Halleux (23) reported that this mechanism developed simultaneously at all the openings in the span subjected to a shear force of high and constant magnitude. This type of mechanism is more likely to develop in beams of short span and long web weld. When the length of the weld joint decreases, so does the magnitude of the secondary bending moment and the stresses become closer to those produced in a full bending situation. Short spans carry a higher allowable load and shear can become the dominant force. It is observed that expanded beams with closely spaced openings or shallow holes would fail predominantly by overall moment collapse.

The failure load for the Vierendeel mechanism was first calculated by Halleux (23). His method was based on the kinematic theorem and gave an upper bound solution. The mechanism assumed is shown in Fig.4.15. The

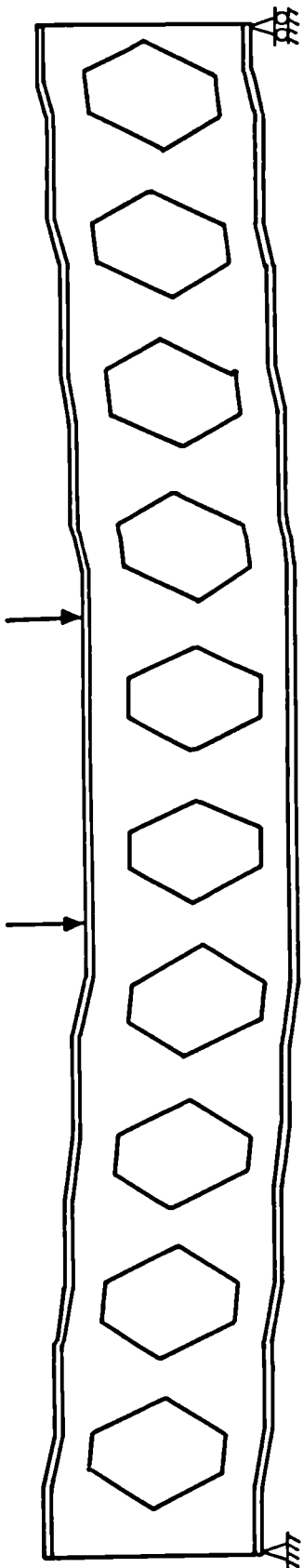


FIG. 4.13. VIERENDEEL MECHANISM

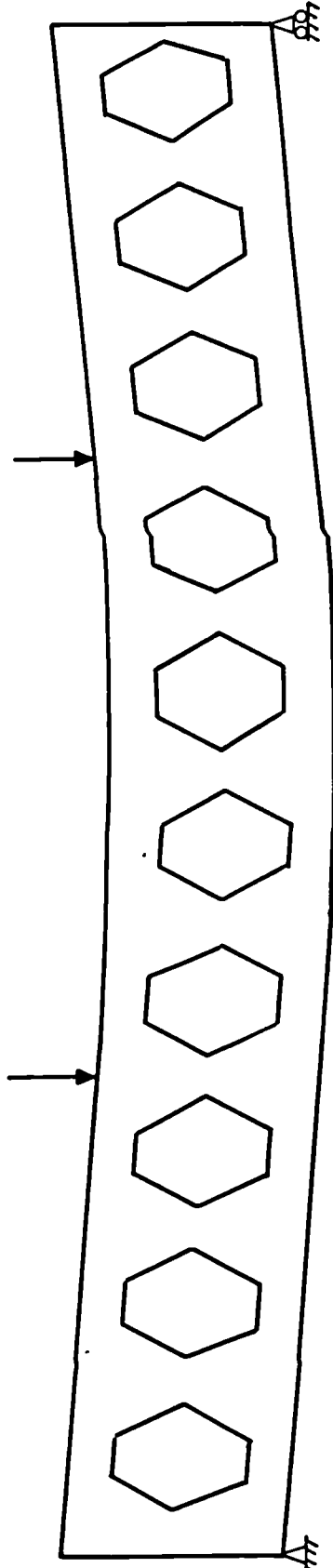
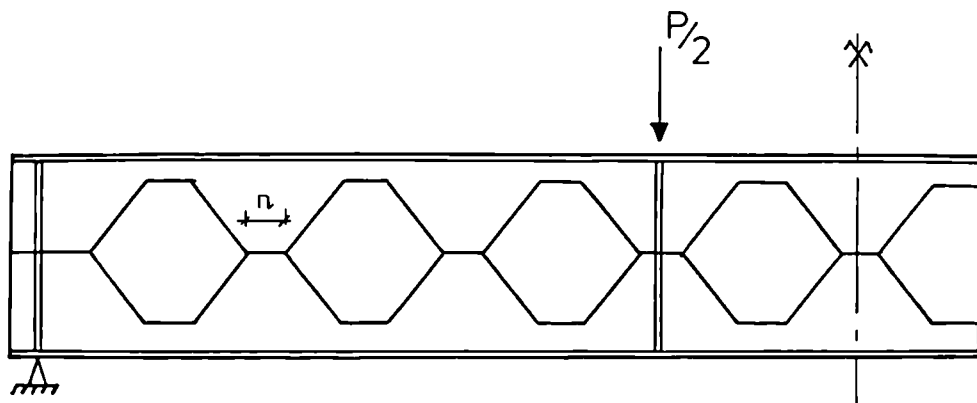
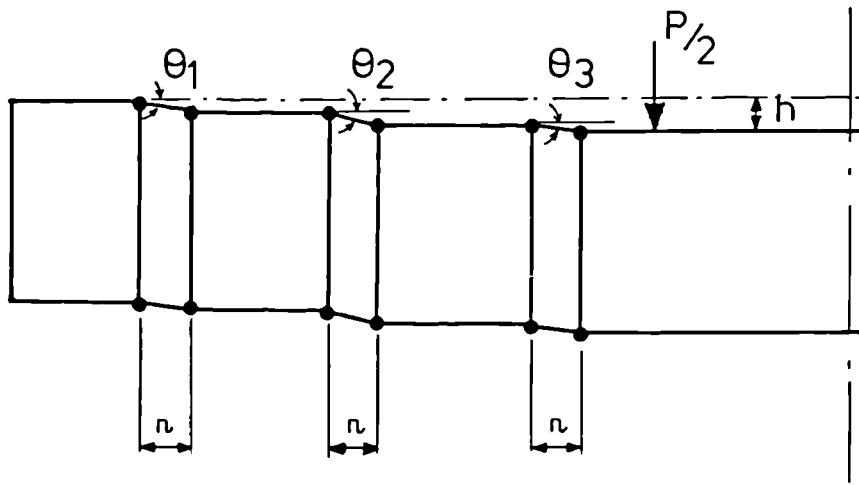


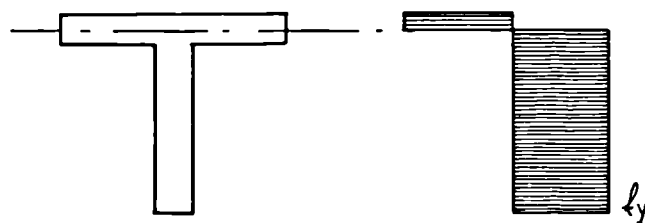
FIG. 4.14. FLEXURAL MECHANISM.



(a)



(b)



(c)

FIG. 4-15. HALLEUX'S SHEAR FAILURE MECHANISM.

failure load P is calculated by equating the internal work due to rotation in the hinges to the work done by the external forces.

$$P = \frac{8S_{tee}p_y}{2n} \quad (4.14)$$

where S_{tee} is the plastic modulus of the tee section
 p_y is the nominal yield stress
 n is the length of the welded joint

The effects of shear and axial forces on the plastic moment of the tee section were neglected by Halleux. The failure load will therefore always be underestimated when the ratios N/N_p and τ/τ_y respectively are higher than 0.15 and 0.5 (N and τ are the axial and shear force acting on the tee section and N_p and τ_y are their ultimate values). In the case of Halleux's results, because the ratios N/N_p and τ/τ_y were small the test results did not indicate any serious overestimate of the failure load whereas Halleux's method used in Hosain's investigation (25) gave predicted loads vastly different from the experimental results.

Inclusion of the axial force effect, which is in many cases the major factor which influences the magnitude of the plastic moment, was considered by Hope and Sheikh (52). Their method which refers to the analysis of a single hole, is based on the determination of the capacity of the tee section to resist the forces to which it is subjected when the beam is under external loading. It consists of plotting the interaction curve for the tee section of the castellated beam to be analysed. The interaction curve is obtained by varying the location of the neutral axis and plotting the resulting values of moment and normal force. When compared with the test results reported in refs. 21, 22 and 25 the predicted failure loads were in good agreement with the test results. The two methods described above were used to calculate

estimates of the shear force which would create a Vierendeel mechanism and a comparison between the various predictions is given in Table 4.13. The table shows that the test beams of the present series are unlikely to develop this form of failure.

Sherbourne and Van Oostrom (82) took into account the interaction between moment, shear and axial force. They used the flexibility method of analysis in order to obtain deflection characteristics and collapse modes of full beams. Although safe solutions for the collapse load were obtained, their method is not easy to use.

A similar mechanism has been shown to develop in beams with a single hole in the web subjected to shear loading (72,73,75) and methods for predicting failure loads in which the effect of axial and shear force were included have been proposed (12,64,74).

It is highly unlikely that castellated beams, which are usually used when light loads are carried over long spans, will fail in a Vierendeel type of mechanism. Furthermore castellated beams of the British type which have closely spaced holes will be less prone to develop this mechanism. However, heavy shear forces will be transmitted in the case of test beams S6-2 and S5-1 and although Table 4.13 showed that the forces necessary to produce the mechanism will not be reached, the approximations used in the derivations of these forces made the failure by Vierendeel mechanism a possibility.

Test Beams	$R_A = M_b / L_{AB}$ (kN)	ref. 23	ref. 52	
		R_A (kN)	R_A (kN)	N/N_p
S6-2	171.	192.	165.	0.841
S5-1	118.2	166.	126.	0.862
M4-2	86.2	161.	109.	0.881
M5-1	97.	168.	125.	0.863
L6-4	115.1	194.	155.	0.856
L4-2	62.	166.	105.	0.887
L5-3	72.	173.	124.	0.869
L4-1	43.6	172.	97.	0.893

Table 4.13 Predicted Failure Loads when Shear Mechanism is considered

CHAPTER 5

TEST RIG

5.1 Test set-up

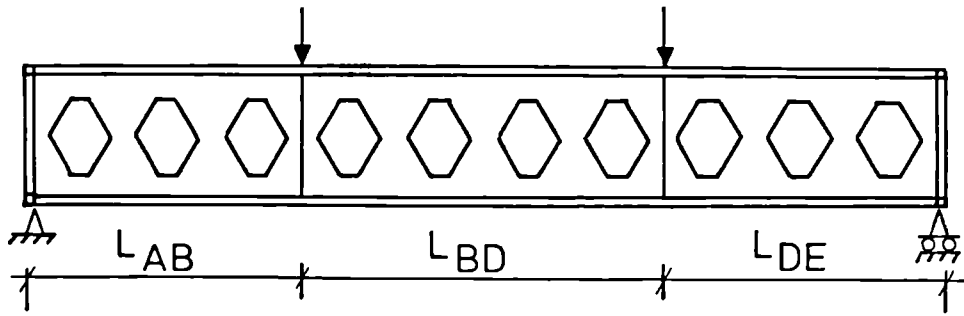
The eight castellated beams chosen for the present series were tested on a laboratory strong floor which could accommodate beams of up to nine metres long. The test rig used had been designed, built and commissioned for a D.Tp research programme (83).

The loading arrangement shown in Fig.5.1 was used. It produced a zone of constant moment and zero shear between the intermediate loading points (Fig.5.1.c). This condition of equal and opposite end moment is the worst possible case of loading for lateral-torsional buckling. The arrangement chosen at the support points provided simply supported type boundary conditions. The beam was free to bend or warp about the major and minor axes of its cross-section, but deflections in both the lateral and transverse directions were prevented, thus allowing the buckled compression flange shape of Fig.5.1.b. The support arrangement which is described in detail below ensured that the test rig was structurally statically determinate.

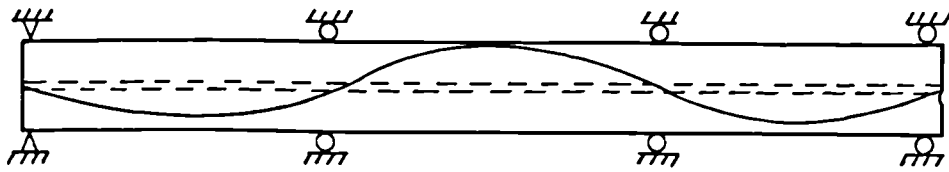
5.2 Loading system

5.2.1 Description of the transfer of load

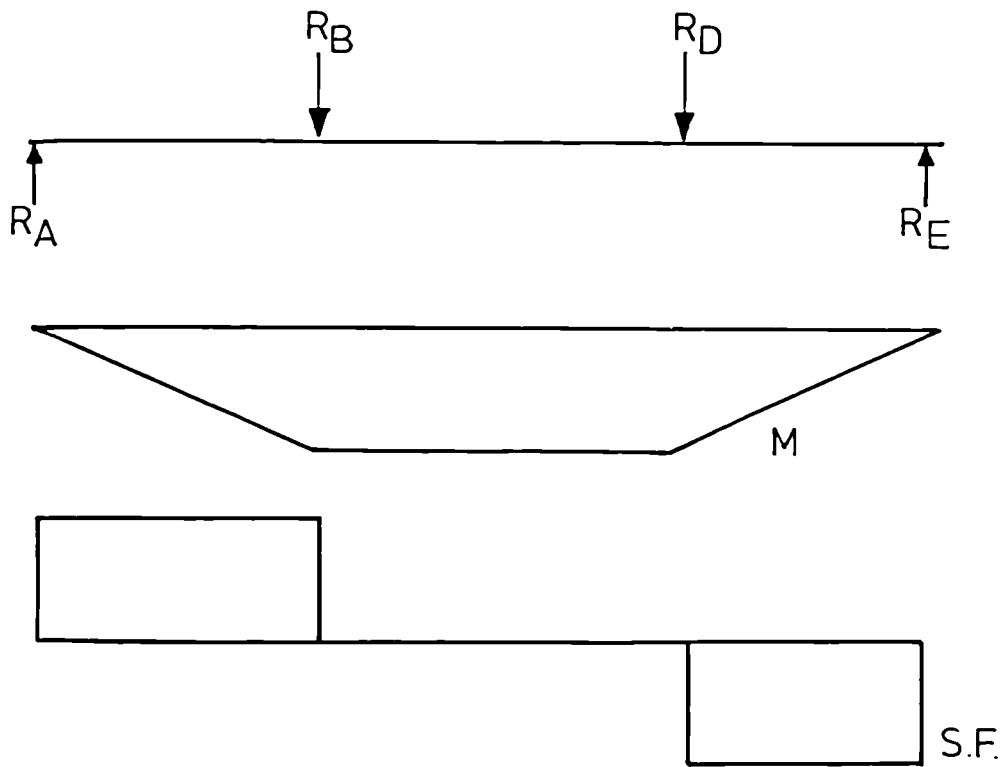
A schematic arrangement of the test rig is shown in Fig.5.2 while Plate 5.1 shows a beam of the present series in the test rig after the completion of a test. Although the test beams were supported in the vertical plane at points A and E, their vertical movement was prevented at points C and E. This was due to the fact that only one jack was utilized in the test rig. This jack was positioned at end A of the test rig. The load applied by the jack at point A induced two reactions at points C and E. The reaction at point C was provided by the central



a) Elevation



b) Possible buckling mode



c) Bending moment and shear force diagram.

FIG.5-1. CASTELLATED BEAM UNDER TWO POINT LOADING.

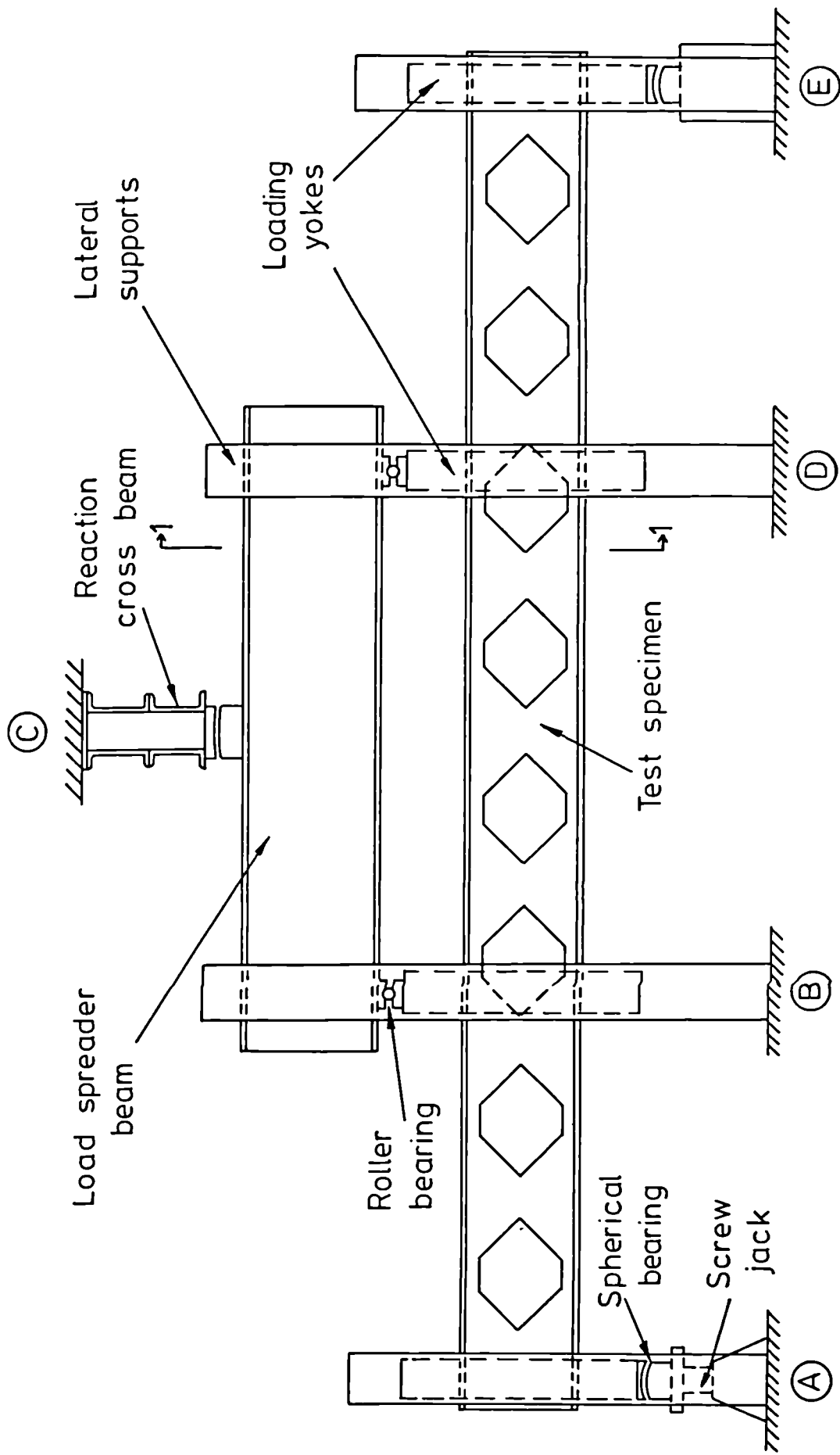


FIG. 5.2. SCHEMATIC ARRANGEMENT OF TEST RIG.

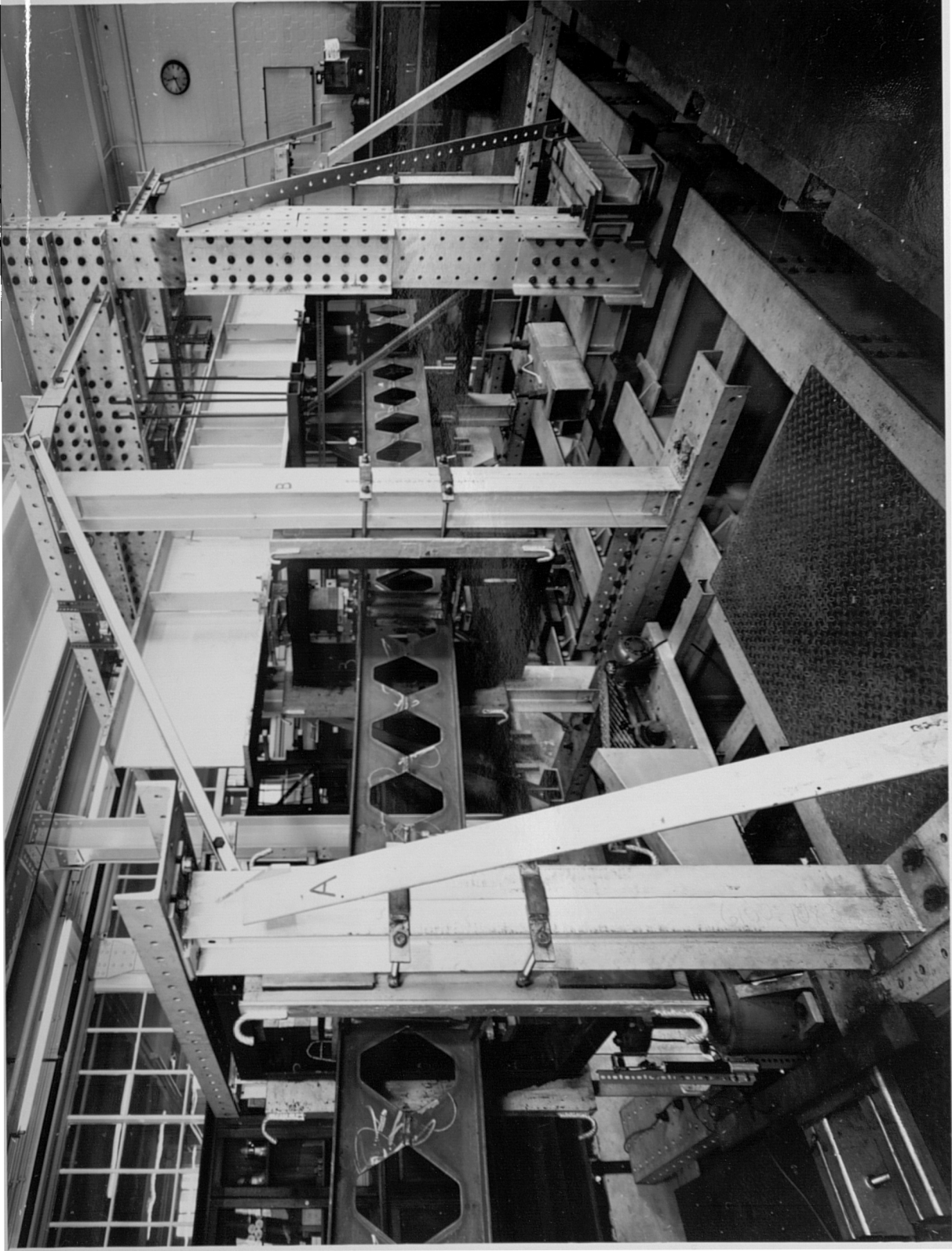


PLATE 5.1 TEST RIG

portal frame through a spherical bearing seated between the portal frame and a spreader beam. This reaction in turn induced the reactions at points B and D through the spreader beam, thereby producing the loading arrangement of Fig.5.1.

5.2.2 Jack system

The jack used was a screw jack of the worm gear type. It had a capacity of 500kN and a possible total lift of about 300mm (12in.). This loading system was preferred to the use of a hydraulic one because it allowed the behaviour of the test beam to be monitored continuously up to and well beyond the point of maximum load.

The servo-controlled straining system which incorporated the screw jack is shown in Plate 5.2. It was considered necessary from considerations of test rig stiffness when the test beam sheds its load after failure. The jack which was driven by a 1/2 H.P. motor via a 1500:1 reduction gear box is shown in Plate 5.3.

The rate of straining of the test beams was determined by the rate of lift of the jack which was controlled throughout the test by a variable speed V-pulley belt drive and a variac device. Any rate of straining varying from a near zero value to the maximum value which depended on the stiffness of the beam under test could be achieved.

5.3 Support system

5.3.1 Lateral support

The prevention of lateral buckling at the supports A, B, D and E was realised by enclosing the test beam in a rectangular box frame made of channel sections (Fig.5.3). The boxes rested on load cells at points A and E and were connected to the spreader beam at points B and D. One

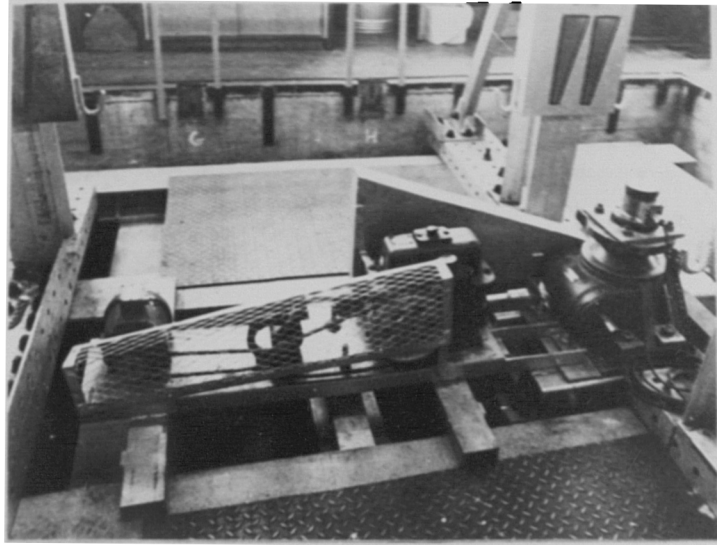


PLATE 5.2 JACK DRIVING MECHANISM

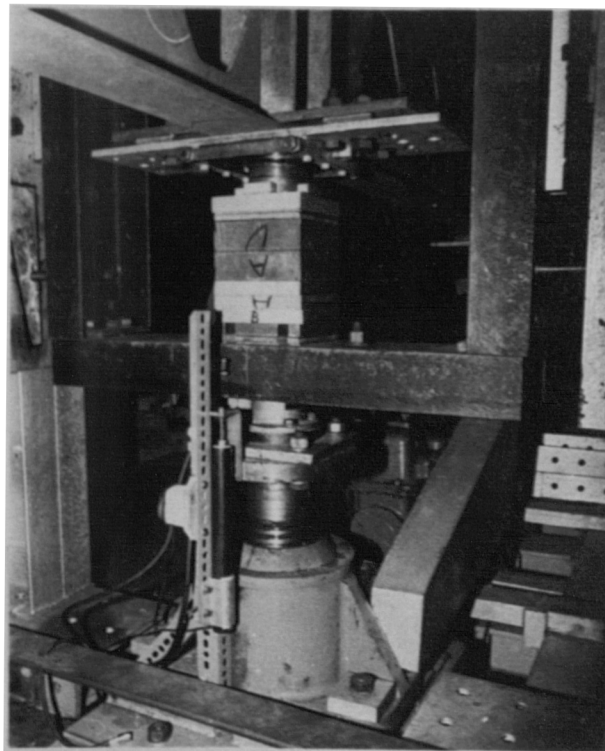


PLATE 5.3 JACK AT END SUPPORT A

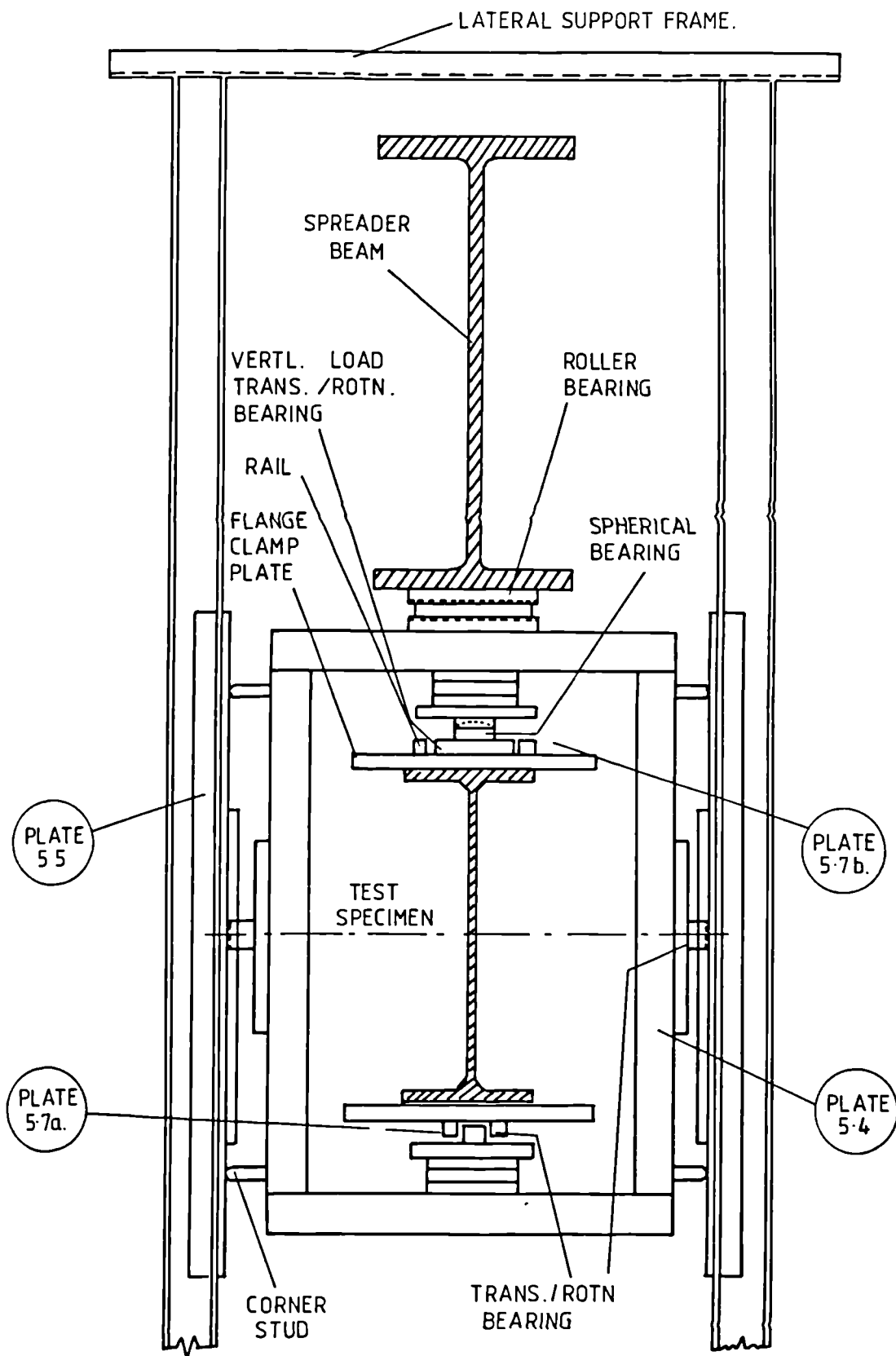


FIG. .5.3. SECTION 1-1 OF FIG 5.2: DETAILS OF TEST GIRDER SUPPORT BOX FRAME AND LATERAL SUPPORT FRAME.

bearing and four studs were attached to each of the two channels which formed part of the box. The bearing and the studs bore against a plate clamped onto the inside of the support frames. The support frames can be seen in Fig.5.2 and partly in Plate 5.1 which shows support frames A and B. One stud was located at each corner of the box thereby preventing lateral movement of the box and consequently that of the beam inside the box. The bearing between two rails was clamped to the plate and allowed the vertical movement and rotation of the box about a horizontal lateral axis passing through the two bearings, one on each side of the box. This arrangement completely prevented the boxes from moving laterally as well as rotating about the vertical and longitudinal axis of rotation of the box frame. Plate 5.4 show the bearing and the four studs on the side channel of one of the boxes whilst the inside plate of the support frame on which bore the studs and the bearing can be seen in Plate 5.5 . The vertical loads were transmitted through bearings at the top of the boxes at B and D and at the bottom of the boxes at points A and E.

5.3.2 Transfer of load within the boxes

Within the box frame, the flanges of the beam were each clamped by a plate, the flange clamping plate (see Fig.5.3) onto which were welded two rails. These rails, along with the plate surface between them, formed the base plate for the two types of bearing used. These bearings could rotate and translate, thereby permitting the boxes to move relative to the beams.

The first type which was a spherical bearing made of two components was used to transmit the vertical loads. They were placed at the bottom of the boxes at points A and E and at the top of the boxes at points B and D. A polytetraflouroethylene/stainless steel interface was provided

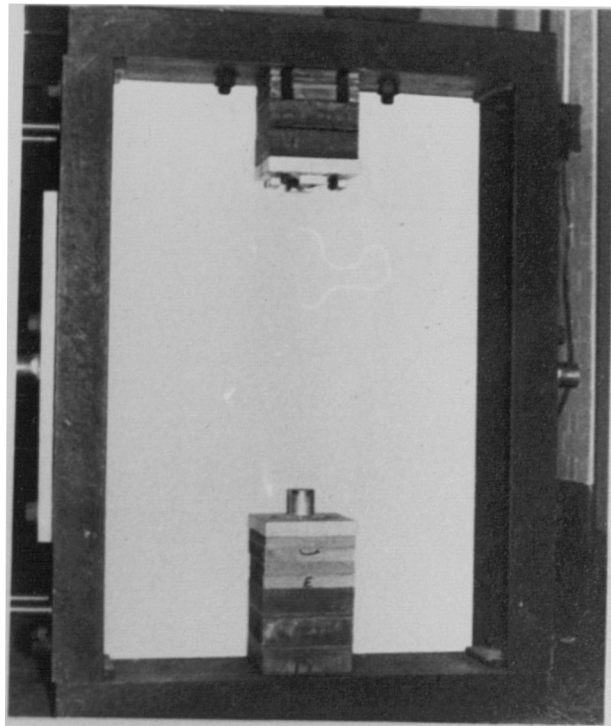
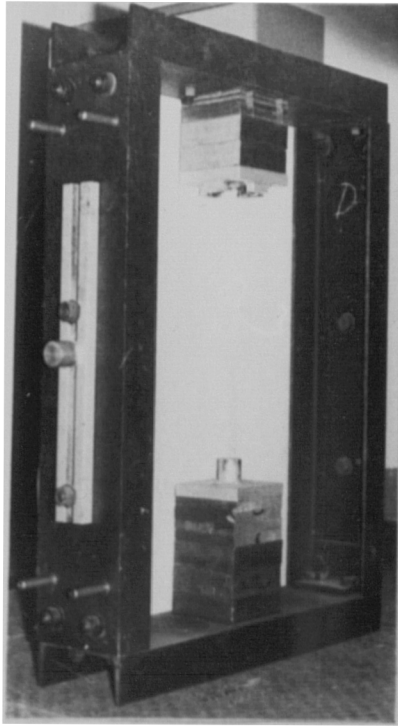


PLATE 5.4 SUPPORT BOX FRAME AND SIDE WALL WITH CORNER STUDS

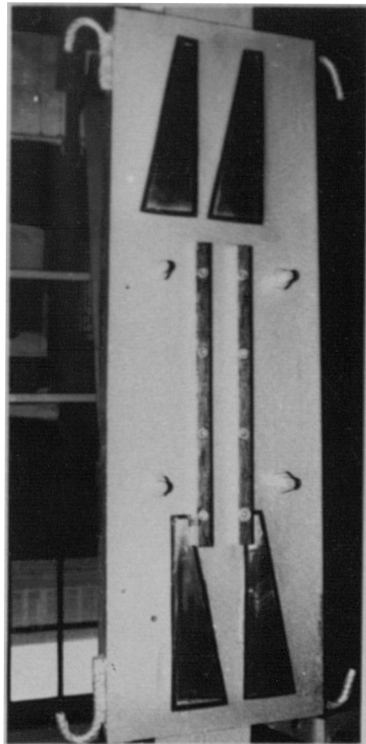


PLATE 5.5 LATERAL SUPPORT PLATE

between the bearing surfaces to allow for translational movement of the beams. The concave faced component of the spherical bearing was attached to the surface of the plate clamped to the test beam while the convex faced component was attached to a plate clamped inside the box thus allowing any rotational movement to take place.

The other type of bearing was used where no vertical forces were transmitted to the beam. The bearing was welded to a plate screwed to the box. It could slide and rotate between the rails welded onto the plate attached to the flange of the beam. Plate 5.6 shows the bearing in relation to a box at point A whilst Plate 5.7 shows the details of the two types of bearing. Plate 5.3 which shows the jack under the box at end support A also shows the bearing between the flange clamping plate and the box.

5.3.3 Vertical supports

Two spherical bearings were inserted between the bottom of the box frame and the supports at points A and E whereas roller bearings were positioned between the top of the box frames and the spreader beam at points B and D. A spherical bearing was situated between the top of the spreader beam and the central portal frame enabling the transfer of load from the jack to the test beam. The spherical bearing can be seen in Fig.5.3. Its importance can be better appreciated in Plate 5.8.a while Plate 5.8.b gives a close-up view of the bearing. The cylindrical bearing can be partially seen in Plate 5.7.a while a side-view of the same bearing is given in Plate 5.9.

The type of bearing chosen to transmit the load throughout the duration of the test ensured that the deformation of the test beams was independent of any flexural or torsional deformation of both the strong

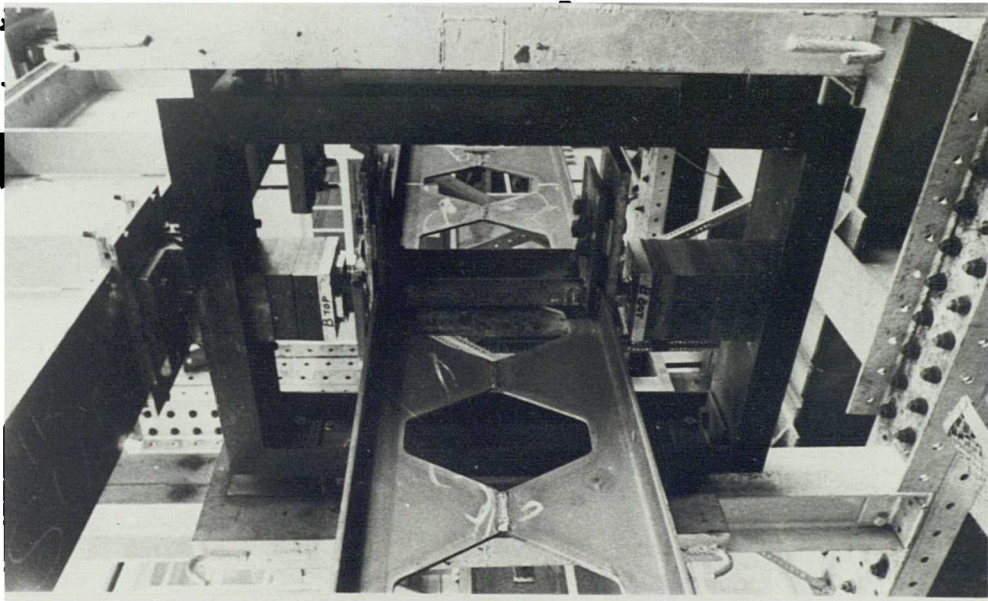
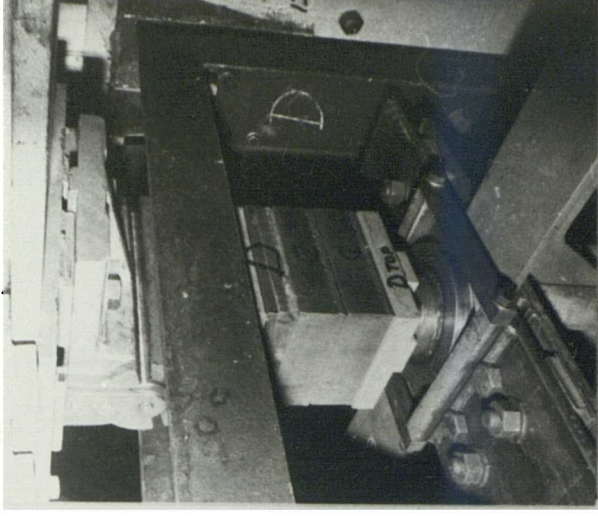
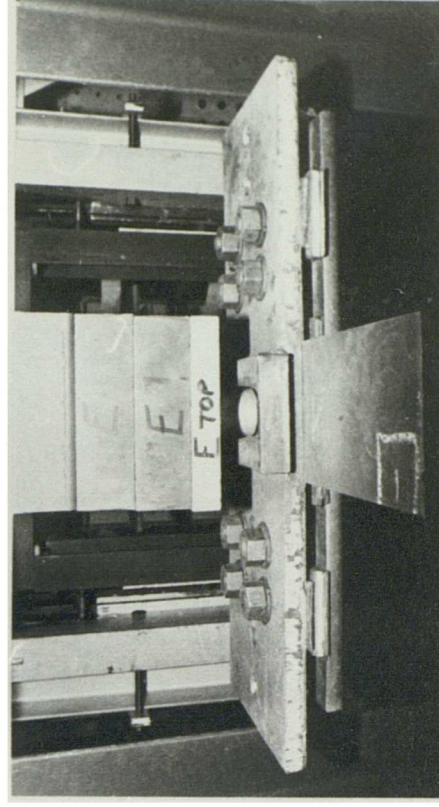


PLATE 5.6 SUPPORT BOX FRAME ENCLOSING THE TEST BEAM



a. Vertical load is transmitted



b. No vertical load is transmitted

PLATE 5.7 BEARINGS

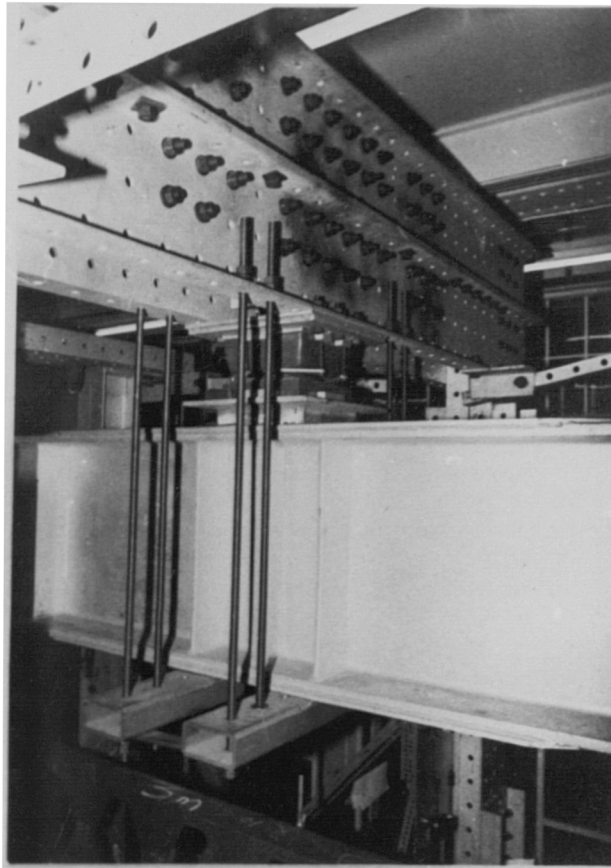


**PLATE 5.8.a SPHERICAL BEARING BETWEEN PORTAL FRAME
AND SPREADER BEAM**

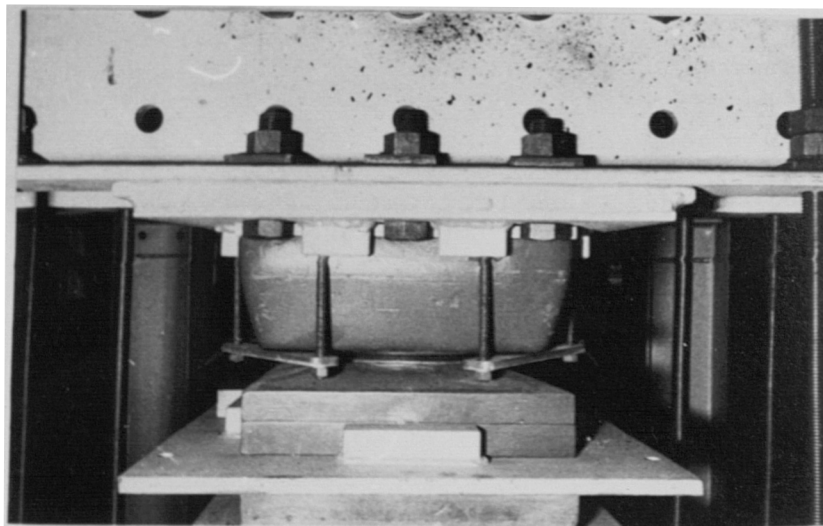


PLATE 5.8.b SPHERICAL BEARING

floor and test rig.

5.3.4 Longitudinal girder movement

The translational movement of the test beams in the longitudinal direction was prevented by stopping the translation of the bearings directly above and below the flanges at end support A. This was achieved by simply welding rails across the flange clamping plate. This arrangement of supports avoided any undesirable side thrust onto the jacking device.

5.3.5 Summary

Simply supported type boundary conditions have been provided to the test beams. The test beams could warp but not twist within the boxes at each support. The boxes were able to move vertically and rotate about a lateral horizontal axis, thus allowing the shortening of the spans when the test beam deflected under loading.

5.3.6 Structural bracing

The structural bracing elements can be seen clearly in Plate 5.1. The four support frames which were linked together by ties made of angle sections were braced to the central portal frame which provided longitudinal stability for the test rig. The support frames were in turn tied to the strong floor beams for lateral stability. The four support frames could be moved to several positions on the strong floor in order to cater for the various lengths of the test beams.

5.3.7 Load bearing stiffeners

The calculations of chapter 4 showed that load bearing stiffeners were required at the support points in order to prevent early failure of the test beams. In order to minimize the costs of the testing programme, re-usable stiffeners were used. They were made of channel section onto which flat bases were welded. Sixteen stiffeners were made, eight for the test beams 458 and 534 and eight for the test beams 609. One stiffener was positioned on each side of the web at points A, B, D and E. Although the stiffeners can be seen in Plates 5.1 and 5.6, Plate 5.10 gives a closer view of them.

5.4 Loading of the beams in the test rig

The transfer of load from the jack to the test beam through the test rig has just been described. The process of placing the beam into position in the test rig and the assembling of the various components enabling the transfer of load will be described now. There were two phases in the preparation of the test beams. A first phase outside the test rig where part of the components were fixed to the beam and a second phase when the beam was loaded in the test rig and the final adjustments took place.

First the three spans AB, BD, and DE were measured on the beam to give the point of application of the loads and thus that of the stiffeners which were placed on each side of the web. The flange clamping plates were then laid across the top and bottom flanges and screwed to the bases of the stiffeners. Boxes were finally put into position at points A, B and D together with the spherical bearings which are shown in Plate 5.7. The beam was now ready to be moved in the test rig.

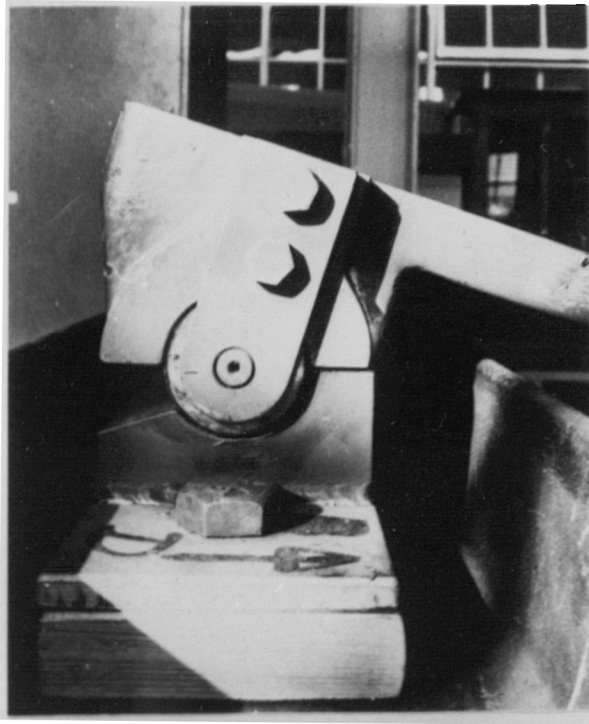


PLATE 5.9 CYLINDRICAL BEARING

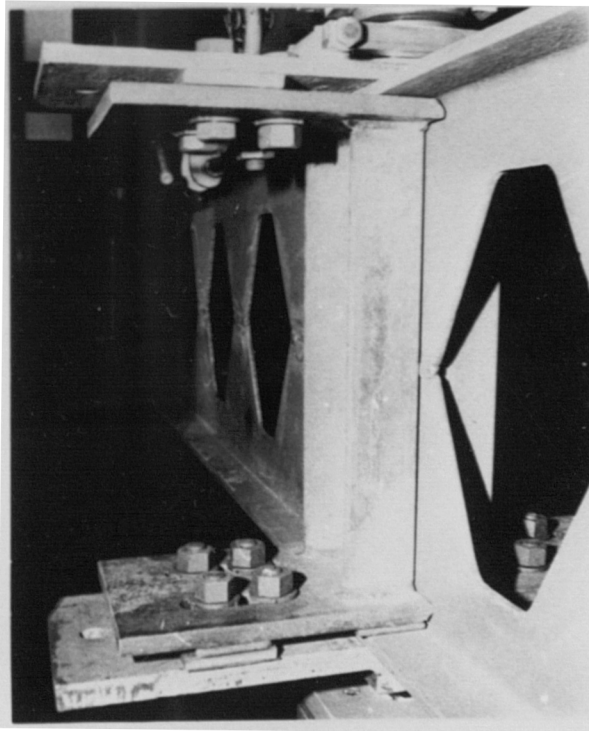


PLATE 5.10 LOAD BEARING STIFFENER

Once the beam was in position in the test rig, the box of end support E was fixed, the cylindrical bearings between the spreader beam and the boxes at B and D were then attached (see Plate 5.9) and finally the studs on each side of the boxes were fixed. The beam could therefore be instrumented.

5.5 Instrumentation

5.5.1 Introduction

The overall behaviour of the eight castellated beams chosen for the present series was observed. Particular attention was given to the middle span under pure bending which was likely to twist and deflect sideways. The displacements of the test beams were monitored throughout each test and the possible distortion of the web posts was looked for. The load applied by the screw jack at the end support A and the resulting reaction at end support E were measured using two Davy load cells of respectively 500 kN and 1000 kN capacity.

5.5.2 Measurement of the displacement of the beams at mid-span

The three components of the displacement of the beams were measured at the mid-span between points B and D, point C on Fig.5.2. The three components were:

1. vertical displacement of the top and bottom flanges of the beams.
2. lateral displacement of the same points.
3. angle of twist of the cross-section.

The deformations of the test beams were measured using an arrangement of wires, pulleys and transducers. Three linear variable displacement transducers (L.V.D.T) were fixed on a board which was set on a plane perpendicular to the plane of the web of the test beams. The

length of the stroke of each transducer was 250mm . Steel wires linked the tops of each transducer via the pulleys fixed on the board to a lightweight frame glued onto the beam under test. Plates 5.11 and 5.12 respectively show photographs of the board with the pulleys and transducers and of the lightweight frame. The use of the lightweight frame fixed onto the beam prevented any cross-sectional distortion during buckling from affecting the transducers readings. As the load was applied, the beam started deflecting downwards, sideways and twisted. The distances between the initial position of the beam and the pulleys changed, thereby altering the lengths of the wires. The transducer probes were therefore pulled upwards or lowered by the change of the distance between the pulleys and the lightweight frame. Because it was not possible to predict before each test the direction in which each test beam could move, the transducer probes were set halfway up so that the maximum displacement that each transducer could record was approximately half the stroke length, i.e. 125mm . Although the displacement of the top flange of the slender beams L4-1, L4-2 and L5-3 would go beyond the maximum that could be recorded by the transducers, it was felt that by that time the beams would be showing large deformations and that the tests would therefore be near completion.

The electrical signals from the three transducers and the two load cells were recorded on a data logger at preset intervals of time. The data logger used was an IMP DATA LOGGER which was programmable and microprocessor based. It had facilities for recording data on up to 128 channels (only 10 were needed in our case). The output was given in kN and mm on a paper roll strip for immediate reading and on paper tape via a paper tape punch which was connected to the data logger. The data obtained was then fed directly in a computer for complete test analysis.

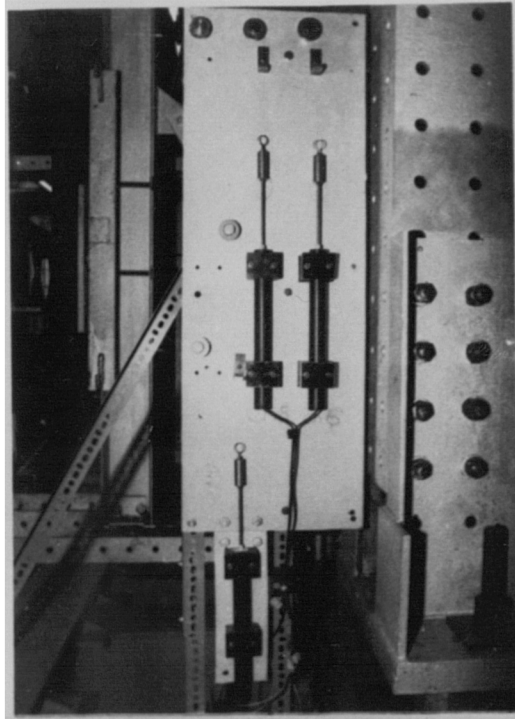


PLATE 5.11 TRANSDUCERS AND PULLEYS ARRANGEMENT

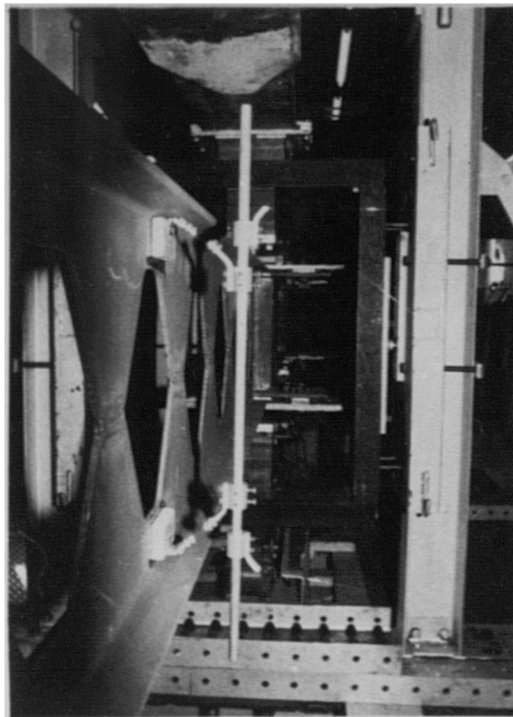


PLATE 5.12 LIGHTWEIGHT FRAME

Plate 5.13 shows the data logger set-up whilst Fig.5.4 shows how by using simple trigonometry the deflections in the vertical and horizontal directions plus the angular distortion were evaluated.

A transducer (L.V.D.T.) which had also a stroke length of 250mm was recording the lift of the jack at end support A. Plate 5.3 shows the transducer fixed on to the jack. Both the transducer and the load cell recording the applied load at support A were connected via the data logger to an X-Y plotter which gave visual indication of the straining of span AB of the beam during the test. From the graphs direct information was obtained on the yielding, failure and unloading of each beam during the test.

The calibration of the transducers was carried out before the testing programme started and after each set of beams were tested (L,M,S). In all they were calibrated four times and very little variation of the calibration factors was noticed. The two load cells were tested only twice, once before the testing programme and once after its completion. Here also very little variation of the calibration factors were recorded

5.5.3 Measurement of the distortion of the web posts

5.5.3.1 Method of measurement

The possibility of web post distortion was raised in previous chapters when the influence of the presence of the holes in the web of castellated beams was discussed in relation to their lateral-torsional buckling strength. Although deformation of the web posts of beams which failed in a purely lateral-torsional mode was never reported by previous authors who were mostly concerned with in-plane behaviour, it was decided to measure the out-of-plane deflection of some of the web posts

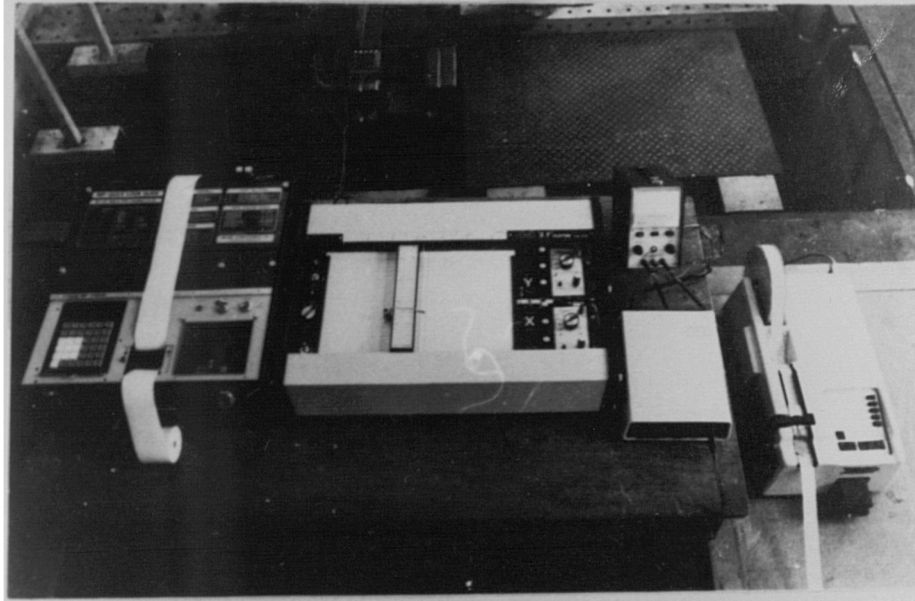
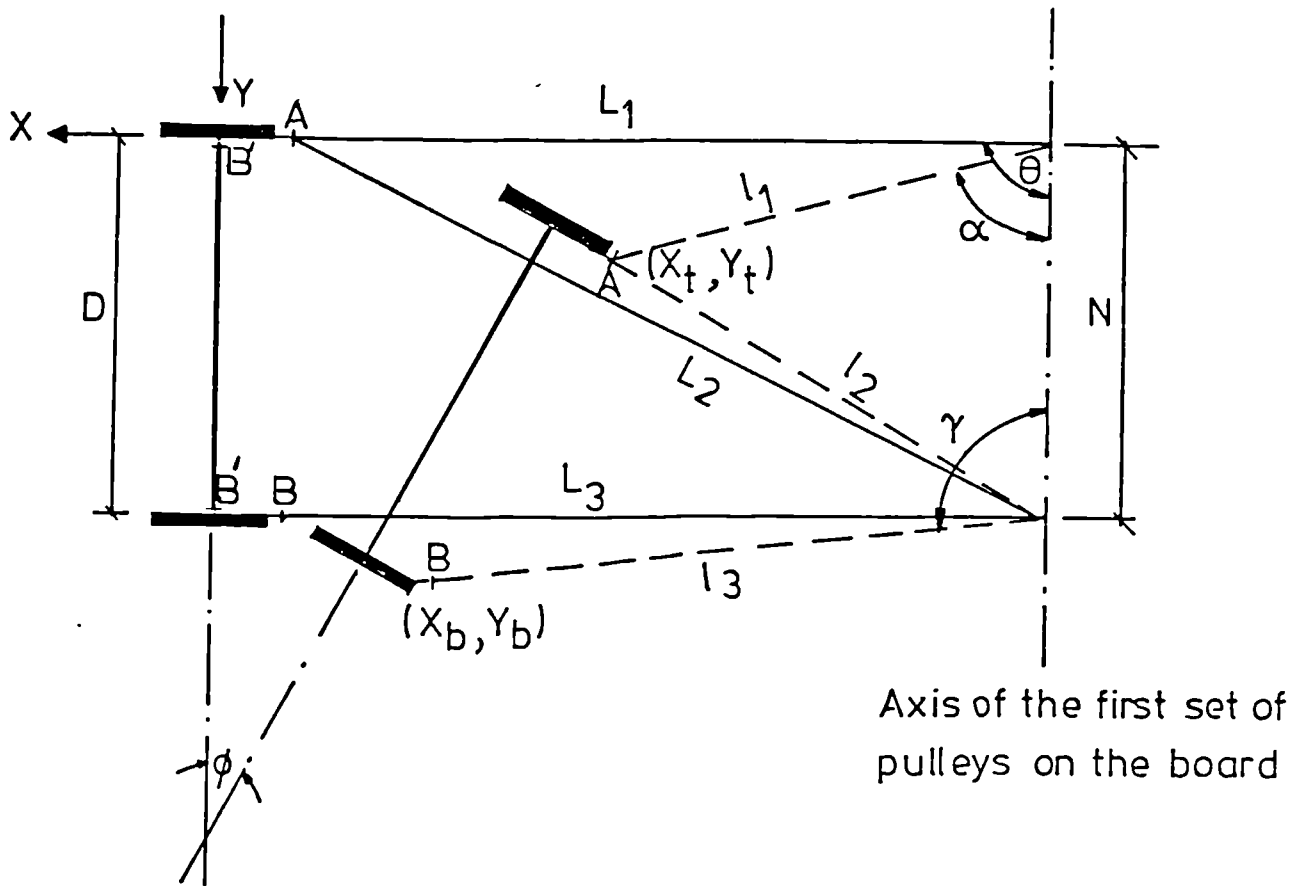


PLATE 5.13 DATA LOGGING ARRANGEMENT



Geometry of the deflected beam at mid-span

$$\theta = \text{Arcos } (N^2 + L_1^2 - L_2^2)/2.N.L_1$$

$$\alpha = \text{Arcos } (N^2 + l_1^2 - l_2^2)/2.N.l_1$$

$$\gamma = \text{Arcos } (N^2 + l_2^2 - l_1^2)/2.N.l_2 + \text{Arcos } (l_2^2 + l_3^2 - D^2)/2.l_2.l_3$$

$$X_t = l_1 \sin \alpha - L_1 \sin \theta$$

$$Y_t = l_1 \cos \alpha - L_1 \cos \theta$$

$$X_b = l_3 \sin \gamma - L_1 \sin \theta$$

$$Y_b = -l_3 \cos \gamma + N - L_1 \cos \theta$$

$$u = (X_t + X_b)/2$$

$$v = (Y_t + Y_b)/2$$

$$\phi = \text{Arctan } ((X_t - X_b)/(Y_t - Y_b))$$

Practical consideration required that points shown as point A and B were actually situated at points A' and B'. This introduced a small error in the calculations.

FIG. 5.4 MID-SPAN DEFLECTIONS.

in order to verify if any distortion could be noticed.

Because of the availability of the instrumentation in the surveying section of the Civil Engineering Department of the University of Sheffield, photogrammetric techniques were used to provide the profile of the distorted test beams at various sections along their length.

The basic principles of photogrammetry can be found in ref.84 and its application to various subjects are described in ref.85. An example of the use of the technique to structural engineering was reported by Scott (86) who measured the structural deformations of a steel model box girder bridge.

5.5.3.2 Description

The principles of the method were those used in aerial photogrammetry. Basically it involved analysing photographs taken by a WILD C40 stereometric camera. This instrument consisted of a stable base tube with a camera fixed at each end, symmetrical about the centre of the tube. The axes of the cameras were accurately set parallel to each other, perpendicular to the base tube and 0.40m apart. The tube with the cameras rested on a tripod which was positioned at a fixed distance from the test beams. Because of the presence of the central portal frame and the support and box frames at point D, only half of span BD could be covered by the cameras. This portion of the test beams was painted white so that black crosses could be drawn on the web posts and flanges and used as targets when analysing the photographs.

Three test beams were instrumented; these were beams L4-2, L5-3 and L6-4. Several crosses were drawn on a vertical line on the web posts and on the edges of the top and bottom flanges of the test beams. Additional crosses were drawn around the edges of the hole next to the centre of

span BD. All the crosses were randomly spaced (the next chapter will give the position of the crosses on each beam). Each camera took a photograph on a glass plate at chosen load increments. The plate size was 65x90mm and the picture format was 60x80mm. The glass plates were then developed accurately in a constant temperature to avoid contraction or expansion of the plates. Each pair of plates corresponding to a load level were analysed on a STEKO 1818 stereocomparator. This instrument measured the X and Y coordinates of the targets on the face of each photograph. The output was given on paper tape which was read as data into a computer for complete analysis of the movements of the points chosen as targets. The results of this analysis are given in the next chapter. The accuracy of the measurements was about $\pm 0.250\text{mm}$.

5.6 Test procedure

The loading system and the instrumentation allowed the test beams to be tested on a continuous basis without pause and prevented any relaxation from occurring. The relevant deformations and loads were continuously recorded on the data logger. The full load-deformation range (including unloading of the specimens) of each test beam was accurately monitored.

The rate lift of the jack controlled the rate of straining of the beams throughout each test. The rate of lift was kept constant at about 0.20mm/min even after reaching the maximum load except for beams L4-2, M4-2 and S6-2. Chapter 6 will give more details about the speeds achieved in each test and the reasons for altering them during the tests.

CHAPTER 6

RESULTS OF THE TEST PROGRAMME

6.1 Introduction

Eight beams were tested, the details of which were given in chapter 4 together with the details of their design. The deformations of the beams were measured, mainly the displacements of the centreline of span BD. The load-displacement behaviour of each beam was monitored continuously throughout the tests.

Two types of information will be presented in this chapter; first, information of a quantitative nature such as displacements and loads recorded during each test and secondly information of a qualitative nature such as the overall shape of the test beams and the shape of their various components, in particular the web posts.

The values of loads obtained from the tests will be used in the next chapter in order to check the validity of the design proposals presented in chapter 4 as well as various other design proposals.

6.2 Failure loads

6.2.1 Presentation

The loads were monitored throughout the tests by means of the two load cells at ends A and E. Although the test rig was designed to provide statically determinate conditions and therefore to make the load applied at end support A and the three reactions at the intermediate loading points B and D and end support E equal, a drift was noticed between the recorded loads at ends A and E, R_A and R_E . There was one exception with test M4-2 where a deliberate moment gradient was chosen. The variation of the end loads at ends A and E is given in Figs. 6.1 and 6.2 in relation to the duration of each test. The figures

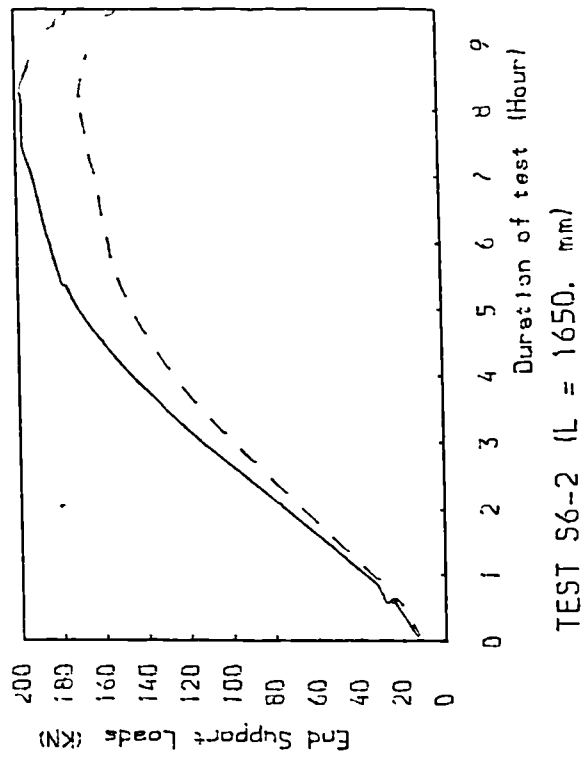
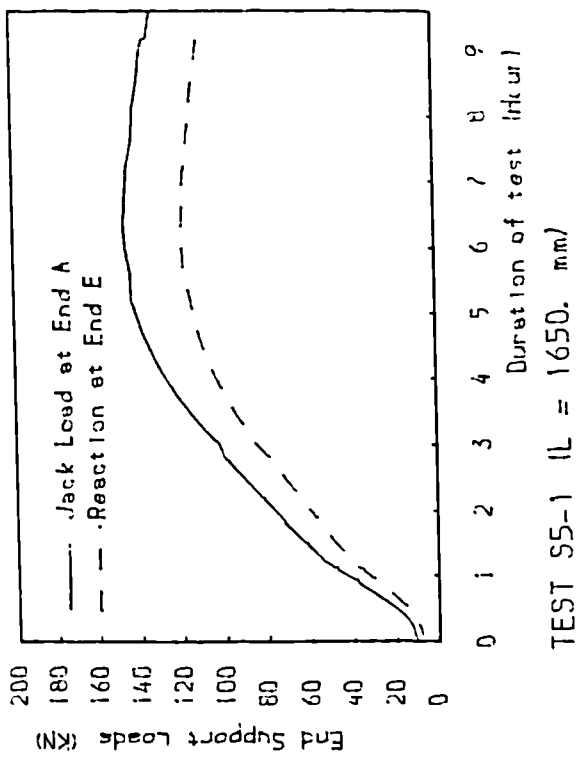
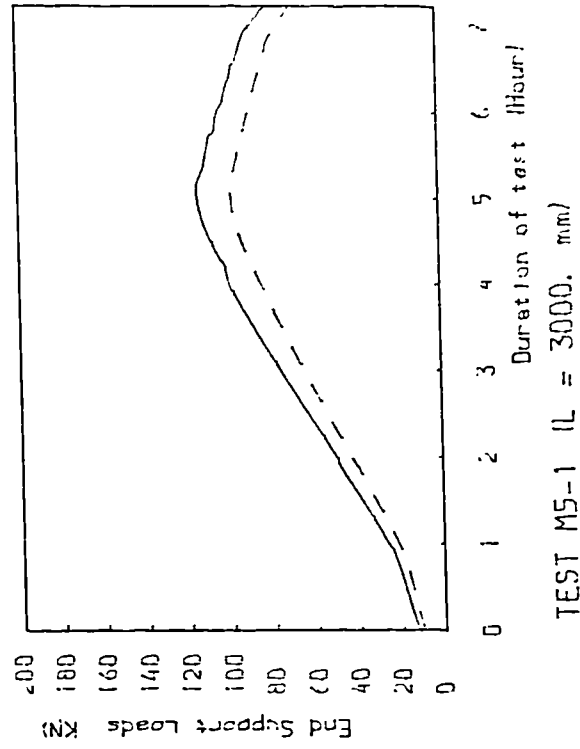
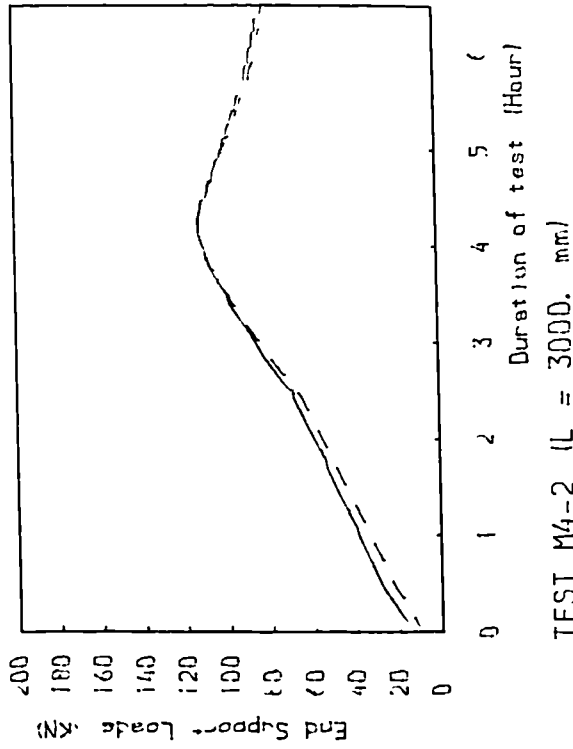


FIG. 6.1 VARIATION OF END SUPPORT LOADS WITH TIME

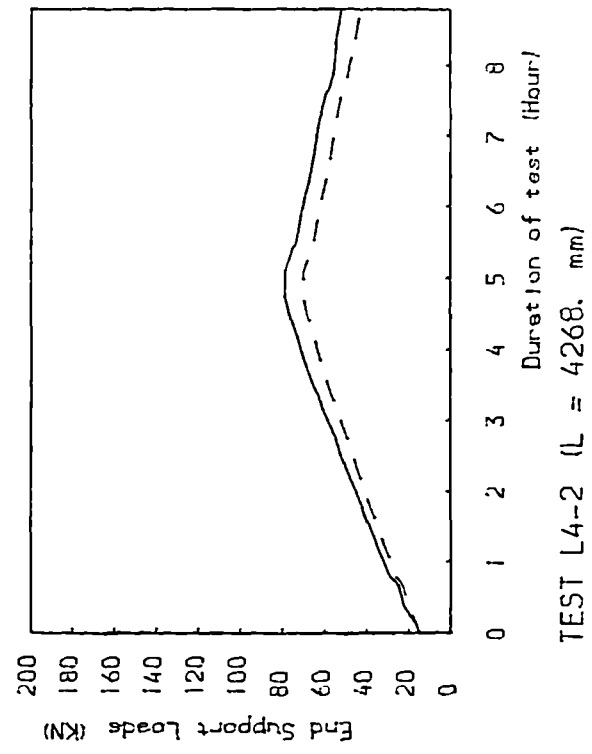
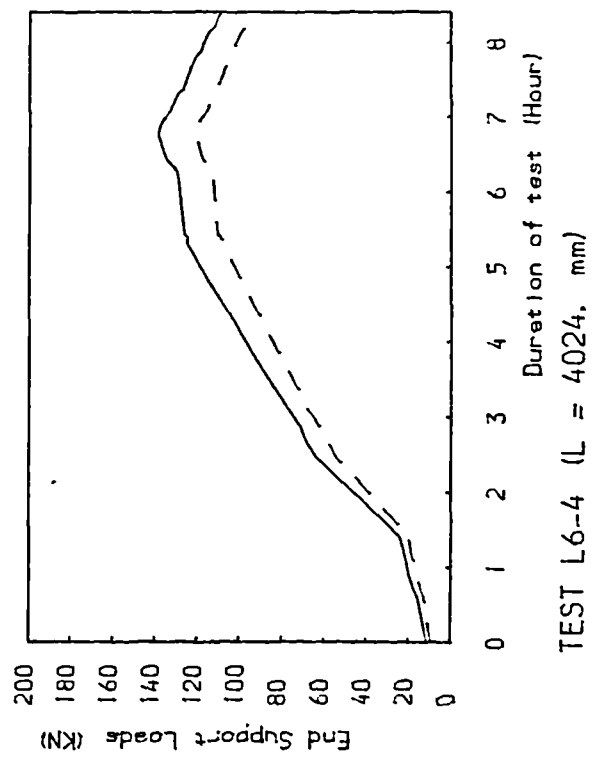
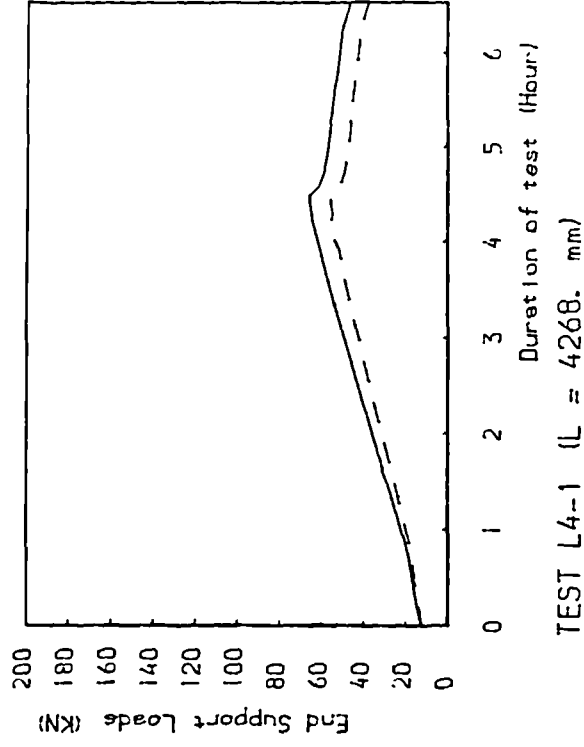
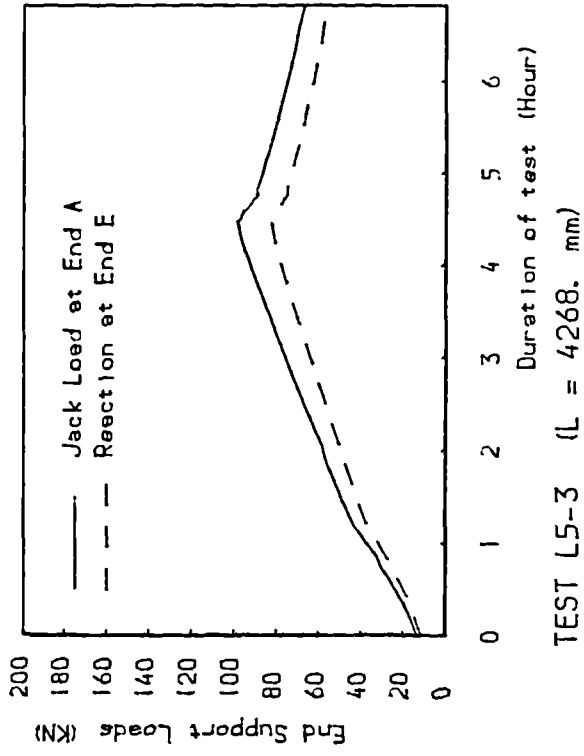


FIG. 6.2 VARIATION OF END SUPPORT LOADS WITH TIME

show that the drift between the load at end A and the reaction at end E was present almost from the beginning of each test and increased with time until failure occurred and then it stabilized. In the case of test M4-2 the two loads tended to become equal as the test approached failure.

The values of failure load which were used in the subsequent calculations were the highest recorded during the test. In all cases the maximum value recorded at A corresponded to the maximum recorded at E. These values of failure load were used to calculate the magnitude of the moments at points B and D, M_B and M_D and subsequently the values of end moment ratios $\beta = M_D/M_B$. Fig.6.3 gives the variation of the ratio of end moments $\beta = M_D/M_B$ versus time (with $M_B = R_A \times L_{AB}$ and $M_D = R_E \times L_{DE}$). It shows that β varied between 0.8 and 0.9 for the seven tests designed to have equal and opposite end moments loading ($\beta = 1.0$).

The values of experimental moments M_{exp} used in the calculations were taken as the average of the values of moments M_B and M_D and corresponded to the moment at mid-span (point C). Table 6.1 gives the values of loads R_A and R_E , the various values of moments and the values of β for each test. In the case of test M4-2, M_{exp} was taken as M_B moment created at point B by the load applied by the jack at end A.

6.2.2 Friction Losses

The presence of moment gradient for span BD different from the one expected could only be explained by friction in the test rig. Although all the bearings transmitting the loads were checked, cleaned and greased carefully before each test, the losses could neither be eliminated nor totally understood. Neither was it possible to gauge the magnitude of the loads which were transmitted through friction as axial

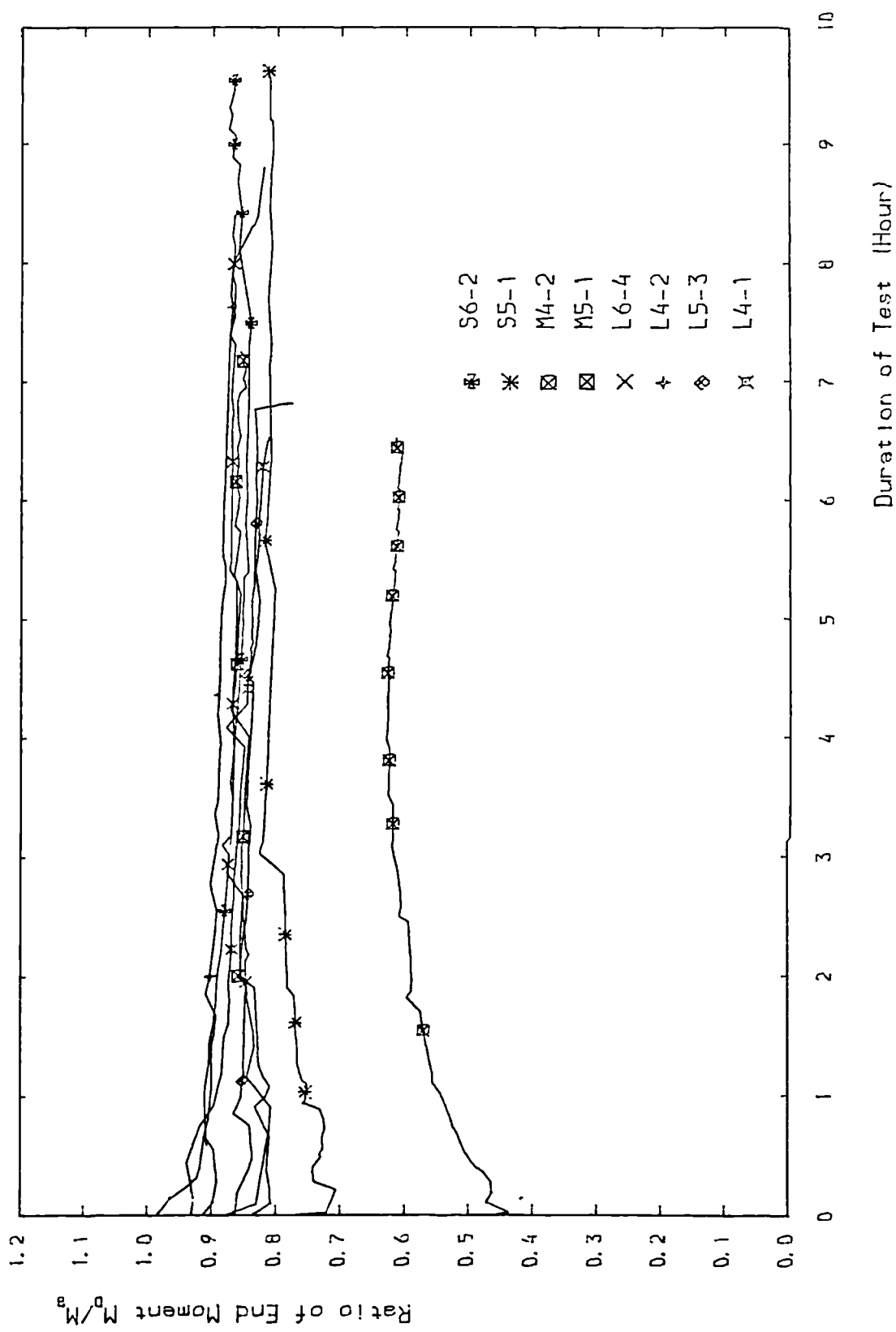


FIG. 6.3 VARIATION OF $\beta = M_0/M_a$ WITH TIME

Test Beams	R_A (kN)	$M_B = R_A \times L_{AB}$ ($\times 10^6$ N.mm)	R_E (kN)	$M_D = R_E \times L_{DE}$ ($\times 10^6$ N.mm)	$\beta = M_D / M_B$	$M_C = M_{exp}$ ($\times 10^6$ N.mm)
S6-2	197.65	3.75	169.67	3.22	0.858	3.49
S5-1	146.64	2.79	119.02	2.26	0.812	2.52
M4-2	112.96	2.15	112.67	1.35	0.630	2.14
M5-1	114.89	2.18	98.85	1.88	0.860	2.03
L6-4	138.62	2.90	120.52	2.52	0.869	2.70
L4-2	78.96	1.55	70.03	1.38	0.887	1.49
L5-3	98.66	1.94	82.71	1.63	0.838	1.79
L4-1	65.98	1.30	55.87	1.10	0.847	1.20

Table 6.1 Ratios of End Moments β of Span BD at Failure

force in the flange under compression.

6.3 Load-deflection behaviour of the test beams

6.3.1 Load-deflection curves

A full set of load-deflection curves is given in Figs. 6.4 to 6.11. For each test three curves are given : load versus lateral deflection u , vertical deflection v and angle of twist of the vertical axis of the web. On the graphs, the vertical axis represents either M/M_p or R . M/M_p is the ratio of mid-span moment to the maximum in-plane capacity of each beam and R is the end load which would create a moment at mid-span equal to $M_c = M_{exp}$. The curves confirm the ability of the apparatus to follow behaviour beyond the point of maximum load. The calculation of the deflections were given in chapter 5. The deflections u and v were those of the centre of gravity of the section of the beams and were calculated as the average of deflections of the top and bottom flanges at mid-span.

6.3.2 Short span beams

Test beams S6-2 and S5-1 which were the stockiest had a middle span of 1650mm long. Because they were designed to fail in a flexural mechanism, i.e. in-plane yielding of the cross-section, they were not expected to show any signs of lateral deflection at least until they approached their maximum in-plane carrying capacity. However from the onset of loading a slight lateral deflection of the flange under compression was noticed in both beams; this kept increasing until the end of the test. The vertical deflection of span BD was very small and was swamped by the lateral deflection of the beams.

Both beams exhibited similar behaviour with linear increase of the lateral deflection and rotation of the vertical axis of the web post

with a very short transition between the end of the straight line and the flat portion of the curves. The vertical deflections of span BD could not be recorded until failure occurred and it is possible that the values calculated were caused by the tilting of the flanges when they deflected sideways.

6.3.3 Long span beams

The behaviour of the long span beams L4-1, L4-2, L5-3, and L6-4 was rather different from that of the short span beams. The vertical deflections were more pronounced from the onset of loading and consequently as well as being non-linear the slope of the three load-deflection curves before failure occurred was bigger. The magnitude of the deflections was nearly three times that of the short span beams at the end of the tests exceeding 60mm for the lateral deflection, 50mm for the vertical deflection and 0.26rad for the rotation of the web in the case of beams L4-1 and L4-2. The shape of the curves and in particular the length of the transition part was due to the fact that the beams did not fail suddenly but showed signs of pronounced lateral buckling very early in the test.

6.3.4 Medium-span beams

The magnitude of the deflections of beams M4-2 and M5-1 was very similar to that of the long span beams although the lateral deflections before failure occurred were not as pronounced. The behaviour of these two beams was generally intermediate between the short and long span beams. The presence of a moment gradient in the case of beam M4-2 did not affect its behaviour and the three load-deflection curves were very similar to those of beam M5-1.

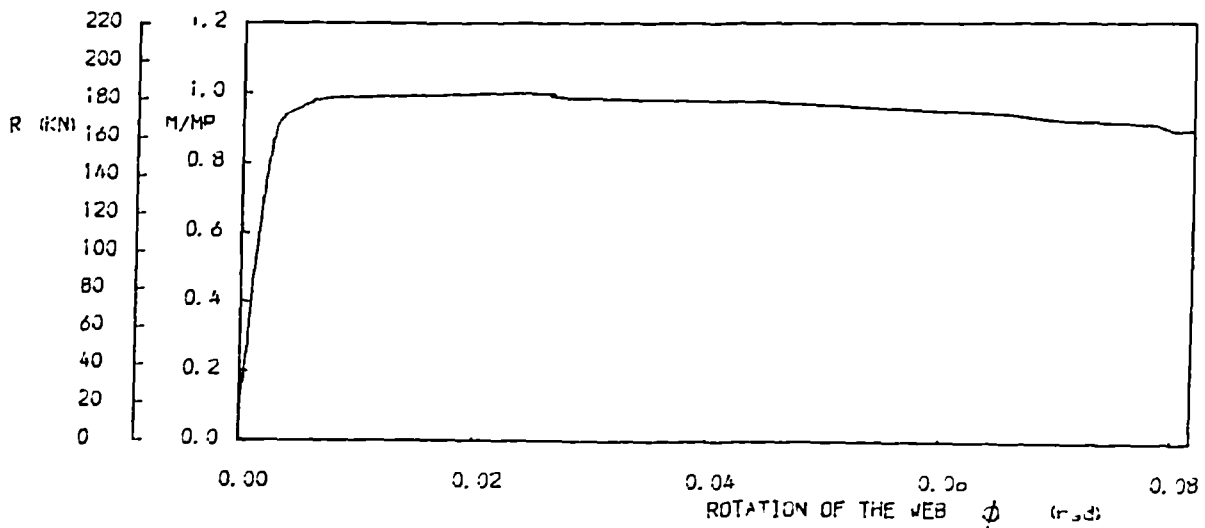
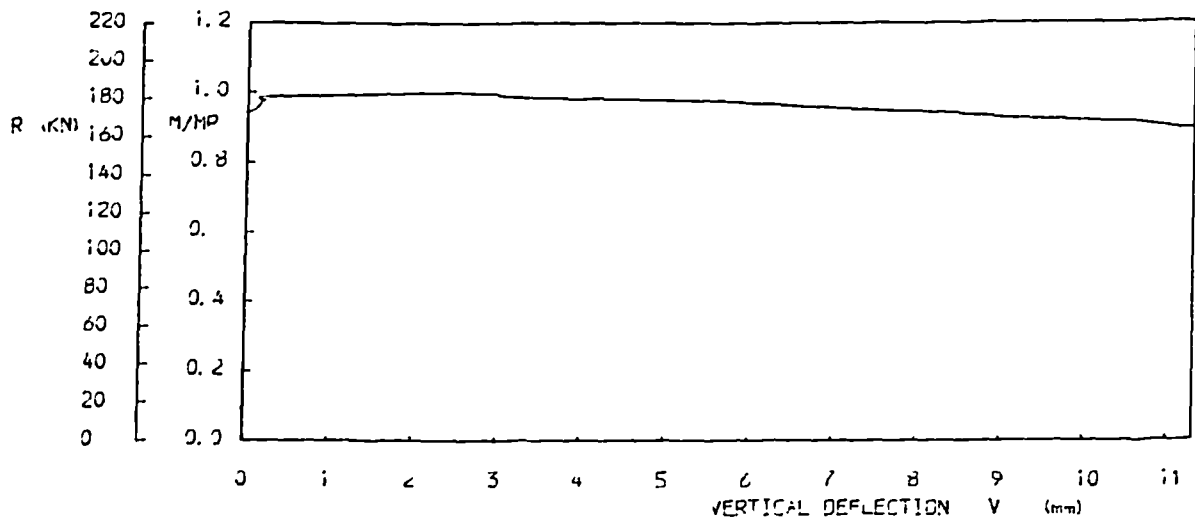
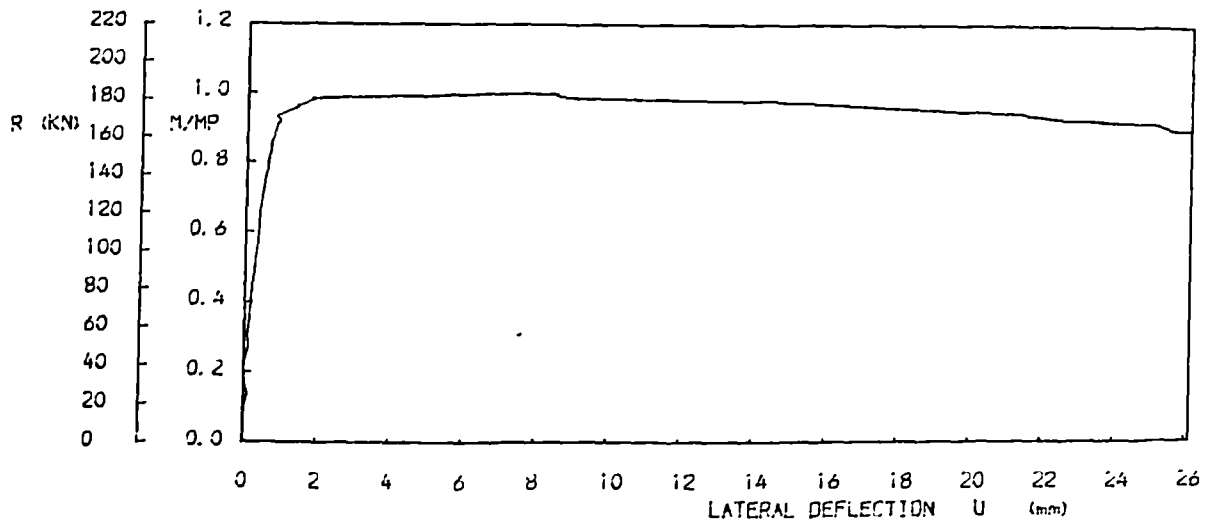


FIG. 6.4 LOAD DEFLECTION CURVES OF BEAM S6-2 ($L=1650$ mm)

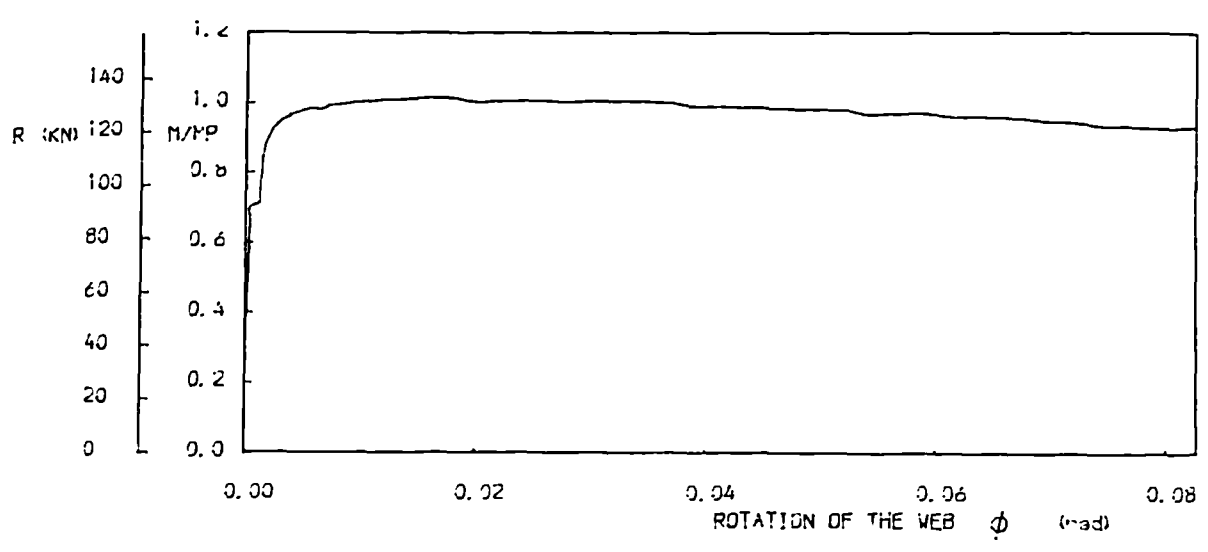
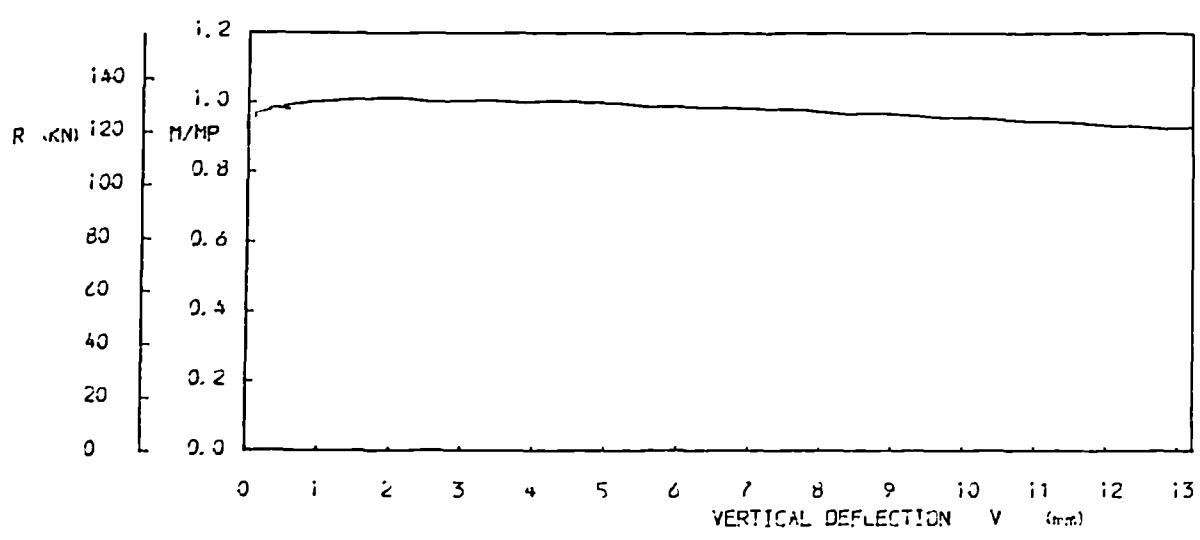
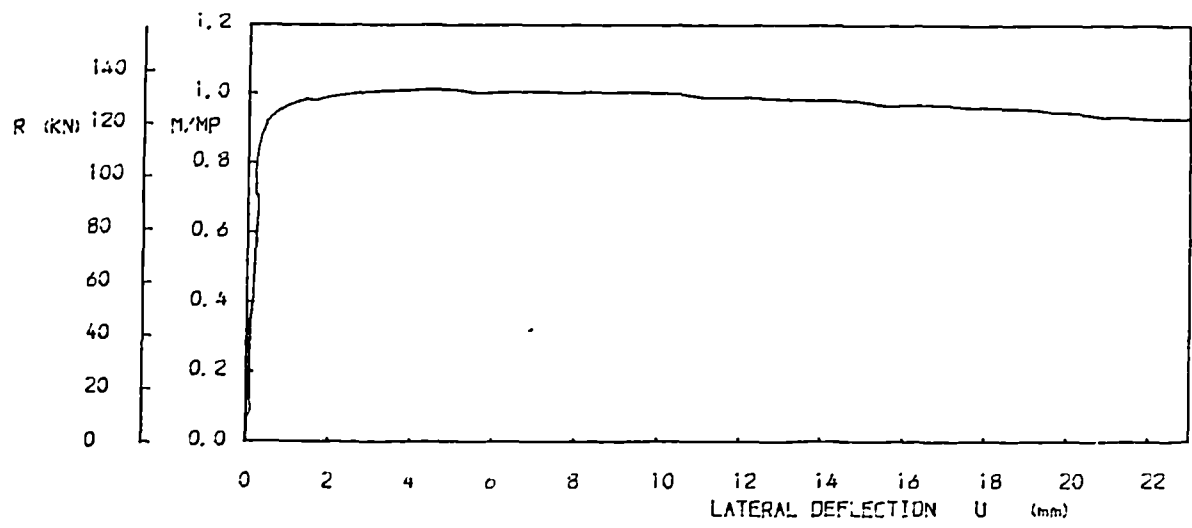


FIG. 6.5 LOAD DEFLECTION CURVES OF BEAM S5-1 (L=1650 mm)

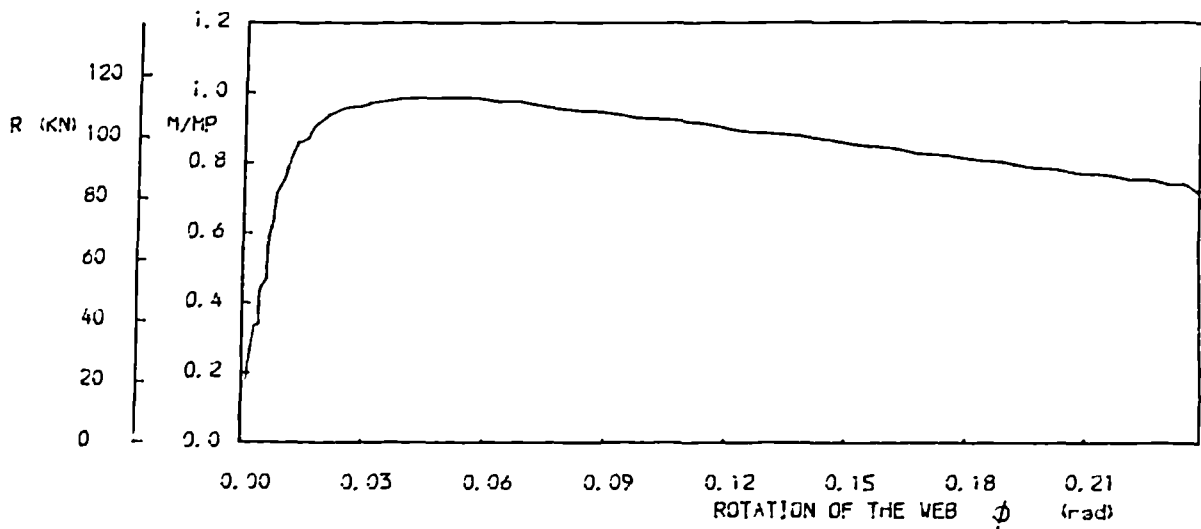
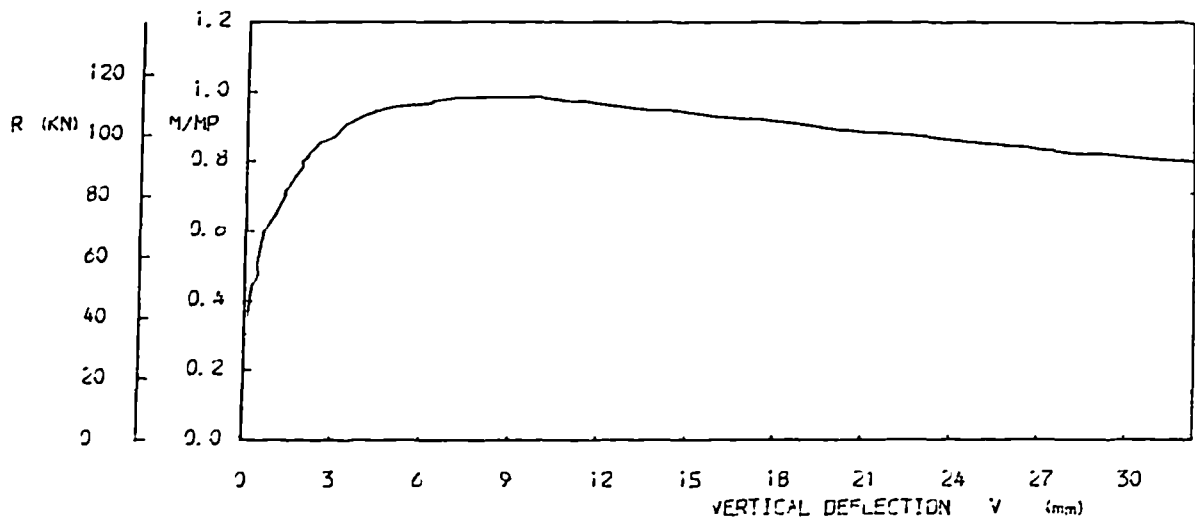
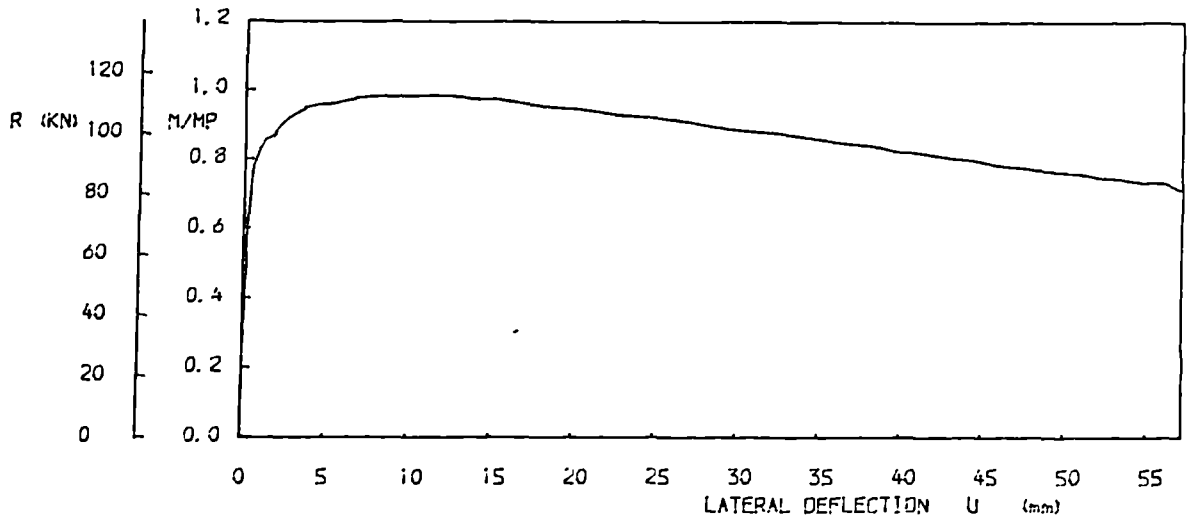


FIG. 6.6 LOAD DEFLECTION CURVES OF BEAM M4-2 (L=3000 mm)

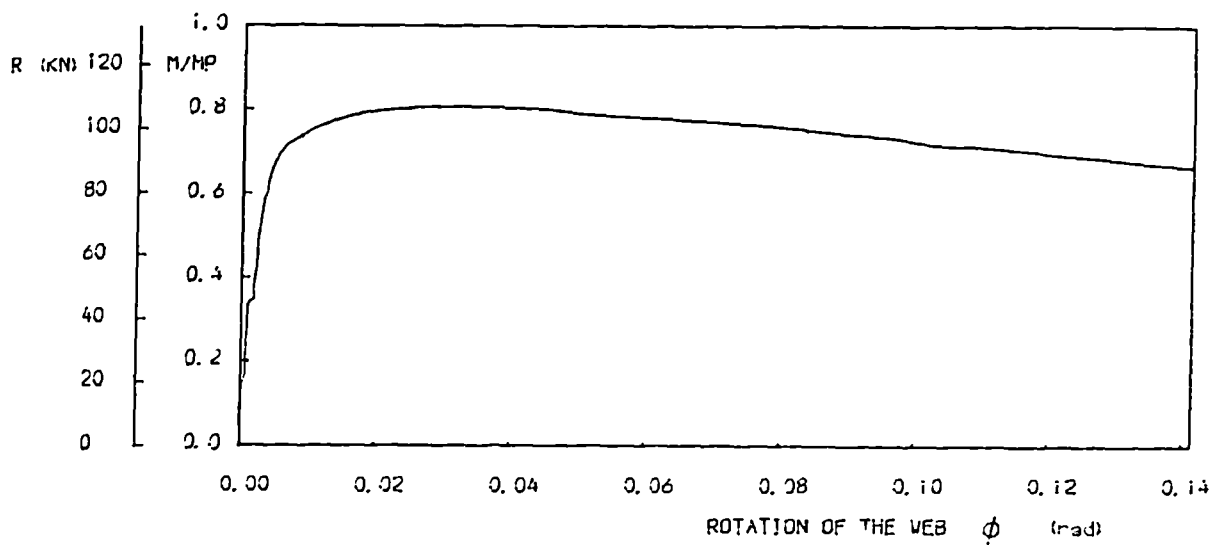
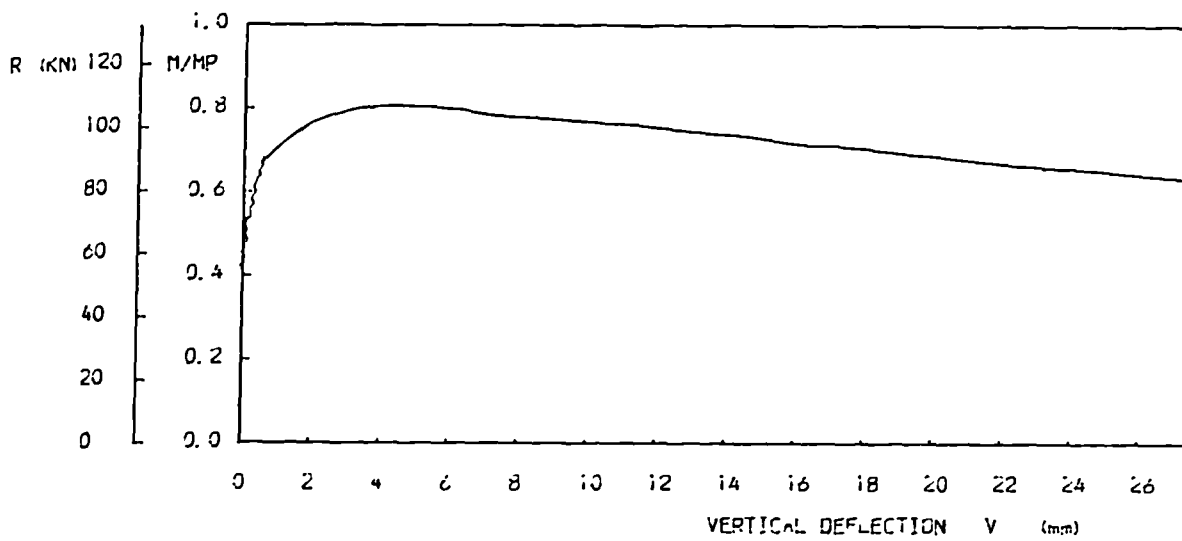
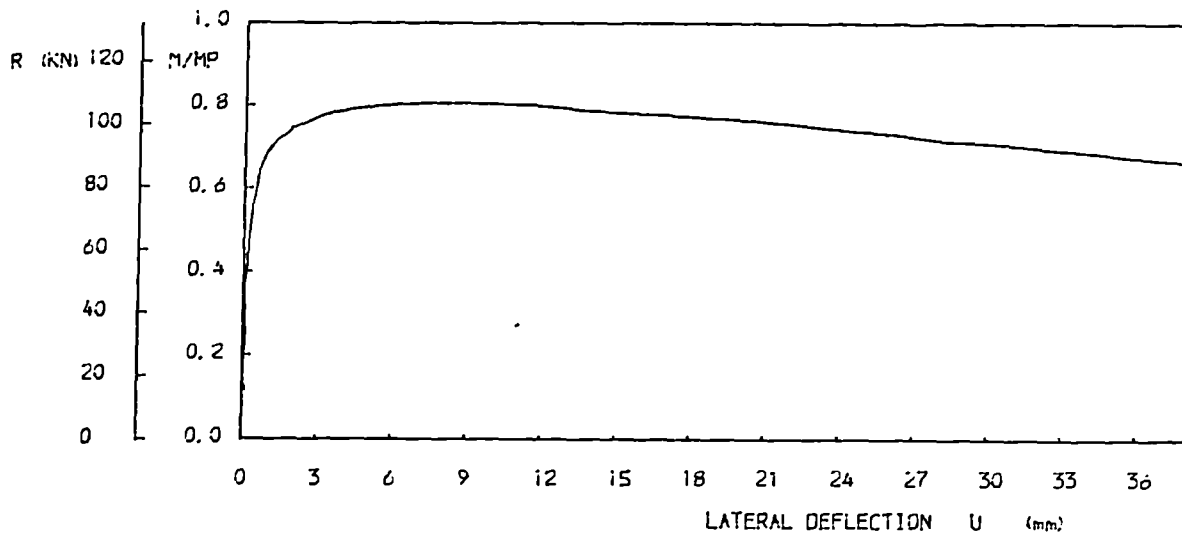


FIG. 6.7 LOAD DEFLECTION CURVES OF BEAM MS-1 (L=3000 mm)

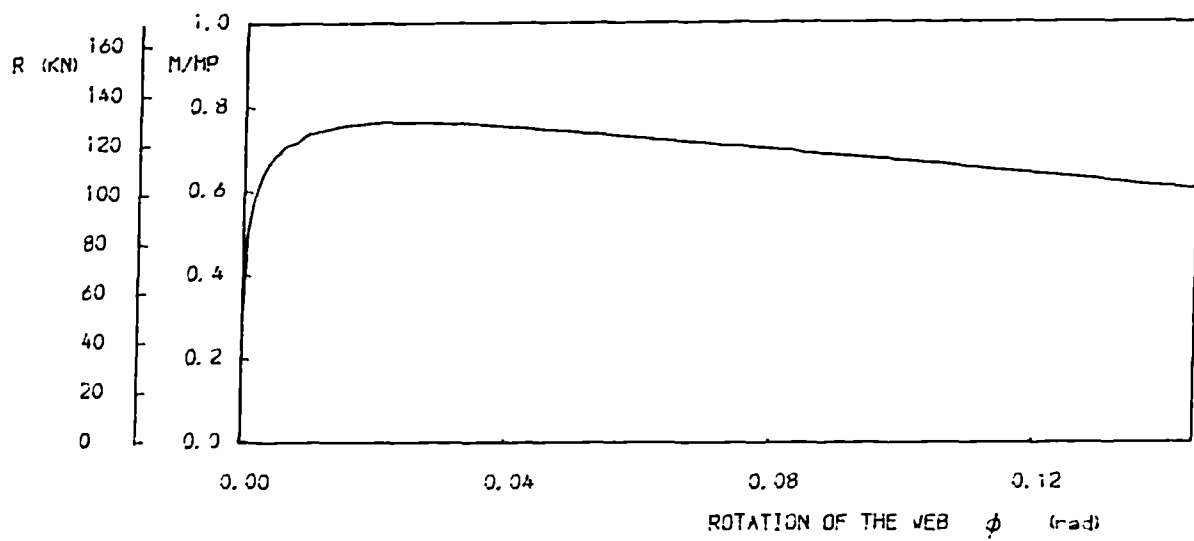
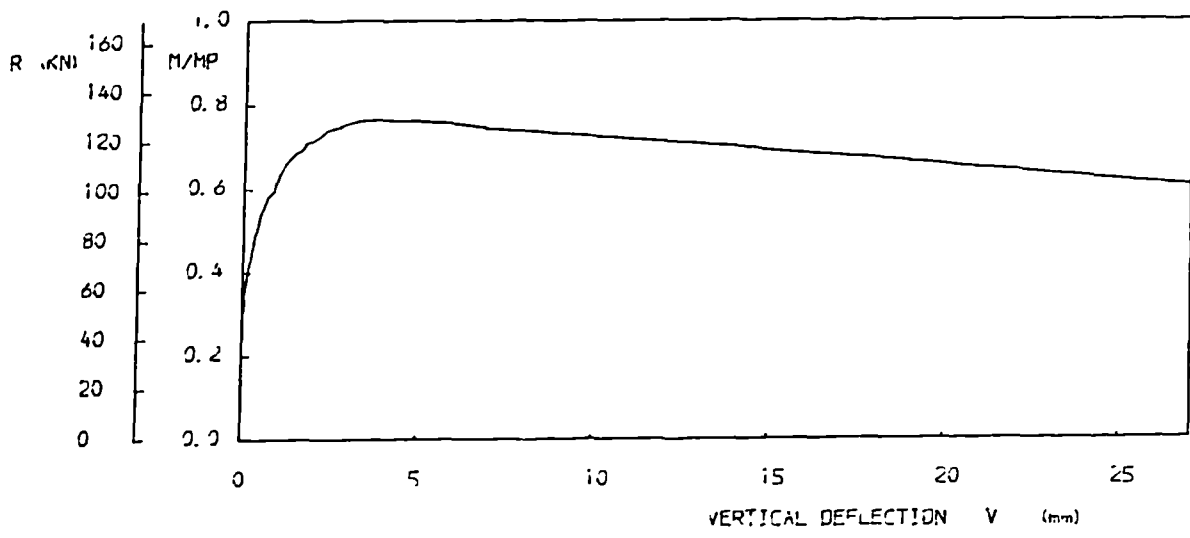
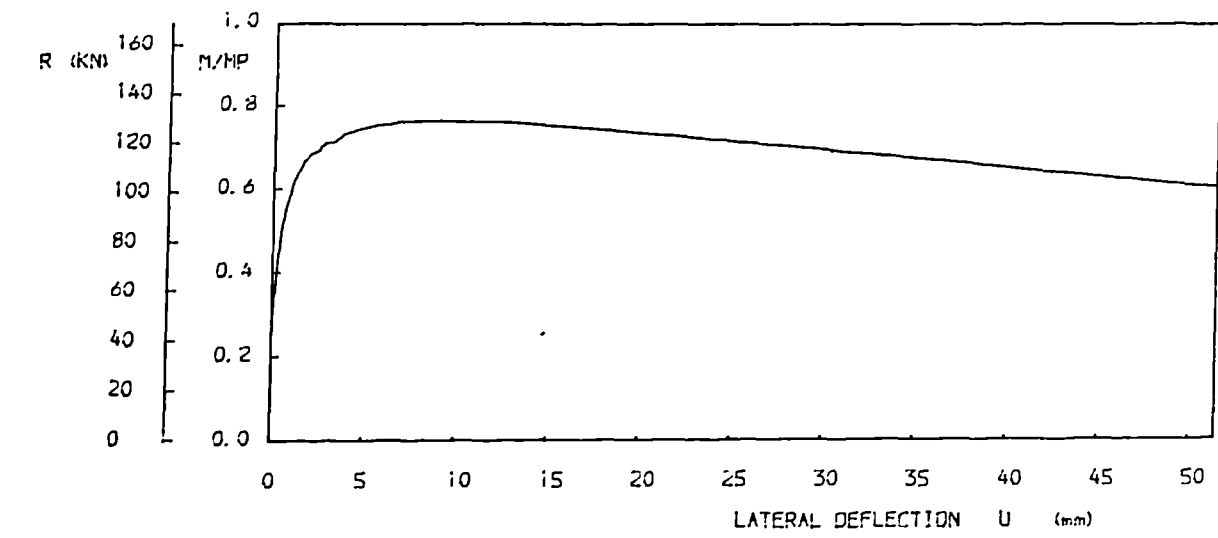


FIG. 6.8 LOAD DEFLECTION CURVES OF BEAM L6-4 (L=4024 mm)

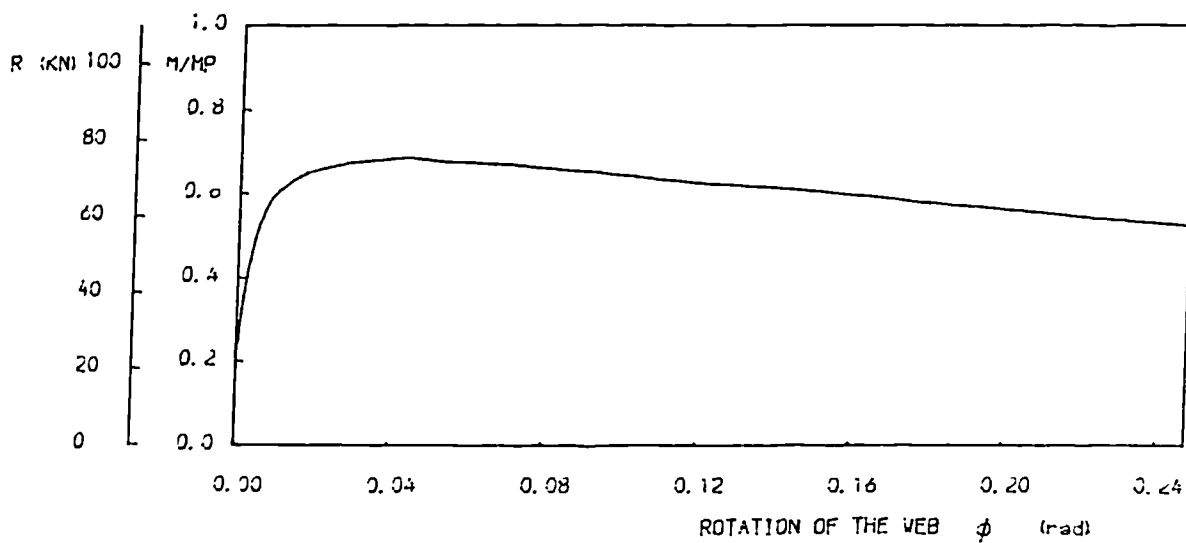
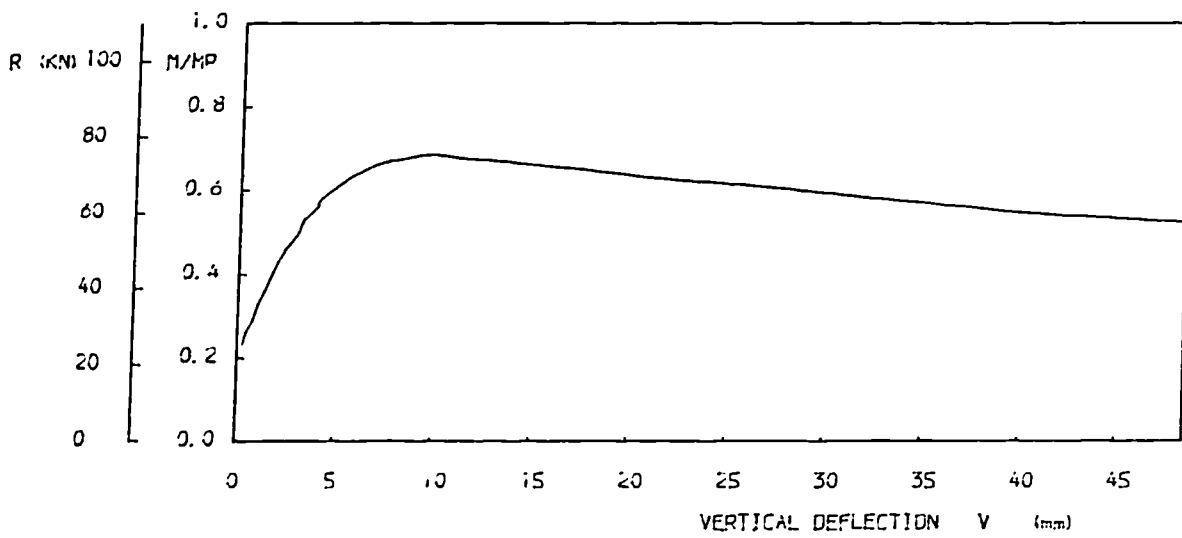
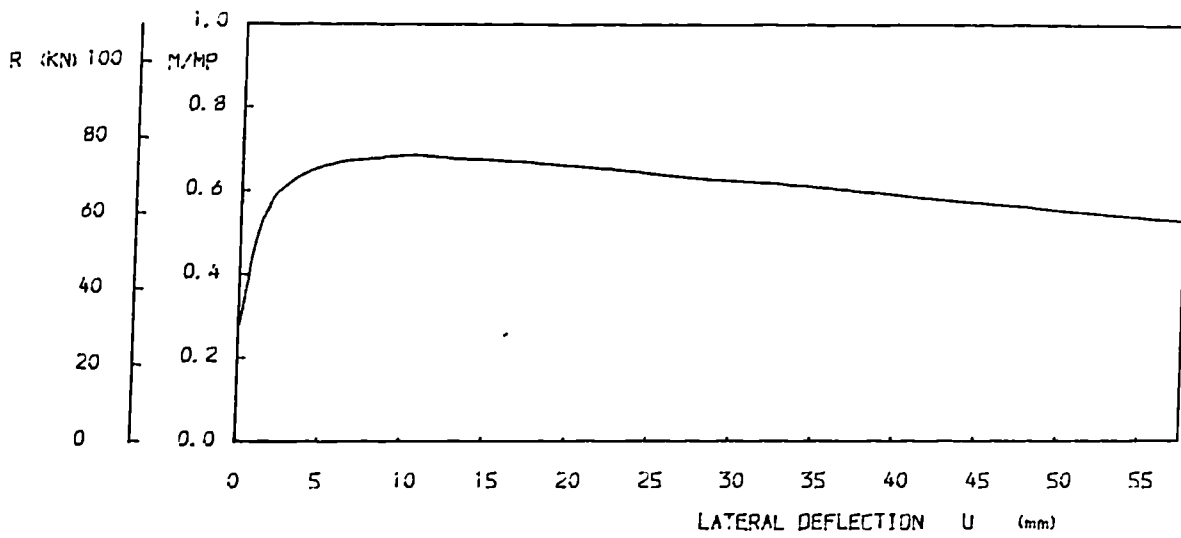


FIG. 6.9 LOAD DEFLECTION CURVES OF BEAM L4-2 (L=4268 mm)

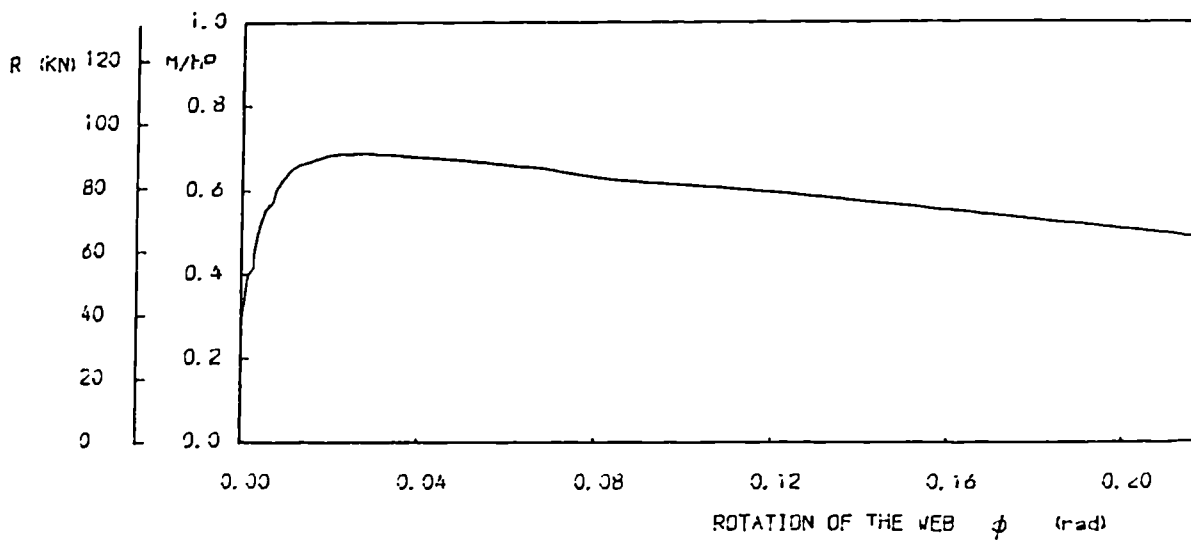
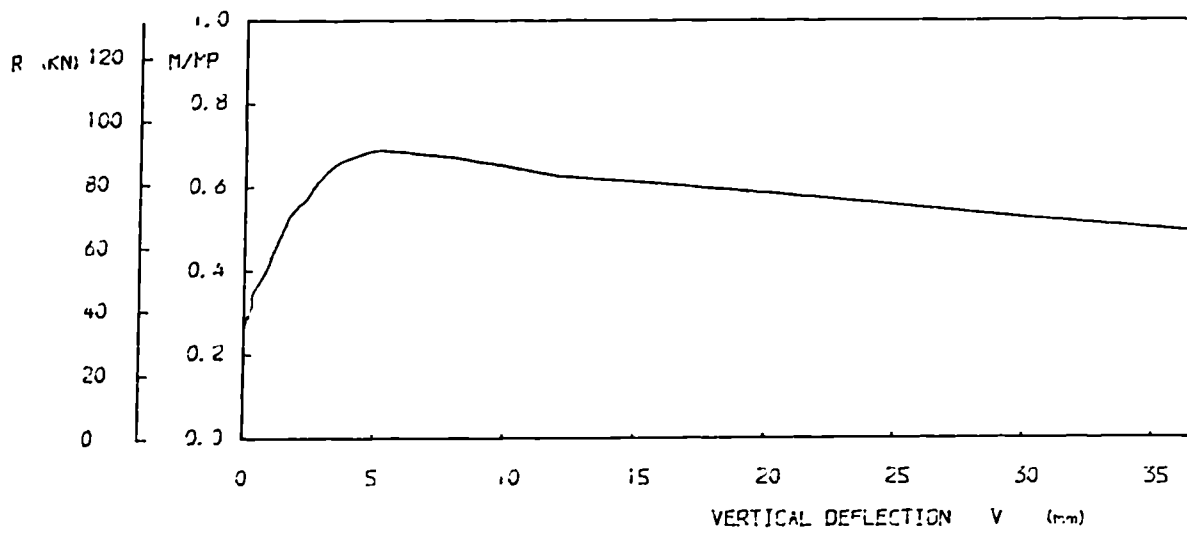
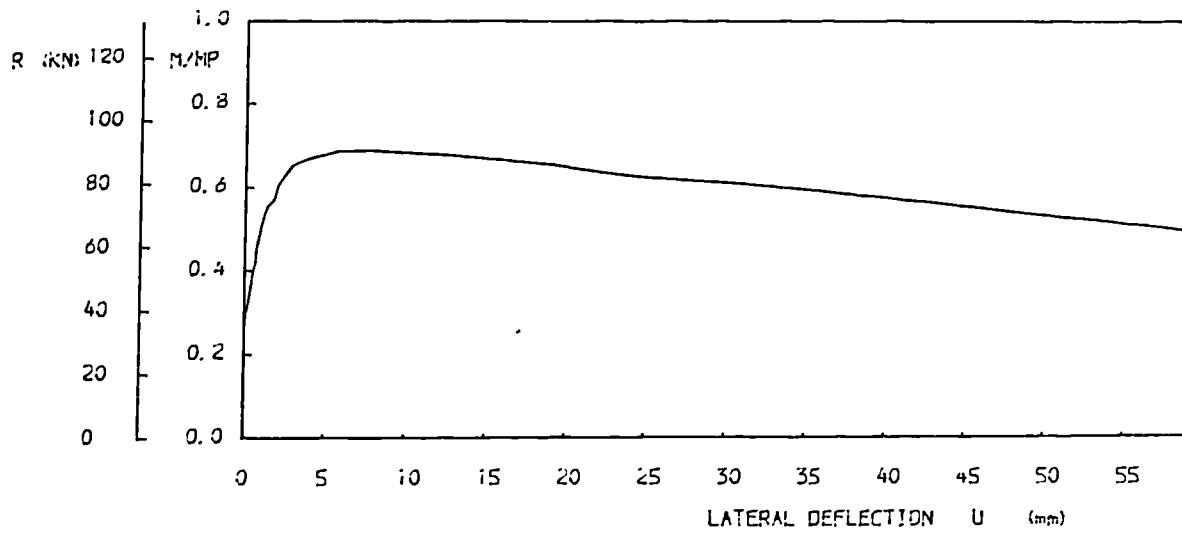


FIG. 6.10 LOAD DEFLECTION CURVES OF BEAM LS-3 (L=4268 mm)

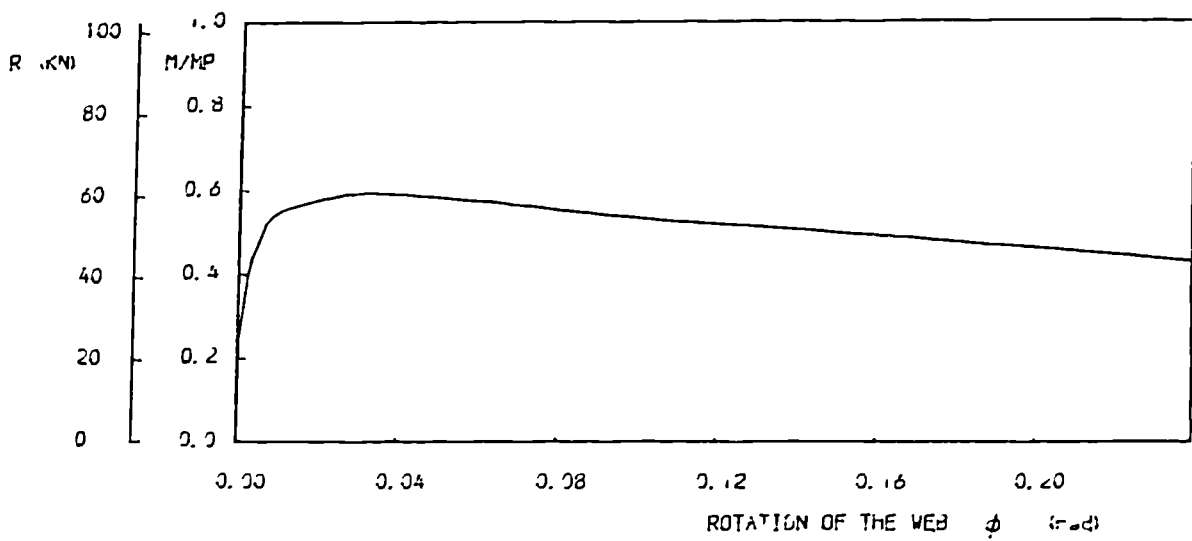
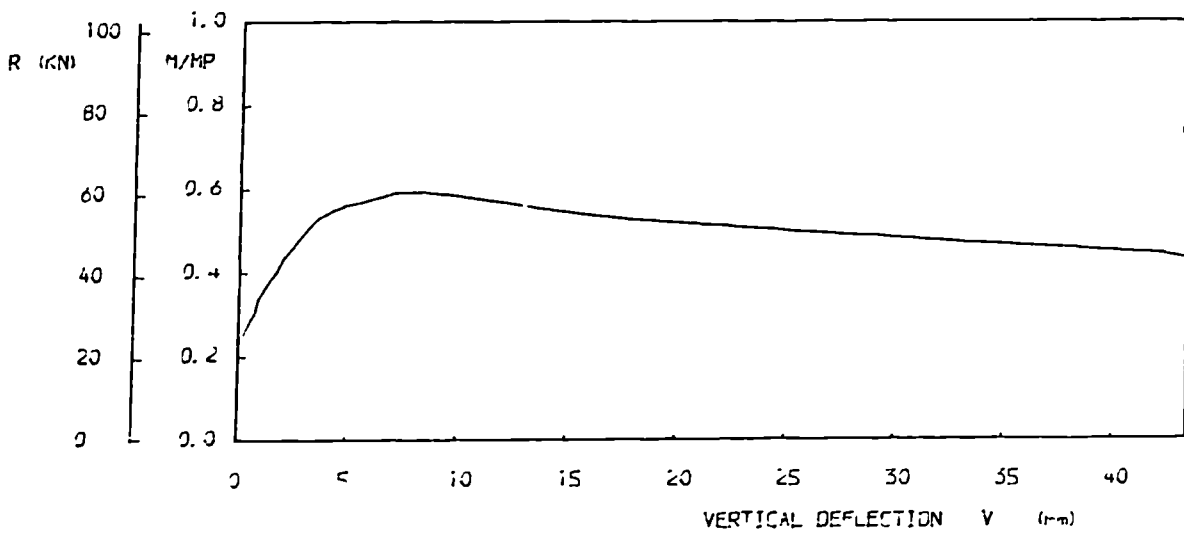
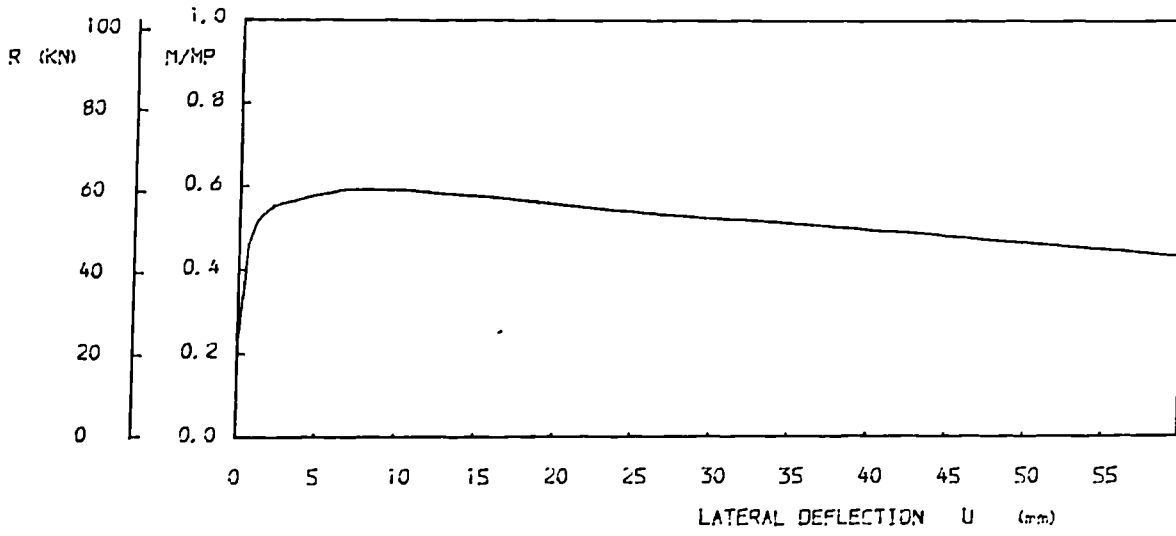


FIG. 6.11 LOAD DEFLECTION CURVES OF BEAM L4-1 (L=4268 mm)

6.3.5 Unloading behaviour

All the test beams were loaded until the displacements of the central span BD were such as to endanger the safety of the components of the test rig. In all cases the deformations were so large, the lateral displacements of the top flange of all the beams except S6-2 and S5-1 had reached at least 120mm, that the beams could have been considered completely unserviceable.

All the beams except beam M4-2 were subjected to a constant rate of lift of the jack equal to about 0.20mm/min until failure occurred. A rate of lift of 0.30mm/min was used in the case of beam M4-2 in order to attain failure at a given time during the test for demonstration purposes. This faster rate of loading did not seem to have adverse effect on the overall behaviour of the beam. In the latter stages of test L4-2 and S6-2 the rate of lift of the jack was increased to about 0.55mm/min for beam L4-2 and 0.50mm/min for beam S6-2 (Fig.6.12 gives the speeds used in all the tests). All the beams could carry between 66% and 90% of the maximum recorded load after the tests were stopped. Beam S5-1 was still able to carry 90% of its failure load 3 hours after reaching the maximum load whilst beam S6-2 for which the rate of loading was speeded up in order to complete the test recorded 88% of the failure load 1.25 hours after it failed. Both these beams attained their maximum in-plane carrying capacity.

In the case of the beams with long and medium spans about 70% of the load at failure was recorded after the maximum load was attained. These tests were usually stopped two hours after this point was reached except in the case of the test of beam L4-2 which was continued for 3.72 hours after failure. The reason for making the test last so long was to see if by distorting the flange considerably any distortion of

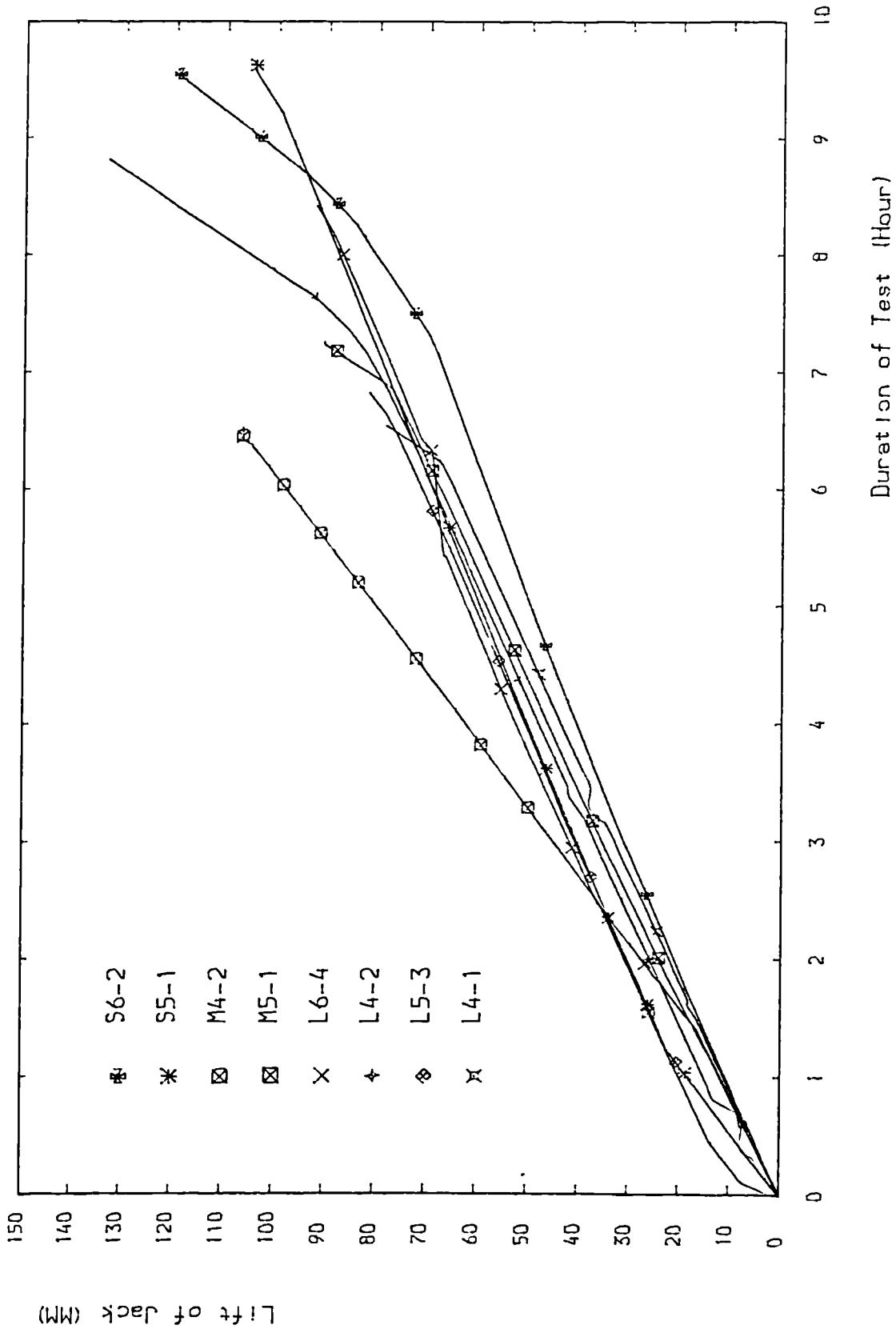


FIG. 6.12 RATE OF LIFT OF JACK

the web post could be noticed. The only consequence of taking the load so far was that it achieved a ratio of the load at termination of test R_{AS} over the load at failure R_{AF} equal to 0.66. This was the lowest percentage achieved as can be seen in Table 6.2 which gives the loads at failure and the loads at the completion of the tests with the corresponding times needed to achieve these loads. The lateral displacement of the top flange of beam L4-2 was measured to be over 140mm when the test was stopped.

6.4 Local buckling failure

The preliminary calculations of the stresses in the castellation just outside loading point B in span AB showed that in the case of test beams S6-2 and S5-1 stresses close or above the value of their material static yield stresses (see Tables 4.9 and 4.10) would be reached and that local failure due to overstressing of the tee sections was possible. Furthermore, a Vierendeel mechanism (formation of four plastic hinges at the corners of a castellation) was also shown to be likely to form (see Table 4.13). It was therefore not surprising that the two beams showed signs of local buckling of the top flange in the upper tee section of the aperture just outside loading point B at a distance from loading point A of 1780mm and 1694mm for beams S6-2 and S5-1 respectively (this corresponds to point 1b of section 2-2 in Fig.4.8).

The two beams behaved in a similar manner as can be seen in Fig.6.13 which gives the load applied by the jack at end A versus the displacement of end A of the beams. Both curves can be divided into five parts IJ, JK, KL, LM and MN. The first part of the curves, IJ, is linear until loads of 118 kN and 133 kN are reached for beams S5-1 and S6-2 respectively. The corresponding values of stresses at point 1b of the

Test Beams	Failure		Test stopped		$\frac{R_{AS}}{R_{AF}}$
	R_{AF} (kN)	time (hour)	R_{AS} (kN)	time (hour)	
S6-2	197.65	8.30	174.44	9.55	0.88
S5-1	146.64	6.35	131.90	9.62	0.90
M4-2	112.96	4.30	80.80	6.53	0.715
M5-1	114.89	5.09	82.70	7.24	0.720
L6-4	138.62	6.76	108.96	8.42	0.786
L4-2	78.96	5.10	51.96	8.82	0.658
L5-3	98.66	4.48	69.49	6.62	0.704
L4-1	65.98	4.45	46.91	6.50	0.712

Table 6.2 Loads at Failure and at End of Test and Time Corresponding to these Loads

section are 261 N/mm^2 and 221 N/mm^2 . If it is considered that the curve of beam S5-1 ceases to be linear at point T where a kink exists, the load of 103.3 kN corresponding to point T gives a stress of 229 N/mm^2 . Yielding must have been present in the section outside point B when part JK of the curve was entered but no signs of distress were yet to be noticed. It is only when the loading was past point K in part KL of the curves that signs of local buckling were noticed in the top flange. The load-deflection behaviour of span AB was constantly monitored on the X-Y plotter. The sharp change of slope recorded at point K meant that failure of span AB must have been well advanced. The load levels were 143 kN and 181 kN for beams S5-1 and S6-2 at point K respectively. However the two beams were able to sustain higher loads until failure of the middle span BD occurred by lateral buckling. In the case of beam S6-2 which had the lowest slenderness ratio, M_p was reached and the load increased from 181 kN to about 198 kN. The flat portion of the curve, LM, was by then entered and this constant load was sustained for about one hour until the load dropped off. The increase in loading was smaller in the case of beam S5-1 which failed when reaching M_p . The flat portion LM of the curve was not as long and marked as that obtained for beam S6-2. The point was made in chapter 4 that the method used for calculating the stresses could predict the loads at which yielding would start in a castellated beam. This is more or less confirmed by the previous calculations. However the stresses computed for point K of the curves are very high. They were found to be equal to 300 N/mm^2 (181 kN) and 316 N/mm^2 (143 kN) for beams S6-2 and S5-1 respectively. It should be remembered that these loads were less than the failure loads of 198 kN and 147 kN recorded for beams S6-2 and S5-1. The nominal stresses at these loads were 328 N/mm^2 and 325 N/mm^2 .

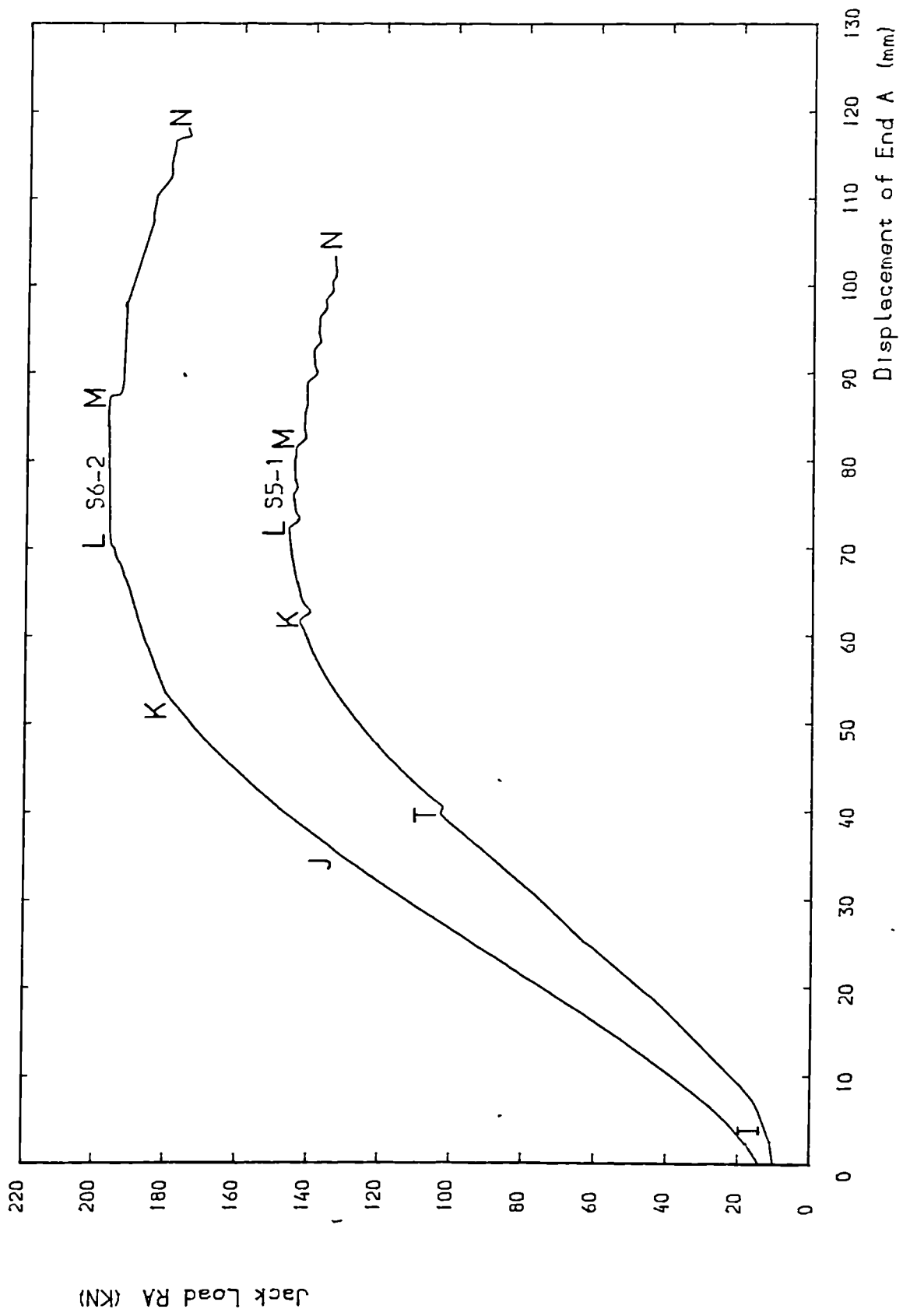


FIG. 6.13 DISPLACEMENT OF END A FOR TEST BEAMS S6-2 AND S5-1

Plates 6.1 and 6.2 show the tee section of the aperture which failed by local buckling. It can be seen clearly on the photographs that the deformations of beam S5-1 were less marked than those of beam S6-2, the increase in load necessary to cause failure in span BD being smaller for beam S5-1.

6.5 Buckled shape

6.5.1 Overall buckled shape

Fig.5.1 showed the loading which was applied to the test beams and the possible buckling mode which could develop. The eight beams tested behaved in the predicted way and all exhibited the same laterally buckled configuration over their central span BD. Plates 6.3 to 6.5 show the eight beams in their laterally deformed state grouped in order of length after their removal from the test rig. Their shape was similar to that of plain-webbed beams which failed in a lateral-torsional buckling mode(89).

Although spans AB and DE appear to be straight on the photographs, they deflected sideways in the direction opposite to that of the middle span during the tests. This deformation which was clearly noticeable by visual inspection disappeared after the unloading of the beams and their removal from the test rig.

6.5.2 Distortion of the web posts

The possibility that the presence of the holes would enhance the distortion of the web posts was raised whilst discussing the lateral buckling of castellated beams. Chapter 5 then described how several beams were instrumented in order to obtain their deformed profile at various sections along their length by using photogrammetric techniques.

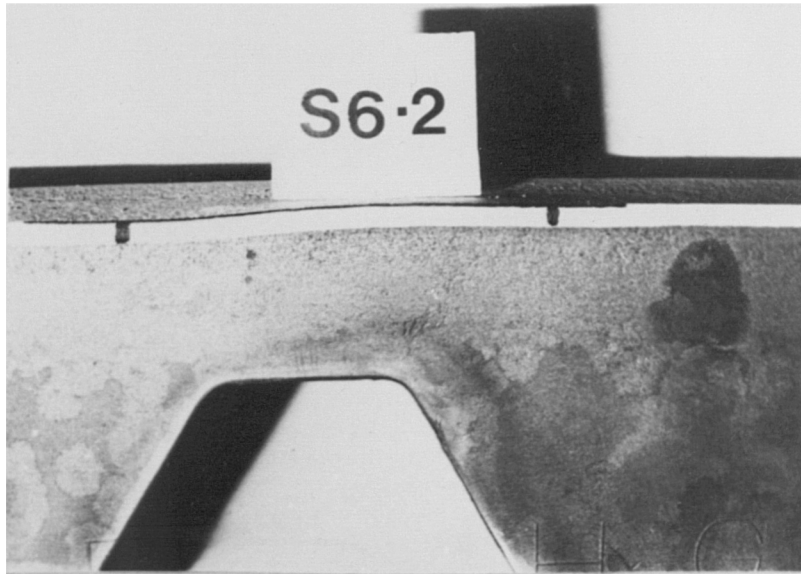


PLATE 6.1 LOCAL BUCKLING FAILURE OF BEAM S6-2

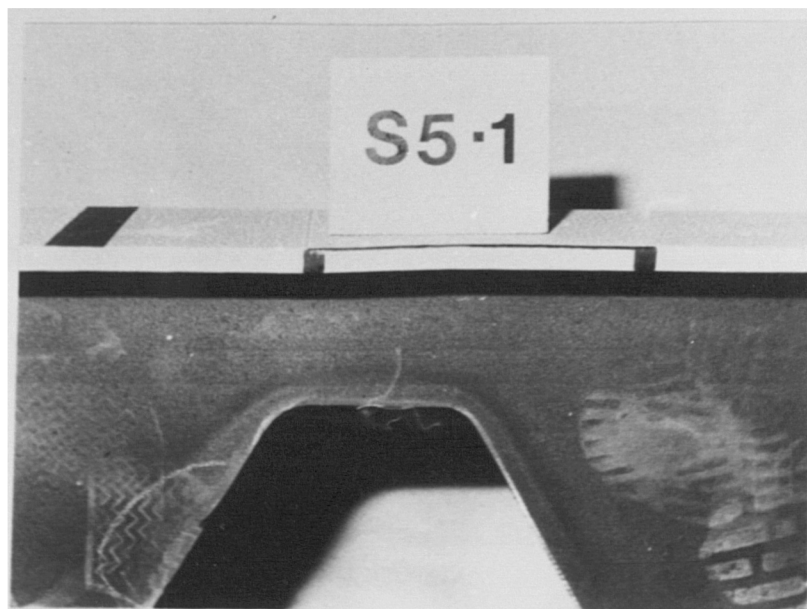


PLATE 6.2 LOCAL BUCKLING FAILURE OF BEAM S5-1

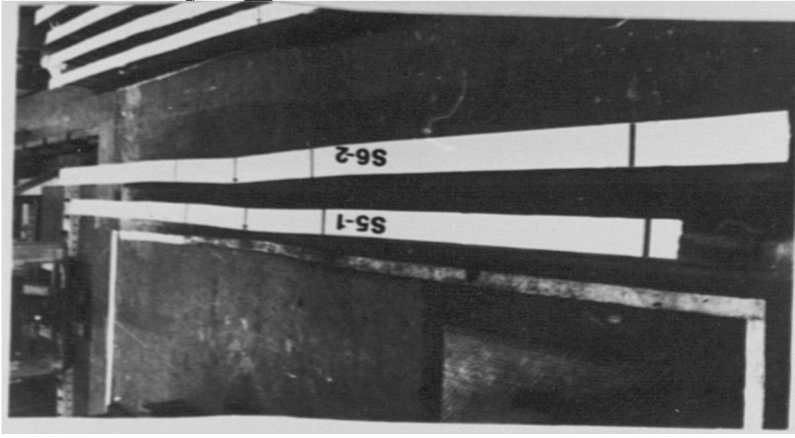


PLATE 6.3 BEAMS S5-1 AND
S6-2 AFTER TEST

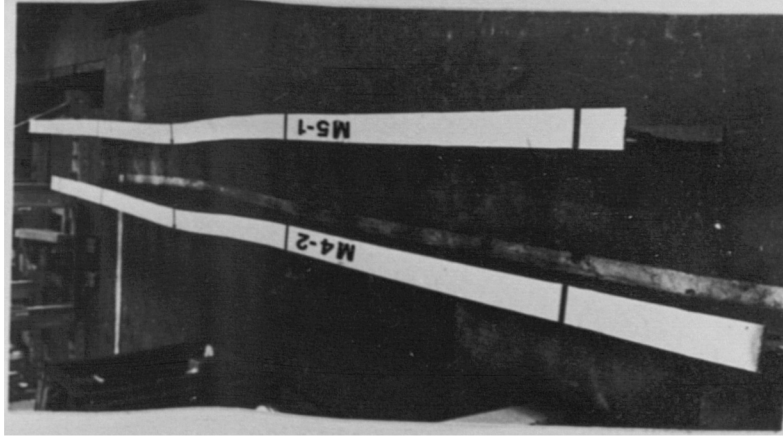


PLATE 6.4 BEAMS M4-2 AND
M5-1 AFTER TEST

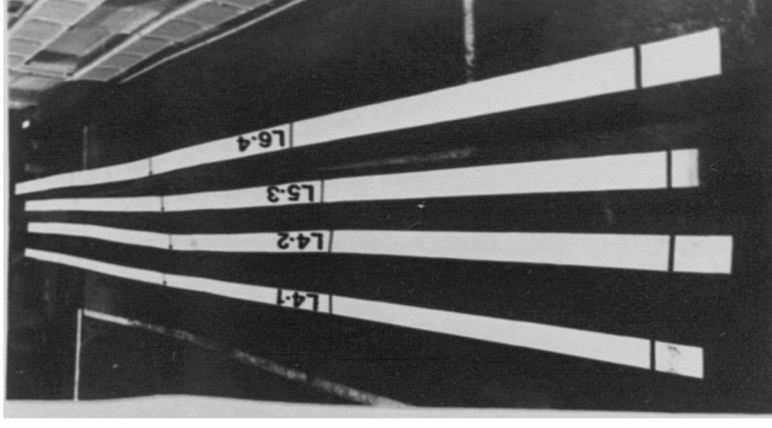
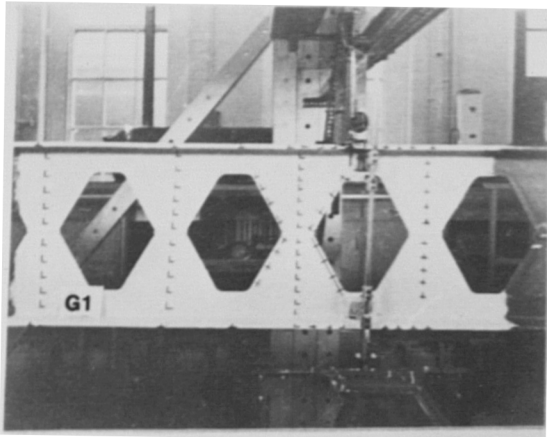


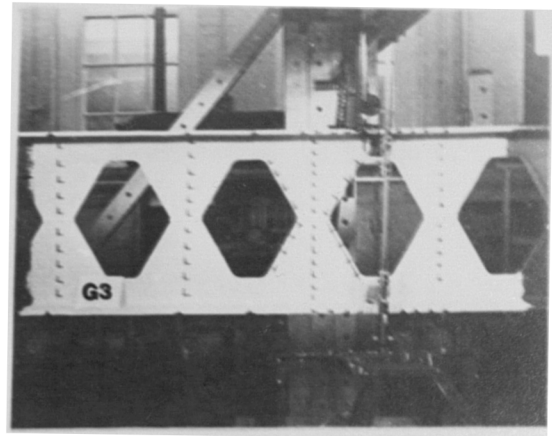
PLATE 6.5 BEAMS L4-1, L4-2,
L5-3 AND L6-4
AFTER TEST

Only the results concerning beam L4-2 will be described herein because of the similarity of the behaviour of the beams.

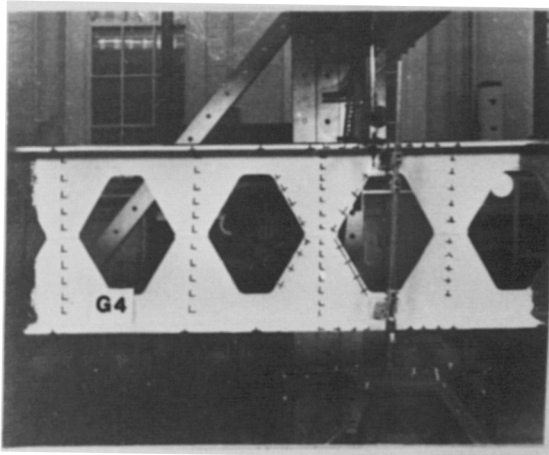
Plate 6.6 gives a set of photographs taken with the left-hand camera of the WILD C40 wide angle stereometric cameras described in chapter 5. Each photograph represents the beam at a load stage. It shows the progressive movement of the beam towards the cameras and in particular the deformation and tilting of the top flange which became very pronounced towards the end of the test especially after the beam passed its failure load of 79 kN (load applied by the jack at end A). The lightweight frame which was connected to the transducers fixed on the board by means of wires can be clearly seen to be accompanying the movement of the beam throughout the test. Although many crosses were drawn on the beam at various locations as seen on the photographs of Plate 6.6, only the displacements of the target points shown in Fig.6.14 are given. Despite the fact that the displacements of the points in the vertical and lateral planes could be calculated, only the values for the lateral displacement are given. Fig 6.15 shows the increasing lateral buckling of the top flange of half span BD. Figs. 6.16 to 6.19 give the displacement of the centreline of web posts W1, W2, W3 and W4 (see Fig.6.14). Some of the points on web posts W3 and W4 could not be seen on the photographs because two cameras were used. The deflection of the beam towards the cameras prevented the right-hand camera from covering all the points (the tilting of the top flange also hid the higher points on the centreline of the web posts from the cameras). The high number of points to be analysed on the STEK0 stereocomparator meant that human errors played a great part in the fact that some of the points plotted out of line on Figs. 6.16 to 6.19. The thickness of the 43 crosses drawn on the beam made the targetting on the same position for each of the



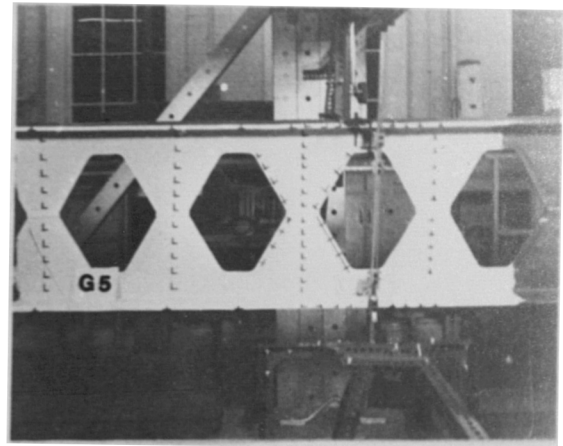
$$21.54\text{kN} = 0.28 R_{\max}$$



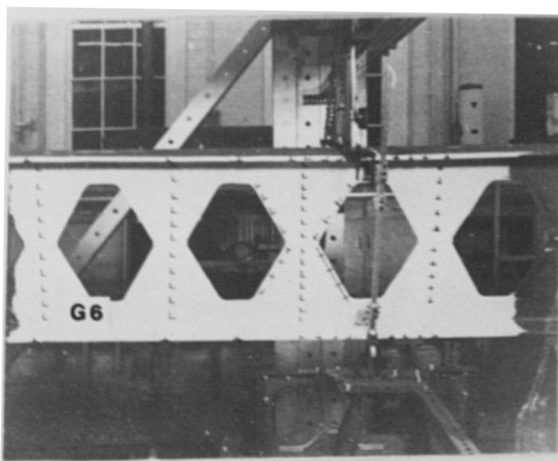
$$70.76\text{kN} = 0.90 R_{\max}$$



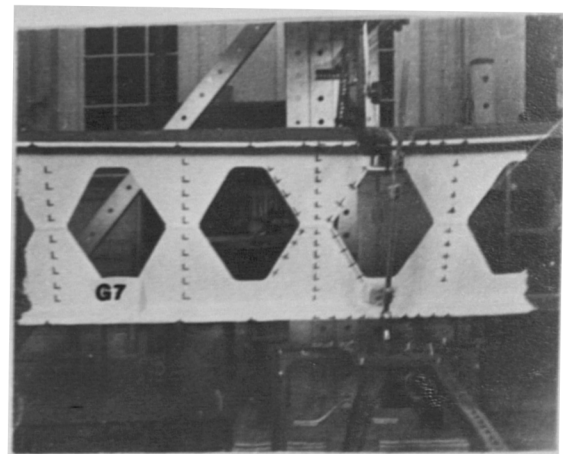
$$78.44\text{kN} = 0.99 R_{\max}$$



$$73.29\text{kN} = 0.93 R_{\max}$$



$$64.21\text{kN} = 0.81 R_{\max}$$



$$55.81\text{kN} = 0.71 R_{\max}$$

$$R_{\max} = 79.0\text{kN}$$

PLATE 6.6 DISPLACEMENTS OF BEAM L4-2 AT VARIOUS STAGES OF LOADING

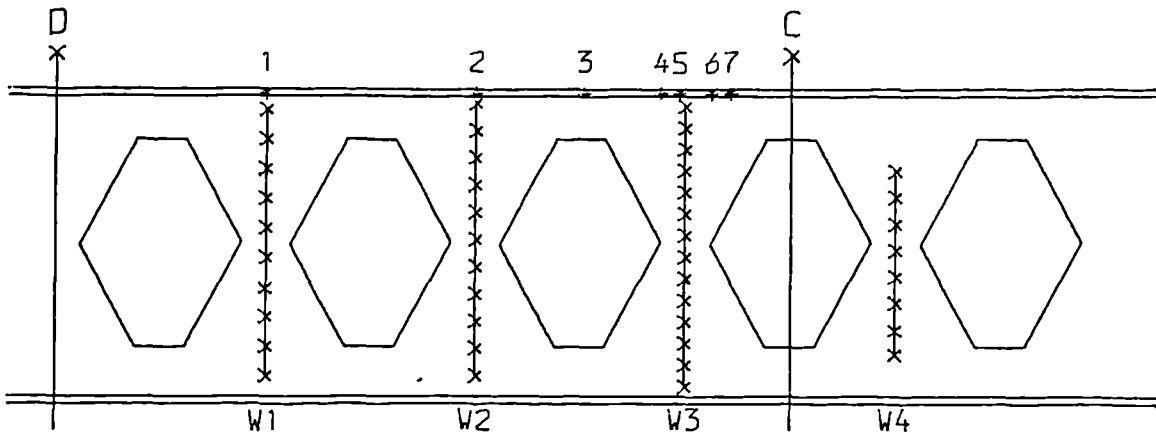


FIG. 6.14 LOCATION OF THE TARGET POINTS ON BEAM L4-2

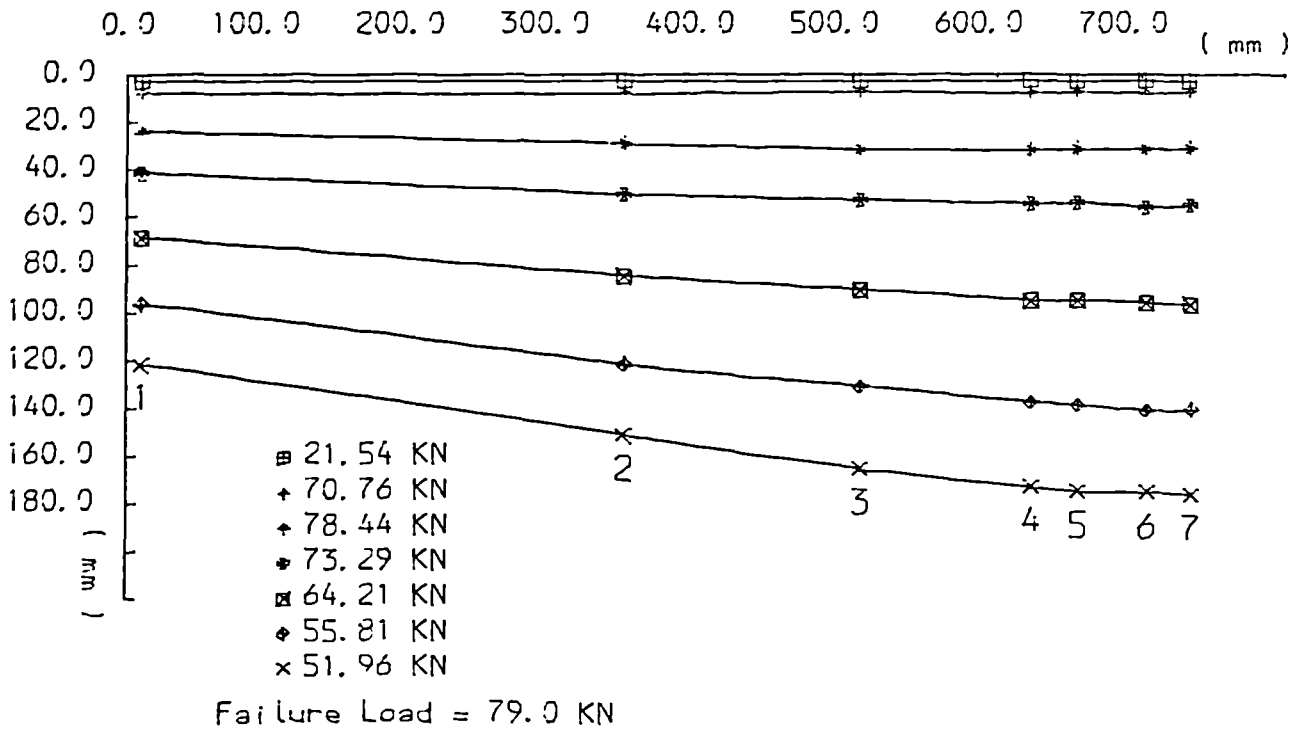


FIG. 6.15 DISPLACEMENTS OF POINTS 1-7 ON BEAM L4-2

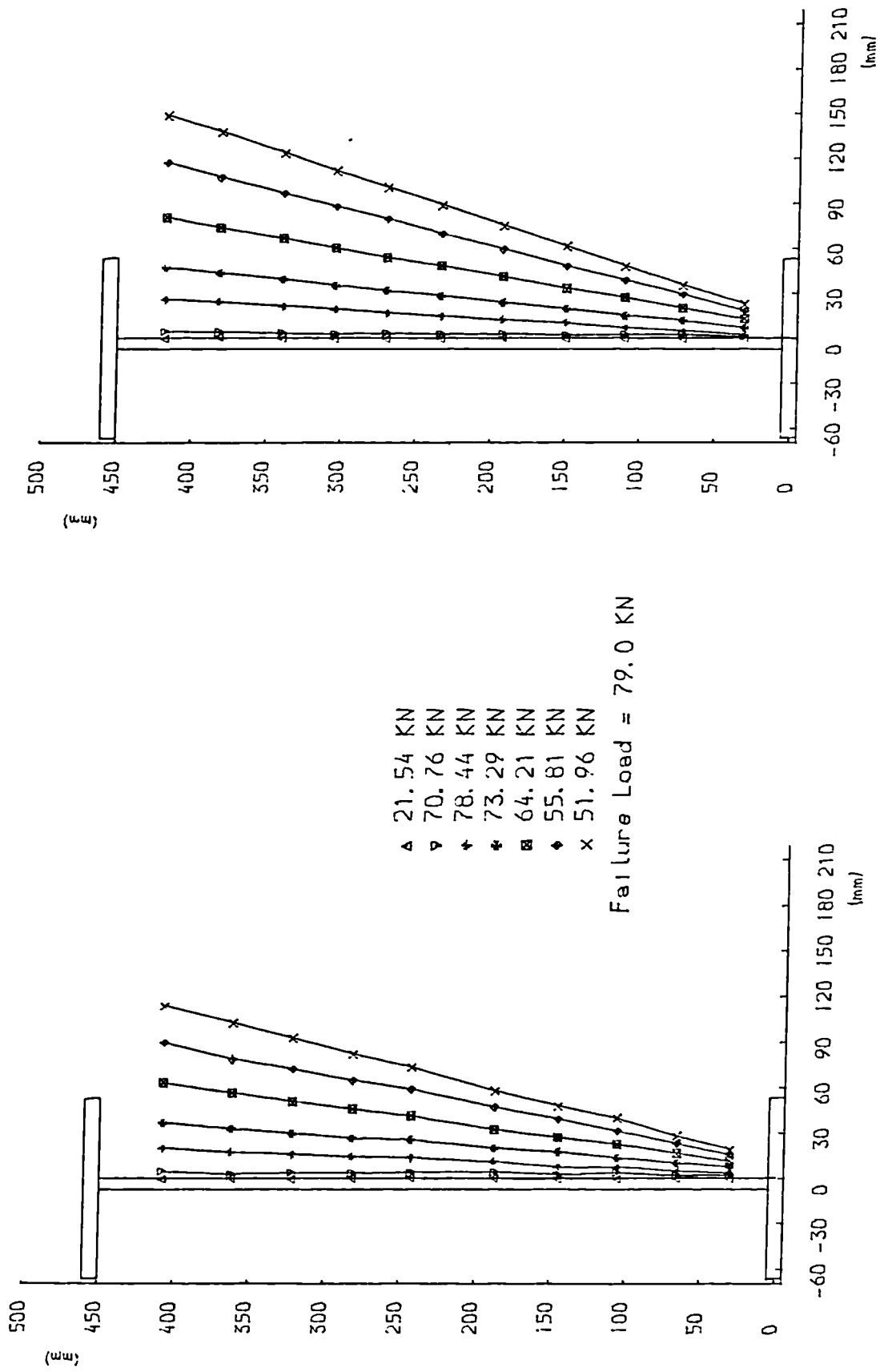
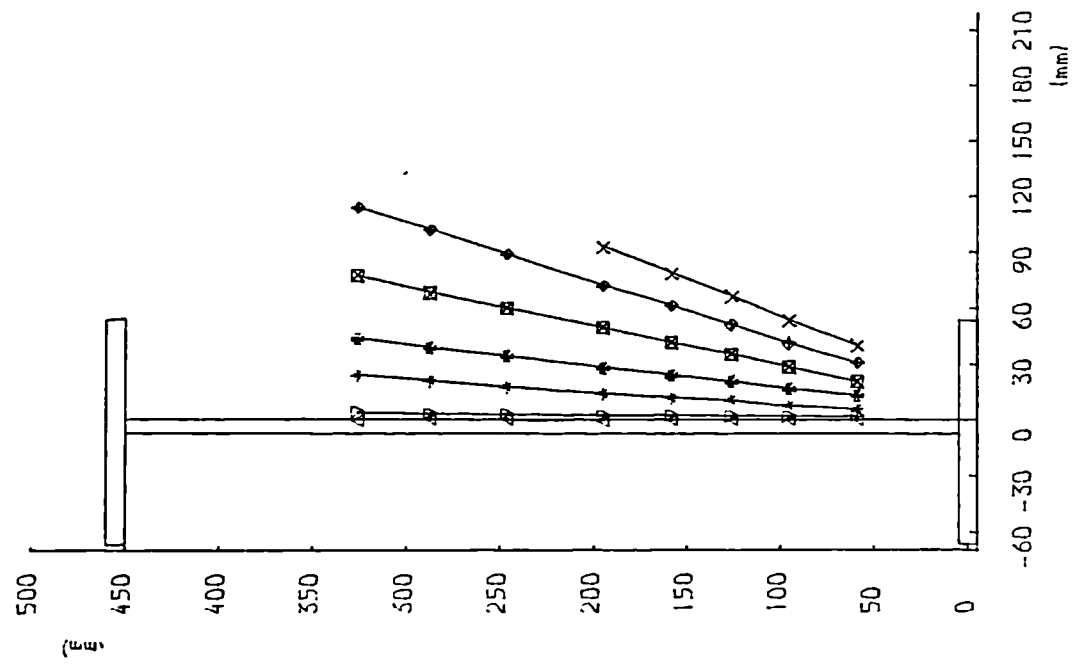


FIG. 6.16 DISPLACEMENT OF WEB POST W1

FIG. 6.17 DISPLACEMENT OF WEB POST W2



- △ 21.54 KN
- ▽ 70.76 KN
- + 78.44 KN
- * 73.29 KN
- 64.21 KN
- ◆ 55.81 KN
- × 51.96 KN

Failure Load = 79.0 KN

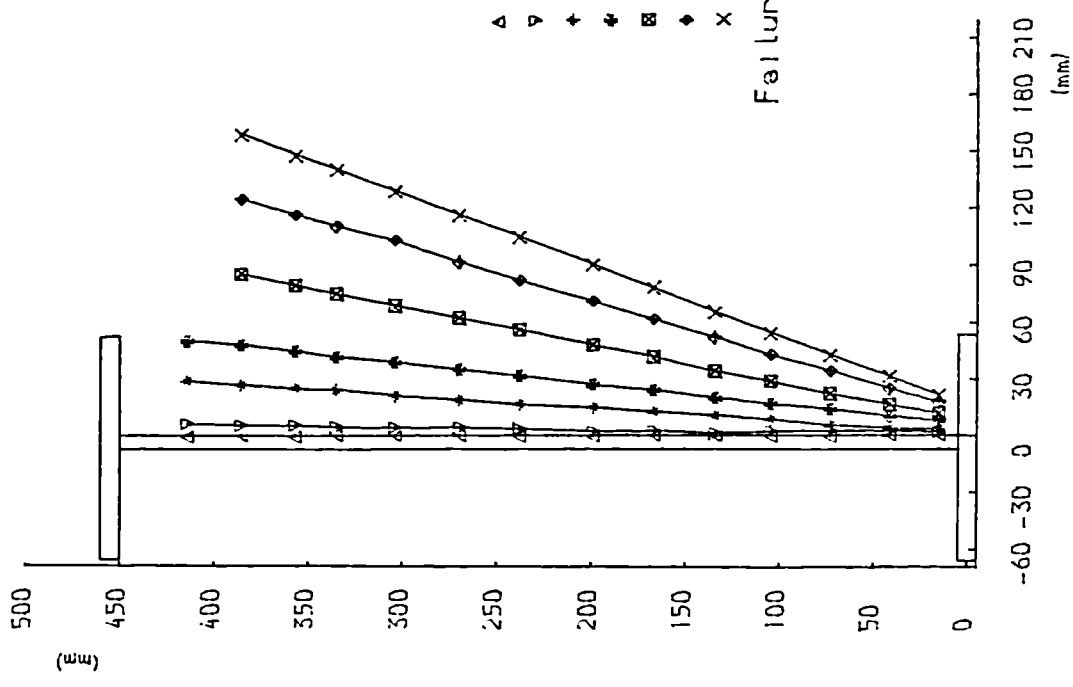


FIG. 6.18 DISPLACEMENT OF WEB POST W3

FIG. 6.19 DISPLACEMENT OF WEB POST W4

loading stages very difficult. Despite these inaccuracies the centreline of each of the web post moved sideways as straight lines and it can be safely said that the web posts did not distort although all the beams were taken well beyond their maximum capacity. The figures also show that the beams deflected very little before reaching the maximum load and then the lateral movement of the beams increased very rapidly. Furthermore no distortion of the web posts between adjacent castellations in the other two spans AB and DE was observed. This is evident in Plates 6.7 and 6.8 which show typical long and short specimens after removal from the test rig as well as in Plate 6.9 showing a late stage in the testing of beam M4-2.

6.6 Comparison of predicted failure loads for collapse modes other than lateral-torsional buckling with the experimental failure loads

6.6.1 Collapse modes

The eight beams chosen in the present investigation were primarily designed to fail by lateral-torsional buckling of their central span BD. Various calculations were then performed in order to check the stability and strength of the components of sidespans AB and DE. These checks were necessary in order to avoid any premature failure of the beams in the sidespans and therefore to obtain the desired failure mode of the central span. These calculations which were carried out in part 2 of chapter 4 showed that only beams S6-2 and S5-1 because of the ratios of lengths of the different spans might have failed in any of the following modes other than lateral-torsional buckling :

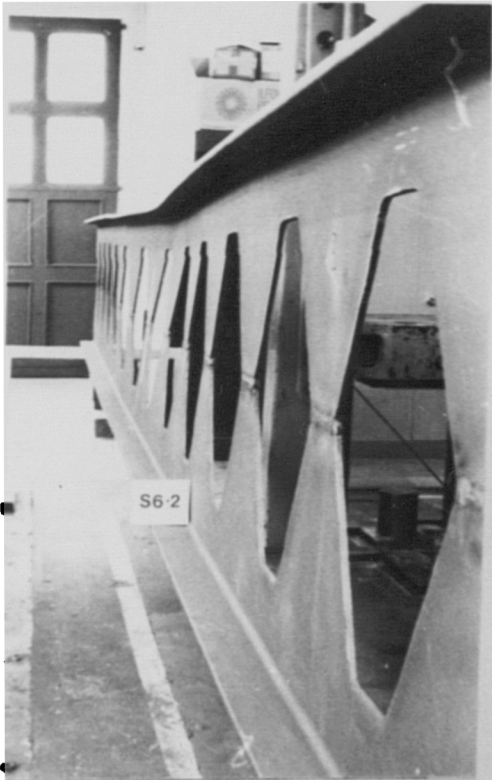


**PLATE 6.7 SIDE-VIEW OF BEAM
S6-2 AFTER TEST SHOWING NO
DISTORTION OF THE WEB POSTS**

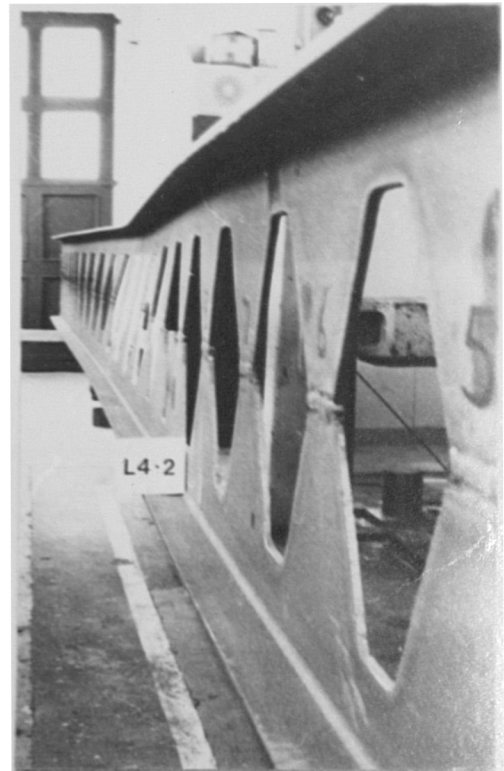


**PLATE 6.8 SIDE-VIEW OF BEAM
L4-2 AFTER TEST SHOWING NO
DISTORTION OF THE WEB POSTS**

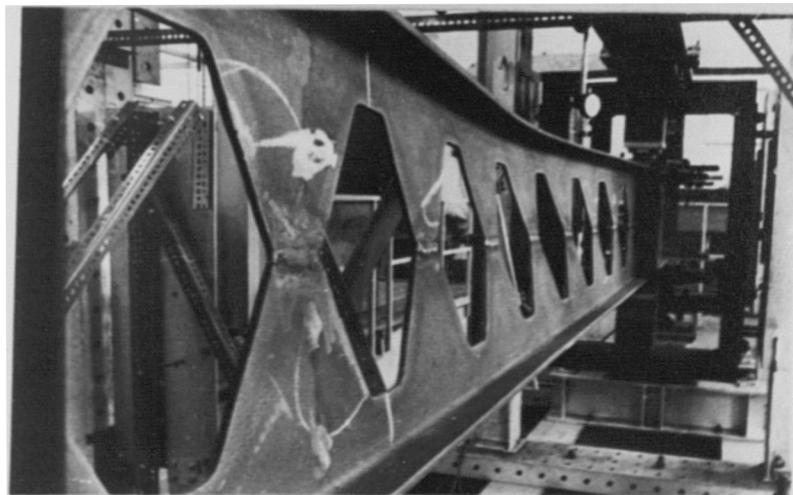


**PLATE 6.9 BEAM M4-2 IN A LATE STAGE OF THE TEST AND SHOWING
NO DISTORTION OF THE WEB POSTS**

1. Vierendeel mechanism.
2. Web post buckling due to - a directly applied force
- the shear force along the web weld
3. Web weld fracture.

The following discussion will therefore compare the beams maximum loads with the predicted loads for each of the possible failure modes for the the two short beams (plus beam M4-2 for the Vierendeel mechanism).

6.6.2 Vierendeel mechanism

This type of mechanism was the most likely to cause premature failure of the sidespans because of the high magnitude of the shear force needed to be applied at end A in order to produce lateral buckling failure of the middle span BD of the two short beams and that of beam M4-2. Although the beams which were reported in the literature to have developed a vierendeel mechanism (22,23,25) had holes which were different in shape than that of the beams used in the present investigation (the beams tested in refs. 22, 23 and 25 had square shaped holes with shallow throats whilst U.K. shaped holes have deeper throats and shorter chords) Table 6.3 below shows that a Vierendeel mechanism could have formed if the method of ref.52 had been used.

Beams	R_{AF} (kN)	R_{AP} (kN)	R_{AF}/R_{AP}
S6-2	199.7	164.9	1.20
S5-1	146.6	125.5	1.17
M4-2	112.9	109.1	1.04

Table 6.3 Failure Loads for Vierendeel Mechanism

A Vierendeel mechanism forms because the stress concentration at the re-entrant corners of the holes lead to the formation of plastic hinges. The values of nominal stresses calculated at these locations (see point 1a of section 1-1 of Fig.4.8) indicated that the stress concentration reported by every author (refs. 22, 23 and 25 in particular) would have been present and therefore although the shape of the holes was different from those of the beams which experienced a Vierendeel type of mechanism, ultimately this mechanism would have developed. Hosain (25) when reporting the collapse of beam A-1 of his test series indicated that yielding started in the top flange at the same point where beams S6-2 and S5-1 showed signs of local buckling. However the lateral buckling failure of the middle spans must have prematurely ended the possible formation of the Vierendeel mechanism.

6.6.3 Web post buckling

6.6.3.1 Web post buckling due to compressive force

The problem of web post buckling due to a directly applied force at points A, B, D and E was dealt with by placing stiffeners at each of the loading points. However in most cases, because of the lengths of the spans chosen, the loads were applied above a castellation between the web posts although previous investigations positioned the applied loads carefully over a web post. This practice is therefore unnecessary as long as load bearing stiffeners are used on each side of the web.

6.6.3.2 Lateral buckling

A number of beams failed either directly(16,23,24) or indirectly (25,30) as a consequence of web post twisting followed by buckling. Although most of these beams were not of the U.K. type, four British castellated beams were found to have failed because of web post buckling(16,30). The possible occurrence of failure brought about by web post buckling was reinforced by the preliminary calculations carried out by using the methods of refs. 45, 46 and 53. Although the values obtained were widely different, the rigorous method proposed by Aglan and Redwood (46) showed that beams S6-2 and S5-1 could fail prematurely because of web post buckling.

Although Hosain (25) came to the conclusion that web post buckling may not be regarded as causing premature failure as far as ultimate load is concerned, two of the three British castellated beams tested in ref.16 failed primarily because of web post buckling at loads well below their maximum in-plane carrying capacity M_p . Table 6.4 gives the dimensions of the section of each beam, their experimental moment and maximum in-plane carrying capacity. The stockiest beams with D/T values lower than 20 and wide flanges could not reach M_p , failing by buckling of the web posts whilst the more slender beam with a narrower flange failed at a load higher than M_p . The three beams had similar web thicknesses.

It is therefore possible to further check the methods of refs. 45, 46 and 53 with the experimental failure loads of Table 6.4. In contrast to the values of Table 4.11, Table 6.5 which summarizes the values of predicted loads gives nearly identical results for both Blodgett's and Aglan's methods. This is because Blodgett relied on an AISC lateral buckling design formula which gives better results as the

Sections	D/T	M_p ($\times 10^8$ Nmm)	M_{exp} ($\times 10^8$ Nmm)	M_{exp}/M_p
381x127x14.0x9.1	27.2	1.89	2.18	1.16
381x203.2x19.9x10.2	19.1	3.82	2.76	0.722
342.9x177.8x21x10.2	16.0	3.11	2.49	0.80

Table 6.4 Moment Capacities of the Beams of Ref.16 which failed by Web Post Buckling

Sections	Ref.45 R_p (kN)	Ref.46 R_p (kN)	Ref.53 R_p (kN)	R_{exp} (kN)	Ref.46 R_{exp}/R_p
381x127x14.0x9.1	61.2	172.1	166.8	422	2.45
381x203.2x19.9x10.2	86.1	193.5	192.5	523	2.70
342.9x117.8x21x10.2	96.2	172.8	175.3	473	2.74

Table 6.5 Comparison of Predicted Failure Loads R_p with Experimental Failure Loads for Beams which failed by Web Post Buckling

slendernesses of the web posts decrease. The beams tested in the present investigation had slender web posts and consequently the formula used by Blodgett gave values of critical loads closer to their elastic critical values, thus considerably under-estimating the actual failure loads. This is also confirmed by the results given by Hosain (25) in the case of the two beams which failed by web post buckling. The safety factor for the beam with the most slender web post was equal to 3.71 while the other beam with the more stocky web post had a safety factor of 1.65. The load factors calculated in Table 6.5 for Aglan's method varied between 2.45 and 2.74. It is therefore not surprising that web post buckling was not reported in the present investigation, failure loads equal to 2.5 times the recorded ones would have been impossible to attain.

6.6.4 Web weld fracture

Hosain (26,27) whilst studying the optimization of castellated beams defined the fracture of the web weld as a possible failure mechanism. However, although the values of the ratios of the lengths of the welded joint to that of the pitch of castellation of the beams he used were smaller than the equivalent ratio for British beams, thus making the possibility of a British beam failing by rupture of the weld very remote, the survey of the literature found that one British beam failed in the aforementioned mode (see Table 2.1). The values of ratios were 0.175 and 0.204 for Hosain's beams as compared to $0.251D_s/1.08D_s = 0.232$ in the case of the beams of the present series. The calculations of the stresses given in table 4.10 showed that there was a real possibility for beams S6-2 and S5-1 to fail in a similar way; the values of stresses due to shear force along the welded joints were

of the order of magnitude of the allowable shear stress of $p_y/\sqrt{3}$. However when similar calculations were performed for the beam of Table 2.1, the stress in the weld had a value of 285 N/mm^2 and the experimental moment was 1.15 times the maximum in-plane carrying capacity. It can therefore be safely suggested that the rupture of the weld was just a consequence of the complete yielding of the cross-section of the beam. This can be further confirmed when the maximum carrying capacity M_p of the six beams tested by Hosain are compared with the moments recorded at failure; three beams reached M_p while the other three just failed to attain the value of M_p . In contrast to the beams of refs. 16 and 26, the beams of the present investigation had longer sidespans which led to the need for comparatively lower shear force in order to attain the desired level of moment for the middle span. This conclusion can apply to all the failure modes in which shear force is the dominant factor.

CHAPTER 7

DISCUSSION OF THE RESULTS

7.1 Introduction

The eight castellated beams used in the investigation were chosen on the basis of the strength of their middle span BD, more specifically the resistance of the span against lateral-torsional buckling. The calculations which used the recommendations of cl. 6.3 of B/20 (14) were described in detail in chapter 4. Although the literature survey had shown that the properties of the beams should be calculated at the minimum section, i.e. through a hole, while calculating the maximum in-plane capacity M_p , this chapter will also compare the experimental strengths with the predicted strengths when the properties of the section are computed at a web post. These calculations will as well as showing the effect of using web post cross-sectional properties on the predicted strengths give a further indication of the influence of the holes on the strength of the beams.

In addition strength predictions were also performed using other available methods of assessing lateral buckling strength. Three were based on the actual British codes of practice BS 449 (9) and BS 153 (10) while the last one compared the B/20 proposals to the European recommendation for structural steelworks (87). These methods were :

1. BS 449 Table 3 for rolled sections
2. BS 449 Tables 8 and 9 for fabricated sections
3. BS 153 Tables 7 and 8
4. ECCS Recommendations cl. R.6.2.13

Hole and web post cross-sections will also be used in all the cases. Because these codes do not provide any recommendations regarding the design of castellated beams, these calculations will be used in

order to assess the safety factors they provide in the case of the beams used in the present investigation. Finally similar calculations will be carried out on the beams found in the literature review to have failed in a lateral-torsional buckling mode.

7.2 Comparison of B/20 with ECCS approach

The ECCS approach is basically very similar to that of B/20. Both give the moment capacity M_b of a beam in terms of the equivalent slenderness ratio $\bar{\lambda}_{LT} = \sqrt{M_p/M_E}$, although the recommendations use the alternative expression

$$\bar{\lambda}_{LT} = \sqrt{\alpha\sigma_r/\sigma_{cr,D}} \quad (7.1)$$

where α is the shape factor for major axis bending

σ_r is the material yield stress

$$\sigma_{cr,D} = M_E/Z_x$$

A limiting design bending stress σ_D is obtained from

$$\sigma_D = \delta_r \alpha \sigma_r \quad (7.2)$$

or

$$\delta_r = \frac{\sigma_D}{\alpha\sigma_r} = \frac{M_b}{M_p} \quad (7.3)$$

where δ_r is a reduction factor equal to

$$\delta_r = \left[\frac{1}{1 + \bar{\lambda}^{2n}} \right]^{\frac{1}{n}} \quad (7.4)$$

where n is a system factor.

δ_r is introduced in order to take into account the unavoidable imperfections and which for whatever value of n tends towards unity for $\bar{\lambda}_{LT}$ tending to zero and to zero for $\bar{\lambda}_{LT}$ tending to infinity. It therefore gives a curve of a shape similar to that of B/20. However by choosing a value of n equal to 2.5, the resulting curve corresponds to a mean value rather than a lower bound which is the case of the B/20 design curve. Another difference with the B/20 design curve is that the ECCS curve is a truly non-dimensional curve. The B/20 values will vary slightly depending on the values of the yield stress chosen. Fig.7.1 compares the two design curves in terms of moment capacity versus $\bar{\lambda}_{LT}$. It makes the point very clear that the B/20 design curve is a lower bound one and therefore the test points calculated by using it will always fall below the ECCS design curve when $M_b < M_p$.

7.3 B/20 other procedures

7.3.1 Description

The procedure adopted in chapter 4 used the idea of a lateral-torsional slenderness $\lambda_{LT} = \sqrt{\pi^2 E / \rho_y} \sqrt{M_p / M_E}$ in order to enter a design curve giving the buckling resistance moment M_b as a fraction of M_p the maximum in-plane moment capacity. It was also shown that by writing M_p and M_E in terms of the beam's geometrical properties λ_{LT} could be written as $\lambda_{LT} = u.v.\lambda$ (expressions for u and v were given in chapter 4). v is an expression which depends on λ , the slenderness ratio, and x , the torsional index. Studies of the values of u for currently available plain webbed sections show that it varies between 0.7 and 1.0, being approximately 0.9 for narrow flanged I-sections, e.g. U.B.s. and channels and approximately 0.85 for wide flanged I-sections, e.g. U.C.s. Furthermore x is found to be approximately equal to D/T for rolled

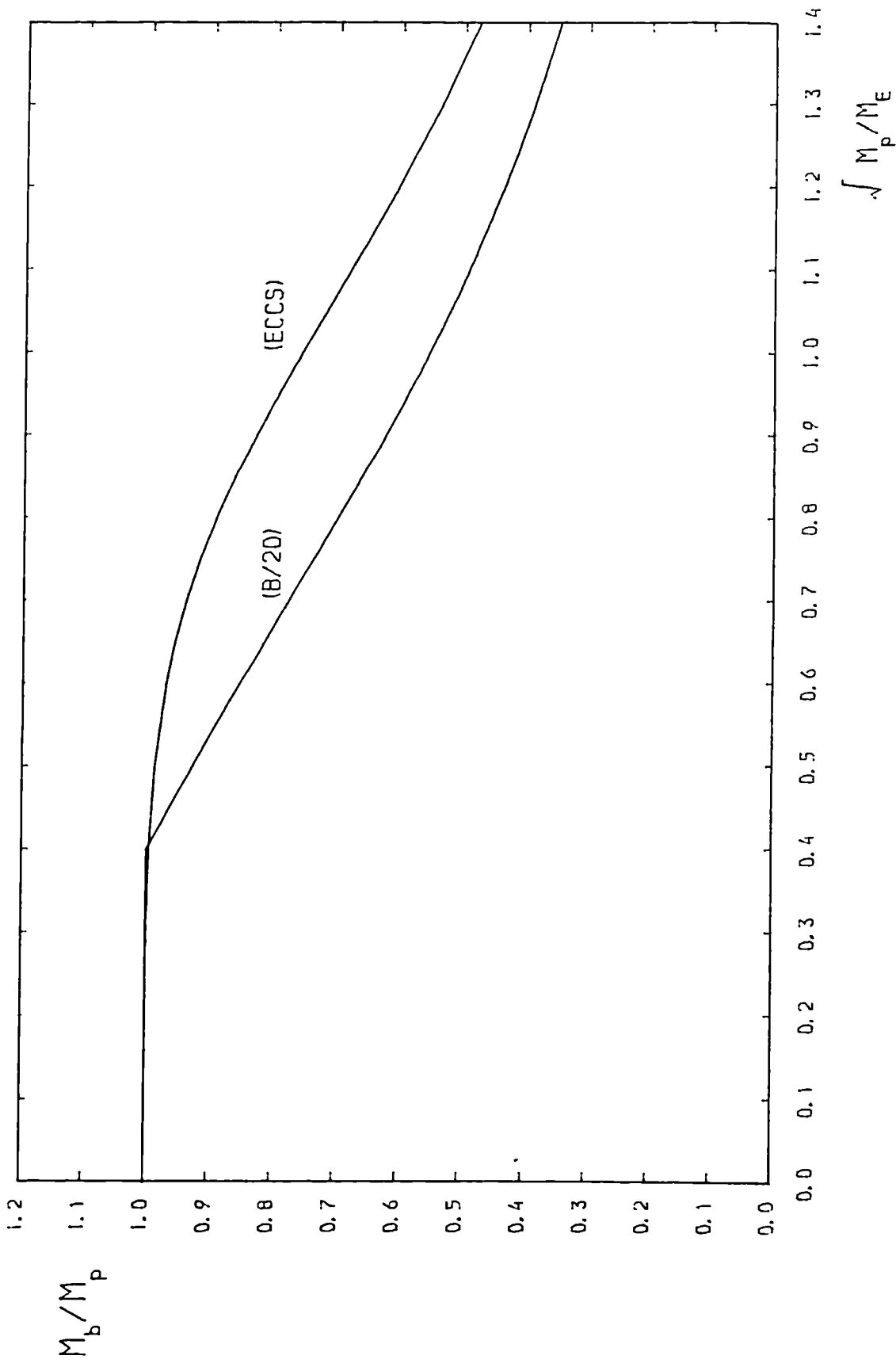


FIG. 7.1 COMPARISON OF B/20 DESIGN CURVE WITH ECCS PROPOSALS
 FOR SOLID WEB BEAMS ($P_y = 280$. N/mm^2)

sections. Therefore various possible interpolations of B/20 are possible depending on the value of λ_{LT} chosen. A final choice as suggested by cl.11.3.2.c of B/20 is to take $\lambda_{LT} = \lambda$ to calculate M_b . As a consequence the various possible approaches can be summarized as follows:

1. cl.11.3.2.c $\lambda_{LT} = kL/r_y$
2. "Exact" method $\lambda_{LT} = \sqrt{\pi^2 E / \rho_y} \sqrt{M_p / M_E}$
3. $\lambda_{LT} = u.v.\lambda$, using " exact " values for u and x
4. $\lambda_{LT} = u.v.\lambda$, using u = 0.9 and x = D/T
5. $\lambda_{LT} = u.v.\lambda$, using u = 1.0 and x = D/T

Once again both hole and web post cross-sectional properties were used. Table 7.1 gives the full list of λ_{LT} values obtained. The corresponding M_b values are given in Table 7.2. The various values of λ_{LT} obtained from procedures 1 to 5 will be compared in the following sub-paragraph.

7.3.2 Comparison between the various λ_{LT} values

The values of λ_{LT} obtained using the procedures 2 and 3 which were termed " exact " are identical when properties are calculated at the same section. The values of λ_{LT} taken at a hole will always be smaller than those calculated at a web post because of the influence of the plastic modulus of the section S_x which is the main factor in the calculation of λ_{LT} . The ratio between the values of λ_{LT} calculated at the two cross-sections will be nearly equal to the square root of the ratios of the values of S_x calculated at the same cross-section. It can be seen from Table 4.7 which gives the properties of the beams used in the present investigation that the average ratio of the two values of S_x is equal to 1.20. The ratio of λ_{LT} 's will therefore be $\sqrt{1.20} = 1.10$. The increase in the values of section properties when they are

	$\lambda = kL/r_y$		$\lambda_{LT} = \sqrt{\frac{M_D}{M_E}}$		$\sqrt{\frac{\pi^2 E}{p_y}}$		$\lambda_{LT} = u.v.\lambda$		$\lambda_{LT} = u.v.\lambda$ and $x = D/T$			
									u = 0.9		u = 1.0	
	hole	web	hole	web	hole	web	hole	web	hole	web	hole	web
S6-2	45.19	58.10	43.56	48.27	43.57	48.29	40.33	51.58	44.81	57.31		
S5-1	48.43	62.66	46.59	51.77	46.61	51.80	43.08	55.32	47.87	61.46		
M4-2	64.91	82.94	61.44	67.48	61.50	67.57	56.85	71.50	63.17	79.44		
M5-1	68.52	88.71	65.20	72.21	65.25	72.29	60.28	76.93	66.97	85.48		
L6-4	74.45	95.32	70.82	78.01	70.87	78.09	65.47	82.69	72.75	91.87		
L4-2	90.23	115.36	83.39	90.98	83.54	91.18	77.16	95.94	85.73	106.60		
L5-3	90.96	117.67	85.22	93.92	85.33	94.08	78.73	99.51	87.48	110.57		
L4-1	111.43	144.70	100.79	110.03	101.02	110.34	93.25	116.35	103.61	129.28		

Table 7.1 Slenderness of Test Beams

calculated at a web post will offset the decrease brought about by the shift to the right of λ_{LT} (horizontal axis in Fig.7.1) when the buckling moments of resistance M_b are calculated at the two sections. The increase will vary with the slenderness of the beams. For the two test beams of the series S the ratio of M_b 's will be equal to 1.18 decreasing to 1.14 for the two test beams of the series M and finally being equal to 1.10 for the last four test beams of the series L.

Approach 1 which approximates λ_{LT} to $\lambda = kL/r_y$ shows that at both locations, hole and web post cross-sections, values of λ_{LT} are higher than those calculated using approaches 2 and 3. However the value of the ratio λ/λ_{LT} differs depending on the cross-section used. When the hole cross-section is used, it varies from 1.04 for the stocky section to 1.10 for the most slender section; when web post cross-sectional properties are used, it becomes 1.21 and 1.32 respectively. The small increase in the value of λ_{LT} when hole cross-section properties are used means that the corresponding values of M_b are about 2% lower than the "exact" values. When web post properties are considered the difference goes up to 10% because of the larger value of the ratio λ/λ_{LT} .

It is interesting to note that the values of λ_{LT} obtained when using the approximate approaches of 4 and 5 are closer to the "exact" values when hole cross-sectional properties are used rather than web post cross-sectional properties. But whereas the values of λ_{LT} are lower and upper bounds to the "exact" values respectively when $u = 0.9$ and $u = 1.0$ for the first set of properties, they are all upper bounds for either values of u for the second set of properties. The corresponding values of M_b become upper and lower bounds to the "exact" values of M_b in the first case but are all lower bounds values in the second case.

A study of the various values of λ_{LT} and M_b obtained shows those

calculated for $u = 1.0$ and at hole cross-section are nearly equal to the "exact" values. Study of the values of u for the commercially available castellated sections showed that it varied between 0.965 and 0.975 with most values being in the range 0.971-0.973 (u was equal to 0.965 in the case of castellated section 458x102x25). It is therefore suggested that in the case of the castellated sections an approximate value of 0.970 can be used in the expression $\lambda_{LT} = u.v.\lambda$.

The approximation $x = D/T$ is also suggested by $B/20$. The comparison between the exact value $x = 0.566h\sqrt{A/J}$ and $x = D/T$ shows that in all cases the approximation is good. It is therefore suggested to keep $x = D/T$.

These approximations were used in the case of the test beams of the present series to calculate various values of λ_{LT} . Table 7.3 gives the details of the comparison between "exact" and approximate values. The table shows that although the exact value of x was 5% higher than the approximate value of x as in the case of beam S6-2, the resulting λ_{LT} value obtained by using $u = 0.970$ is only 0.2% lower than the exact value. In general the difference between accurate and approximate λ_{LT} varies between 0.20% and 0.5%. Because the sections chosen in the present investigation had large D/T values ($42.8 < x < 54.5$) the same calculations were performed on the British castellated sections used in previous experimental programmes (15,16,20,30). These beams were shallower having D/T values between 23.8 and 35.4 and Table 7.4 which gives the results of the calculations shows that similar conclusions are reached.

Test Beams	$x = D/T$	$x=0.566 h \sqrt{A/J}$ "exact"	u "exact"	$\lambda = kL/r_y$	$\lambda_{LT} = u.v.\lambda$ ($x = D/T$)	$\lambda_{LT} = u.v.\lambda$ "exact"	$\lambda_{LT} = u.v.\lambda$ $u=0.97, x=D/T$
S6-2	54.5	57.16	0.973	45.2	43.61	43.57	43.47
S5-1	49.5	51.55	0.973	48.43	46.57	46.61	46.43
M4-2	42.8	41.04	0.972	64.91	61.40	61.50	61.30
M5-1	49.6	51.66	0.973	68.52	65.17	65.25	64.97
L6-4	53.5	56.09	0.973	74.45	70.79	70.87	70.57
L4-2	42.3	43.21	0.972	90.23	83.32	83.54	83.15
L5-3	49.5	51.57	0.973	90.96	85.12	85.33	84.86
L4-1	43.0	44.63	0.971	111.43	100.64	101.02	100.54

Table 7.3 Comparison of Accurate and Approximate Values of λ_{LT} for the Beams of the Present Series

Ref.	Sections	$x = D/T$	$x=0.566 h \sqrt{A/J}$	u "exact"	$\lambda - kL/r_y$	$\lambda_{LT} = u.v.\lambda$ $x = D/T$	$\lambda_{LT} = u.v.\lambda$ "exact"	$\lambda_{LT} = u.v.\lambda$ $u=0.97$ $x=D/T$
15	266.7x101.6x9.8x6.3	27.21	27.01	0.973	28.91	27.75	27.74	27.65
16	381x114.3x12.8x7.6	29.77	30.16	0.975	75.80	68.90	69.0	68.55
16	342.9x101.6x11.6x7.6	29.56	29.80	0.974	47.80	45.15	45.17	44.97
20	457.2x127x12.9x8.38	35.44	36.27	0.973	35.50	34.12	34.14	34.0
30	228.6x76.2x9.6x5.8	23.81	23.65	0.975	16.60	16.09	16.05	16.0
30	228.6x76.2x9.6x5.8	23.81	23.65	0.975	24.84	23.90	23.90	23.83
30	228.6x76.2x9.6x5.8	23.81	23.65	0.975	33.12	31.37	31.55	31.32

Table 7.4 Comparison of Accurate and Approximate Values of λ_{LT} for Beams with U.K. Shaped Holes from other Test Series

7.4 Beams S6-2 and S5-1

7.4.1 Hole cross-sectional properties

7.4.1.1 B/20 approach

Table 7.5 which gives the moment capacities of beams S6-2 and S5-1 shows that in both cases the beam attained its theoretical capacity M_p calculated at a hole cross-section. Table 7.8 gives values of the ratio M_{exp}/M_{pred} . When considering these ratios it is of course necessary to bear in mind the point that whereas both B/20 and the ECCS recommendations are written in terms of limit state, BS 449 and BS 153 are permissible stress codes. Thus predictions using the latter documents already contain the full allowance for the load factor whilst the B/20 predictions make no such allowance, nor do the ECCS predictions. It should be also pointed out that the value of M_b from B/20 have been determined directly from the Perry formula for M_b in terms of M_p and M_E (cl.3.11 and chapter 4) Alternatively M_b can be determined from Tables 6.31 of B/20. These tables give values of p_b , the bending strength, in terms of λ_{LT} . It should be noted that the derivation of M_b from these tables include the use of a material factor $\gamma_m = 0.93$ which is not included when M_b is determined directly from the Perry formula.

Each of the tests yields a value for M_{exp}/M_p and a value for λ_{LT} . These test points can therefore be plotted and compared graphically to the B/20 and ECCS design curves. Fig.7.2 shows how for test beams S6-2 and S5-1 the experimentally obtained capacities exceed those obtained using the most rigorous approach of B/20 by about 10% whilst Fig.7.6 shows that they are nearly equal to the ECCS predictions. Although the slenderness of the two beams were higher than the limiting value for the attainment of M_p , they were just able to reach this load.

7.4.1.2 Permissible stress approaches

Table 7.5 shows that the moment capacities for the two beams obtained by using the method of BS 153 are 17% and 14% higher respectively than those obtained by using the two methods of BS 449. This is because in this range of slenderness, the maximum design stresses allowed by the two methods of BS 449 are equal but lower than that allowed by BS 153. This is therefore reflected in Table 7.8 which shows that the load factors associated with the BS 449 predictions are higher than 1.70, reaching 1.83 in the case of beam S5-1, but is less than 1.70 in the case of BS 153 predictions although these can be considered to be satisfactory not being less than 1.53. Table 7.11 gives the values of bending stresses allowed by BS 449 and BS 153. A design stress of 193 N/mm^2 is allowed by BS 153 in the case of beam S6-2 compared with only 165 N/mm^2 for both methods of BS 449.

7.4.2 Web post properties

7.4.2.1 Effect of using web post properties on the slenderness

The use of the properties of a web post cross-section rather than those of a hole cross-section leads to an increase in kL/r_y (due to a 22.6% reduction in r_y as shown in Table 4.7) and an increase in S_x of between 23.6% and 24.7% for the sections used herein as shown in Table 4.7. Because the predicted buckling moment is thus dependant upon two conflicting effects the result of this change will vary with beam slenderness; for low slenderness M_b will tend to increase whereas for sufficiently high slenderness it will decrease. Because of the different ways in which the various design approaches are formulated these decreases are most noticeable for the methods of BS 153 and for the Tables 8 and 9 approach of BS 449. The plateau in Table 3 of BS 449

delays the appearance of the reductions in M_b .

7.4.2.2 Comparison of the various approaches

Table 7.5 lists the predicted strength for each method while Table 7.8 gives the comparison of the test moments with the various design predictions. Since the theoretical values of M_p are now some 24% higher neither beam was able to attain this failing at loads somewhat below those predicted by B/20. If the proportion of M_b attained was 91% and 95% when the B/20 predictions are considered, the percentage drops to only 70% when the ECCS predictions are taken into consideration. In the case of the permissible stress predictions the load factors are reduced below those obtained for the cross-sectional properties except for BS 153 where they remain constant. In the case of the method of Table 3, the load factors are now below 1.7 while those obtained by using the other BS 449 method are just equal to 1.7. By studying the permissible stresses given in Table 7.11, it can be seen that the stresses obtained from Table 3 of BS 449 are still equal to the maximum 165 N/mm^2 while those obtained from the other methods are lower than the stresses calculated for hole cross-sectional properties although BS 153 design stresses are still higher than those of BS 449.

7.5 Beams M4-2 and M5-1

7.5.1 Allowance for moment gradient

Beam M4-2 was the only one of the series to be subjected to a deliberate moment gradient in its central span. The lengths of end spans AB and DE were such as to create a ratio of end moments $\beta = M_D/M_B = 0.8$. This condition is a less severe condition of loading than the condition of equal and opposite end moments. Allowance for the case of non-uniform

bending will therefore lead to economies in design. The usual approach to the problem is to base the modification to the design procedure presented in chapter 4 on a comparison of the elastic critical load for the actual case with the elastic critical load for the basic case, equal and opposite end moments(88).

The number of possible moment diagrams between points of effective lateral restraint can be classified under two main types:

1. Loading by end moments as is frequently encountered in practice when a beam is subjected to loads which act only at points of effective lateral restraints e.g. loads transferred to the main beam by cross beams.
2. Loading between points of effective lateral restraints as would occur for example on a crane girder.

Two procedures are given in cl. 6.3 of B/20 for dealing with these two types of problem. They are both based on the use of an "equivalent uniform moment factor" m . Its value gives a direct measure of the severity of the actual pattern of moments as compared with the basic pattern of equal and opposite end moments used in establishing the design curve. m is approximated as

$$m = 0.57 + 0.33\beta + 0.1\beta^2 \leq 0.43 \quad (7.5)$$

where β is the ratio of end moments. For any value of β the value of moment M at which instability will occur may be obtained as M_E/m .

The two ways of using the factor m in design are:

1. Use the value of the equivalent uniform moment $\bar{M} = m M_{\max}$ when checking the capacity against M_b (the correction is made on the vertical axis in the design curve).
2. In calculating M_b from the Perry formula (see eq.4.4) replace M_E by M_E/m , i.e. enter Fig.7.1 the B/20 design curve, with an effective value $\lambda_{LT} = \lambda_{LT} \sqrt{m}$ (the correction is made here on the horizontal axis).

Method 1 has been found to be appropriate in all cases where the loads are applied at points of effective lateral restraint which is the case for the present experimental investigation. The restriction of yielding to a region near the supports results only in a relatively small reduction in lateral buckling strength. Method 2 is appropriate when the point of maximum strength occurs within the span and reduction in stiffness due to yield usually exceeds the benefit of the less severe pattern of moments (88).

These proposals constitute a major revision of BS 449 and BS 153 approaches for which the omission of such guidance meant that all beams were designed for uniform moment loading, a process that is unnecessarily conservative in many cases, particularly where slender beams are concerned.

7.5.2 Hole cross-sectional properties

7.5.2.1 B/20 predictions

Values of M_{exp} for the two beams M4-2 and M5-1 are compared with the various predicted strengths in Table 7.6. In both cases failure occurred by inelastic lateral-torsional buckling at moments below the theoretical values of M_p calculated for a hole cross-section. Table 7.9

Lists the various ratios M_{exp}/M_{pred} . The discrepancy between the values of M_{exp}/M_p for the two beams is due to the fact that in the case of beam M5-1, $M_{exp} = M_c$ (moment calculated at the centre of span BD) whereas for beam M4-2, $M_{exp} = M_{max} = M_{AB}$. However as shown in Table 7.9 as well as on the graphical comparison of Fig.7.2, use of the most rigorous B/20 approach leads to slight under-predictions. For beam M4-2 the test point appears at first to plot slightly high. This is because no allowance has been made for the less severe pattern of moments. For the purpose of Figs. 7.2 to 7.5 the allowance is illustrated as an increase in the design curve for $\beta \neq 1.0$ instead of a scaling down of the test point by m . It was reported in chapter 5 that the ratio of end moments β varied between 0.812 and 0.887 (Table 6.1) with a mean value of 0.853 and a standard deviation of 0.022. Making the comparison on this revised basis ($\beta = 0.8$) suggests that the margin between the experimental strengths and the B/20 predictions is approximately the same for this test as for the others in the series.

7.5.2.2 ECCS predictions

Allowance for non-uniform moments in the ECCS method is always by means of a correction to λ_{LT} which should be calculated using the value of M_E for the actual load arrangement (this corresponds to a correction on the horizontal axis in Fig.7.1). For test M4-2 this reduces λ_{LT} by 5.3% with a corresponding increase in the predicted M_b of 1.75%.

The ECCS predictions in this range of slenderness are rather less satisfactory than those of the B/20. Fig.7.6 which compares the test data with the ECCS design curve shows that the experimental strength of beam M5-1 reached 88% of the predicted strength while test M4-2 plotted slightly above the curve.

7.5.2.3 Other predictions

Predictions using the methods of BS 449 become less satisfactory for this range of slenderness in the case beam M5-1, the load factors recorded being less than 1.7 for the three approaches. Use of the Table 3 method of BS 449 produces a low value of load factor equal to 1.47 because the design stress allowed is still equal to the maximum value of 165 N/mm^2 (Table 7.11) whereas a design stress of only 146 N/mm^2 is given by Tables 8-9 of BS 449.

All the load factors recorded for beam M4-2 are well above the safe value of 1.7 reaching 2.06 for the Tables 8-9 approach of BS 449. It shows that not allowing for the beneficial effects of unequal end moments under-predicts considerably the strength of the beam when permissible design methods are used.

7.5.3 Web post cross-sectional properties

Use of web post properties causes the B/20 predicted strength of beam M5-1 to exceed the experimental strength by 3% while that of beam M4-2 is under-estimated by the same amount (see Table 7.9). This is apparent in Fig.7.3 where test point M4-2 plots above the design curve while test point M5-1 plots below it. However both predictions are less satisfactory than when hole properties were used. Similarly for the Table 3 method of BS 449 the load factors are reduced to 1.3 and 1.65 respectively for beams M5-1 and M4-2. These decreases are due to the fact that the design stresses are still equal to those allowed when hole properties were used. For the other permissible stress methods, however, the increases in slenderness are sufficient to reduce the design stresses and thus produce increases in load factors generally above 1.7.

7.6 Beams L6-4, L4-2, L5-3 and L4-1

7.6.1 Hole cross-section

7.6.1.1 Limit state approaches

Table 7.7 gives the moment capacities of the beams with the longest central span while Table 7.10 compares the test moments with the various design predictions. The Table shows that each of the four beams failed at moment significantly below both M_p and M_E with the most slender specimen L4-2 reaching some 89% of M_E . The stockiest specimen L6-4 meanwhile developed only 52% of M_E . Although the central span length of beam L6-4 made it fall into the group L of the series, its slenderness ratio of only 70.82 made it to belong more to group M of the series rather than to group L. In particular its similarity with beam M5-1 whose slenderness was 65.20 and which reached 47% of M_E and 80% of M_p (the value of the ratio M_{exp}/M_p being 0.77 for beam L6-4) is very striking.

Table 7.10 shows that in each case the strength obtained from the most rigorous B/20 design approach using the properties at a hole cross-section was exceeded. The load factors varied between 1.12 for the stockiest beam (L6-4) to 1.40 for the most slender beam (L4-1). Beams L4-2 and L5-3 which had an intermediate slenderness value of 85.0 showed that the design strength was exceeded by more than 22%. These results are in accordance with previous comparisons (89,90) for solid web beams which also exhibit significant under-predictions in the region of high slenderness.

Fig.7.6 indicates that the ECCS design curve tends to over-predict the test results, the one exception being the most slender beam L4-1 for which the test point falls on the curve. The other three points reached about 90% of the ECCS predicted strength.

7.6.1.2 Permissible stress approaches

Results based on the Table 3 method of BS 449 give rise to some concern. The method which is a permissible approach gives a slightly higher predicted strength for beam L4-1 than that of B/20; the predictions for beams L4-2 and L5-3 are nearly equal to that of B/20. The margins of failure shown in Table 7.10 are consequently very low and of the order of 1.3 (these have to be compared with an allowable load factor of 1.7). These low load factors can be explained by the high design stresses that BS 449 allows for slendernesses less than 90. Only beam L4-1 whose slenderness ratio λ_{LT} was higher than 90 ($\lambda_{LT} = 110.4$) had a design stress of 145 N/mm^2 which was below the maximum permitted of 165 N/mm^2 .

Use of the two-stage procedure of both BS 449 and BS 153 does however lead to more satisfactory load factors although those obtained from the latter are between 5.4% and 9.6% lower than those obtained from the former. In both cases the highest value of slenderness leads to the highest value of load factors with those from BS 449 being generally higher than 1.7 and those from BS 153 lower than 1.7. In this range of slenderness, the design stresses allowed by both methods are lower than those obtained from Table 3 of BS 449.

The comparison between the ratios obtained for beam L6-4 and those of beam M5-1 still furthers the similarity between the two beams. Tables 7.9 and 7.10 show that the load factors for both the two-stage approaches are nearly equal, the difference being only 7% for the Table 3 approach.

	M_E	M_p	B / 20 M_b	ECCS M_b	BS 449 Table 3 M_b	BS 449 Tables 8-9 M_b	BS 153 M_b	M_{exp}
Properties at a hole	S6-2	3.53	3.25	3.48	1.96	1.96	2.29	3.49
	S5-1	8.38	2.25	2.46	1.38	1.38	1.57	2.52
Properties at a web post	S6-2	13.58	3.83	4.93	2.16	2.05	2.27	3.49
	S5-1	8.46	3.14	3.58	1.57	1.45	1.59	2.52

Table 7.5 Moment Capacities for Beams with Short Central Spans (x10⁹ Nmm)

	M_E	M_P	B / 20 M_b	ECCS M_b	BS 449 Table 3 M_b	BS 449 Tables 8-9 M_b	BS 153 M_b	M_{exp}
Properties at a hole	M4-2	2.18	1.82*	2.05*	1.55	1.04	1.15	2.14
	M5-1	2.55	1.84	2.32	1.38	1.22	1.33	2.03
Properties at a web post	M4-2	2.68	2.08*	2.87*	1.30	1.02	1.11	2.14
	M5-1	3.18	2.10	3.50	1.57	1.16	1.26	2.03

* enhanced values to take account of moment gradient effect

Table 7.6 Moment Capacities for Beams with Medium length Central Spans ($\times 10^6$ Nmm)

	M_E	M_p	$B/20$ M_b	ECCS M_b	BS 449 Table 3 M_b	BS 449 Tables 8-9 M_b	BS 153 M_b	M_{exp}
Properties at a hole	L6-4	3.54	2.41	3.12	1.97	1.64	1.80	2.70
	L4-2	2.18	1.22	1.66	1.16	0.858	0.930	1.49
	L5-3	2.58	1.42	1.95	1.39	1.01	1.06	1.79
	L4-1	1.98	0.858	1.17	0.901	0.622	0.661	1.20
Properties at a web post	L6-4	4.36	2.69	4.26	2.19	1.53	1.65	2.70
	L4-2	2.68	1.35	2.18	1.12	0.764	0.817	1.49
	L5-3	3.22	1.56	2.55	1.32	0.877	0.925	1.79
	L4-1	2.47	0.943	1.55	0.782	0.551	0.566	1.20

Table 7.7 Moment Capacities for Beams with Long Central Spans ($\times 10^8$ Nmm)

	M_{exp}/M_E	M_{exp}/M_p	$B/20$ M_{exp}/M_b	ECCS M_{exp}/M_b	BS 449 Table 3 M_{exp}/M_b	BS 449 Tables 8-9 M_{exp}/M_b	BS 153 M_{exp}/M_b
Properties at a hole	S6-2	0.989	1.07	1.002	1.78	1.78	1.53
	S5-1	1.00	1.12	1.03	1.83	1.82	1.60
Properties at a web	S6-2	0.799	0.911	0.709	1.62	1.70	1.54
	S5-1	0.803	0.951	0.704	1.61	1.74	1.58

Table 7.8 Comparison of Test Moments with Various Design Predictions for Beams with Short Central Span

Properties at a hole	M_{exp}/M_E	M_{exp}/M_p	$B/20$ M_{exp}/M_b	ECCS M_{exp}/M_b	BS 449 Table 3 M_{exp}/M_b	BS 449 Tables 8-9 M_{exp}/M_b	BS 153 M_{exp}/M_b
Properties at a hole	M4-2	0.982	1.18*	1.04*	1.86	2.06	1.86
	M5-1	0.797	1.10	0.878	1.47		
Properties at a web post	M4-2	0.799	1.03*	0.746*	1.65	2.09	1.93
	M5-1	0.639	0.968	0.581	1.29		

* M_b allows for moment gradient

Table 7.9 Comparisons of Test Moment with Various Design Predictions for Beams with Medium Central Spans

	M_{exp}/M_E	M_{exp}/M_p	$B/20$ M_{exp}/M_b	ECCS M_{exp}/M_b	BS 449 Table 3 M_{exp}/M_b	BS 449 Tables 8-9 M_{exp}/M_b	BS 153 M_{exp}/M_b
Properties at a hole	L6-4	0.764	1.12	0.868	1.37	1.65	1.51
	L4-2	0.681	1.22	0.895	1.28	1.73	1.60
	L5-3	0.692	1.26	0.914	1.28	1.77	1.68
	L4-1	0.605	1.40	1.024	1.33	1.93	1.81
Properties at a web post	L6-4	0.511	1.005	0.635	1.24	1.77	1.64
	L4-2	0.651	1.10	0.682	1.33	1.94	1.82
	L5-3	0.689	1.14	0.699	1.35	2.04	1.93
	L4-1	0.850	1.27	0.775	1.53	2.18	2.12

Table 7.10 Comparison of Test Moments with Various Design Predictions for Beams with Long Central Span

Test Beams	D/T	$\lambda = kL/r_y$		BS 449 Table 3 P_{bc}		BS 449 Tables 8-9 P_{bc}		BS 153 P_{bc}	
		hole	web	hole	web	hole	web	hole	web
S6-2	54.5	45.2	58.1	165.	165.	165.	157.	193.	173.
S5-1	49.5	48.4	62.7	165.	165.	165.	153.	187.	167.
M4-2	42.8	64.9	82.9	165.	165.	149.	130.	165.	141.
M5-1	49.6	68.5	88.7	165.	165.	146.	122.	159.	133.
L6-4	53.5	74.4	95.3	165.	163.	138.	114.	150.	123.
L4-2	42.3	90.2	115.4	165.	141.	122.	96.	132.	103.
L5-3	49.5	90.9	117.7	165.	138.	120.	92.	127.	97.
L4-1	43.0	111.4	144.7	145.	111.	100.	78.	107.	80.

Table 7.11 Values of Allowable Bending Stresses P_{bc} Calculated using BS 449 and BS 153 Methods (N/mm²)

7.6.2 Web post properties

Use of web post properties causes some reduction in the ratio M_{exp}/M_b obtained from the B/20 approach but in contrast to the short and medium length beams, all the load factors are now greater than 1.0 and the four test points plot above the B/20 design curve of Fig.7.3. However Fig.7.7 shows that the test points plot well below the ECCS design curve and Table 7.10 shows that the beam L6-4 attained only 64% of its ECCS predicted strength while the more slender beam L4-1 reached 78% of M_b .

For each of the permissible stress approaches the safety margins are with one exception increased. However those for the Table 3 approach of BS 449 remain significantly less than 1.7, beam L6-4 giving a load factor lower than that obtained with hole properties. The reason for these lower predicted strengths is that the increase in λ which follows from the reductions in r_y shown in Table 4.7 is now more significant than the increase in section modulus (even for the Table 3 method for which the λ values now exceed the plateau value of 90.0). Table 7.11 shows that the λ values vary between 95.0 for beam L6-4 to 144.0 for beam L4-1 while the permissible stresses from Table 3 vary respectively from 163 N/mm² to 110.7 N/mm² (the value of 163 N/mm² explains the lower load factor of 1.24 obtained for beam L6-4).

7.7 Results from other tests

7.7.1 Introduction

A total of ten beams failed by lateral buckling when tested by previous authors for in-plane behaviour (15,16,20,22,24) while three beams (30) which were tested for lateral-torsional buckling behaviour failed in a flexural mode. The range of slenderness ratios varied

between 16.6 and 75.0 while the D/T ratios varied between 23.8 and 58.5. Some were expanded according to the British module (15,16,30) while the others were expanded differently (20,22,24). Similar calculations to those carried out on the eight beams of the present test programme were performed and the results are presented in Tables 7.12 to 7.15. A detailed comment on these results is given below.

7.7.2 Hole Cross-section

7.7.2.1 Permissible stress approaches

All the beams had slendernesses which indicated that they were likely to reach their maximum in-plane moment capacity M_p . As was explained in chapters 2 and 4 the only beam which did not (castellated section 381x114x12.8x7.6) failed prematurely because of the inability of the bracing to hold the beam in position (16). The value of failure load given was approximate and no conclusion can be drawn from the test (apart from a reminder about the importance of the bracing).

The slendernesses of the other beams were in the low range with values varying from 16.6 to 47.8 with four beams having slendernesses below 30.0, six beams having slendernesses between 30.0 and 40.0 and two between 30.0 and 47.8. This means that the maximum predicted strength can be calculated when both methods of BS 449 are used (Table 7.12). This is because in both cases the maximum design stress of 165 N/mm^2 is allowed. In the case of moments predicted by BS 153, only in the case of the beams of refs. 16, 20 and the shallowest beam from ref.22 ($D/T = 52$) was the allowable stress not equal to the maximum permitted. Because in this range of slenderness the design stresses allowed by BS 153 are higher than those from BS 449, the ratio M_{exp}/M_b obtained from the former are lower than those from the latter. Neglecting the test from

Ref.	Sections	kL/r _y	D/T	BS 449 Table 3		BS 449 Tables 8-9		BS 153		B / 20	ECCS	M _b ^{exp}
				P _y *	M _b *	P _y	M _b	P _y	M _b			
15	266.7x101.6x9.8x6.3	28.9	27.2	165	0.469	165	0.469	174	0.495	0.782	0.727	0.847
16	381x114.3x12.8x7.6	75.8	29.8	165	1.02	141.5	0.871	139	0.856	1.15	1.46	1.03
16	342.9x101.6x11.6x7.6	47.8	29.6	165	0.749	165	0.749	167	0.758	1.08	1.16	1.154
20	457.2x127x12.9x8.38	35.5	35.4	165	1.43	165	1.43	154	1.50	2.26	2.20	2.26
22	266.7x101.6x5.1x4.57	42.7	52.	165	0.289	165	0.289	195	0.341	0.500	0.525	0.499
	299.9x100.3x5.13x4.83	34.3	58.1	165	0.317	165	0.317	198	0.381	0.566	0.558	0.577
	297.2x99x5.08x4.7	29.0	58.5	165	0.309	165	0.309	198	0.370	0.603	0.576	0.574
24	295.9x100.3x5.15x4.4	33.4	57.5	165	0.310	165	0.310	198	0.372	0.595	0.589	0.605
	500x135x10.2x6.6	30.4	49.	165	1.36	165	1.36	198	1.63	2.52	2.43	2.62
30	500x135x10.2x6.6	38.	49.	165	1.36	165	1.36	198	1.63	2.39	2.41	2.52
	228.6x76.2x9.6x5.8	16.6	23.8	165	0.292	165	0.292	198	0.351	0.617	0.537	0.591
		24.8	23.8	165	0.292	165	0.292	198	0.351	0.581	0.537	0.581
		33.1	23.8	165	0.292	165	0.292	198	0.351	0.612	0.535	0.612

* P_y N/mm² ; * M_b x10⁶ Nmm

Table 7.12 Moment Capacities Calculated at a Hole Cross-section

Ref.	Sections	M_{exp}/M_b				
		BS 449 Table 3	BS 449 Tables 8-9	BS 153	B/ 20	ECCS
15	266.7x101.6x9.8x6.3	1.80	1.80	1.71	1.08	1.17
16	381x114.3x12.8x7.6	1.01	1.19	1.20	0.896	0.705
16	342.9x101.6x11.6x7.6	1.54	1.54	1.52	1.07	0.995
20	457.2x127x12.9x8.38	1.58	1.58	1.50	1.0	1.03
22	266.7x101.6x5.1x4.57	1.73	1.73	1.46	0.998	0.95
	299.9x100.3x5.13x4.8	1.82	1.82	1.52	1.02	1.03
	297.2x99x5.08x4.7	1.86	1.86	1.55	0.952	0.997
	295.9x100.3x5.15x4.4	1.95	1.95	1.63	1.02	1.03
24	500x135x10.2x6.6	1.93	1.93	1.60	1.04	1.03
	500x135x10.2x6.6	1.85	1.85	1.56	1.05	1.05
30	228.6x76.2x9.6x5.8	2.02	2.02	1.68	0.858	1.10
		1.99	1.99	1.66	1.0	1.08
		2.10	2.10	1.74	1.12	1.14

Table 7.13 Comparison of Test Moments with Various Design Predictions-
properties at a Hole Cross-section

Ref.	Sections	kL/r _y	D/T	BS 449 Table 3		BS 449 Tables 8-9		BS 153		B/20	ECCS	M _{exp}
				P _y	M _b	P _y	M _b	P _y	M _b			
15	266.7x101.6x9.8x6.3	31.16	27.2	165	0.517	165	0.517	174	0.545	0.848	0.847	0.847
16	381x114.3x12.8x7.6	86.8	29.8	165	1.133	165	1.065	150.5	1.034	1.34	1.71	1.03
	342.9x101.6x11.6x7.6	50.22	29.6	165	0.844	165	0.844	167.5	0.857	1.35	1.39	1.154
20	457.2x127x12.9x8.38	44.7	35.4	165	1.61	165	1.61	193.5	1.89	2.66	2.67	2.26
22	266.7x101.6x5.1x4.57	50.14	52.	165	0.305	165	0.305	184	0.340	0.543	0.594	0.499
	299.9x100.3x5.13x4.83	43.93	58.1	165	0.355	165	0.355	193	0.416	0.674	0.711	0.577
	297.2x99x5.08x4.7	37.17	58.5	165	0.347	165	0.347	198	0.416	0.711	0.709	0.574
	295.9x100.3x5.15x4.4	42.2	57.5	165	0.345	165	0.345	195.4	0.409	0.702	0.715	0.605
24	500x135x10.2x6.6	37.8	49.	165	1.517	165	1.517	198	1.82	2.92	2.97	2.62
	500x135x10.2x6.6	46.2	49.	165	1.517	165	1.517	190	1.75	2.80	3.00	2.52
30	228.6x76.2x9.6x5.8	20.2	23.8	165	0.327	165	0.327	198	0.392	0.633	0.633	0.591
		30.29	23.8	165	0.327	165	0.327	198	0.392	0.633	0.632	0.581
		40.4	23.8	165	0.327	165	0.327	198	0.392	0.633	0.630	0.612

* P_y = N/mm² ; * M_b = x10⁸ Nmm

Table 7.14 Moment Capacities Calculated at a Web Post Cross-section

Ref.	Sections	M_{exp}/M_b				
		BS 449 Table 3	BS 449 Tables 8-9	BS 153 Tables 7-8	ECCS	B/20
15	266.7x101.6x9.8x6.3	1.64	1.64	1.55	1.0	0.999
16	381x114.3x12.8x7.6	0.909	0.97	0.997	0.602	0.769
	342.9x101.6x11.6x7.6	1.37	1.37	1.35	0.83	0.855
20	457.2x127x12.9x8.38	1.41	1.41	1.20	0.847	0.850
22	266.7x101.6x5.1x4.57	1.63	1.63	1.47	0.840	0.919
	299.9x100.3x5.13x4.8	1.62	1.62	1.39	0.811	0.856
	297.2x99x5.08x4.7	1.65	1.65	1.38	0.810	0.807
	295.9x100.3x5.15x4.4	1.75	1.75	1.48	0.846	0.862
24	500x135x10.2x6.6	1.73	1.73	1.44	0.882	0.897
	500x135x10.2x6.6	1.66	1.66	1.44	0.840	0.9
30	228.6x76.2x9.6x5.8	1.81	1.81	1.51	0.934	0.934
		1.78	1.78	1.48	0.918	0.918
		1.87	1.87	1.56	0.971	0.967

Table 7.15 Comparison of Test Moments with Various Design Predictions.

Properties at a Web Post Cross-section

ref.16 the mean value of M_{exp}/M_b for the twelve tests is equal to 1.85 with a standard deviation of 0.162 for the methods of BS 449, ten tests having ratios above 1.7 while two tests have recorded load factors below 1.6. If BS 153 is considered, the mean value drops below 1.7 and is equal to 1.59 with a standard deviation of 0.086. It has to be noticed that the three beams tested by Sherbourne gave values of the ratio M_{exp}/M_b between 2.0 and 2.10.

7.7.2.2 B/20 and ECCS approaches

When the B/20 accurate design procedure is used, all the beams except two managed to reach their predicted design strength. However the load factors although higher than 1.0 are not very favourable when compared to those obtained for the test beams of the writer's series S. The mean value for the ratio M_{exp}/M_b is only 1.017 with a standard deviation of 0.064. If the ECCS recommendations are used the mean value increases to 1.05 with a standard deviation of 0.060. This is a reverse of the findings for the beams of the writer's series which showed that the ECCS ratios were lower than those of B/20.

7.7.3 Web post cross-section

The moment capacities calculated for the properties taken at a web post cross-section are given in Table 7.14 while the ratios of experimental moments versus the various predicted moments are given in Table 7.15. The results are also similar to those obtained for the beams of the series S although the load factors were somewhat different because the slenderness of the beams was generally lower.

The mean value of the ratio M_{exp}/M_b was 1.66 for both methods of BS 449 but only 1.44 for BS 153 about 8% lower than the means of the

test results of series S.

Both the ECCS and B/20 procedures yielded very similar mean values. Values equal to 0.877 and 0.897 respectively were recorded and they have to be compared to mean values of 0.706 and 0.931 when beams S6-2 and S5-1 are considered.

7.8 Comparisons based on the full set of results

7.8.1 B/20 Recommendations

Fig.7.2 compares all eight test results with the design curve for rolled sections given in B/20. Each point is plotted using values of M_b and λ_{LT} obtained from the "exact" method for the properties of a hole cross-section. In each case the points plot significantly above the design curve. Neglecting the result of test M4-2 the mean value of M_{exp}/M_b for the remaining seven tests is 1.184 with a standard deviation of 0.108.

When web post properties are substituted for hole section properties Fig.7.3 shows that only the four most slender beams plus test M4-2 now have strengths which plot above the B/20 design curve. Once again omitting test M4-2 the mean value of M_{exp}/M_b is now reduced to 1.05 with a corresponding standard deviation of 0.118. However, for slendernesses λ_{LT} below about 70.0 the use of web post properties is clearly unsatisfactory, principally because it leads to values of M_p which cannot be attained even for fully braced beams, i.e. $\lambda_{LT} \rightarrow 0$. The use of web post properties is therefore unsound.

Use of the simplified design approach provided in cl.11.3.2.c of B/20 (taking $\lambda_{LT} = \lambda$ which amounts to neglecting the contributions of the web and tension flange towards providing lateral stability) produces safe predictions of strength for each test even when used in conjunction

with web post properties, see Tables 7.1 and 7.2. However, Fig.7.5 suggests that beams with slenderness below the minimum considered in this series i.e. $\lambda < 60.0$ would tend to have their strength over-predicted due to the high values of S_x . It is the low values of p_b resulting from the safe approximation $\lambda_{LT} \approx \lambda$ that cause the test points for the more stocky beams to plot above the design curve; once $\lambda_{LT} \leq \lambda_{Lo}$ and $p_b = p_y$ this benefit disappears. When this approach is used with hole section properties Table 2 and Fig.7.4 show that it gives predicted strengths which are safer than those of the "exact" method of Fig.7.2. In this case the mean value of M_{exp} / M_b for the seven uniform moment tests is 1.220 with a standard deviation of 0.123 (for web post properties the mean value of M_{exp} / M_b is 1.158 with a standard deviation of 0.146).

Table 7.2 lists the values of M_b obtained using the other possible interpolations of the B/20 method as set out in section 7.3. The general trend is for these to under-predict when used with hole cross-sectional properties and to over-predict when used with web post properties although this latter point is masked somewhat by the conservatism attached to using safe (high) values of λ_{LT} .

No comparisons have been made against the B/20 design curve proposed for welded beams. This recognises the more severe patterns of residual stress produced by the web to flange welds by being depressed below the rolled section curve in the range of intermediate λ_{LT} values ($40.0 < \lambda_{LT} < 100.0$). Since the welding used to fabricate castellated beams is arranged differently, being located in the web comparatively near the neutral axis, it is unlikely to produce the same type of reductions in strength. This view is supported by all the comparisons above.

7.8.2 ECCS recommendations

Figs. 30 and 31 compare the test results with the design curves given in the ECCS recommendations. The point has already been made, see Fig.7.1, that this curve is up to 35% higher than the B/20 curve. Even when used with the properties of a hole cross-section this approach tends to over-predict all but the results for the most stocky and the most slender beams as shown in Fig.7.5 with the mean value of M_{exp}/M_b being only 0.944. Changing to web post properties causes all points to fall significantly below the design curve and the mean value of M_{exp}/M_b drops to 0.684.

7.8.3 Permissible stress approaches

Of the three permissible stress approaches, only the two-stage method of BS 449 gives a satisfactory mean load factor when hole cross-sectional properties are considered, the mean value of M_{exp}/M_b being 1.77 with a standard deviation of 0.088 (these calculations do not take into account beam M4-2). When the test results are compared to BS 153 and the Table 3 approach of BS 449, the mean values of M_{exp}/M_b are only 1.61 and 1.48 respectively with standard deviations of 0.098 and 0.216. Even when using web post properties only BS 153 mean value of M_{exp}/M_b increases above 1.7 while the mean from Table 3 decreases to 1.42. It is interesting to note that the largest standard deviations are obtained when the Table 3 approach of BS 449 is used while the smallest standard deviations are obtained with the limit state approach of ECCS and B/20. Table 7.16 all the values of means and standard deviations obtained from the various approaches.

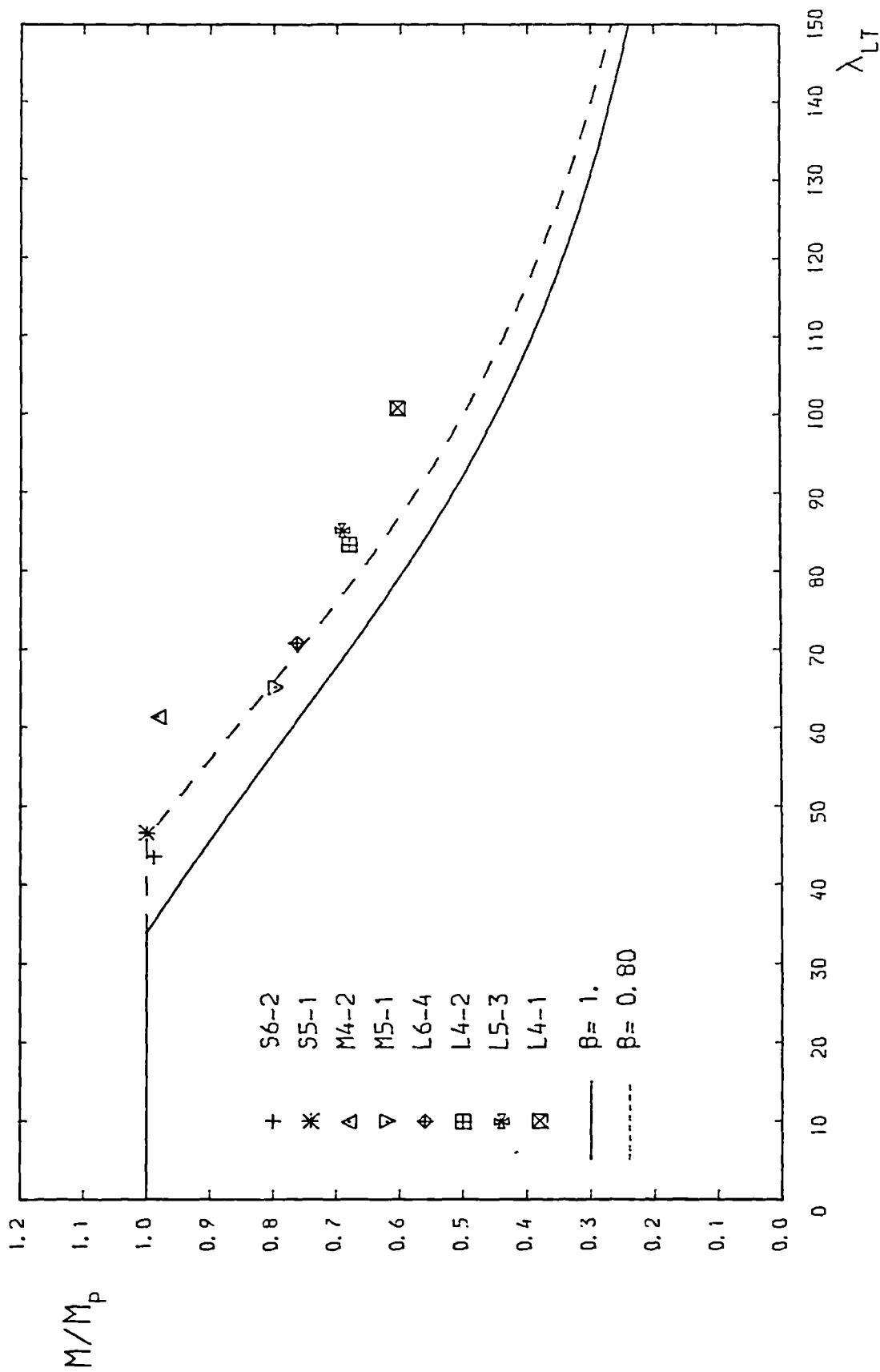


FIG. 7.2 COMPARISON OF TEST DATA WITH B/20 PROPOSALS FOR SOLID WEB BEAMS
 HAVING THE PROPERTIES OF THE HOLE CROSS-SECTION
 ($P_y = 280. \text{ N/mm}^2$)

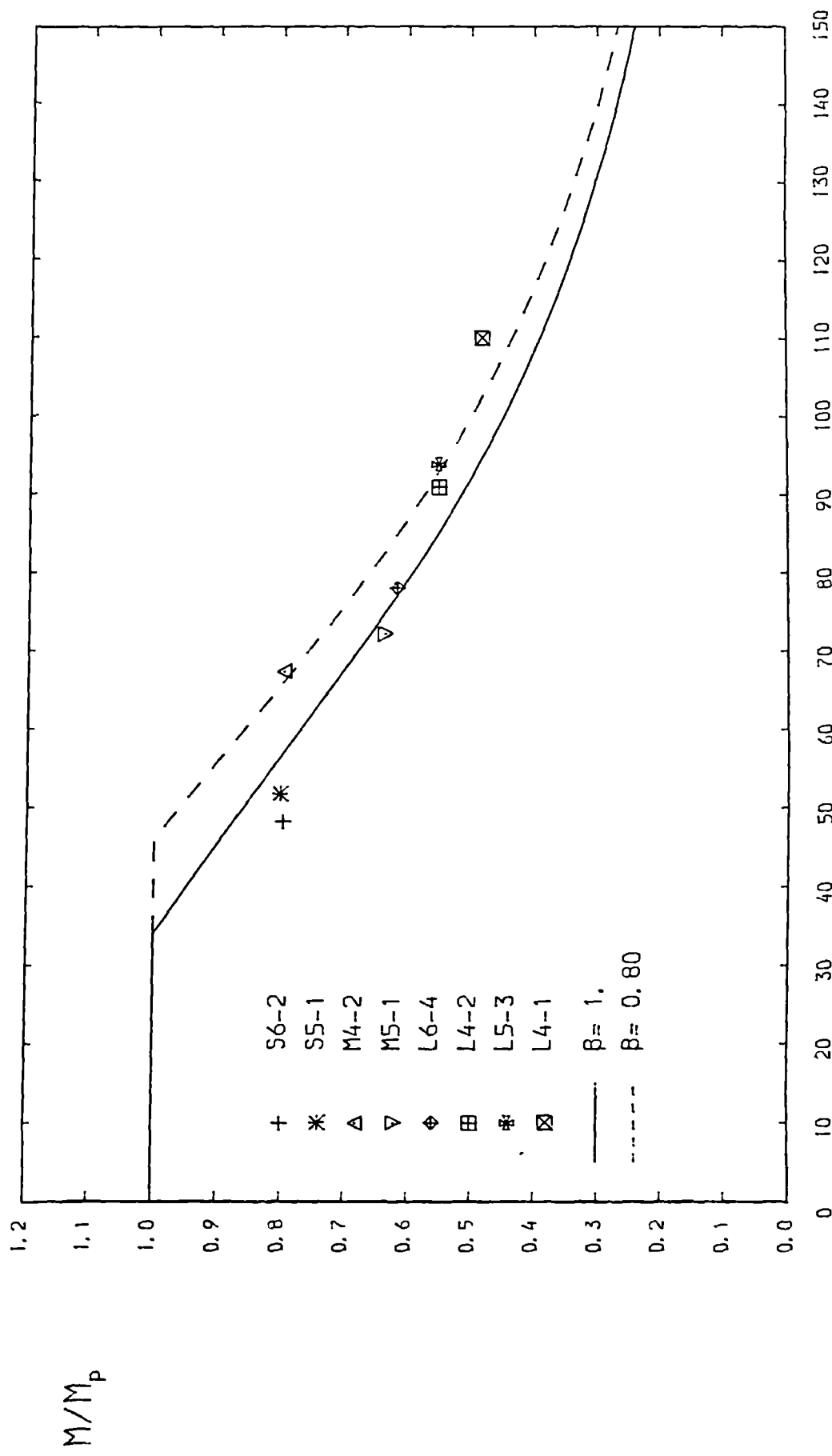


FIG. 7.3 COMPARISON OF TEST DATA WITH B/20 PROPOSALS FOR SOLID WEB BEAMS
 HAVING THE PROPERTIES OF THE WEB POST CROSS-SECTION
 ($P_y = 280. \text{ N/mm}^2$)

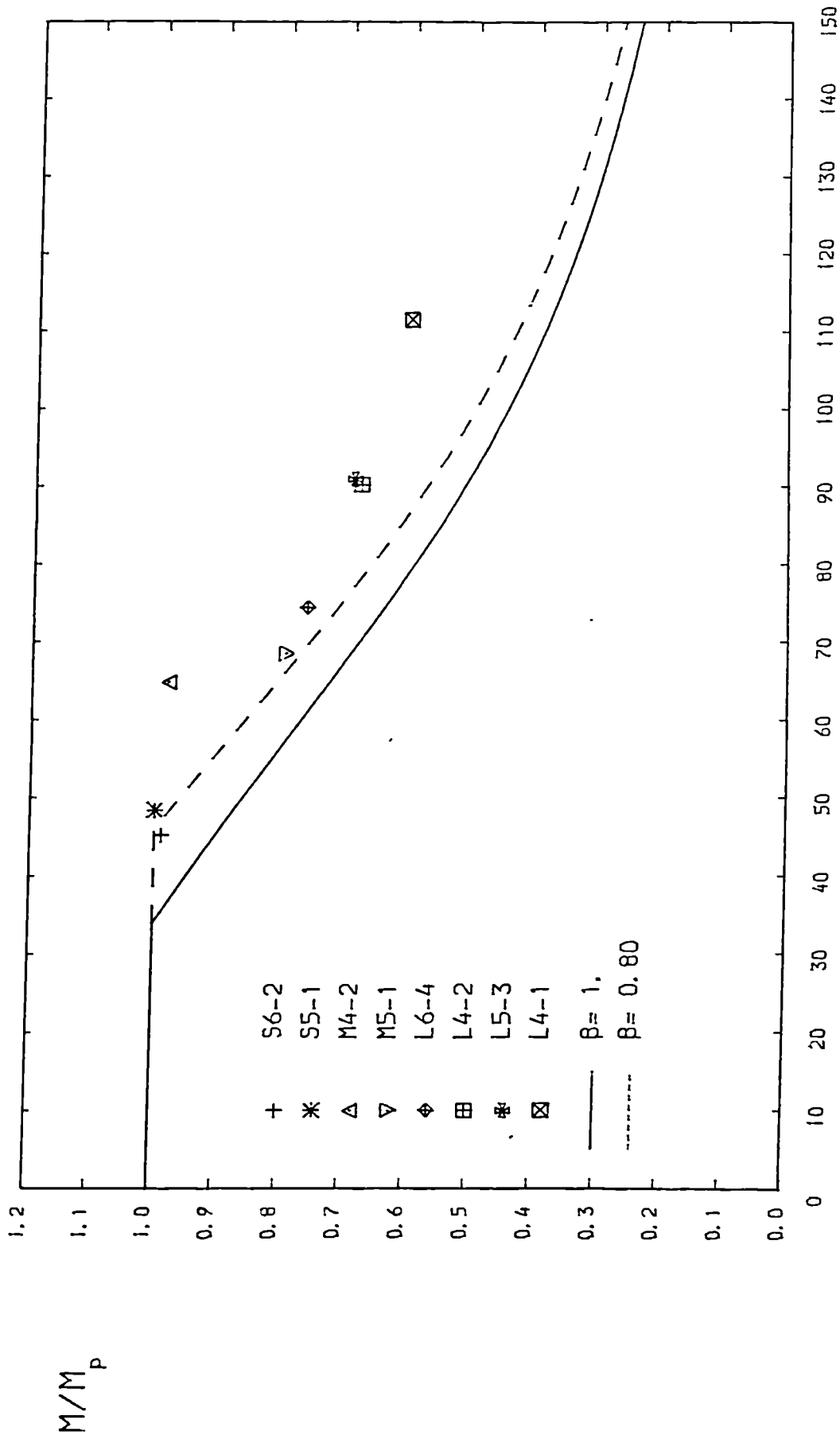


FIG. 7.4 COMPARISON OF TEST DATA WITH APPROXIMATE B/20 PROPOSALS FOR SOLID WEB BEAMS HAVING THE PROPERTIES OF THE HOLE CROSS-SECTION
 ($\lambda_{LT} = \lambda$, $U=1.0$, $X \rightarrow \infty$) ($P_y = 280$, N/mm^2)

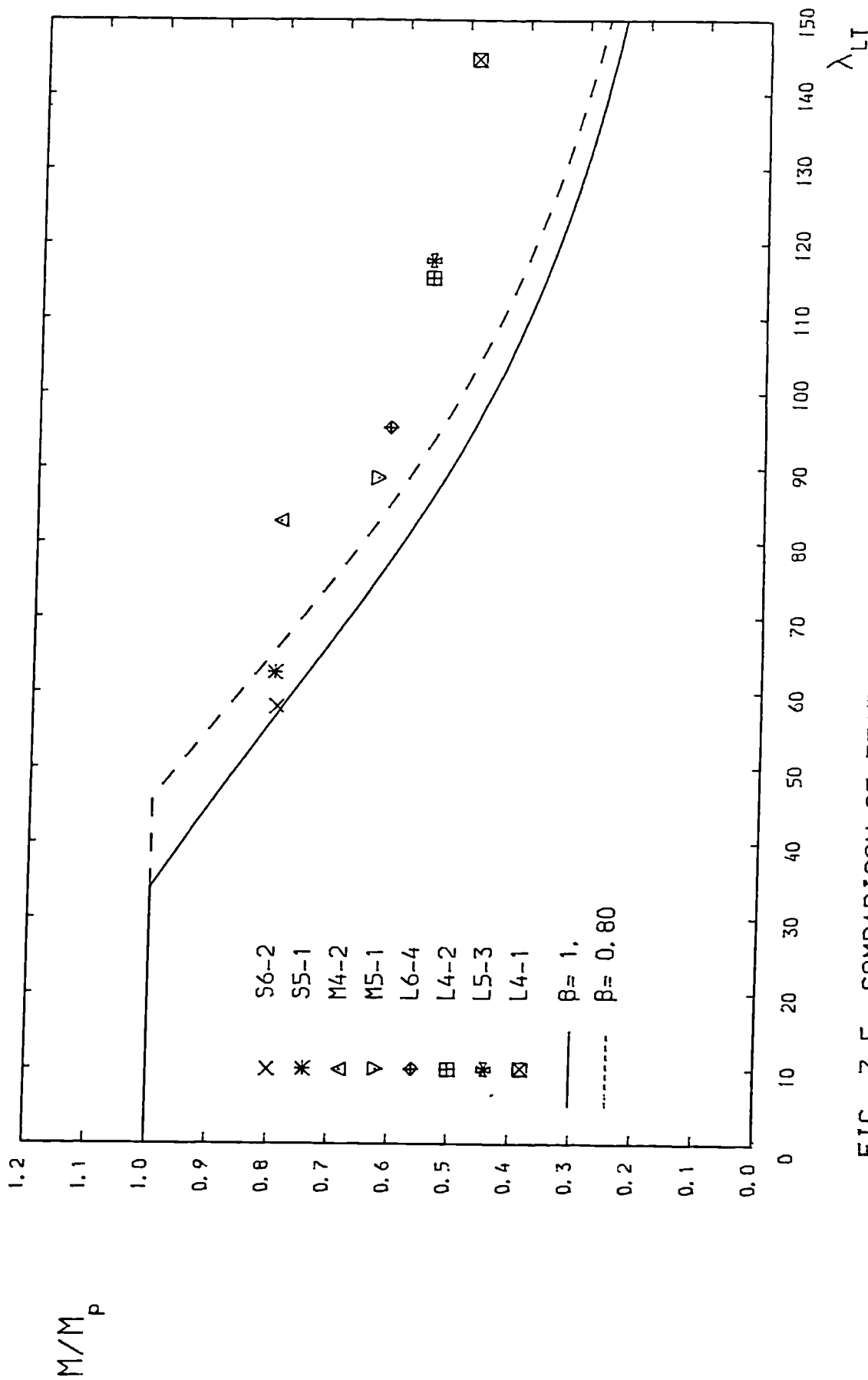


FIG. 7.5 COMPARISON OF TEST DATA WITH APPROXIMATE B/20 PROPOSALS FOR SOLID WEB BEAMS HAVING THE PROPERTIES OF THE WEB POST CROSS-SECTION
 ($\lambda_{LT} = \lambda$, $U=1.0$, $X \rightarrow \infty$) ($P_y = 280$, N/mm^2)

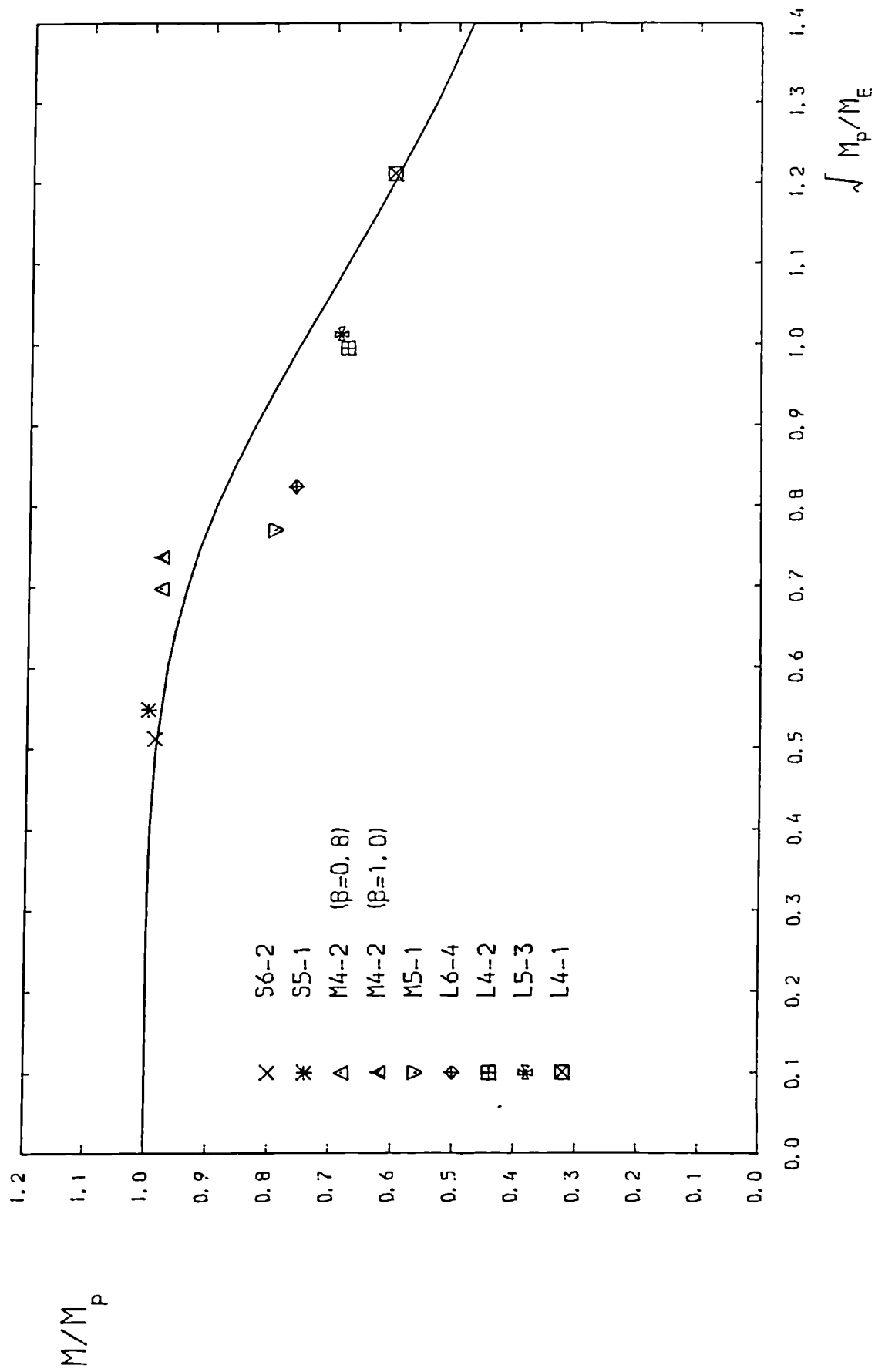


FIG. 7.6 COMPARISON OF TEST DATA WITH ECCS PROPOSALS FOR SOLID WEB BEAMS HAVING THE PROPERTIES OF THE HOLE CROSS-SECTION

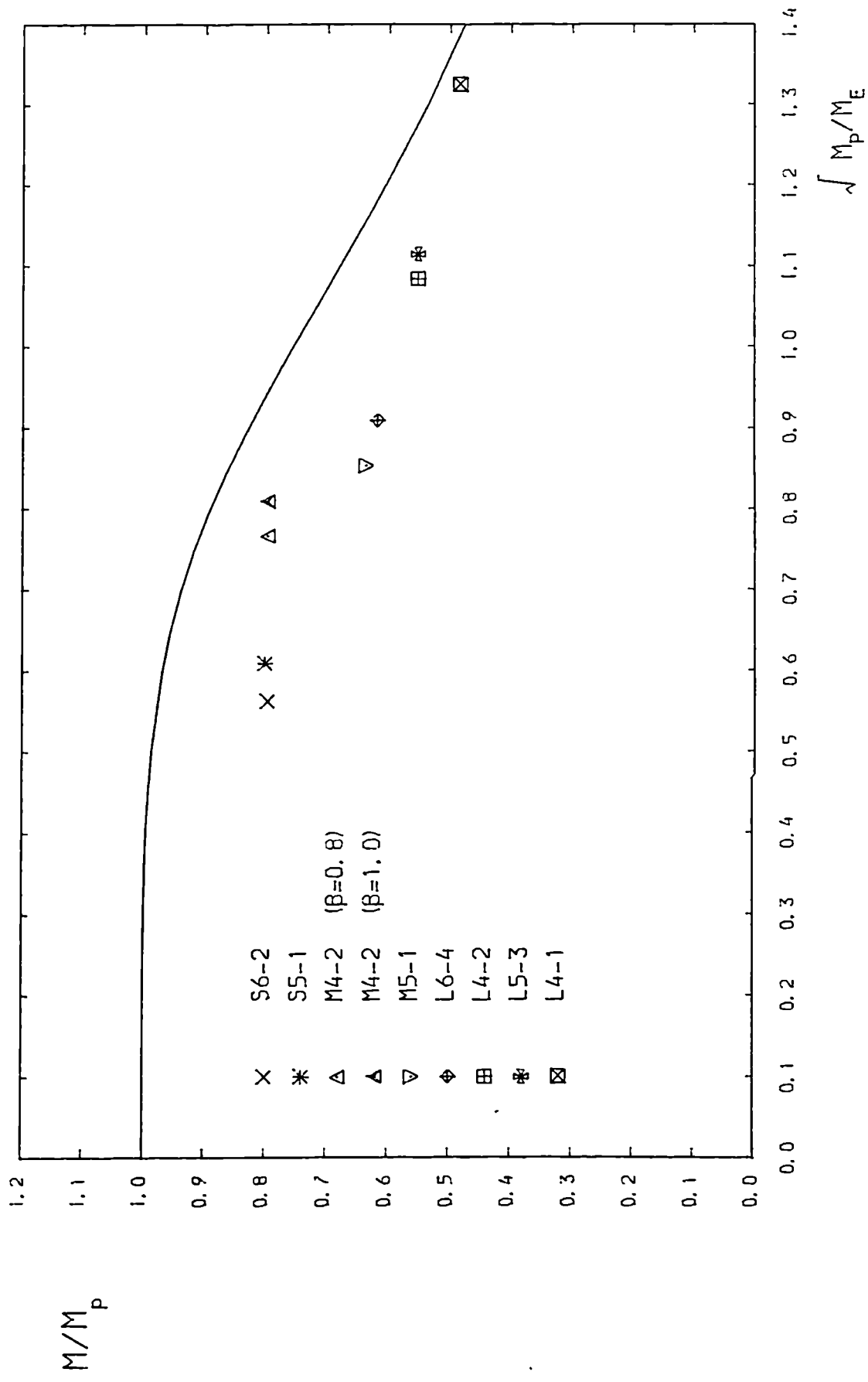


FIG. 7.7 COMPARISON OF TEST DATA WITH ECCS PROPOSALS FOR SOLID WEB BEAMS HAVING THE PROPERTIES OF THE WEB POST-CROSS-SECTION

	BS 449 Table 3		BS 449 Tables 8-9		BS 153		ECCS		B / 20	
	mean	s.d.*	mean	s.d.	mean	s.d.	mean	s.d.	mean	s.d.
Present Series	hole	1.48	1.77	0.088	1.61	0.098	0.944	0.066	1.184	0.108
	web post	1.42	1.87	0.169	1.75	0.199	0.684	0.056	1.05	0.118
Previous Tests	hole	1.85	1.85	0.162	1.59	0.086	1.05	0.063	1.017	0.064
	web post	1.66	1.66	0.142	1.44	0.094	0.877	0.061	0.897	0.0519

* s.d. = standard deviation

Table 7.16 Means and Standard Deviation Values Obtained for the Various Predictions for the Beams of the Present Series

CHAPTER 8

ANALYSIS OF THE CASTELLATED BEAM BY THE STIFFNESS METHOD

8.1 Introduction

The idealisation of the castellated beam as a plane frame has been used extensively in the Vierendeel analogy (see chapters 2 and 4) in order to calculate the internal forces in the members of the beam. The castellated beam was also treated as a frame with vertical and horizontal members by methods based on the stiffness (25,31,42) and flexibility (44) approaches. These methods, in addition to giving a distribution of stresses in the members very similar (31) to that obtained by the simpler Vierendeel analogy, could also automatically compute the deflections of the frame (25,42). The deflections were found to compare well with those of beams constrained to move in the plane of loading (25,42). The stiffness method because of its easier use was more popular than the flexibility method.

However, although these programs were limited to the analysis of in-plane behaviour, it was possible to expand their scope by adding the analysis of the out-of-plane behaviour. The program developed herein will therefore predict the elastic critical load for lateral-torsional buckling and subsequently draw the laterally buckled shape of the idealised castellated beam and more particularly that of the deformed web posts. The effect of varying the size of the holes will also be investigated.

8.2 Out-of-plane analysis

8.2.1 Stability analysis of a frame

The calculation of the elastic critical load for lateral-torsional buckling is part of the general problem of stability of structures. The instability of a plane frame structure may be classified (91) in accordance with its load-deformation characteristic as being of the

bifurcation type or the non-bifurcation type (see Fig.8.1). For the bifurcation type of instability, the structure deforms in a stable configuration as the load is increased from zero until a critical load (at the point of bifurcation on the load-deformation path) is reached. The structure will then deform suddenly to find its new stable configuration. Structures can also exhibit the non-bifurcation type of instability in which the deflections increase until a maximum load is reached beyond which static equilibrium can only be sustained by decreasing the load. The stiffness or displacement method can only be used in these two fundamentally different approaches to calculate the failure load of frames: The load-deflection approach is linked to the non-bifurcation type of instability whilst the eigenvalue approach is linked to the non-bifurcation type of instability.

8.2.2 Load-deflection approach

The load deflection approach will attempt to solve the stability problem of a frame by determining the load-deflection behaviour over its entire range of loading including the unloading branch of the curve. The solution technique is performed by applying the load incrementally and calculating the resulting deflections. Equilibrium iterations are usually performed until the internal forces balance the externally applied load. The overall stiffness matrix of the structure is constantly modified along the load-deformation path and the maximum load is obtained from the full load-deformation characteristic. The advantages of the method are that geometrical (initial out-of-straightness) and material (residual stresses) imperfections can be included in the analysis. Its drawbacks are its complexity in calculating the deflections in the elastic-plastic range of the material. Structures with three dimensional loading will exhibit the

non-bifurcation type of instability.

8.2.3 Eigenvalue approach

This method was first used by Euler in 1759 when he considered the buckling of slender columns. The critical load of a frame can be found without calculating any deflections by mathematically testing the equilibrium of the frame; the critical load is reached when the equilibrium path separates into two possible configurations. This load is known as the buckling or bifurcation load. The point of bifurcation for the frame is shown in Fig.8.1. At the critical load the equilibrium path may either continue on the vertical axis or the lateral deflections may become indetermined. This simpler analysis overestimates the maximum load carrying capacity of real structures whose members are not perfectly straight nor free of residual stresses. The eigenvalue approach can be easily adapted to the stiffness matrix method which is then referred to as the determinantal stiffness method. The determinant of the overall stiffness matrix is calculated at different load levels and the critical load causes it to become equal to zero.

8.2.4 Application to castellated beams

The lateral-torsional buckling of a castellated beam idealised as a plane frame subjected to loading in its plane is of the bifurcation type. The out-of-plane deformations remain zero until the critical loading condition is reached. Therefore the in-plane behaviour of the frame can be analysed independently of the out-of-plane buckling behaviour. The solutions from the in-plane analysis, which is performed first, can thus be used to solve the out-of-plane analysis. The critical load which causes the frame to buckle laterally can be found from the condition that the

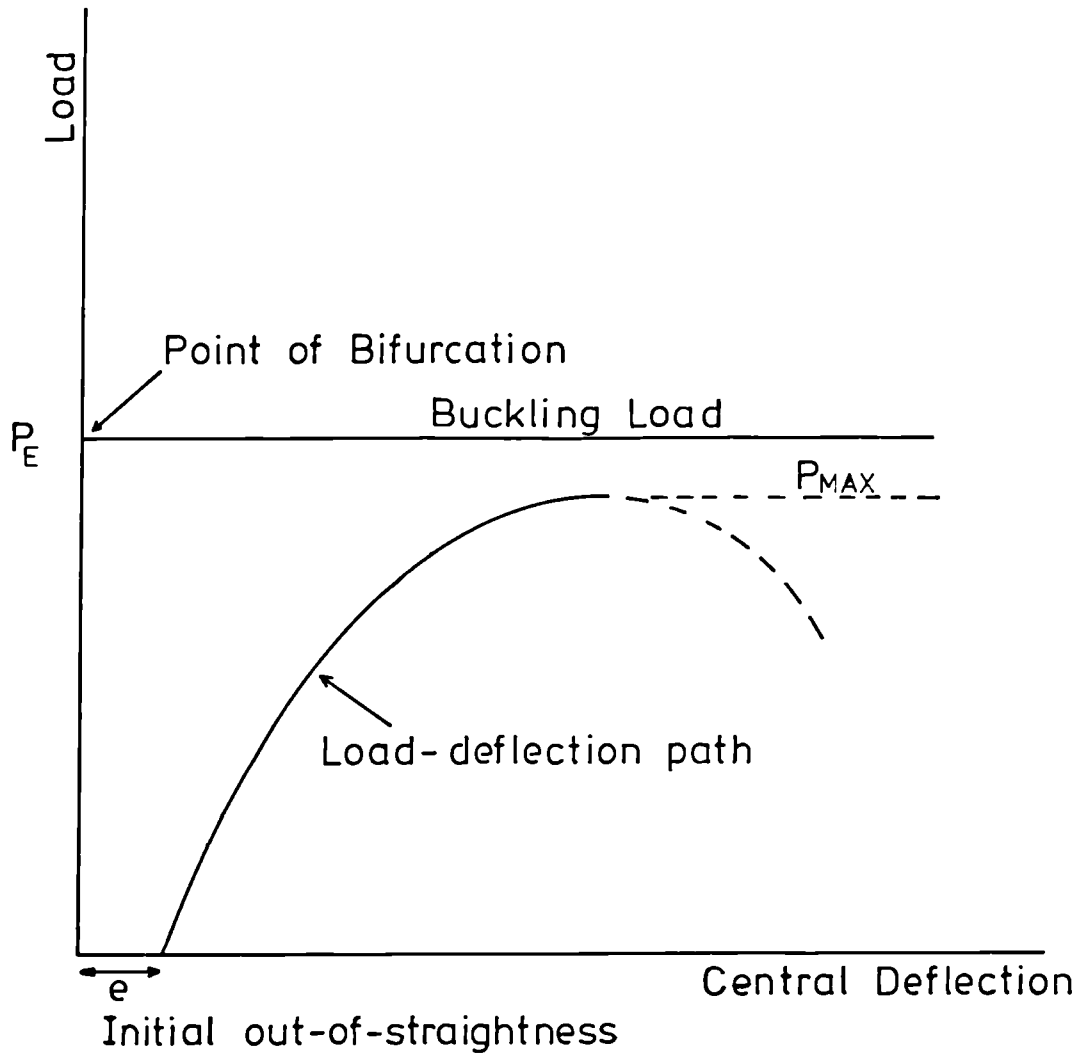


FIG. 8.1 COMPARISON OF EIGENVALUE AND LOAD-DEFLECTION METHODS

determinant of the overall matrix which governs the out-of-plane behaviour should be zero.

A number of assumptions regarding the properties of the beam-frame have to be made when the critical load is computed by the eigenvalue approach.

1. the beam is free of geometrical and material imperfections (the beam is straight and no residual stresses are present).
2. the material is perfectly elastic.
3. the loads act in the plane of the web and remain vertical.

8.3 Analysis of the castellated beam treated as a plane frame

8.3.1 Matrix stiffness method

The matrix stiffness method is a standard structural analysis technique which is described in many standard textbooks (92,93) and it is not necessary to give a detailed description of the technique. For this reason, only a brief outline of the technique will be given when its application to the calculation of the elastic critical load of castellated beams is described.

8.3.2 Geometry of the frame

The castellated beam is treated as a frame whose members are horizontal and vertical. The proportions and properties of these members are calculated from the known dimensions of the actual beam. The properties are assumed to act at their centroidal axis. The vertical members will be made from the web posts while the horizontal members which span the holes are made from the upper and lower tee sections of the beam. The resulting frame is shown in Fig.8.2. The heavy lines indicate the location of the centroidal axis of the members and therefore the effective location of the members themselves.

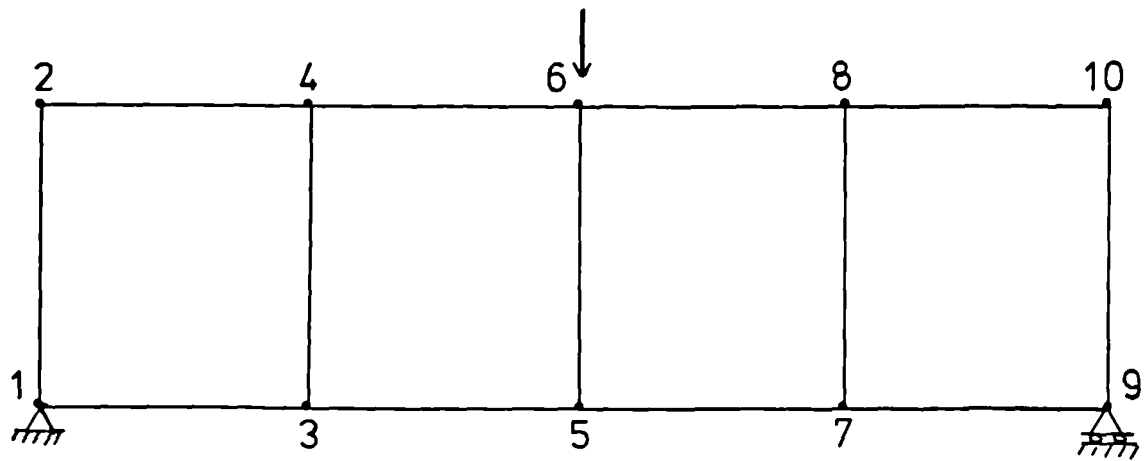
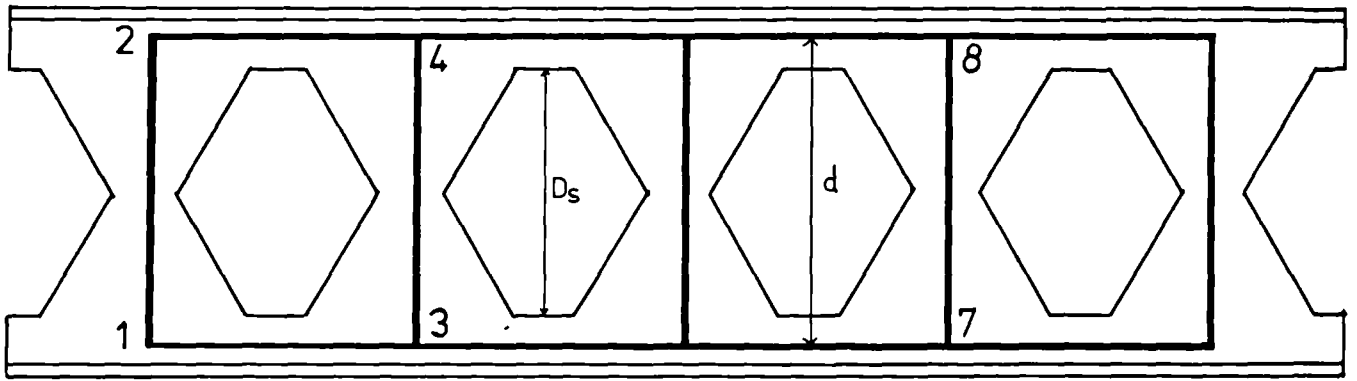
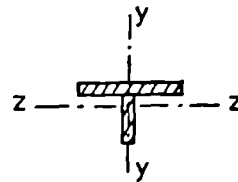
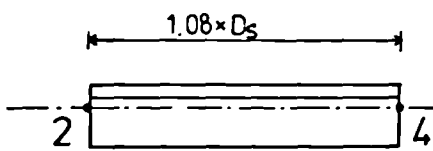
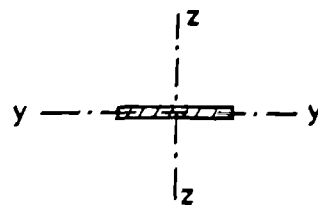
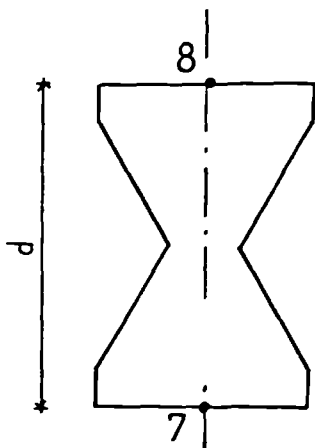


FIG. 8.2 CASTELLATED BEAM TREATED AS A PLANE FRAME



a. chord



b. web post

FIG. 8.3 PROPERTIES OF THE MEMBERS

The vertical members were at first taken to comprise all the web between the neutral axis of the lower and upper tee sections (see Fig.8.3). However, in order to obtain the deflected shape of the web posts it was necessary to add three extra nodal points across the vertical members which had to be subdivided into four elements (Fig.8.4). Two members were made from the web common to the tee sections whilst the middle two members were formed from the tapered part of the web between two consecutive holes. The length and properties of each member are given in the figures.

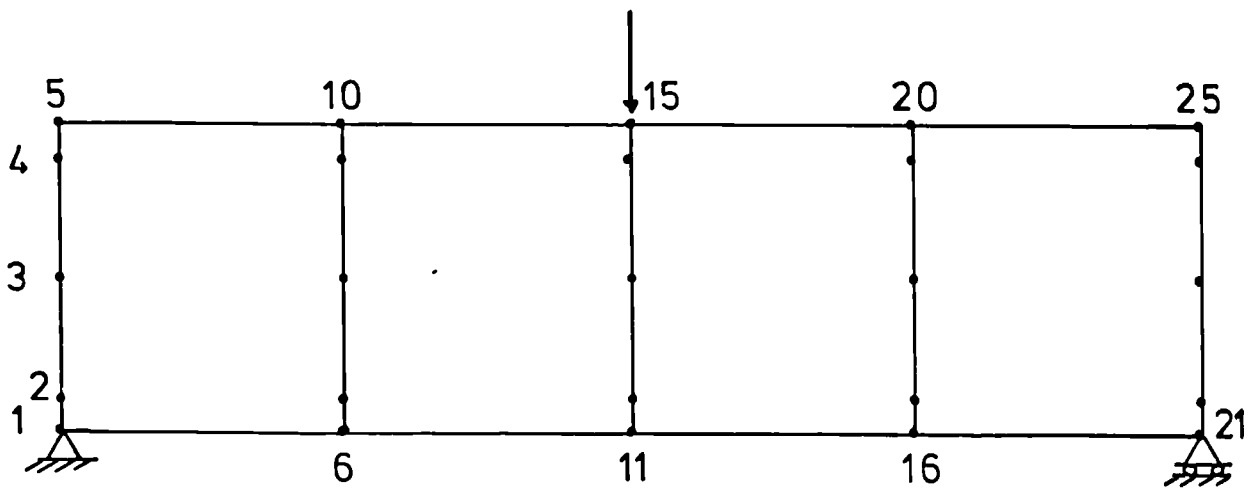
8.4 Flow chart of the computer program

8.4.1 General description

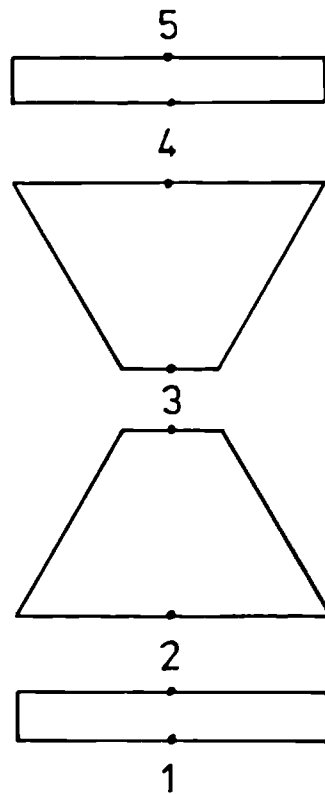
It has already been said that the lateral-torsional buckling of a plane frame is of the bifurcation type and that the analysis of the out-of-plane behaviour can be carried out independently of the in-plane behaviour. The flow chart (which is shown in Fig.8.5) of the computer program written to find the elastic critical load of the frame by the matrix stiffness method will therefore be divided into the following parts:

1. input of data, calculation of member properties, automatic node and member numbering, preliminary evaluation of critical load.
2. in-plane analysis which will yield the internal forces in the members and the deflections of the nodes.
3. out-of-plane analysis carried out by using the internal forces obtained from the in-plane analysis; once the critical load is found the deflected shape is calculated.
4. print results: critical load and deflected shape.

Details of parts 1 to 4 are expanded upon in the next sections.



a. Frame



b. Vertical members

FIG. 8.4 SECOND IDEALISATION OF THE CASTELLATED BEAM

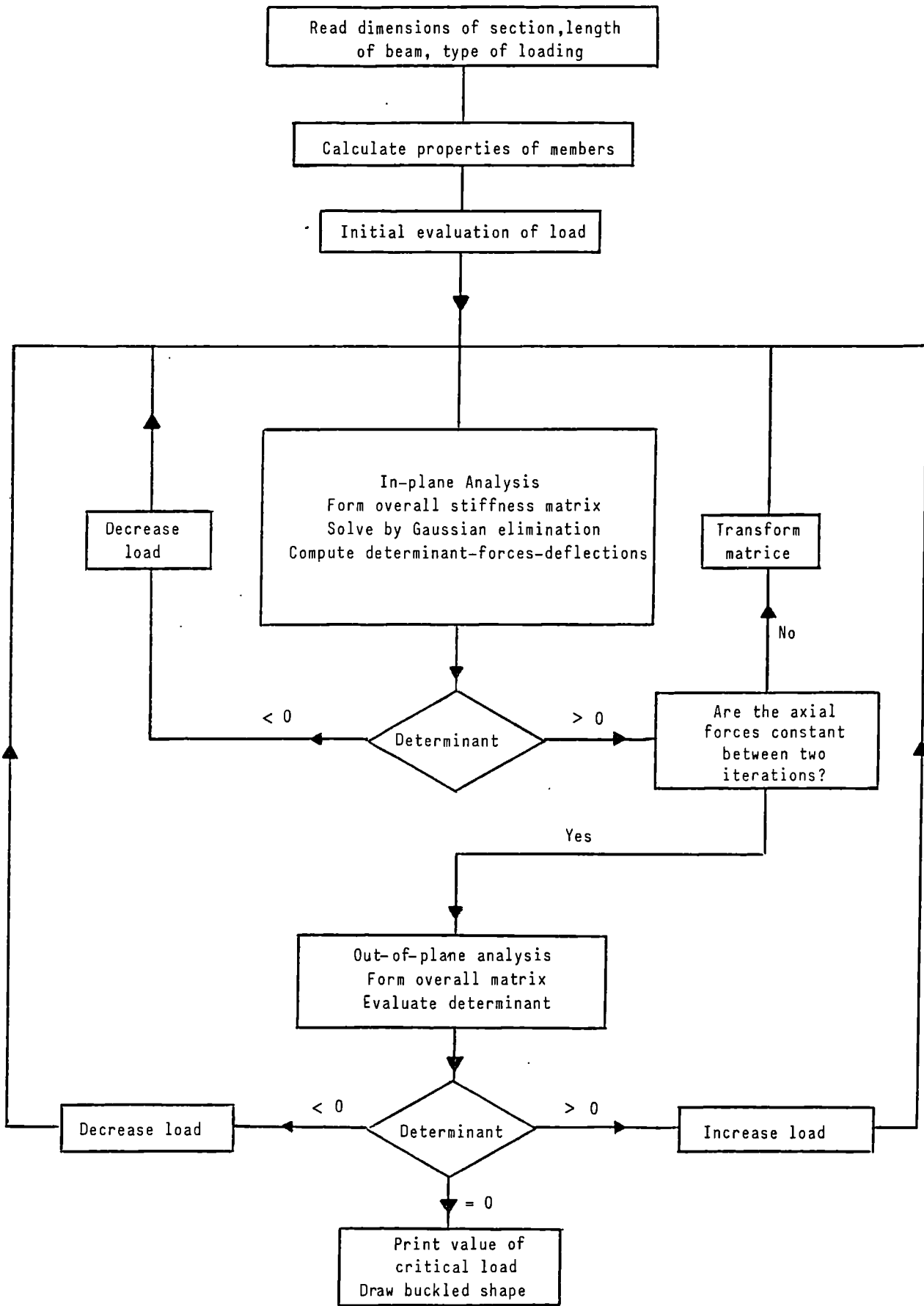


Fig. 8.5 Flow-chart of Computer Program

8.4.2 Preliminary

The first step involves the reading of the data which consists of the dimensions of the cross-section to be analysed, the length of the beam given as the number of castellations in the beam (this is also equal to the number of panels in the frame) and the type of loading to be treated. The nodes and members of the frame will be automatically numbered and each member will be assigned the various properties needed in the calculations of the element matrices such as lengths, areas, second moment of area, torsion constant and the stiffness coefficients used in the slope deflections equations and the stiffness matrices. The properties have to be calculated about the two axes of the section for the in-plane and out-of-plane matrices needed for each element. Finally an estimate of the critical load can be calculated or input as data.

8.4.3 In-plane analysis

Once the properties of the individual elements of the frame have been established it is necessary to assemble the overall in-plane stiffness matrix of the whole frame. This is done by adding the contributions for each member in their numerical order. The element stiffness matrices are assembled into the overall stiffness matrix after due account has been taken of the orientation of each member in relation to the set of reference axes. Because of the presence of non-prismatic element in the vertical members the element stiffness matrix for a member is written as:

$$[k_I^e] = \begin{bmatrix} \frac{EA}{L} & 0 & 0 & -\frac{EA}{L} & 0 & 0 \\ 0 & f_1 \frac{EI_z}{L^3} \phi_1 & f_2 \frac{EI_z}{L^3} \phi_2 & 0 & -f_1 \frac{EI_z}{L^3} \phi_1 & f_3 \frac{EI_z}{L^3} \phi_3 \\ 0 & f_2 \frac{EI_z}{L^3} \phi_2 & f_4 \frac{EI_z}{L^3} \phi_4 & 0 & -f_2 \frac{EI_z}{L^3} \phi_2 & f_5 \frac{EI_z}{L^3} \phi_5 \\ -\frac{EA}{L} & 0 & 0 & \frac{EA}{L} & 0 & 0 \\ 0 & -f_1 \frac{EI_z}{L^3} \phi_1 & -f_2 \frac{EI_z}{L^3} \phi_2 & 0 & f_1 \frac{EI_z}{L^3} \phi_1 & -f_3 \frac{EI_z}{L^3} \phi_3 \\ 0 & f_1 \frac{EI_z}{L^3} \phi_1 & f_2 \frac{EI_z}{L^3} \phi_2 & 0 & -f_1 \frac{EI_z}{L^3} \phi_1 & f_3 \frac{EI_z}{L^3} \phi_3 \end{bmatrix} \quad (8.1)$$

where L is the length of the element, A is the cross-sectional area, I_z is the second moment of area about the plane of loading and E is the material elastic modulus. The ϕ_i 's are stability coefficients and the f_i 's are stiffness coefficients. The coefficients f_i 's can be expressed as :

$$\begin{aligned}
 f_1 &= C_{11} + C_{22} + 2C_{21} & f_4 &= C_{11} \\
 f_2 &= C_{11} + C_{21} & f_5 &= C_{22} \\
 f_3 &= C_{22} + C_{21} & f_6 &= C_{21}
 \end{aligned} \quad (8.2)$$

When the members have a constant cross-section the coefficients C_{ij} 's are equal to the usual values of :

$$\begin{aligned}
 C_{21} &= 2 \\
 C_{11} &= C_{22} = 4 \\
 C_{11} + C_{21} &= C_{22} + C_{21} = 6
 \end{aligned} \quad (8.3)$$

Values for the coefficients C_{ij} 's can be found in chapter 5 of ref.94.

The coefficients ϕ_i 's are stability functions which are used to take

into account the destabilising effect of the axial forces in the members of the frame. They can be found in ref.92. Because the axial forces are unknown at the beginning, an iterative process is used whereby the axial forces calculated in the first iteration are used to compute values for the stability functions which are then used to modify the stiffness matrix of each element. New axial forces are calculated and compared to the previous ones. This is repeated several times until the difference between consecutive axial forces becomes negligible. Node displacements are also obtained at this stage.

These axial forces are used in the next stage of the program which analyses the out-of-plane behaviour of the frame. Throughout this stage, the determinant of the in-plane matrix is evaluated to check for in-plane buckling failure.

8.4.4 Out-of-plane analysis

Following the calculation of the axial forces, the member stiffness matrices for the out-of-plane analysis are formed and the overall stiffness matrix $[K_L]$ for the frame is assembled. Because there are no applied loads acting on the structure which directly cause out-of-plane displacement, the out-of-plane load vector $[P_L]$ is zero and the following equation is solved:

$$[P_L] = [K_L] [\delta_L] = 0. \quad (8.4)$$

Thus the solution for the flexural-torsional buckling is obtained when the magnitude of the in-plane loads are such that the determinant of $[K_L]$ is zero. An iterative procedure is used to find the applied load which causes the determinant of $[K_L]$ to become zero. The stiffness matrix for each member can be written as:

$$[k_L^e] = \begin{bmatrix}
 \frac{GJ}{L} & 0 & 0 & -\frac{GJ}{L} & 0 & 0 \\
 0 & f_1 \frac{EI_y}{L^3} \phi_1 & -f_2 \frac{EI_y}{L^2} \phi_2 & 0 & -f_1 \frac{EI_y}{L^3} \phi_1 & -f_2 \frac{EI_y}{L^2} \phi_2 \\
 0 & -f_2 \frac{EI_y}{L^2} \phi_2 & f_1 \frac{EI_y}{L} \phi_1 & 0 & -f_2 \frac{EI_y}{L^2} \phi_2 & f_1 \frac{EI_y}{L} \phi_1 \\
 -\frac{GJ}{L} & 0 & 0 & \frac{GJ}{L} & 0 & 0 \\
 0 & -f_1 \frac{EI_y}{L^3} \phi_1 & f_2 \frac{EI_y}{L^2} \phi_2 & 0 & f_1 \frac{EI_y}{L^3} \phi_1 & f_2 \frac{EI_y}{L^2} \phi_2 \\
 0 & -f_2 \frac{EI_y}{L^2} \phi_2 & f_1 \frac{EI_y}{L} \phi_1 & 0 & f_2 \frac{EI_y}{L^2} \phi_2 & f_1 \frac{EI_y}{L} \phi_1
 \end{bmatrix} \quad (8.5)$$

where J is the torsion constant and G is the shear modulus of elasticity. The other coefficients have the same meaning as those given for the element in-plane matrix but are calculated about the axis y-y.

The procedure used to find the load level at which the determinant of the overall matrix vanishes is based on checking its change sign from positive to negative. The determinant is positive when the structure is stable and negative when it is in an unstable state. Once the sign change has been obtained, the Newton secant method is used to approach the value of external load which causes the determinant to be zero. However it is not sufficient to control the sign change of the determinant to find the lowest buckling mode. A safety measure is added to the routine which calculates the value of the determinant of the overall matrix. The signs of the coefficients of the leading diagonal of the overall matrix $[K_L]$ are checked (95). When the structure is stable, all the coefficients of the diagonal are positive and only one needs to change sign for the determinant to become negative and the structure to be in an unstable

state of equilibrium. The determinant will still be positive for the second buckling mode when two coefficients of the leading diagonal are negative (the determinant is calculated as the product of the coefficients of the diagonal after the matrix has been triangularized by Gaussian elimination) and it is not impossible that an initial coarse iteration will miss the first buckling mode.

8.4.5 Determination of the buckled shape

Once the load which causes the determinant of the overall matrix to vanish has been found it is possible to obtain the shape of the beam in its unstable configuration. However, because there are no out-of-plane loads and the determinant of $[K_L]$ is null, the system of equations 8.4 has only a trivial solution. The system of equations can only be solved by assigning an arbitrary value usually equal to 1 to one of the unknown lateral displacements (the node which will produce the largest displacement is chosen) and the other displacements can be calculated as a ratio of the prescribed one. This will give the buckled shape of the frame.

8.5 Results

8.5.1 Initial verification of the computer program

A computer program was written in FORTRAN IV to perform the analysis described in the previous paragraphs. This was developed using the ICL-1906S computer of the university of Sheffield. Its validity had first to be examined before any calculation of the elastic critical load for out-of-plane buckling could be done. This verification was carried out in two stages; the first one was carried out for the in-plane part of the program whilst the second one, which will be described when the

calculation of the elastic critical load is discussed, checked the out-of-plane part of the program.

A frame centrally loaded (see Fig.8.2) was used to compare the internal forces in the members and the displacements of the nodes calculated by the in-plane part of the program with those obtained from the plane frame package available on the ICL-1906S computer. They were found to be equal within a few percent and the next part of the program could therefore be added with confidence.

8.5.2 Calculation of the elastic critical load

8.5.2.1 Frame used in the analysis

The elastic critical load was calculated for equal end moment loading. This was the easiest that could be treated analytically and an exact solution of the problem existed (see eq.4.1). The equal end moment loading had also the advantage of making the resulting nodal deflections and internal forces symmetrical about the centreline of the frame if the number of panels in the particular frame under consideration was kept equal to an even number. The length of the frames was therefore increased by two for each increment of length. In this case, only half of the frame needed to be analysed, thus halving the number of simultaneous equilibrium equations to be solved. This considerably reduced the amount of computer time required for the complete analysis. The symmetrical half frame is shown in Fig.8.6. The equal end moment loading is equivalent to two concentrated loads applied at one end of the frame and of equal and opposite magnitude.

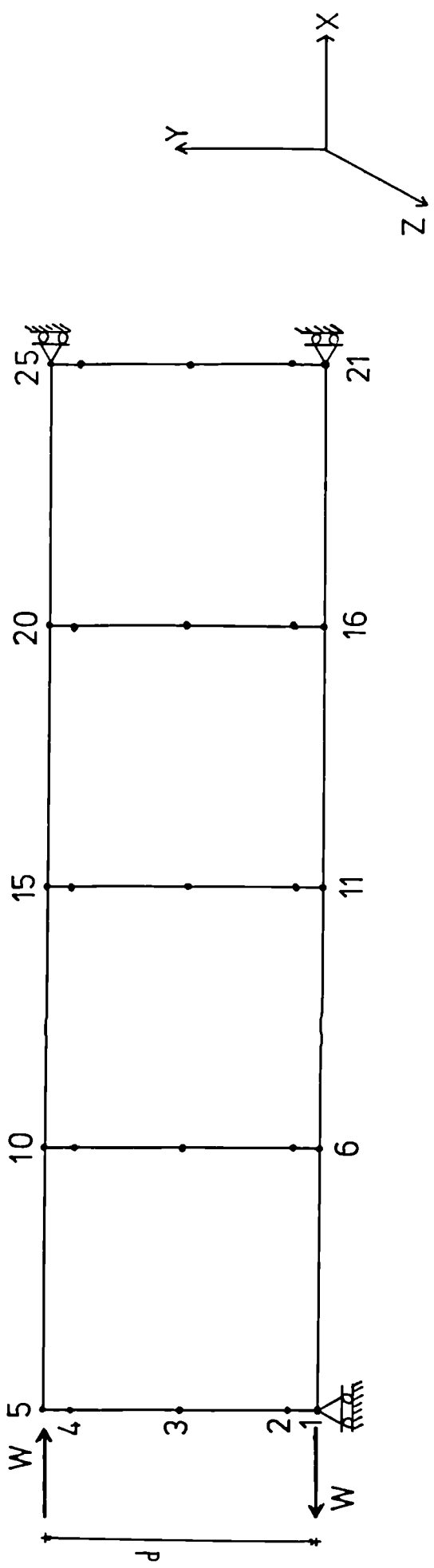


FIG. 8.6 SYMMETRICAL HALF-FRAME

8.5.2.2 Verification of the out-of-plane part of the program

This was done by neglecting the contributions of the vertical members to the overall stability of the frame and was therefore equivalent to studying the buckling of two struts made of the horizontal members linked by web members of negligible area and stiffness. The results from the program were checked with values of buckling loads of struts, having a length equal to the length of the frame, calculated from Euler's expression

$$P_E = \frac{\pi^2 EI}{L^2} \quad (8.6)$$

The results were found to agree as Table 8.1 below suggests when several sections were studied. The table gives the results for section 458x102x33.

N	6	8	10	12	14	16	18
L (mm)	1976	2635	3294	3953	4611	5270	5929
P _E (kN)	501.41	282.04	180.51	125.35	92.1	70.51	55.71
W (kN)	501.4	282.1	180.5	125.4	92.1	70.5	55.7

Table 8.1 Comparison of Euler Buckling Load P_E with program buckling load W.

8.5.2.3 Elastic critical load

The elastic critical loads of eight frames for each of the section used in the present experimental programme were calculated. The lengths of the frames varied from 6 to 20 panels (castellations). The results are shown in Tables 8.2 to 8.5. The loads given as the applied load W of

Fig.8.6 are equal to

$$W = \frac{M_E}{d} \quad (8.7)$$

with d being equal to the distance between the neutral axes of the top and bottom sections (see Fig.8.6) and M_E the end moment. The values of critical load were usually calculated within 100N of the "exact" failure load. This was due to the difficulty in obtaining the exact point where the determinant vanished.

The values obtained were compared to the elastic critical load calculated by using eq.4.1. It can be seen from the tables that the values from the present approach are slightly lower than those of eq.4.1 but that the approximation improves as the length of the frame increases. In the case of two sections (see Tables 8.2 and 8.4), the program failure loads actually become larger than the loads from eq.4.1 when the length of the frames reached 18 castellations.

8.5.2.4 Influence of the size of the holes on the elastic critical load

The computer program could also be used to study the influence of the holes on the elastic lateral buckling. This had been shown to be rather small in chapter 4. However it was soon realised that the program could only deal with variations in the width of the hole and not its depth. This was because the depth of the hole dictated the depth of the resulting frame. A decrease in the depth of the hole in a particular frame would lower the position of the neutral axis of the bottom and top chords (tee sections) thus reducing the total depth of the frame and making the comparison between frames derived from the same section impossible. For this reason, only variations in the width of the holes was studied as this kept the depth of the frames constant. The elastic critical loads of

Section 458x102x33				
N	L (mm)	P_{ME} (kN)	W (kN)	$\frac{P_{ME}^{-W}}{P_{ME}} \times 100$
6	1976	572.9	564.3	4.66
8	2635	339.0	328.3	3.17
10	3294	230.0	224.1	2.69
12	3953	170.2	165.9	2.53
14	4612	133.5	130.9	1.95
16	5270	109.3	109.4	-0.20
18	5929	92.2	92.8	-0.68
20	6588	79.7	80.7	-1.34

Table 8.2 Elastic Critical Loads

Section 458x127x37				
N	L (mm)	P_{ME} (kN)	W (kN)	$\frac{P_{ME}^{-W}}{P_{ME}} \times 100$
6	1976	971.3	919.6	5.32
8	2635	567.4	543.8	4.16
10	3294	379.7	369.0	2.83
12	3953	277.2	269.8	2.65
14	4612	214.7	212.4	2.28
16	5270	173.7	171.6	1.21
18	5929	145.1	143.8	0.91
20	6588	124.3	124.1	-0.11

Table 8.3 Elastic Critical Loads

Section 534x127x39				
N	L	P_{ME} (kN)	W (kN)	$\frac{P_{ME}-W}{P_{ME}} \times 100$
6	2307	753.5	714.9	5.11
8	3076	439.3	421.2	4.11
10	3845	293.3	284.6	2.99
12	4614	213.6	209.6	1.91
14	5383	165.2	164.3	1.68
16	6152	133.3	132.9	0.28
18	6921	111.1	111.6	-0.43
20	7690	95.0	95.9	-0.98

Table 8.4 Elastic Critical Loads

Section 609x140x46				
N	L (mm)	P_{ME} (kN)	W (kN)	$\frac{P_{ME}-W}{P_{ME}} \times 100$
6	2631	870.2	825.4	5.15
8	3508	505.8	483.8	4.36
10	4385	335.6	324.5	3.32
12	5262	243.2	238.2	2.11
14	6139	187.0	184.3	1.47
16	7016	150.3	148.4	1.25
18	7893	124.8	123.5	1.03
20	8770	106.3	105.1	1.10

Table 8.5 Elastic Critical Loads

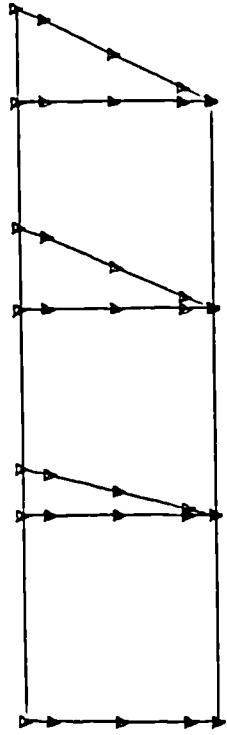
castellated beams were calculated for three sizes of holes which were of a rectangular shape. The length of the web welds in one frame was equal to the pitch of the castellation thus making the width of the holes equal to $0.251D_s$ (this was equivalent to a plain-webbed beam) whilst the width of the web members was equal to $0.251D_s$ and $0.829D_s$ in the other two beams (giving width of holes of $0.829D_s$ and $0.251D_s$ respectively). The results for the three sizes of holes are compared to the "exact" values in Table 8.6. The table shows that the critical loads for plain-webbed beams are between 2.34% and 7.25% higher than those for the beams with the smaller sized holes ($0.251D_s$) and that the values of "exact" critical load fall between the values of critical load for the small size hole and the larger size hole as expected. These results seem to confirm that the holes have very little influence on the lateral buckling strength of the castellated beams.

8.5.3 Shape of the buckled frames

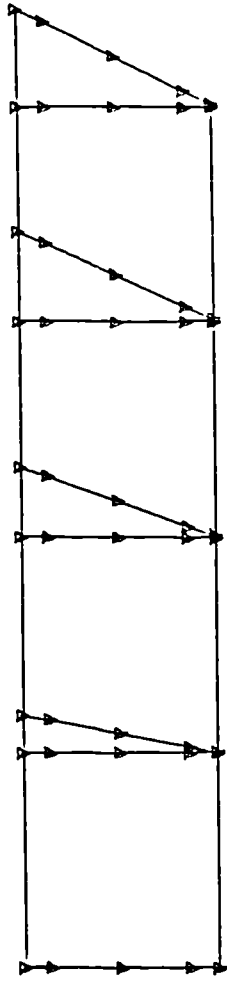
The shape of the frames in their laterally buckled state was also obtained when the elastic critical load was calculated. The results were very similar for all the sections analysed with no lateral movement of the bottom members in tension while the top members displaced in a half wave fashion. The web posts did not show any distortion when accompanying the lateral movements of the top members. Fig.8.7 shows the buckled shape of the web posts of section 609x140x46 for lengths of frame varying from 6 to 16 castellations. The figures show each frame in its initial and final state. The displacements of each node were multiplied by a factor of a 100 in the figures.

N	W (kN)			
	0.251xD _S	"Exact"	0.829xD _S	1.08xD _S
6	822.2	825.4	835.5	841.4
8	480.1	483.8	491.1	496.2
10	320.9	324.5	330.8	335.6
12	234.7	238.2	243.2	246.8
14	182.0	184.3	189.5	192.7
16	147.4	148.4	154.1	157.3
18	123.2	123.6	129.4	132.10

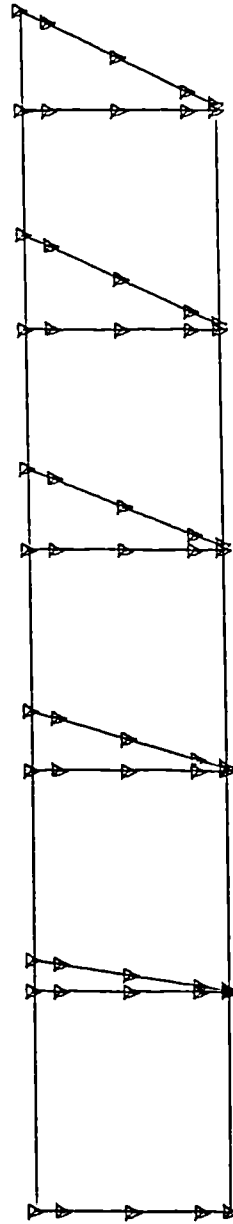
Table 8.6 Elastic Critical Loads for Different Widths of
Web Post for Section 609x140x46



6 PANELS

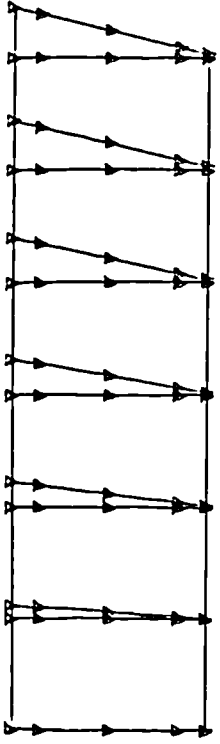


8 PANELS

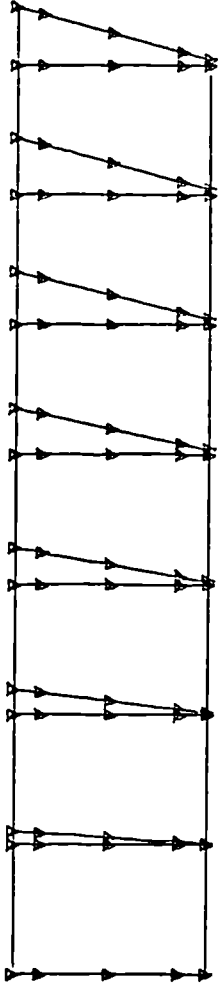


10 PANELS

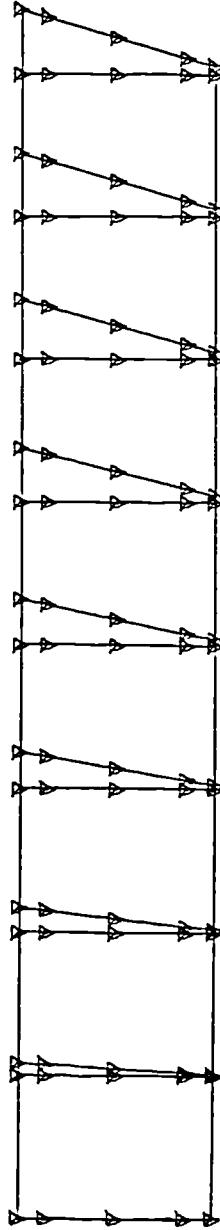
FIG. 8.7. a BUCKLED SHAPE OF THE WEB POSTS FOR SECTION 609x140x46



12 PANELS



14 PANELS



16 PANELS

FIG. 8.7.b BUCKLED SHAPE OF THE WEB POSTS FOR SECTION 609x140x46

8.6 Conclusions

The elastic critical loads of 32 frames having the properties of four sections have been calculated. The approximation used has proved to be reasonable although the computational effort involved might seem excessive when it is compared to that needed when eq.4.1 is used. However, eq.4.1 is also an approximation because it treats the castellated beam as a plain-webbed beam with a reduced section. The advantages of the method developed herein over eq.4.1 is that the sizes of the holes can be changed and that the influence of the holes on the lateral-buckling behaviour of castellated beams can be studied although changes need to be made to the program in order to cater for variation in the depth of the holes. The findings from the experimental programme regarding the possible distortion of the web posts when the beam deflected sideways seem to have been corroborated by the results of the computer program.

CHAPTER 9

CONCLUSIONS AND SUGGESTIONS FOR FUTURE WORK

9.1 General behaviour of castellated beams

The work carried out in this thesis has highlighted the influence that the type of loading, the slenderness and the geometry of the cut have on the behaviour and consequently the failure modes of castellated beams. The relative importance of these factors will determine whether a beam can be treated as a plain-webbed beam i.e. a member of a structure or as a structure in its own right the members of which are the chords and the web posts.

The review of the literature showed that previous authors who were concerned with in-plane behaviour treated the beams as structures designed to reach their maximum in-plane carrying capacity. Therefore most of the failure modes recorded involved isolated members of the structure. However in a few cases castellated beams were reported to have failed in modes involving an entire span: flexural failure and lateral-torsional buckling failure modes. In these two cases the beams were usually subjected to equal end moments loading.

The beams of the present experimental programme were made of three laterally continuous spans under a four-point loading system. Thus the three spans had to be designed separately because of the different failure modes involving each of the spans. The middle span under equal end moments loading provided the missing experimental data with which to evaluate various design methods. On the other hand the sidespans which were designed as structures whose members were liable to fail in any of several failure modes provided an opportunity for an appraisal of existing design procedures.

9.2 Design of the sidespans

Although the magnitude of the shear force transmitted to the middle span were low enough in all cases but two to prevent the formation of any of the failure modes involving the chords or the web posts, the calculations performed on beams S6-2 and S5-1 plus the beams tested in refs. 15 and 16 demonstrated the limitations of most of the methods available for designing the sidespans. Some of the conclusions reached are as follow:

1. Buckling of the web posts due to a directly applied force could not be predicted with any degree of precision.
2. Out of the three methods which existed for calculating the shear force responsible for lateral buckling of the web post, only that of Aglan and Redwood (46) gave reasonable predictions although safety factors between 2.45 and 2.74 were obtained for the three beams of ref.16.
3. Web weld fracture will not occur in castellated beams made of British castellated sections before the maximum in-plane carrying capacity has been reached.
4. The calculations showed that a Vierendeel mechanism could have formed in the case of beams S6-2 and S5-1 although this particular mechanism had never been reported for a British castellated section.
5. The Vierendeel analogy used to calculate the stresses up to the start of yielding has again proved reasonably accurate.

9.3 Lateral-torsional buckling

Two series of tests were performed, the first on small scale specially fabricated castellated beams of the same general proportions as full scale beams and a second on eight full scale beams.

The results of the first series in which the beams were tested as cantilevers under dead weight loading suggested that the presence of holes in the web had negligible effect on the beams lateral stability.

The second series of tests covered a wide range of beam slendernesses ranging from stocky, for which the full in-plane strength was anticipated, to much more slender sections, which were expected to buckle laterally at loads less than 50% of their in-plane capacity. All eight beams collapsed in a lateral-torsional mode, although in no case was this accompanied by rapid unloading as shown by the comparatively shallow slope of the load-deflection curves. The experimentally observed maximum loads have been compared with the strengths predicted by various interpretations of the new draft steelwork code B/20 as well as with those of BS 449, BS 153 and the ECCS Recommendations. From these comparisons the following conclusions may be drawn regarding an appropriate basis for the calculation of the lateral buckling strength of castellated beams having the proportions currently used in the U.K.

1. All cross-sectional properties used in determining bending strength, e.g. S_x , r_y , should be calculated for the cross-section at the centre of a castellation, and methods of determining the lateral buckling strength of normal solid web beams, cl.6.3 of B/20, may be used without modification. It appears to be unduly conservative to neglect the contribution of the web and tension flange as is implied by the method of cl.11.3.2.c of B/20.

2. The design curve presently specified in B/20 for rolled sections gives about 10% underprediction of buckling strength for the present series, with the degree of conservatism tending to increase with slenderness.
3. The assessments of the design approaches of BS 449, Table 3, and the two-stage procedure of Table 8 and 9, against the results of the tests, showed again the similarity in behaviour of castellated and plain-webbed beams. The use of Table 3 leads to rather unsafe load factors (as low as 1.3 in the case of the longer beams), whereas the two-stage procedure of BS 449 provided more satisfactory load factors of about 1.7.

9.4 Suggestions for future work

The work undertaken herein has fulfilled its primary purpose which was mainly to provide an assesement of the procedure of B/20 for the prevention of lateral-torsional buckling of castellated beams. However the work can be extended in order to achieve a better understanding of British castellated beams and obtain a clear relationship between loading and failure modes (the choice of British made beams would remove the geometry of the cut as a variable). This can be done by testing castellated beams under moments gradient of increasing magnitude or alternatively by developing an analytical model which could achieve similar results. This would help define the transition between a castellated beam treated as a structure and a castellated beam treated as a member of a structure (as in the case of lateral buckling). Finally the procedures for designing the various members of the castellated beams irrespective of the geometry of their cut could be improved when available e.g. web post buckling due to shear, or provided when missing

e.g. web post buckling due to a directly applied force. This would certainly help designers use castellated beams more extensively as structural elements in their own right and replace welded plate girders more often and not only when light loads are carried over long spans.

REFERENCES

REFERENCES

1. LITZKA, H., "Production of castellated beams in all types and sizes by automation", ACIER-STAHL-STEEL, Vol. 25, No. 11, Nov. 1960, pp. 483-487.
2. HETTICH, W., "Special type of latticed girder saves 200,000 dollars in cost of multi-storey steel framed building", ACIER-STEEL-STAHL, Vol. 25, No. 9, Sept. 1960, pp. 355-358.
3. STRUCTURAL STEELWORK HANDBOOK, Sections to BS 4: Part 1, Properties and safe table loads, Published by BCSA and CONSTRADO.
4. JOHNSON, H. I., "Open-web beams for Seattle office building", Civil Engineering, ASCE, Vol. 30, No. 3, March 1960, pp. 168-171.
5. WILLIAMS, G. M. J. and RUTTER, P. A., "The design of two buildings with suspended structures", The Structural Engineer, April 1967, Vol. 45, No. 4, pp. 143-151.
6. LAVEND'HOMME, R., "New building 'Delta-Hainaut' at Mons (Belgium)", ACIER-STAHL-STEEL, Vol. 28, No. 10, Oct. 1963, pp. 413-419.
7. VARSÌ, G. C., "Some interesting applications of castellated beams in Italy", ACIER-STAHL-STEEL, Vol. 32, No. 3, March 1967, pp. 117-120.
8. GARCIA, J., "Superphosphate store for the Cros Company, Madrid", ACIER-STAHL-STEEL, Vol. 32, No. 1, Jan. 1967, pp. 17-20.
9. BS 449, "Specification for the use of structural steel in building: Part 2, London, British Standards Institution, 1969.
10. BS 153, "Specification for steel girder bridges: Parts 3B and 4, London, British Standards Institution, 1972.
11. CSA-S16.1-1974, "Steel structures of buildings-limit state design, Rexdale, Ontario, Canadian Standards Association, 1974.
12. Sub-committee on beams with web openings of the Task Committee on flexural members of the Structural Division, "Suggested design guide for beams with web holes", Journal of the Structural Division, ASCE, Vol. 97, No. ST11, Nov. 1971, pp. 2702-2728.

13. HALLEUX, P., "Etude expérimentale et technique du comportement élastique des poutres métalliques à âme évidée", Revue Française de Mécanique, Mémoires du Groupement pour l'Avancement des Méthodes d'Analyse des Contraintes, Nos. 19 et 18, 1966, pp. 123-140.
14. B/20., "Draft standard specification for the structural use of steelwork in building, Part 1: Simple construction and continuous construction", London, British Standards Institution, 1978
15. THE UNITED STEEL CO. LTD., Res. and Dev. Dep., Swinden laboratories, Rotherham, "Properties and strengths of castella beams. Consideration of previous tests", Report D.GE. 71/262, 27th April 1957.
16. THE UNITED STEEL CO. LTD., Res. and Dev. Dep., Swinden laboratories, Rotherham, "Properties and strengths of castella beams. Further tests", Report D.GE. 71/261/1, 26th July 1958.
17. THE UNITED STEEL CO. LTD., Res. and Dev. Dep., Swinden laboratories, Rotherham, "Properties and strengths of castella beams. Deflection characteristics", Report D.TS. 6/262/2, 25th August 1960.
18. THE UNITED STEEL CO. LTD., Res. and Dev. Dep., Swinden laboratories, Rotherham, "Web strength of castella beams", report D.TS. 6/262/6, 23rd may 1962.
19. GIBSON, J. E. and JENKINS, W. M., "An investigation of the stresses and deflections in castellated beams", The Structural Engineer, Vol. 35, No. 12, Dec. 1957, pp. 467-479.
20. KOLOSOWSKI, J., "Stresses and deflections in castellated beams", The Structural Engineer, Vol. 42, No. 1, Jan. 1964, pp. 19-24.
21. ALTFILLICH, M. D., COOKE, B. R. and TOPRAC, A. A., "An investigation of welded open-web expanded beams", Journal of the American Welding Society, Welding res. supp., Feb. 1957, pp. 77-88.
22. TOPRAC, A. A. and COOKE, B. R., "An experimental investigation of open-web beams", Welding Research Council Bulletin Series, No. 47, Feb. 1959.
23. HALLEUX, P., "Limit analysis of castellated steel beams", ACIER-STAH-STEEL, Vol. 32, No. 3, March 1967, pp. 133-144.
24. BAZILE, A. and TEXIER, J., "Essais de poutres ajourées", Construction Métallique, No. 3, Sept. 1968, pp. 12-25.

25. HOSAIN, M. U. and SPEIRS, W. G., "Experiments on castellated beams", Journal of the American Welding Society, Welding res. supp. Vol. 52, No. 8, Aug. 1973, pp. 329-342.
26. HOSAIN, M. U. and SPEIRS, W. G., "Failure of castellated due to rupture of welded joints", ACIER-STAH-STEEL, Vol. 36, No. 1, Jan. 1971, pp. 34-40.
27. GALAMBOS, A. R., HOSAIN, M. U. and SPEIRS, W. G., "Optimum expansion ratio of castellated steel beams", Engineering Optimization, Vol. 1, No. 4, 1975, pp. 213-225.
28. CLARK, P. R., "Shear stresses and web stability in castellated steel beams", MEng thesis, Nova Scotia Technical College, Halifax, 1964.
29. DOUTY, R. T. and BALDWIN, J. W., "Measured and computed stresses in three castellated beams", AISC Engineering Journal, Vol. 3, Part 1, 1966, pp. 15-18.
30. SHERBOURNE, A. N., "The plastic behaviour of castellated beams", Proc. 2nd Commonwealth Welding Conference, Institute of Welding, London, 1966, No. C2, pp. 1-5.
31. MANDEL, J. A., BRENNAN, P. J., WASIL, B. A., ANTONI, C. M., "Stress distribution in castellated beams," Journal of the Structural Division, ASCE, Vol. 97, No. ST7, July 1971, pp. 1947-1967.
32. MATEESCO, D. and MERCEA, G., "Un nouveau type de poutres ajourées", Construction Métallique, No. 3, 1981, pp. 3-14.
33. GARDNER, N. J., "An investigation into the deflection behaviour of castellated beams", Transactions of the EIC, Vol. 9, No. A-7, Sept. 1966, pp. 1-8.
34. HALLEUX, P., "Le calcul des flèches des poutres à âmes évidees", Centre de Recherches Scientifique et Techniques de l'Industrie des Fabrications Métalliques, Janvier 1968.
35. SHOUKRY, Z., "Elastic flexural stress distribution in webs of castellated beams", Journal of the American Welding Society, Welding Res. Supp., Vol. 44, No. 5, May 1965, pp. 231-240.
36. HUMPHREY, A. T. and SUNLEY, V. K., "A finite element analysis of an expanded I-section beam and an axi-symmetric flanged cylinder", Conference records, Advanced stress analysis, 3-14, Joint British Conference for stress analysis, Vol. 3, No. 14, 1968.
37. CHENG, W. K., HOSAIN, M. U. and NEIS, V. V., "Analysis of castellated beams by the finite element method", Proc. of the speciality conference on Finite Element Method in Civil Engineering, Montreal, Canada, June 1-2, 1972, pp. 1105-1140.

38. GOTOH, K., "Stress analysis of castellated beams", Transactions of JSCE, Vol. 7, Nov. 1976, pp. 37-38.
39. HOSAIN, M. U., CHENG, W. K. and NEIS, V. V., "Deflection analysis of expanded open-web steel beams", Computers and Structures, Vol. 4, No. 2, March 1974, pp. 327-336.
40. HRABOK, M. M. and HOSAIN, M. U., "Castellated beam deflections using substructuring", Journal of the Structural Division, ASCE, Vol. 103, No. ST1, January 1977, pp. 265-269.
41. MAEDA, Y. and MATSUI, S., "Stress and deflection analysis of open-web steel beams", Technology reports, Osaka University, Vol. 27, No. 1362, 1977, pp. 271-281.
42. SRIMANI, S. L. and DAS, P. K., "An investigation of deflection in castellated beams", Journal Institution of Engineers, Civil Eng. Div. (India), Vol. 58, pt. CI-1, July 1977, pp. 46-49.
43. SRIMANI, S. L. and DAS, P. K., "Finite element analysis of castellated beams", Computers and Structures, Vol. 9, August 1978, pp. 169-174.
44. VAN OOSTROM, J. and SHERBOURNE, A. N., "Plastic analysis of castellated beams, part 2, analysis and tests", Computers and Structures, Vol. 2, Nos. 1/2, February 1972, pp. 111-140.
45. DELESQUES, R., "Stabilité des montants des poutres ajourées", Construction Métallique, No. 3, 1968, pp. 26-33.
46. AGLAN, A. A. and REDWOOD, R. G., "Web buckling in castellated beams", Proc. of the ICE, Part 2, Vol. 57, June 1974, pp. 307-320.
47. DOUGHERTY, B. K., "Buckling of web posts in perforated beams", Journal of the Structural Division, ASCE, Vol. 107, No. ST3, March 1981, pp. 507-519.
48. BAZILE, A., "Etude de la resistance des poutrelles ajourées", Construction Métallique, No. 3, 1964, pp. 10-11.
49. FALTUS, F., "Calculation of castellated girders", ACIER-STAH-STEEL, Vol. 31, No. 5, May 1966, pp. 227-230.
50. BOYER, J. P., "Castellated beams - New developments", AISC, Engineering Journal, Vol. 1, No. 3, July 1964, pp. 104-108.
51. DELESQUES, R., "Le calcul des poutres ajourées", Construction Métallique, Vol. 6, No. 4, 1969, pp. 41-51.
52. HOPE, B. B. and SHEIKH, M. A., "The design of castellated beams", Transaction of the EIC, Vol. 12, No. A-8, Sept. 1969.

53. BLODGETT, O. W., "Cost-saving open-web expanded beams and girders, Design of welded structures", The James F. Lincoln Arc Welding Foundation, Cleveland, Ohio, 1969.
54. McCORMICK, M. M., "Open-web beams - behaviour analysis and design", BHP Melbourne Research Laboratories Report 17/18, Feb. 1972.
55. PATTANAYAK, U. C. and CHESSON, E., "Lateral instability of castellated beams", Engineering Journal, AISC, Vol. 11, No. 3, 3rd quarter, 1974, pp. 73-79.
56. NETHERCOT, D. A. and ROCKEY, K. C., "A unified approach to the elastic lateral buckling of beams", The Structural Engineer, Vol. 49, No. 7, July 1971, pp. 321-330.
57. American Institute of Steel Construction, "Manual of Steel Construction", 8th ed., AISC, New York, 1978.
58. AS 1250-1975 Steel Structure Code, Standard Association of Australia, Sydney, 1975.
59. WORLEY, W. J., "Inelastic behaviour of alloy I-beams with web cut-outs, Bulletin No. 448, Engineering Experiment Station, University of Illinois, 1958.
60. COULL, A. and ALVAREZ, M., "Effect of openings on lateral buckling of beams", Journal of the Structural Division, ASCE, Vol. 106, No. ST12, December 1980, pp. 2553-2560.
61. NETHERCOT, D. A., "The effective length of cantilevers as governed by lateral buckling", The Structural Engineer, Vol. 51, No. 5, May 1973, pp. 161-168.
62. TIMOSHENKO, S. P. and GERE, J. M., "Theory of elastic stability", Chapt. 6, 2nd ed., New York, McGraw-Hill.
63. GALAMBOS, T.V., "Structural members and frames", Chapt. 3, Englewood Cliffs, N.J., Prentice Hall.
64. REDWOOD, R. G., "Design of beams with web holes", Canadian Steel Industries Construction Council, Ontario, Canada.
65. DOUGHERTY, B. K., "The effects of rectangular web holes on the behaviour of steel beams", thesis presented to the University of Natal, Durban, South Africa, in 1978, in partial fulfillment of the requirements for the degree of Doctor of Philosophy.
66. NETHERCOT, D. A., "Factors affecting the buckling stability of partially plastic beams", Proc. of the ICE, Part 2, Vol. 53, Sept. 1972, pp. 285-385.

67. NETHERCOT, D. A., "Inelastic buckling of steel beams under non-uniform moment", *The Structural Engineer*, Vol. 53, No. 2, Feb. 1975, pp. 73-78.
68. KITIPORNCHAI, S. and TRAHAIR, N. S., "Buckling of inelastic I-Beams under moment gradient", *Journal of the Structural Division, ASCE*, Vol. 101, No. ST5, May 1975, pp. 991-1004.
69. KITIPORNCHAI, S. and TRAHAIR, N. S., "Inelastic buckling of simply supported steel I-Beams", *Journal of the Structural Division, ASCE*, Vol. 101, No. ST7, July 1975, pp. 1333-1347.
70. NETHERCOT, D. A. and TRAHAIR, N. S., "Inelastic buckling of determinate beams", *Journal of the Structural Division, ASCE*, Vol. 102, No. ST4, April 1976, pp. 701-717.
71. HOLLINGER, B. H. and MANGELSDORF, M., "Inelastic lateral-torsional buckling of beams", *Journal of the Structural Division, ASCE*, Vol. 107, No. ST8, Aug. 1981, pp. 1551-1567.
72. SEGNER, E. P., "Reinforcement requirements for girder web openings", *Journal of the Structural Division, ASCE*, Vol. 90, No. ST3, June 1964, pp. 147-164.
73. REDWOOD, R. G. and McCUTCHEON, J., "Beam tests with unreinforced web openings", *Journal of the Structural Division, ASCE*, Vol. 94, No. ST1, Jan. 1968, pp. 1-17.
74. BOWER, J. E., "Ultimate strength of beams with rectangular holes", *Journal of the Structural Division, ASCE*, Vol. 94, No. ST6, June 1968, pp. 1315-1337.
75. CONGDON, J. B. and REDWOOD, R. G., "Plastic behaviour of beams with reinforced holes", *Journal of the Structural Division, ASCE*, Vol. 96, No. ST9, Sept. 1970, pp. 33-1955.
76. COOPER, P. B. and SNELL, R. R., "Tests on beams with reinforced web openings", *Journal of the Structural Division, ASCE*, Vol. 98, No. ST3, March 1972, pp. 611-632.
77. BS 4360, "Specification for weldable structural steels", London, British Standards Institution, 1979.
78. NETHERCOT, D. A. and TRAHAIR, N. S., "Lateral-buckling approximation for elastic beams", *The Structural Engineer*, Vol. 54, No. 6, June 1976, pp. 197-204.
79. TRAHAIR, N. S., "Discussion of Lateral-torsional buckling of I-sections in grade 55 steel by J.E. Dibley", *Proc. of the ICE*, Vol. 46, 1970, pp. 97-104.
80. BS 18, "Methods for tensile testing of metals: part 2, London, British Standards Institution, 1971.

81. Transport and Road Research Laboratory, "Recommended Standard Practices for Structural Testing of Steel Models", TRRL Supplementary Report 254, DoE and DTp, 1977.
82. SHERBOURNE, A. N. and VAN OOSTROM J., "Plastic analysis of castellated beams - Part 1, Interaction of moment, shear and axial force", Computers and Structures, Vol. 2, Nos. 1/2, February 1972, pp. 79-109.
83. O'HEACHTAIRN, P. and NETHERCOT, D. A., "Lateral-torsional buckling tests on reduced scale welded plate girders", Res. Rept. No. BE 22/2/065/2, submitted to DTp, BED, Sept. 1978.
84. KILFORD, W.K., "Elementary air survey", Chapt. 7, 4th ed., Pitman publishers.
85. "American Society of Photogrammetry", Handbook of non-topographic photogrammetry, ed. H. M. KARARA, 1st ed., 1979.
86. SCOTT, P. J., "Structural deformation measurement of a model box girder bridge", The Photogrammetric Record, Vol. 9, No. 51, April 1978, pp. 361-377.
87. "European Recommendations for Steel Construction", European Convention for Structural Steelwork, 1978.
88. KIRBY, P. A. and NETHERCOT, D. A., "Design for structural stability", Constrado Monographs, Crosby Lockwoods Staples, Granada Publishing, 1971.
89. DIBLEY, J. E., "Lateral-torsional buckling of I-sections in grade 55 steel", Proc. of the ICE, Vol. 43, Aug. 1969, pp. 599-627.
90. European Convention for Constructional Steelwork, Second International Colloquium on Stability, Introductory report ECCS, Chapt. 5.
91. CHEN, W. F. and ATSUTA, T., "Theory of beam-columns, Vol.2, Space behaviour and Design, Chapt. 3", New York, McGraw-Hill.
92. MAJID, K., "Non-linear structures", London, Butterworths.
93. LIVESLEY, R. K., "Matrix methods of structural analysis", 2nd ed., Pergamon Press.
94. PARCEL, J. I. and MOORMAN, R. B. B., "Analysis of statically indeterminate structures, chapt. 5", John Wiley and Sons, New York.
95. WITTRICK, W. H. and WILLIAMS, F. W., "An algorithm for computing critical buckling loads of elastic structures", Journal of Structural Mechanics, Vol. 1, No. 4, 1973, pp. 497-518.